

Université catholique de Louvain
de Duve Institute

**Role of Akt/PKB and PFKFB isoenzymes in the
control of glycolysis, cell proliferation and protein
synthesis in mitogen-stimulated thymocytes**

Amina HOUDDANE

Thesis submitted in fulfillment of the requirements for a PhD
degree in Biomedical and Pharmaceutical Sciences

Promoter: Prof. Mark H. RIDER

Co-promoter: Prof. Stefan CONSTANTINESCU

2017

COMMITTEE

Prof. Jean-Baptiste Demoulin (President)
Université catholique de Louvain

Prof. Mark H. Rider (Promoter)
Université catholique de Louvain

Prof. Stefan Constantinescu (Co-promoter)
Université catholique de Louvain

Prof. Luc Bertrand
Université catholique de Louvain

Prof. Olivier Feron
Université catholique de Louvain

Prof. Almut Schulze
Universität Würzburg

TABLE OF CONTENTS

| | |
|--|-----------|
| ABBREVIATIONS | 1 |
| SUMMARY | 5 |
| RÉSUMÉ | 7 |
| INTRODUCTION | 10 |
| I. Glycolysis | 11 |
| I.1. Introduction | 11 |
| I.2. Control points in the glycolytic pathway. | 11 |
| I.2.1. <i>Glucose transporters</i> | 13 |
| I.2.2. <i>Hexokinase</i> | 13 |
| I.2.3. <i>Phosphofructo-1-kinase</i> | 14 |
| I.2.4. <i>Pyruvate kinase</i> | 15 |
| I.3. Fructose-2,6-bisphosphate..... | 17 |
| I.3.1. <i>Synthesis and degradation of Fru-2,6-BP</i> | 17 |
| I.3.2. <i>Structure of PFK-2/FBPase-2</i> | 19 |
| I.3.3. <i>Gene expression and post-translational regulation of PFK-2/FBPase-2 isoenzymes</i> | 20 |
| I.3.3.1. PFKFB1 | 22 |
| I.3.3.2. PFKFB2..... | 24 |
| I.3.3.3. PFKFB3..... | 26 |
| I.3.3.4. PFKFB4..... | 28 |
| I.3.4. <i>Roles of Fru-2,6-BP</i> | 28 |
| I.4. Glycolysis in cancer and rapidly-proliferating cells..... | 30 |
| I.4.1. <i>PFKFB isoenzymes in cancer and normal proliferating cells</i> | 31 |
| I.4.2. <i>PFKFB3 inhibitors</i> | 34 |
| I.5. TIGAR..... | 34 |

| | |
|--|------------|
| II. Thymocytes as a non-cancer proliferating cell model | 35 |
| II.1. Mitogenic stimulation..... | 35 |
| II.1.1. <i>Concanavalin A: a mitogenic plant lectin</i> | 35 |
| II.1.2. <i>Interleukin-2</i> | 36 |
| II.1.2.1. Interleukin-2 receptors | 36 |
| II.1.2.2. The interleukin-2 signaling pathway..... | 37 |
| II.1.2.2.1. The Jak-STAT signaling pathway..... | 39 |
| II.1.2.2.2. The Ras-MAP kinase pathway..... | 39 |
| II.1.2.2.3. The PI3K pathway..... | 40 |
| II.2. The PKB pathway | 41 |
| II.2.1. <i>The PI3K/PKB axis</i> | 41 |
| II.2.2. <i>PKB/Akt isoforms</i> | 42 |
| II.2.3. <i>Structure of PKB</i> | 43 |
| II.2.4. <i>Cellular functions of PKB</i> | 44 |
| II.2.5. <i>PKB inhibitors</i> | 48 |
| II.3. Metabolic changes in ConA-stimulated thymocytes..... | 49 |
| RESEARCH OBJECTIVES | 53 |
| RESULTS | 55 |
| Paper 1: Role of Akt/PKB and PFKFB isoenzymes in the control of glycolysis, cell proliferation and protein synthesis in mitogen-stimulated thymocytes..... | 56 |
| DISCUSSION | 74 |
| ANNEXES..... | 82 |
| PAPER 2: A conserved phosphatase destroys toxic glycolytic side products in mammals and yeast..... | 83 |
| PAPER 3: 6-phosphofructo-2-kinase/fructose-2,6-bisphosphatase 4 is essential for p53-null cancer cells..... | 96 |
| REFERENCES | 121 |

ABBREVIATIONS

| | |
|----------|---|
| 2,3-BPG | 2,3-bisphosphoglycerate |
| 4E-BP1 | Eukaryotic initiation factor 4E-binding protein-1 |
| AK | Adenylate kinase |
| AMPK | AMP-activated protein kinase |
| APC/C | Anaphase-promoting complex/cyclosome |
| AR | Androgen receptor |
| AS160 | Akt substrate of 160 kDa |
| ATF | Activating transcription factor |
| BAD | Bcl-2-associated death promoter |
| BIM | Bcl-2-like protein 11 |
| Ca/CAMK | Ca ²⁺ /calmodulin-dependent protein kinase |
| cAMP | Cyclic 3',5'-adenosine monophosphate |
| c-myc | v-myc avian myelocytomatosis viral oncogene cellular homolog |
| ConA | Concanavalin A |
| CREB | Cyclic AMP response element-binding protein |
| Elk-1 | Ets-like transcription factor 1 |
| eNOS | Endothelial nitric oxide synthase |
| ERK | Extracellular-signal-regulated kinase |
| FBPase-1 | Fructose-1,6-bisphosphatase |
| FBPase-2 | Fructose-2,6-bisphosphatase |

| | |
|------------|--|
| FOXO | Forkhead box, Class O |
| Fru-1,6-BP | Fructose-1,6-bisphosphate |
| Fru-2,6-BP | Fructose-2,6-bisphosphate |
| Fru-6-P | Fructose-6-phosphate |
| GAP | GTPase activating protein |
| GAPDH | Glyceraldehyde-3-phosphate dehydrogenase |
| Glu-6-P | Glucose-6-phosphate |
| GLUT | Glucose transporter |
| GOT1 | Glutamic oxaloacetate transaminase 1 |
| GSK-3 | Glycogen synthase kinase-3 |
| HGF | Hepatocyte growth factor |
| HIF | Hypoxia-induced factor |
| HK | Hexokinase |
| HMIT1 | H ⁺ /myoinositol co-transporter 1 |
| IGF-1 | Insulin-like growth factor 1 |
| IKK | I κ B kinase |
| IL-2 | Interleukin-2 |
| IL-2R | Interleukin-2 receptor |
| Jak | Janus tyrosine kinase |
| JNK | c-Jun N-terminal kinase |
| LDHA | Lactate dehydrogenase A |
| MACC1 | Metastasis associated in colon cancer 1 |
| MAPK | Mitogen-activated protein kinase |

| | |
|---------|---|
| MDH1 | Malate dehydrogenase 1 |
| MDM2 | Mouse double minute 2 homolog |
| MEK | Mitogen-activated protein kinase/extracellular-signal-regulated kinase kinase |
| MNK | MAPK-interacting kinase |
| mTOR | mammalian target of rapamycin |
| mTORC1 | mammalian target of rapamycin complex 1 |
| mTORC2 | mammalian target of rapamycin complex 2 |
| NO | Nitric oxide |
| OxPhos | Oxidative phosphorylation |
| p53 | Tumour protein 53 |
| p38MAPK | p38 mitogen-activated protein kinase |
| p90Rsk | 90-kDa ribosomal S6 kinase |
| PDK1 | Phosphoinositide-dependent kinase-1 |
| PDK2 | Pyruvate dehydrogenase kinase isoform 2 |
| PEP | Phosphoenolpyruvate |
| PFK-1 | 6-phosphofructo-1-kinase |
| PFK-2 | 6-phosphofructo-2-kinase |
| PFKFB | 6-phosphofructo-2-kinase/fructose-2,6-bisphosphatase isoenzyme |
| PHA | Phytohemagglutinin |
| PI3K | Phosphatidylinositol-3-kinase |
| PK | Pyruvate kinase |
| PKA | cAMP-dependent protein kinase |
| PKB | Protein kinase B |
| PKC | Protein kinase C |

| | |
|-----------------------------|--|
| PPi:PFK | Pyrophosphate-dependent 6-phosphofructo-1-kinase |
| PPP | Pentose phosphate pathway |
| PRAS40 | Proline-rich Akt/PKB substrate 40 kDa |
| PtdIns-4,5-P ₂ | Phosphatidylinositol-4,5-bisphosphate |
| PtdIns-3,4,5-P ₃ | Phosphatidylinositol-3,4,5-triphosphate |
| PTEN | Tumor suppressor phosphatase and tensin homolog deleted on chromosome 10 |
| Rheb | Ras homologue enriched in brain |
| ROS | Reaction oxygen species |
| S6K1 | p70 ribosomal protein S6 kinase-1 |
| SAPK | Stress-activated protein kinase |
| SGK3 | Serum and glucocorticoid-inducible kinase-3 |
| SH2 | Src Homology 2 |
| STAT | Signal transducer and activator of transcription |
| TCA | Tricarboxylic acid |
| TIGAR | Tumour protein 53-induced glycolysis and apoptosis regulator |
| TSC1 | Tuberous sclerosis protein 1 (hamartin) |
| TSC2 | Tuberous sclerosis protein 2 (tuberin) |
| VEGF | Vascular endothelial growth factor |

SUMMARY

Proliferating cells increase glucose metabolism to generate ATP and to supply precursors for macromolecular biosynthesis. Despite the fact that aerobic respiration produces more ATP, cancer cells convert most of their glucose to lactate under aerobic conditions, a phenomenon known as the “Warburg effect”, but which is not restricted to cancer cells. Fructose-2,6-bisphosphate (Fru-2,6-BP) is the most potent positive allosteric effector of 6-phosphofructo-1-kinase (PFK-1), and hence of glycolysis. Fru-2,6-BP is synthesized and degraded by a bifunctional, homodimeric enzyme, called 6-phosphofructo-2-kinase (PFK-2)/fructose-2,6-bisphosphatase (FBPase-2). Four PFK-2/FBPase-2 isoenzymes, designated PFKFB1-4, have been identified in mammals encoded by four genes and each gene generates several isoforms by alternative splicing. Previous studies showed that Fru-2,6-BP concentrations in cancer cells can reach levels 10 – 100 times higher than required to stimulate PFK-1. Therefore, we investigated whether Fru-2,6-BP might play a role in coupling glycolysis to cell proliferation and protein synthesis.

Freshly isolated rat thymocytes were chosen as a non-cancerous model to study the metabolic changes that occur during the transition from the resting to the proliferating state. Mitogen stimulation of rat thymocytes with concanavalin A (ConA) induced time-dependent increases in medium lactate accumulation (6-fold), Fru-2,6-BP content (4-fold), expression of PFKFB3 and PFKFB4 isoenzymes (~2-fold and ~15-fold, respectively) and rates of cell proliferation (~40-fold) and protein synthesis (~10-fold) after 68 h of incubation compared with resting cells. In parallel, increased expression and phosphorylation of translation factors, such as eukaryotic initiation factor-4E-binding protein-1 (4E-BP1) and ribosomal protein S6 (rpS6), were observed in ConA-stimulated thymocytes. In a parallel *in vitro* study, protein kinase B (PKB) was shown to phosphorylate PFKFB3 at Ser461, leading to PFK-2 activation. However, in ConA-stimulated

cells, only a slight increase in PFKFB3 Ser461 phosphorylation was detected. Therefore, although PFKFB3 is expressed in many proliferating and cancer cells, the importance of PKB-induced PFKFB3 phosphorylation is unclear. Treatment of ConA-stimulated thymocytes with low doses of PKB inhibitor (MK-2206) resulted in reduced levels of the PFKFB3 and PFKFB4 proteins, suggesting regulation of expression of the two PFKFB isoenzymes by PKB. In parallel, we also showed that MK-2206 induced significant decreases in Fru-2,6-BP content, medium lactate and rates of cell proliferation and protein synthesis in ConA-stimulated thymocytes. As expected, treatment with the PFK-2 inhibitor (3PO) reduced Fru-2,6-BP content and medium lactate accumulation, without affecting PFKFB3 and PFKFB4 expression in ConA-stimulated cells. Surprisingly, rates of cell proliferation and protein synthesis were also significantly decreased by exposure of ConA-stimulated cells to low doses of 3PO. These data were confirmed by siRNA knockdown of PFKFB3, PFKFB4 and PKB α/β in the more easily transfectable Jurkat E6-1 cell line. The findings suggest that increased PFKFB3 and PFKFB4 expression, but not increased PFKFB3 Ser461 phosphorylation, plays a role in stimulating glycolysis in ConA-stimulated thymocytes and implicate PKB in the upregulation of PFKFB3 and PFKFB4 expression. Taken together, the findings support a role of Fru-2,6-BP in the control of glycolysis, cell proliferation and protein synthesis in mitogen-stimulated thymocytes, through a mechanism involving PKB.

RÉSUMÉ

Les cellules en prolifération augmentent considérablement le métabolisme du glucose en lactate pour générer de l'ATP et fournir des précurseurs de la biosynthèse de macromolécules. Bien que la production d'ATP soit plus efficace en aérobose, les cellules cancéreuses utilisent majoritairement la fermentation lactique même en présence d'oxygène, un phénomène appelé l'effet Warburg, qui n'est pas limité aux cellules cancéreuses. Le fructose-2,6-bisphosphate (Fru-2,6-BP) est l'effecteur allostérique positif le plus puissant de la 6-phosphofructo-1-kinase (PFK-1), et donc de la glycolyse. Le Fru-2,6-BP est synthétisé et dégradé par une enzyme homodimérique bifonctionnelle, appelée 6-phosphofructo-2-kinase (PFK-2)/fructose-2,6-bisphosphatase (FBPase-2). Quatre isoenzymes de la PFK-2/FBPase-2, désignées PFKFB1-4, ont été identifiées chez des mammifères et sont codées par quatre gènes, chacun générant plusieurs isoformes par épissage alternatif. Des études précédentes ont montré que les concentrations de Fru-2,6-BP dans les cellules cancéreuses peuvent être 10 à 100 fois supérieures à celles requises pour stimuler la PFK-1. Par conséquent, nous avons investigué si le Fru-2,6-BP pourrait jouer un rôle dans le couplage de la glycolyse à la prolifération cellulaire ainsi qu'à la synthèse protéique.

Des thymocytes fraîchement isolés de rat ont été choisis comme modèle cellulaire non cancéreux afin d'étudier les adaptations métaboliques induites par une stimulation mitogénique par la concanavaline A (ConA). Par rapport aux cellules quiescentes, les thymocytes stimulés par la ConA augmentent l'accumulation de lactate dans le milieu de culture (6 fois), la concentration en Fru-2,6-BP (4 fois), l'expression des isoenzymes PFKFB3 et PFKFB4 (2 fois et 15 fois, respectivement) et les vitesses de prolifération cellulaire (40 fois) et de synthèse protéique (10 fois) après 68 h d'incubation. Parallèlement, l'expression et la phosphorylation de facteurs de traduction, telles que la protéine liée au facteur

d'initiation eucaryote 4E (4E-BP1) et la protéine ribosomale S6 (rpS6), sont augmentées. Dans une étude réalisée *in vitro*, nous avons montré que la protéine kinase B (PKB) phosphoryle le résidu Ser461 de la PFKFB3, conduisant ainsi à l'activation de la PFK-2. Cependant, l'augmentation de la phosphorylation de la Ser461 détectée dans les cellules stimulées par la ConA était faible. Dès lors, bien que l'isoenzyme PFKFB3 soit exprimée dans de nombreuses cellules en prolifération et cellules cancéreuses, la signification et l'importance de la phosphorylation de la PFKFB3 induite par la PKB reste à clarifier. Le traitement de thymocytes stimulés par la ConA en présence de faibles doses de l'inhibiteur de la PKB (MK-2206) a provoqué une diminution de l'expression de la PFKFB3 et PFKFB4, suggérant un contrôle de l'expression de ces deux isoenzymes par PKB. Parallèlement, nous avons également montré que, dans des thymocytes stimulés par la ConA, MK-2206 a réduit significativement la concentration de Fru-2,6-BP, l'accumulation de lactate dans le milieu et les vitesses de prolifération cellulaire et de synthèse protéique. Comme attendu, l'inhibiteur de la PFK-2 (3PO) a diminué la concentration en Fru-2,6-BP et l'accumulation de lactate dans le milieu de culture des cellules stimulées par ConA, et ceci sans affecter l'expression des isoenzymes PFKFB3 et PFKFB4. De façon intéressante, les vitesses de prolifération cellulaire et de synthèse protéique ont également été significativement réduites dans des cellules stimulées par ConA en présence de faibles doses de 3PO. Ces résultats ont été confirmés au moyen d'ARN interférents (siRNA) ciblant la PFKFB3, la PFKFB4 ou la PKB α/β dans des cellules Jurkat E6-1, lignée cellulaire facilement transfectable. Les résultats suggèrent que l'augmentation de l'expression des deux isoenzymes PFKFB3 et PFKFB4, mais pas l'augmentation de la phosphorylation de la Ser461 de la PFKFB3, joue un rôle dans la stimulation de la glycolyse dans des thymocytes stimulés par des mitogènes et impliquent PKB dans la régulation de l'expression de la PFKFB3 et PFKFB4.

Ainsi, les résultats confirment le rôle de la Fru-2,6-BP dans le contrôle de la glycolyse, de la prolifération cellulaire et de la synthèse protéique dans les thymocytes stimulés par des mitogènes, par un mécanisme impliquant la PKB.

INTRODUCTION

I. Glycolysis

I.1. Introduction

Glycolysis is the metabolic pathway that transforms glucose into pyruvate while generating two ATPs per glucose molecule consumed. Further metabolism of pyruvate depends on oxygen availability. Under aerobic conditions, pyruvate can be completely oxidized to CO₂ by the tricarboxylic acid (TCA) cycle coupled to the mitochondrial respiratory chain, which generates maximum 38 ATPs for each molecule of glucose oxidized. Under anaerobic conditions, glycolysis becomes the sole source of ATP and is greatly enhanced to provide the cell with sufficient ATP. Pyruvate is reduced to lactate to regenerate NAD⁺, which is required to allow glycolytic flux to proceed via glyceraldehyde-3-phosphate dehydrogenase (GAPDH). Besides its energetic role, glycolysis can also provide precursors for biosynthetic processes, such as lipid and nucleic acid biosynthesis.

In the presence of oxygen, glycolysis is inhibited, a phenomenon discovered by Louis Pasteur and known as the Pasteur effect. Glycolysis can also be modulated by energy demand, substrate availability, hormones and nutritional status. In addition, in cancer cells and in rapidly-proliferating cells, glycolysis is greatly increased and prevails even in the presence of oxygen. This characteristic feature is known as the Warburg effect and is further discussed below (see section I.4.)

I.2. Control points in the glycolytic pathway.

Glycolytic flux is controlled at the following steps: (i) glucose transport by glucose transporters (GLUTs); (ii) phosphorylation of glucose by hexokinases (HKs)/glucokinase; (iii) phosphorylation of fructose-6-phosphate (Fru-6-P) to

fructose-1,6-bisphosphate (Fru-1,6-BP) catalyzed by 6-phosphofructo-1-kinase (PFK-1); and (iv) the last reaction catalyzed by pyruvate kinase (PK).

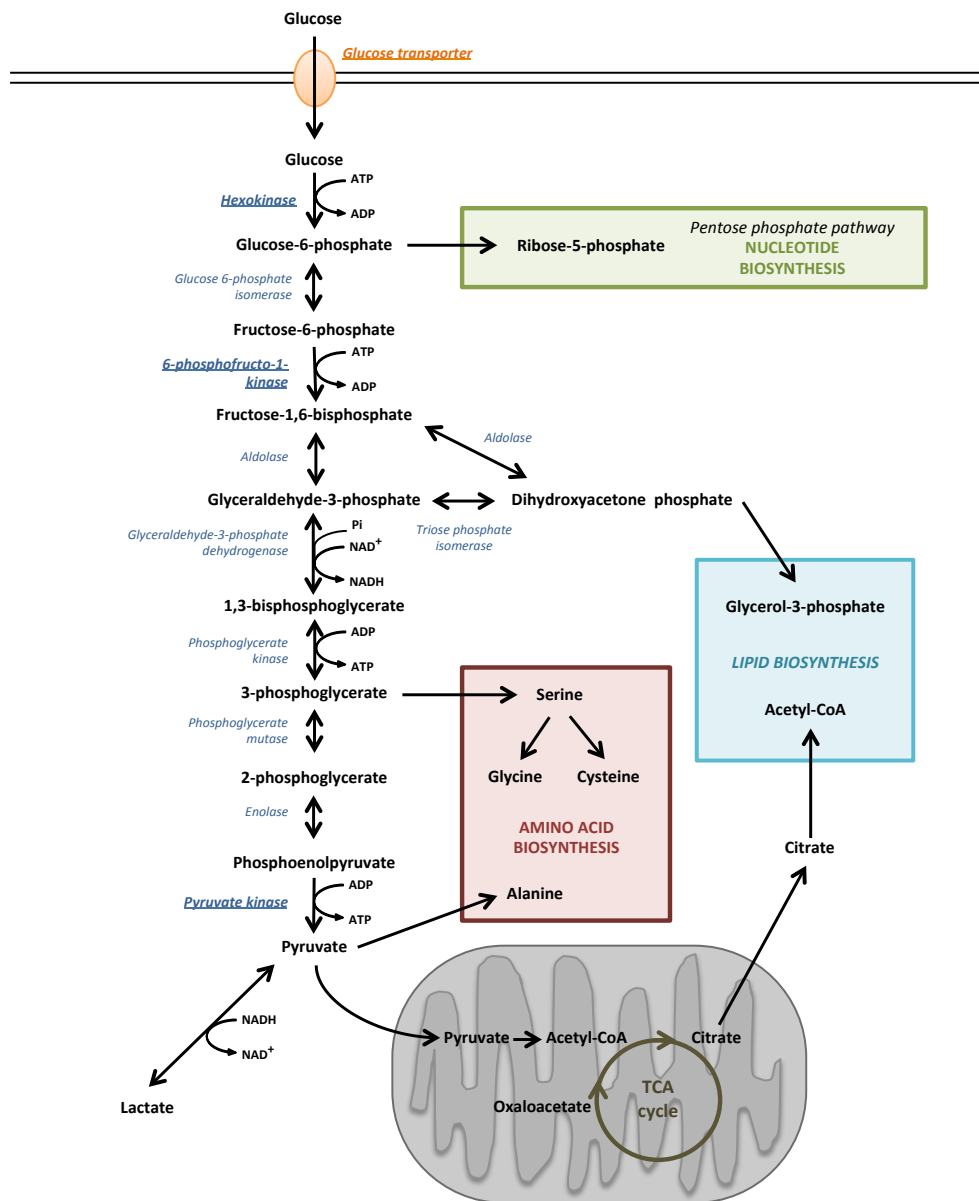


Figure 1. Glycolytic pathway and its contribution to the supply of biosynthetic precursors. Enzymes that control critical steps are underlined in bold.

1.2.1. Glucose transporters

Glucose transport across cell membranes is mediated by specific GLUTs, via ATP-independent, facilitative diffusion. GLUTs are encoded by different genes and belong to a family of thirteen transmembrane proteins called GLUT1-12 and H⁺/myoinositol co-transporter 1 (HMIT1) (Joost and Thorens, 2009). These diverse transporters display different specificities and affinities for sugars as well as different tissue distributions and physiological functions (Wood and Trayhurn, 2003). The main GLUTs, namely GLUT1, 2 and 4, will only be considered here.

GLUT1 is ubiquitously distributed. It is highly expressed in many foetal and adult tissues (such as brain, erythrocytes and endothelial cells), in most immortalized cell lines and in a variety of human malignant tumours (Brown and Wahl, 1993; Noguchi et al., 2000; Wang et al., 2000; Yamamoto et al., 1990). Overexpression of *GLUT1* gene seems to be one of the first effects of oncogenesis essential for tumour growth (Flier et al., 1987). GLUT2 is mainly expressed in liver, kidney cortex and small intestine. Its high K_M together with its high activity in liver favor either glucose uptake or release depending on the glucose gradient across the liver plasma membrane: uptake when the concentration of blood glucose rises as after a meal, or glucose production during glycogen breakdown and gluconeogenesis in the fasted state. GLUT4 has a high affinity for glucose and its activity depends on its concentration at the cell surface. It is present in insulin sensitive tissues (such as adipose tissue, heart and skeletal muscle), where this hormone promotes the rapid recruitment of GLUT4 from intracellular vesicles to the plasma membrane, thereby stimulating glucose entry and its subsequent phosphorylation.

1.2.2. Hexokinase

Phosphorylation of glucose to glucose-6-phosphate (Glu-6-P) by ATP is catalyzed by HK and glucokinase. This reaction maintains a glucose concentration gradient

that facilitates its entry into cells and the initiation of all major pathways of glucose utilization. Also, Glu-6-P is located at a metabolic crossroad in the cell. It is the starting point of glycolysis, the pentose phosphate pathway (PPP) and glycogen synthesis. Four hexokinase isoenzymes encoded by distinct genes are expressed in mammals, named HKI, HKII, HKIII and HKIV (also known as glucokinase). The four HK isoenzymes display differences in kinetic properties, regulation, intracellular distribution and tissue expression. HKI, HKII and HKIII have high affinity for glucose (50 – 100 μ M) and are inhibited by the reaction product Glu-6-P. However, HKIII is distinguishable from the other two high affinity HKs by inhibition via physiological concentrations of glucose (Wilson, 2003). By contrast with the other isoenzymes, HKIV, which is expressed in liver and pancreatic beta cells, presents a low affinity for glucose (5 -10 mM) and is not inhibited by Glu-6-P (Postic et al., 2001; Robey and Hay, 2006). HKI is constitutively expressed in most mammalian adult tissues. HKII is mainly expressed in muscles and adipose tissue (Wilson, 2003). Nevertheless cancer cells express high levels of HKII (Mathupala et al., 2001; Shinohara et al., 1994), unlike normal cells, which could explain increased glycolysis. HKIII is also widely expressed, but not in a predominant manner. Interestingly both HKI and HKII are associated with the mitochondrial membrane where they might preferentially utilize ATP provided by oxidative phosphorylation. Also, mitochondrial location of both HKI and HKII could play a role in cell survival (Gottlob et al., 2001; Majewski et al., 2004).

1.2.3. Phosphofructo-1-kinase

PFK-1 catalyzes the phosphorylation of Fru-6-P to Fru-1,6-BP using ATP and represents the first committed step of glycolysis (Marshall et al., 1978; Weber, 1977). In mammals, there are three PFK-1 genes, each encoding a different isoenzyme. PFK-M is mainly expressed in muscle, PFK-L is predominant in liver and PFK-P is expressed in brain, platelets and other tissues. PFK-1 exists as homo-

tetramers or as hetero-tetramers depending on cell type (Moreno-Sanchez et al., 2007). PFK-1 is a key multi-modulated enzyme controlling glycolysis. Indeed PFK-1 plays a central role in adjusting glycolytic flux to environmental conditions and cellular metabolic requirements. Its activity is controlled by its substrates and a variety of ligands. Allosteric inhibitors include ATP, citrate, long-chain fatty acids and protons (Jenkins et al., 2011; Van Schaftingen et al., 1981). Allosteric stimulators are Fru-6-P, AMP and notably fructose-2,6-bisphosphate (Fru-2,6-BP). PFK-1 activity is finely tuned to adapt glycolytic flux to cellular needs. By stimulating PFK-1, a rise in AMP helps to maintain the energy status of the cell, when ATP levels fall, as during hypoxia. In the most eukaryotes, Fru-2,6-BP is the most potent positive allosteric effector of all PFK-1 isoenzymes (see section I.3.). Interestingly Fru-2,6-BP can stimulate PFK-1 activity even in the presence of inhibitory concentrations of ATP. Indeed physiological concentrations of Fru-2,6-BP (1 - 10 μ M) are sufficient to relieve inhibition by ATP (Moreno-Sanchez et al., 2007; Okar and Lange, 1999; Van Schaftingen, 1987; Van Schaftingen et al., 1982; Wu et al., 2006). Thus Fru-2,6-BP allows the inhibitory effect of ATP to be bypassed and to enhance glycolysis even if energy supply is sufficient, suggesting that Fru-2,6-BP could increase PFK-1 flux when oxygen is available in cancer and normal proliferating cells.

1.2.4. Pyruvate kinase

PK catalyzes the transformation of phosphoenolpyruvate (PEP) and ADP to pyruvate and ATP. Four isoenzymes have been identified in mammals, termed PKM1, PKM2, PKR and PKL. Both PKM1 and PKM2 are produced from the *PKM2* gene on chromosome 15, while PKR and PKL are encoded by the *PKLR* gene located on chromosome 1 (Noguchi et al., 1986; Noguchi et al., 1987). PKL is the major isoenzyme in liver and minor in kidney. PKR is exclusively found in red blood cells. PKM1 is found in tissues with high energy demand, such as skeletal

muscle, heart and brain. PKM2 is the embryonic isoenzyme and is present in most cells, except adult muscle, brain and liver. PKM2 is preferentially expressed in both cancer and normal proliferating cells (Chaneton and Gottlieb, 2012; Imamura and Tanaka, 1972; Imamura et al., 1972; Mazurek, 2011; Netzker et al., 1992). However, lack of proliferation does not necessarily correspond to the absence of PKM2. PKM2 is also found in many differentiated tissues, including adipose tissue and lung (Eigenbrodt et al., 1983; Imamura and Tanaka, 1972).

PK isoenzymes are mostly active as homotetramers. Interestingly PKM2 and PKM1 exhibit distinct regulatory properties although their sequences only differ by 22 amino acids. Unlike PKM1, PKM2 is not a constitutive tetramer and is controlled by allosteric effectors and posttranslational modifications. In both normal and cancer proliferative cells, PKM2 undergoes a conformational switch between dimeric and tetrameric forms, corresponding to low and high PK activities respectively (Tamada et al., 2012). The expression of low-activity-dimeric PKM2 has been claimed to be necessary for the shift in cell metabolism to aerobic glycolysis (Warburg effect), which could provide a selective growth advantage for tumour cells *in vivo* (Christofk et al., 2008). In addition, the low activity of the PKM2 dimeric form could favour the routing of glycolytic intermediates through branch pathways, such as the pentose phosphate pathway (PPP), which generates NADPH to reduce levels of reactive oxygen species (ROS) (Tamada et al., 2012). Interestingly, PKM2 also has non-glycolytic functions in the nucleus. Nuclear PKM2 has been reported to activate gene transcription (Gao et al., 2012) and cell proliferation (Hoshino et al., 2007). Therefore, through both the glycolytic and non-glycolytic functions, PKM2 could contribute to growth and survival of cancer cells, suggesting that it may be a target for cancer therapy, as proposed (Iqbal et al., 2014).

I.3. Fructose-2,6-bisphosphate

Fru-2,6-BP is an osylphosphate, with a β anomeric configuration, found in all mammalian tissues studied so far, in plants, fungi and certain unicellular eukaryotes (such as yeasts and trypanosomes), but is absent from prokaryotes. Unlike Fru-1,6-BP, Fru-2,6-BP is acid-labile and its concentration ranges from 0.1 to 100 μM depending upon the tissue and the experimental conditions. The highest concentrations ($\geq 100 \mu\text{M}$) have been observed in proliferating cells (Hue and Rousseau, 1993), although concentrations needed to regulate the activities of its target enzymes, PFK-1 and fructose-1,6-bisphosphatase (FBPase-1), are at least 10-fold lower, between 1 and 10 μM (Hue and Rider, 1987; Van Schaftingen, 1987).

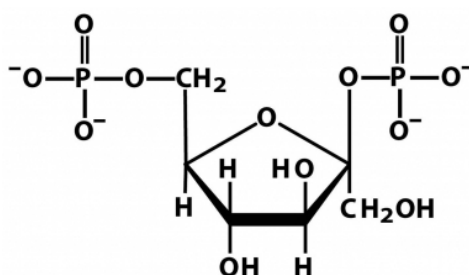


Figure 2. Structure of β -D-fructose-2,6-bisphosphate

I.3.1. Synthesis and degradation of Fru-2,6-BP

Fru-2,6-BP is synthesized from Fru-6-P and ATP by 6-phosphofructo-2-kinase (PFK-2) in a side reaction of glycolysis. Its concentration rises in response to increasing glucose concentrations via an increase in Fru-6-P and when PFK-2 activity is increased. The hydrolysis of Fru-2,6-BP to Fru-6-P is catalyzed by fructose-2,6-bisphosphatase (FBPase-2). Therefore, the steady state concentration of Fru-2,6-BP in the cell depends on the balance between its rates of synthesis and

degradation by PFK-2 and FBPase-2, respectively. These two enzyme activities are catalyzed at different sites of a bifunctional, homodimeric protein, called PFK-2/FBPase-2 (Okar et al., 2001; Rider et al., 2004). The kinase and phosphatase reactions are catalyzed in the N-terminal and C-terminal halves of each enzyme subunit respectively, which are flanked by regulatory domains at each extremity. Unlike PFK-1, PFK-2 is not inhibited by ATP. Interestingly, Pi stimulates both PFK-2 and FBPase-2 activities. Citrate, sn-glycerol-3-phosphate and PEP inhibit PFK-2 activity. FBPase-2 activity is stimulated by GTP and sn-glycerol-3-

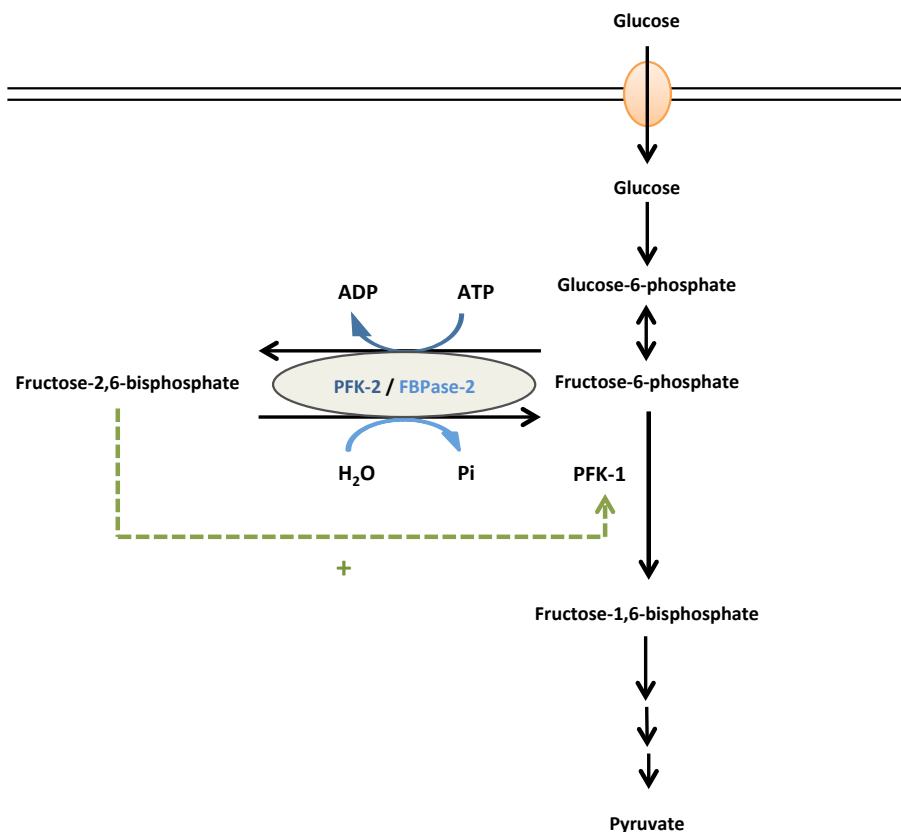


Figure 3. The synthesis and degradation of Fru-2,6-BP are catalyzed by a bifunctional homodimeric enzyme, named PFK-2/FBPase-2. Fru-2,6-BP is the most potent positive allosteric effector of PFK-1.

phosphate, which antagonize product inhibition of the enzyme by Fru-6-P (Ros and Schulze, 2013).

1.3.2. Structure of PFK-2/FBPase-2

The PFK-2 domain was proposed to be related to bacterial PFK-1 (Bazan et al., 1989), but later PFK-2 was shown to share sequence similarities with nucleotide-binding proteins, such as adenylate kinase (AK) (Bertrand et al., 1997). The FBPase-2 domain shares sequence, mechanistic and structural similarity with the histidine phosphatase family of enzymes, including the acid phosphatases and phosphoglycerate mutase (Okar et al., 2001; Pilkis et al., 1995). Unlike AK, PFK-2 functions as a homodimer and the PFK-2 domains come together in a head-to-head fashion whereas the FBPase-2 domains are almost independent, with only one connecting salt bridge (Hasemann et al., 1996).

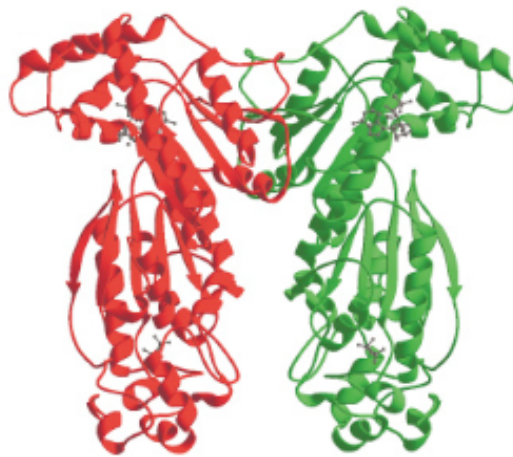


Figure 4. Crystal structure of the homodimeric bifunctional enzyme PFK-2/FBPase-2. The protein monomers are colored red and green, and the ATP γ S and PO $_4$ ligands are in grey. The rotation axis is vertical as shown here, with a 180° rotation relating the red and green monomers. It is clear that the FBPase-2 domains (the lower domains) are independent of one another. Only a single salt bridge interconnects the two domains (Hasemann et al., 1996).

The PFK-2 domain is composed of a six-stranded β -sheet surrounded by seven α -helices and its sequence contains two regions called “Walker A” and “Walker B” motifs for nucleotide-binding that are found in AK and Ras (Hasemann et al., 1996). An essential residue for catalysis was identified as Lys54, located within the Walker A motif (Vertommen et al., 1996). This residue interacts with both the β - and γ -phosphates of ATP and stabilizes the transition state of the PFK-2 reaction during phosphate transfer. Thr55 of the Walker A motif (Vertommen et al., 1996) and Asp130 in the Walker B (Rider et al., 1994) motif provide two ligands for the octahedral Mg^{2+} ion, another two being provided by the β - and γ -phosphates of ATP (Hasemann et al., 1996). ATP is also bound by stacking of the adenine ring against non-polar side chains. The binding site for Fru-6-P is predicted to correspond to the AMP site in AK, with the 6-phosphate group of Fru-6-P bound by Arg104, Arg138 and Arg195 (Bertrand et al., 1998). By analogy with AK, the PFK-2 domain is also predicted to contain two mobile segments that trap Fru-6-P and ATP (Hasemann et al., 1996), thus excluding water to protect against ATP hydrolysis.

1.3.3. Gene expression and post-translational regulation of PFK-2/FBPase-2 isoenzymes

In mammals, four PFK-2/FBPase-2 isoenzymes were originally identified in liver/muscle, heart, brain/placenta and testis, respectively. The PFK-2/FBPase-2 isoenzymes were subsequently found to be encoded by four different genes located on different chromosomes and the PFK-2/FBPase-2 isoenzymes were accordingly termed PFKFB1, 2, 3 and 4. The corresponding genes are: *PFKFB1* (also called gene A, on human chromosome 1) (Darville et al., 1989), *PFKFB2* (gene B, on human chromosome 10) (Darville et al., 1991), *PFKFB3* (on human chromosome 10) (Navarro-Sabate et al., 2001) and *PFKFB4* (on human chromosome 3) (Manzano et al., 1999). These genes all share a similar genomic organization,

revealing how each generates several isoforms by alternative splicing, and for even more mRNAs due to the presence of several promoters and 5' non-coding exons.

Despite the high sequence homology within their core catalytic domains, the four PFKFB isoenzymes display different PFK-2:FBPase-2 activity ratios (Okar et al., 2001). When assayed under optimal condition with saturating substrate concentrations, the PFK-2:FBPase-2 activity ratios of PFKFB1, PFKFB2 and PFKFB4 are ≈ 1 . By contrast, PFKFB3 is unusual in that its PFK-2:FBPase-2 activity ratio is much higher and strongly favors Fru-2,6-BP synthesis, such that PFKFB3 expression would be expected to result in enhanced glycolytic flux. The low FBPase-2 activity of PFKFB3 is due to the presence of Ser at position 302 instead of Arg required for Fru-2,6-BP binding and conserved in the other PFKFB isoenzymes (Cavalier et al., 2012; Kim et al., 2006b). Interestingly, several PFKFB isoenzymes can be co-expressed in a given tissue, sometimes with an isoform predominating, suggesting that different isoforms play different roles in regulating Fru-2,6-BP content in response to different physiological conditions or stimuli.

| Gene name | Chromosomal location | mRNA | Protein isoform | PFK-2/FBPase-2 activity ratio |
|---------------|----------------------|----------------|--|-------------------------------|
| <i>PFKFB1</i> | Human Xp11.21 | L M F | L-PFK-2/FBPase-2 (liver) M-PFK-2/FBPase-2 (muscle) M-PFK-2/FBPase-2 (foetal) | 1.2 (bovine liver) |
| <i>PFKFB2</i> | Human 1q31 | H1/H2/H4 H3 | H-PFK-2/FBPase-2 (heart) long 58 kDa H-PFK-2/FBPase-2 (heart) short 54 kDa | 1.8 (bovine heart) |
| <i>PFKFB3</i> | Human 10p14-p15 | U I | u-PFK-2/FBPase-2 (placental, brain, ubiquitous) i-PFK-2/FBPase-2 (inducible) | > 700 (human placenta) |
| <i>PFKFB4</i> | Human 3p21-p22 | T | T-PFK-2/FBPase-2 (testis) | 0.9 (human testis) |

Figure 5. PFKFB isoenzymes – chromosomal location, tissue distribution and PFK-2:FBPase-2 activity ratio. Properties of the PFK-2/FBPase-2 enzymes. Information on chromosomal location and relative enzyme activities of the different isoforms has been taken from Okar et al. (2001).

The PFKFB isoenzymes can be regulated by post-translational modifications. In response to hormones, growth factors or cellular stress, PFK-2 activity can be modulated by phosphorylation by protein kinases, such as cyclic AMP-dependent protein kinase (PKA), protein kinase B (PKB, also known as Akt) and AMP-activated protein kinase (AMPK).

1.3.3.1. PFKFB1

PFKFB1 gene

This gene (60kb) contains 17 exons and encodes three different mRNAs (L, M and F, respectively) from distinct promoters (named L, M and F from 3' to 5'). These mRNAs differ only within their first exon (Darville et al., 1992; Dupriez et al., 1993). An additional 5' coding exon (exon_{1L}), coding for 32 amino acids, is present in the L mRNA and gives rise to a protein with a Ser residue at position 32 which can be phosphorylated by PKA (discussed in detail below). This isoform is mainly expressed in liver, but was also detected in skeletal muscle and white adipose tissue (Bruni et al., 1999). The M mRNA contains exon_{1M} coding only nine amino acids, none of which provides a substrate for phosphorylation. From the M promoter, the M isoform is expressed in skeletal muscle and white adipose tissue. The two F mRNAs, which contain two non-coding exons upstream (1_{Fa} and 1_{Fb}) and part of exon_{1M}, also code for the M isoform. This isoform is also generated from promoter F and expressed in fibroblasts, fetal tissues and proliferating cells.

PFKFB1 isoenzyme

The liver isoform PFKFB1 (L-PFK-2/FBPase-2) contains, within its N-terminal regulatory domain, Ser32 phosphorylated by PKA (Pilkis et al., 1995).

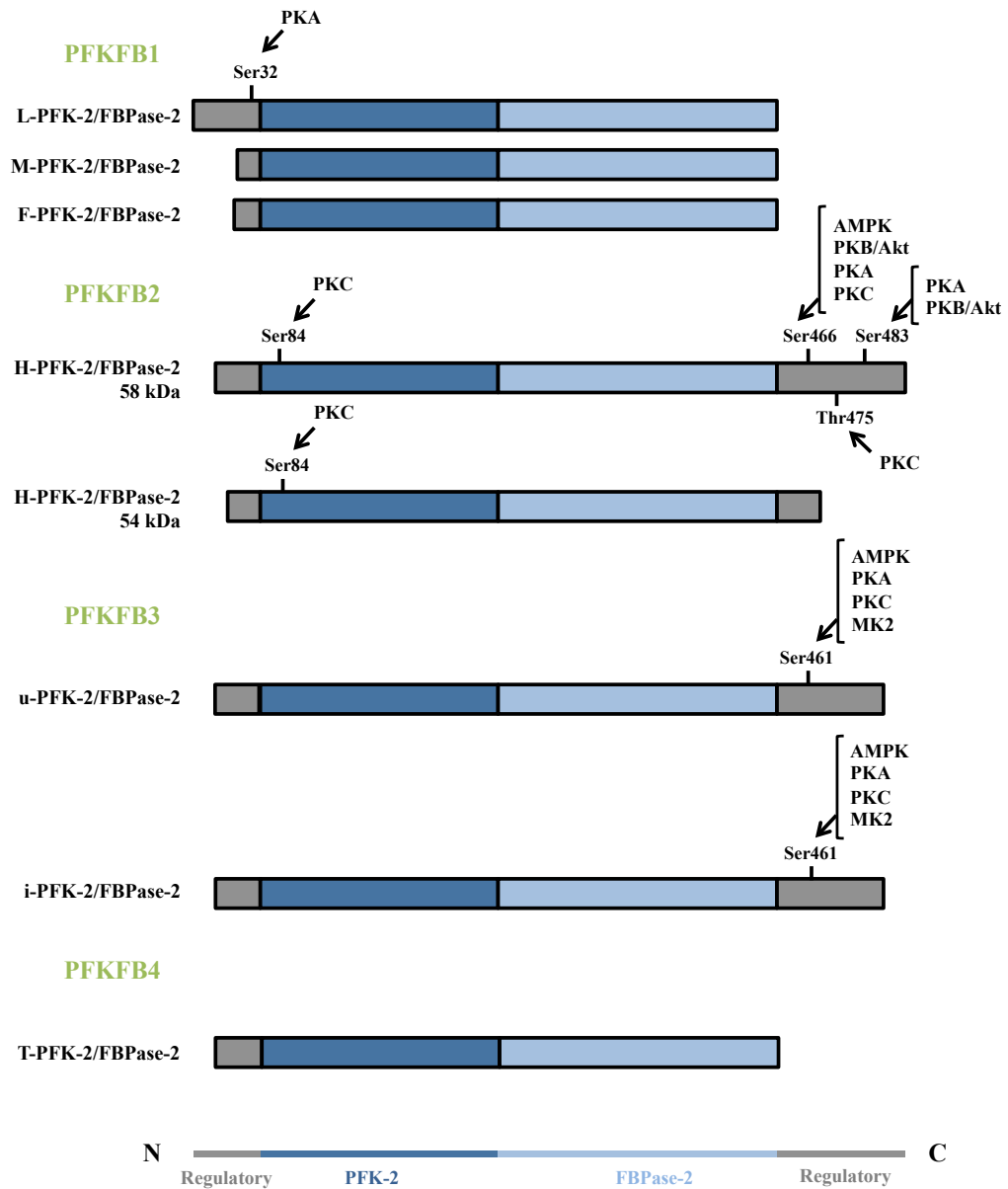


Figure 6. Domain organizations and phosphorylation of PFKFB isoenzymes. The N-terminal PFK-2 domain is shown in dark blue, the C-terminal FBPase-2 domain is shown in light blue and the regulatory domains are shown in grey. Phosphorylation sites and the kinases capable of phosphorylation are indicated for each of the main isoforms. The domain structure of human PFK-2/FBPase-2 isoenzymes is based on Rider et al. (2004) and Ros and Schulze (2013)

Thus, in response to glucagon, PKA is activated and phosphorylates Ser32 of L-PFK-2/FBPase-2, leading to PFK-2 inactivation and FBPase-2 activation. The subsequent fall in Fru-2,6-BP content decreases glycolytic flux while increasing gluconeogenesis in hepatocytes (Bartrons et al., 1983). In intact hepatocytes, by contrast with incubation with glucagon, treatment with vasopressin, phorbol ester or calcium ionophore did not increase phosphorylation of L-PFK-2/FBPase-2 (Garrison et al., 1984). Insulin stimulates glycolysis in white adipose tissue and skeletal muscle. However, several studies have shown that increased glycolysis is mainly due to the well-known stimulation of glucose transport (Pessin et al., 1999) and PFK-2 activity in adipose tissue and muscle is unaffected by insulin.

1.3.3.2. PFKFB2

PFKFB2 gene

This gene encodes the heart isoenzyme and its two isoforms. The rat gene (22 kb) contains 20 exons (Chikri and Rousseau, 1995). Exons 3 to 14 are very similar to those of the *PFKFB1* gene that code for the core catalytic domain. Several phosphorylation sites for protein kinases are found within exon 15. In bovine heart, alternative splicing via deletion of exon 15 leads to the short isoform (54 kDa, instead of 58 kDa) (Tsuchiya and Uyeda, 1994; Vidal et al., 1993). Four different mRNAs are derived from distinct promoters and differ only by non-coding sequences at the 5' end (Chikri and Rousseau, 1995; Heine-Suner et al., 1998). However, it is unknown how these different 5' ends are related to the three mRNAs (H1, H2 and H4) that give rise to the 58 kDa isoform and the mRNA (H3) that encodes the short isoform. Also, none of these mRNAs are strictly heart-specific and for example, an alternatively spliced product of gene B was detected in kidney (Rider et al., 2004).

PFKFB2 isoenzyme

PFKFB2 protein contains several phosphorylation sites that control PFK-2 activity. Unlike the liver isoenzyme, phosphorylation of heart PFK-2/FBPase-2 leads to increased PFK-2 activity.

Insulin stimulates glycolysis in the heart by a combination of an increase in glucose transport and PFK-2 activation (Depré et al., 1998; Hue et al., 2002). Rat heart PFK-2 is activated by insulin *in vivo* through a 2-fold increase in V_{MAX} with no change in K_M for Fru-6-P (Rider and Hue, 1984). Heart PFK-2 was shown to be phosphorylated and activated *in vitro* by PKB in response to insulin and the phosphorylation sites were identified as Ser466 and Ser483 within the C-terminal regulatory domain (Deprez et al., 1997). Moreover, insulin-induced heart PFK-2 activation was demonstrated to involve phosphatidylinositol-3-kinase (PI3K), but not p70 ribosomal protein S6 kinase-1 (S6K1, also referred to as p70S6K) (Lefebvre et al., 1996). *In vitro* and *in vivo* experiments also indicated that the serum- and glucocorticoid-inducible protein kinase-3 (SGK3) was not required for insulin-induced heart PFK-2 activation and this effect is likely mediated by PKB α (Mouton et al., 2010). Interestingly, it was found that 14-3-3 proteins bind to phosphorylated Ser483 in response to insulin or in cells stimulated with insulin-like growth factor 1 (IGF-1) or transfected with active forms of PKB, leading to the stimulation of glycolysis by growth factors (Pozuelo Rubio et al., 2003).

Adrenaline, a positive inotropic hormone, also activates heart PFK-2 presumably involving Ser466 and Ser483 phosphorylation via PKA. Phosphorylation of heart PFK-2/FBPase-2 by PKA increased the V_{MAX} of PFK-2 and decreased the K_M for Fru-6-P which would be expected to stimulate glycolysis in heart (Kitamura et al., 1988; Rider et al., 1992).

Glycolysis in heart is also stimulated in response to increased workload, involving increased Fru-2,6-BP content and heart PFK-2 activation (Beauloye et al., 2002; Depré et al., 1993). Ca²⁺/calmodulin-dependent protein kinase (Ca/CAMK) phosphorylates and activates heart PFK-2 *in vitro* (Depré et al., 1993).

Also, increased workload activated PKB in heart, without affecting S6K1 (Beauloye et al., 2002) and PFK-2 activation was blocked by wortmannin, but was rapamycin-insensitive.

Activation of AMPK occurs during ischemia or hypoxia in heart and leads to increased PFK-2 activation along with increased Fru-2,6-BP content and glycolysis. AMPK was found to phosphorylate heart PFK-2/FBPase-2 at Ser466 *in vitro*, resulting in an increase in V_{MAX} of PFK-2 with no change in K_M for Fru-6-P (Marsin et al., 2000). AMPK activation could also stimulate glycolysis by increasing GLUT4 translocation (Russell et al., 1999).

Heart PFK-2 is also a substrate of protein kinase C (PKC), which phosphorylates Ser84, Ser466 and Thr475. However, the physiological significance of PKC-induced phosphorylation of these residues is unclear. It seems that phosphorylation of Ser466 and Thr475 does not lead to a change in PFK-2 activity. This might be due to phosphorylation of Ser84 in the PFK-2 domain which could counteract the effects of phosphorylation at the activating C-terminal sites (Kitamura et al., 1988; Rider et al., 1992).

Interestingly, the C-terminal phosphorylation sites are absent from the short heart isoform (54 kDa) indicating that this isoform might have an overall reduced PFK-2 activity and would be insensitive to cellular signaling events.

1.3.3.3. PFKFB3

PFKFB3 gene

This gene codes for an isoenzyme originally cloned from bovine brain (Ventura et al., 1995) and human placenta (Sakai et al., 1996). It contains 19 exons spanning a genomic region of about 90 kb. Alternative splicing of exon 15 generates two main isoforms that vary in a short C-terminal sequence (Navarro-Sabate et al., 2001). These are the ubiquitous/constitutive PFK-2/FBPase-2 (u-PFK-2/FBPase-2, 15 exons) (Hamilton et al., 1997) and inducible PFK-2/FBPase-2 (i-PFK-2/FBPase-2,

16 exons) (Chesney et al., 1999) isoforms. The i-PFK-2/FBPase-2 isoform is weakly expressed in adult tissues, but highly expressed in tumour cell lines and increased by pro-inflammatory and stress stimuli. Additional splice variants of this gene have been reported, six in rat brain (Watanabe and Furuya, 1999) and four in human brain (Kessler and Eschrich, 2001).

PFKFB3 isoenzyme

AMPK phosphorylates both the u-PFK-2/FBPase-2 and i-PFK-2/FBPase-2 isoforms at Ser461 within their C-terminal regulatory domain, which increases PFK-2 activity and stimulates glycolysis (Marsin et al., 2002). This phosphorylation site is equivalent to Ser466 present in the 58 kDa heart isoform (see above). Ser461 of human placental PFK-2/FBPase-2 can also be phosphorylated by PKC and PKA which would render the PFKFB3 isoenzyme responsive to multiple external signals (Okamura and Sakakibara, 1998). Moreover, it was demonstrated that the p38/MK2 pathway and RSK are implicated in PFK-2 activation by phosphorylating Ser461 (Novellademunt et al., 2013; Novellademunt et al., 2012) and *in vitro* phosphorylation of PFKFB3 resulted in an increase in V_{MAX} of PFK-2 activity as well as a decrease in K_M for Fru-6-P. The major PFKFB isoform expressed in astrocytes is i-PFK2/FBPase-2 (Almeida et al., 2004). In these cells, but not in neurons where i-PFK-2/FBPase-2 is undetectable, nitric oxide (NO) activates glycolysis and increases Fru-2,6-BP content. This effect is due to mitochondrial respiratory chain inhibition at cytochrome oxidase by NO, leading to a rise in AMP, AMPK activation and PFK-2 activation (Almeida et al., 2004). As the C-terminal region of PFKFB3 is subject to alternative splicing, the structural organization around this site may differ between various splice variants. Interestingly, PFKFB3 is also regulated by modulation of its stability. PFKFB3 contains a KEN box motif that is not present in other PFKFB isoenzymes. The KEN box is a target for anaphase-promoting complex/cyclosome (APC/C)-Cdh1, an E3 ubiquitin ligase complex controlling G1- to S-phase transition via

degradation of several cell cycle proteins. ACP/C-Cdh1 promotes PFKFB3 degradation, while a decrease in ubiquitin ligase activity resulted in PFKFB3 accumulation and enhanced glycolysis (Almeida et al., 2010). Thus, regulation of PFKFB3 during the cell cycle suggests that Fru-2,6-BP might play a role in proliferation (see section I.4.1.).

I.3.3.4. PFKFB4

PFKFB4 gene

This gene (44 kb) contains at least 14 exons and codes for an isoenzyme originally identified in testis (Sakata et al., 1991). Several splice variants of the *PFKFB4* mRNA have been reported not only in testis but also in various rat tissues (Minchenko et al., 1999a). Among these splice variants, some transcripts carry deletions or inserts within the FBPase-2 region or differ in length and amino acid sequence of the C-terminal region. However, the PFK-2 catalytic domain is conserved in all. This might implicate different *PFKFB4* splice variants in cell-specific and/or tissue-specific regulation of glycolysis.

PFKFB4 isoenzyme

Up to now, no post-translational modifications have been reported for PFKFB4. However, as for the other PFKFB isoenzymes, PFK-2 and FBPase-2 activities of PFKFB4 would nevertheless be modulated in response to changes in the concentrations of substrates and effectors.

I.3.4. Roles of Fru-2,6-BP

Fru-2,6-BP was discovered more than three decades ago during studies on the effects of glucagon on hepatic gluconeogenesis. Fru-2,6-BP acts both as an inhibitor of FBPase-1, a regulatory enzyme of gluconeogenesis, and as a potent

positive allosteric effector of PFK-1. Therefore Fru-2,6-BP controls liver glucose homeostasis by allowing a switch between the opposing pathways of glycolysis and gluconeogenesis. In the liver, three states can be defined and distinguished by different glycolytic and gluconeogenic fluxes. Firstly, during starvation or after glucagon treatment (i), gluconeogenesis is active while glycolysis is inhibited. Fru-2,6-BP content is low (below 1 μM) (Hers and Hue, 1983) due to PKA-induced PFK-2 inactivation and FBPase-2 activation (see section I.3.3.1.). Glycolytic flux is also blocked via the PKA-induced phosphorylation and inactivation of PK. It is noteworthy that a decrease in Fru-2,6-BP concentrations is also observed during liver regeneration and in hepatocytes incubated with ethanol, adenosine or fatty acids (Hue and Rider, 1987; Rosa et al., 1990). Under these conditions, changes in concentrations of cAMP and regulators of PFK-2/FBPase-2, such as sn-glycerol-3-phosphate and citrate, occur. Conversely, after a carbohydrate-rich meal (ii), Fru-2,6-BP levels increase to stimulate glycolysis. Part of the glucose taken up is stored as glycogen, while the rest is metabolized into lactate and fatty acids. The third state corresponds to the stimulation of glycolysis during anoxia (iii) (Pasteur effect). Although this extreme situation probably never occurs in liver under physiological conditions, it can be induced in hepatocytes incubated *in vitro* without oxygen (Hue, 1982). By contrast, in ischemic hearts, Fru-2,6-BP plays a role in the stimulation of glycolysis. Under these conditions, increased glycolysis is due to an increase in Fru-2,6-BP as well as changes in adenine nucleotides. A fall in ATP is translated into a substantial rise in AMP by the equilibrium AK reaction. This not only increases glycolysis by allosterically stimulating PFK-1, but also activates AMPK, which in turn phosphorylates and activates the heart PFK-2/FBPase-2 isoenzyme (see section I.3.3.2.). In the heart, a rise in Fru-2,6-BP is also involved in the stimulation of glycolysis by insulin. This is due to heart PFK-2/FBPase-2 activation by PKB (see section I.3.3.2), the protein kinase that mediates many of the metabolic effects of insulin. The different glycolytic

responses of liver and heart partly reside in the different PFK-2/FBPase-2 isoenzymes expressed in these tissues (see section I.3.3.).

It is noteworthy that Fru-2,6-BP controls the activity of pyrophosphate-dependent 6-phosphofructo-1-kinase (PPi:PFK) found in plants and euglenoids (Miyatake et al., 1986; Sabularse and Anderson, 1981). Interestingly the glycolytic target of Fru-2,6-BP in trypanosomes is PK rather than PFK-1 (Van Schaftingen et al., 1985).

In rapidly-dividing cells, Fru-2,6-BP seems to be essential for maintaining elevated aerobic glycolysis (Warburg effect). Indeed, several studies showed that Fru-2,6-BP levels are much higher in cancer cell lines than in normal cells. Moreover, treatment of chick embryo fibroblasts with growth factors or mitogens (Bosca et al., 1985) leads to both increased glycolysis and Fru-2,6-BP content, which can partly be explained by differences in expression of PFK-2/FBPase-2 isoenzymes (see section I.3.3.).

In summary, although Fru-2,6-BP can not be considered as the universal and ubiquitous regulator of glycolysis under all conditions, it acts as an intracellular messenger controlling PFK-1, a key glycolytic enzyme. It does not belong to a particular anabolic or catabolic pathway, but represents a final product crucial as a metabolic signal. Although Fru-2,6-BP was discovered more than 30 years ago, no targets outside glycolysis/gluconeogenesis have ever been described.

I.4. Glycolysis in cancer and rapidly-proliferating cells

Rapidly-dividing cells use glucose as the main source of energy to proliferate. Proliferating cells need to increase glucose metabolism not only to rapidly generate ATP but also to supply adequate levels of intermediates for macromolecular synthesis. Glucose can indeed provide precursors for amino acid, lipid and nucleotide biosynthesis. Some 90 years ago, Otto Warburg discovered that cancer cells display increased glycolysis even in the presence of oxygen (Warburg et al., 1924). Despite the fact that aerobic respiration produces more ATP, cancer cells

convert most of their glucose to lactate under aerobic conditions, a phenomenon known as the “Warburg effect”. This characteristic feature is not restricted to cancer cells. Indeed, increased glucose uptake and lactate production have been observed in proliferating non-cancer cells (Brand, 1985; Hedeskov, 1968; Hume et al., 1978; Munyon and Merchant, 1959; Wang et al., 1976). Warburg suggested that mitochondria were defective in cancer cells, however in many cancer and proliferating cells mitochondrial function is normal (Fantin and Leder, 2006; Moreno-Sanchez et al., 2007; Zu and Guppy, 2004). Thus most proliferating cells do not have a defect in mitochondrial oxidative phosphorylation.

1.4.1. PFKFB isoenzymes in cancer and normal proliferating cells

As already mentioned, the concentration of Fru-2,6-BP is hugely increased in several transformed cell lines, and several oncogenes and growth factors increase Fru-2,6-BP synthesis. Therefore, the potential roles of the different PFKFB isoenzymes in cancer and normal rapidly-dividing cell metabolism have been studied. All PFKFB mRNAs have been reported to be overexpressed in human lung cancers compared with corresponding normal tissues (Minchenko et al., 1999b).

- ***PFKFB1***. Compared with the three other isoenzymes, to date there is little evidence concerning the possible involvement of PFKFB1 in cancer.

- ***PFKFB2***. This isoenzyme is upregulated in prostate cancer cells, as a consequence of transcriptional changes induced by the androgen receptor (AR), with probable control through the AR-CAMKII-AMPK signaling pathway (Massie et al., 2011). Using a synthetic androgen (methyltrienolone, also called R1881), PFKFB2 expression was induced in LNCaP prostate cancer cells by direct recruitment of the ligand-activated AR to the *PFKFB2* promoter (Moon et al.,

2011). PFKFB2 silencing or inhibition of PFK-2 activity lead to decreased glucose uptake and lipogenesis, suggesting that the induction of *de novo* lipid synthesis by androgen requires the transcriptional upregulation of PFKFB2 in prostate cancer cells (Moon et al., 2011). In hepatocellular carcinoma, high expression of MACC1 (metastasis associated in colon cancer 1), which is a key regulator of the hepatocyte growth factor (HGF)-HGF receptor (also named MET) pathway, correlated with elevated PFKFB2 expression (Ji et al., 2014).

• **PFKFB3.** Due to its high PFK-2:FBPase-2 ratio, PFKFB3 seems to contribute most to Fru-2,6-BP levels and glycolysis in transformed and proliferating cells. Early studies reported that PFKFB isolated from hepatoma cells, in which Fru-2,6-BP had been induced by the oncogene *src*, was unusual in that it displayed no FBPase-2 activity (Hue and Rousseau, 1993). Although several PFKFB isoenzymes are co-expressed in these cells, the absence of FBPase-2 activity supports the notion that PFKFB3 is predominantly expressed. The i-PFK-2/FBPase-2 isoform is often strongly expressed in cancer cells as well as in rapidly-dividing normal cells, which have high rates of glycolysis even in the presence of oxygen (Warburg effect). In cancer cell lines from various tissues, such as gastric and pancreatic cancer, PFKFB3 mRNA and protein product are markedly induced by hypoxia through a hypoxia-inducible factor 1 α (HIF-1 α)-dependent mechanism (Bobarykina et al., 2006). PFKFB3 has also been identified as a progesterone responding gene in breast cancer. Indeed, treatment of breast cancer cell lines with synthetic progestins lead to PFKFB3 induction, resulting in a rapid increase in Fru-2,6-BP content (Hamilton et al., 1997). Other cancer types, including colon, prostatic and ovarian cancer, express high levels of PFKFB3 relative to non-malignant adjacent tissue (Atsumi et al., 2002).

On the other hand, PFKFB3 silencing in HeLa cells (cervical cancer cells) decreased Fru-2,6-BP synthesis and glycolytic flux, leading to reduced cell viability and anchorage-independent growth (Calvo et al., 2006). Compared to

wild-type mice, oncogenic *H-ras*^{V12} did not promote anchorage-independent growth of lung fibroblasts derived from *PFKFB3*^{+/-} mice. It was also shown that the heterozygotic genomic deletion of PFKFB3 induced a reduction in Fru-2,6-BP levels, leading to decreased glucose uptake and lactate production, suggesting that PFKFB3 could be a selective target for the development of antineoplastic agents (Telang et al., 2006). Furthermore, PFKFB3 is highly phosphorylated at Ser461, the phosphorylation site for protein kinases downstream of growth factor signaling (see section I.3.3.3.), in colon and breast carcinoma compared to epithelial cells from normal tissue, suggesting enhanced PFK-2 activity of PFKFB3 in cancer (Bando et al., 2005). PFKFB3 is the only PFKFB isoenzyme found in the nucleus (Yalcin et al., 2009). Due to its nuclear localization, the expression and activity of cyclin-dependent kinase-1 was proposed to be increased by Fru-2,6-BP, thus inducing cell proliferation.

• ***PFKFB4***. This isoenzyme is highly expressed in several malignant tumors compared with non-malignant tissue. PFKFB4 mRNA and protein expression are also induced under hypoxia in several cancer cell lines (Bobarykina et al., 2006; Minchenko et al., 2005). Interestingly, PFKFB4 has been shown to play an important role in the survival of glioma stem-like cells (Goidts et al., 2012). PFKFB4 knockdown caused decreased ATP production and lactate release, and ultimately induced apoptosis in these cells. PFKFB4 expression was also increased in brain cancer stem-like cells relative to adult normal brain tissue, whereas PFKFB3 mRNA was downregulated. These observations therefore suggest PFKFB4 is the main PFKFB isoenzyme controlling glycolysis in malignant glioma cells. It was also reported that PFKFB4 silencing was detrimental for the survival of prostate cancer cell (Ros et al., 2012). Surprisingly, PFKFB4 depletion resulted in increased Fru-2,6-BP content in prostate cancer cells. This led to the conclusion that, in response to PFKFB4 silencing, metabolic intermediates are redirected into glycolysis and away from the oxidative arm of the PPP, resulting in a fall in

NAPDH production. As NAPDH is necessary for *de novo* synthesis of fatty acids and the maintenance of antioxidant glutathione (GSH), the level of ROS would increase to reduce cell viability. Although the role of PFKFB4 in cancer metabolism requires further investigation, this isoenzyme could be a possible target for cancer therapy.

1.4.2. PFKFB3 inhibitors

A small molecule inhibitor of PFK-2, called 3-(3-pyridinyl)-1-(4-pyridinyl)-2-propen-1-one (3PO) (Clem et al., 2008), interferes with Fru-6-P binding to the PFK-2 domain. 3PO (i) reduces Fru-2,6-BP content and suppresses glycolytic flux in transformed cells (IC₅₀ 1.4 - 24 µM); (ii) is selectively cytostatic towards *ras*-transformed human bronchial epithelial cells with negligible effects on normal human bronchial epithelial cells; (iii) decreases Fru-2,6-BP synthesis and ¹⁸F-2-DG uptake by tumors *in situ*; (iv) suppresses tumorigenic growth of leukemia cells as well as breast and lung adenocarcinoma cells *in vivo*. However, due to strong conservation of the Fru-6-P binding site in the PFK-2 domain of all four PFKFB isoenzymes, 3PO might not be selective for PFKFB3, as proposed (Ros and Schulze, 2013).

Other PFKFB3 inhibitors have been developed using a structure-based approach (Seo et al., 2011). As for 3PO, these compounds bind to the Fru-6-P pocket of PFKFB3 and inhibit Fru-2,6-BP synthesis, leading to reduced glycolysis and eventual necrosis of cultured cancer cells.

1.5. TIGAR

The p53-induced protein TIGAR (TP53 (tumour protein 53)-Induced Glycolysis and Apoptosis Regulator), also called *C12orf5* (Chromosome 12 open reading Frame 5), has been reported to inhibit glycolysis and redirect glucose carbon

towards the PPP, thereby providing antioxidant protection through increased NADPH levels (Bensaad and Vousden, 2007). TIGAR shares structural and functional similarities with the FBPase-2 domain of PFKFB isoenzymes (Bensaad et al., 2006). However, a recent study reported that TIGAR has an active site similar to that of phosphoglycerate mutase, an enzyme hydrolyzing 2,3-bisphosphoglycerate (2,3-BPG), and that its activity towards Fru-2,6-BP was almost negligible (Gerin et al., 2014). Moreover, it was recently demonstrated that there is a crosstalk between PFKFB3 and TIGAR mediated by PKB/Akt (Simon-Molas et al., 2016). Indeed, following PFKFB3 inhibition, cells undergo oxidative stress which led to PKB/Akt activation via Ser473 phosphorylation. This resulted in induction of TIGAR to redirect glycolytic intermediates into other signaling pathways for the synthesis of biomolecules, also maintaining ROS homeostasis to reduce cell death. How these effects are mediated by changes in 2,3-BPG levels is a mystery. However, inhibition of both PFKFB3 and TIGAR could represent a more efficient strategy for impairing tumour growth, rather than targeting PFKFB3 alone.

II. Thymocytes as a non-cancer proliferating cell model

II.1. Mitogenic stimulation

II.1.1. Concanavalin A: a mitogenic plant lectin

Several plant lectins bind to sugar residues on receptors at the cell surface. The first to be studied was phytohemagglutinin (PHA) extracted from the bean (*Phaseolus vulgaris*), which binds *N*-acetyl D-galactosamine or galactose penultimate to *N*-acetylneuraminic acid (Nowell, 1960). Concanavalin A (ConA) is a lectin extracted from the jack bean (*Canavalia ensiformis*). ConA exists as a homotetramer

(subunit mass 27 kDa) with one saccharide-binding site per monomer, which specifically binds α -D-mannopyranosyl, α - and β -D-glucopyranosyl and β -D-fructofuranosyl groups present on cell surface (Dutton, 1972). ConA exerts a powerful mitogenic activity and was first used as an activator of suppressor cells in mouse mixed lymphocyte reactions (Rich and Rich, 1975). Activation of resting thymocytes by ConA leads to both interleukin-2 (IL-2) secretion and IL-2 receptor (IL-2R) expression through a complex signaling cascade (see section II.1.2.2.).

II.1.2. Interleukin-2

IL-2 is a 15.5-kDa glycoprotein cytokine discovered in 1976 as a T-cell growth factor in activated T cells (Morgan et al., 1976). IL-2 was the first type I cytokine to be cloned (Taniguchi et al., 1983) as well as the first cytokine for which a receptor was cloned (Leonard et al., 1984; Nikaido et al., 1984). IL-2 mediates its effects via a cell surface binding site with all of the characteristics of classical hormone receptors, including high affinity, stereospecificity and saturability (Robb et al., 1981).

II.1.2.1. Interleukin-2 receptors

IL-2 binds to specific cell surface IL-2R (Robb, 1984; Robb et al., 1984). Three independent genes encode three IL-2R polypeptide chains (Kim et al., 2006a): IL-2R α (also known as CD25 or Tac antigen), IL-2R β (also called CD122) and IL-2R γ (now denoted as the common cytokine receptor γ chain (γ c) or CD132).

The IL-2R α chain contains a short 13-amino acid residue-long intra-cytoplasmic domain, which is necessary for IL-2 binding and internalization, and does not appear to be critically involved in intracellular signaling. By contrast, the β and γ c chains belong to the hematopoietin receptor (type I cytokine receptor family) with

an extracellular domain characterized by four positionally conserved cysteine residues and a Trp-Ser-X-Trp-Ser (WSXWS) motif, close to the membrane spanning region, that is responsible for stabilization of the receptor on the cell surface (Gesbert et al., 1998). IL-2R β and γ_c chains are responsible for initiating intracellular signal transduction. It has been shown that heterodimerization of the IL-2R β and γ_c cytoplasmic domains appears necessary and sufficient for IL-2 signaling in T cells (Nakamura et al., 1994; Nelson et al., 1994).

Following mitogenic stimulation of T cells, strong induction of IL-2R α occurs, resulting in approximately a 10:1 ratio of low:high affinity IL-2 receptors (Robb et al., 1987). The three dimensional structure of the high affinity receptor has been solved and supports a model whereby IL-2 initially binds to IL-2R α , then IL-2R β is recruited, and finally γ_c (Stauber et al., 2006; Wang et al., 2005). The intermediate and high affinity receptor forms are functional, transducing IL-2 signals.

II.1.2.2. The interleukin-2 signaling pathway

IL-2 receptors, like receptors for many other cytokines, do not contain catalytic domains typical of intrinsic protein kinases. As mentioned above, IL-2-signaling requires heterodimerization of the IL-2R β and γ_c cytoplasmic domains. This leads to the activation of several protein tyrosine kinases that phosphorylate a large array of intracellular substrates including the receptor complex. Phosphorylated tyrosine residues within the receptor then serve as docking sites for multimolecular signaling complexes that initiate three major pathways (Kim et al., 2006a; Liao et al., 2011): (i) the Janus tyrosine kinase (Jak) – signal transducer and activator of transcription (STAT) pathway controlling gene transcription; (ii) the Ras/mitogen-activated protein kinase (MAPK) pathway leading to cell proliferation and gene transcription; and (iii) the PI3K pathway involved in anti-apoptotic signaling, organization of the cytoskeleton and probably in metabolic control.

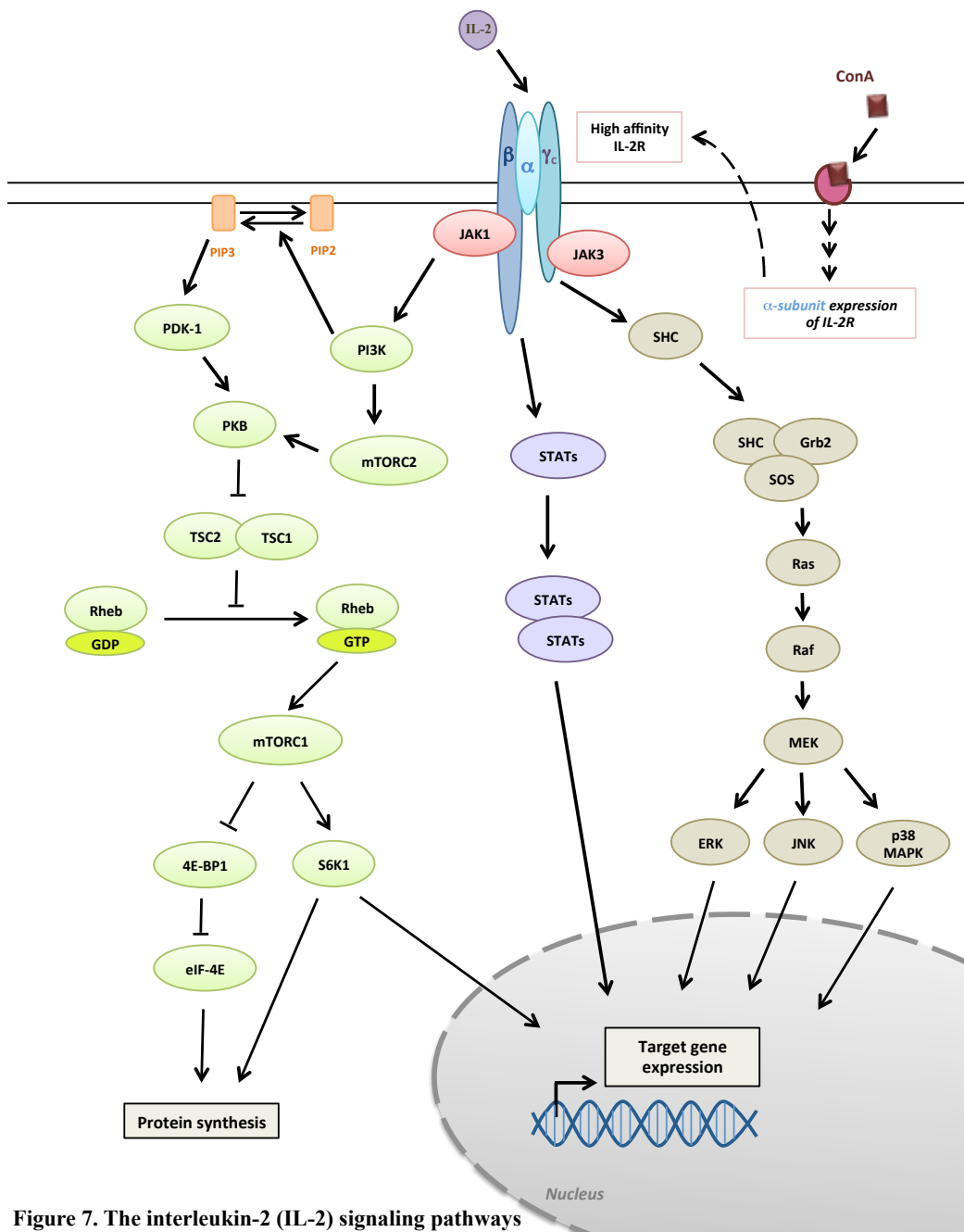


Figure 7. The interleukin-2 (IL-2) signaling pathways

II.1.2.2.1. The Jak-STAT signaling pathway

Jak family – STAT signaling is involved in the signaling pathway of many cytokines (Leonard, 2001). Activation of Jaks by IL-2-induced heterodimerization of IL-2R β and γ_c is likely to be one of the earliest events in the IL-2-induced signaling cascade. Two Jak family members, Jak1 and Jak3, are physically associated with β and γ chains of the IL-2R, respectively, and activated by IL-2 stimulation. The membrane-proximal region of IL-2R β , the so-called serine-rich region (S region), is critical for Jak1 association and the cytoplasmic domain of IL-2R γ directly participates in Jak3 association. Jak1 and Jak3 are thus brought in proximity by dimerization of the receptor and activate each other. The crucial role of Jak3 in IL-2-induced proliferation is clear, however it has been reported that Jak1 may be dispensable for IL-2-mediated cell growth (Higuchi et al., 1996) and suggests that alternative modes of Jak3 activation may exist. Once activated, Jaks recruit cytosolic STAT proteins and in turn phosphorylate them. Phosphorylation of STAT1 α and STAT1 β , STAT3, and most consistently and prominently STAT5A and STAT5B leads to their homo- or heterodimerization and nuclear translocation where they function as transcription factors (Frank et al., 1995; Gilmour et al., 1995; Nielsen et al., 1994). The Jak-STAT pathway serves to rapidly regulate expression of target genes. Two of the genes induced by IL-2 are IL-2R α and IL-2R β . Interestingly, the former is clearly dependent on STAT5 activation (Lin and Leonard, 1997; Lin and Leonard, 2000).

II.1.2.2.2. The Ras-MAP kinase pathway

Upon IL-2 stimulation, activation of the Ras/MAPK pathway begins with the recruitment of the adaptor Shc (Ravichandran and Burakoff, 1994). Shc binds via

its phosphotyrosine-binding (PTB) domain to phosphorylated Y338 of the IL-2R β chain, becomes tyrosine phosphorylated, and in turn recruits the Grb2/Sos complex. The Shc/Grb2/Sos trimer then transduces a signal to Ras, a small GTP binding protein. Activation of Ras leads to activation of a Ser/Thr protein kinase cascade. Ras-GTP binds to and activates Raf-1, which results in turning on MAPK/extracellular-signal-regulated kinase (ERK) kinase (MEK) 1/2, which activates and phosphorylates ERK1/2 (de Vries-Smits et al., 1992; Perkins et al., 1993). The phosphorylated ERK dimer can regulate targets in the cytosol and nucleus by activating other protein kinases, such as the 90-kDa ribosomal S6 kinase (p90Rsk) and MAPK-interacting kinase (MNK), which then phosphorylate proteins involved in chromatin remodeling, or transcription factors such as c-Jun, c-Fos and ATF (activating transcription factor), Elk-1 (Ets-like transcription factor 1) and c-myc (v-myc avian myelocytomatosis viral oncogene cellular homolog) (Binétruy et al., 1991; Smeal et al., 1991). Interestingly it has been shown that stress-activated protein kinase (SAPK)/c-Jun N-terminal kinase (JNK) and p38MAPK also participate in IL-2-induced mitogenesis (Crawley et al., 1997).

II.1.2.2.3. The PI3K pathway

PI3K proteins are ubiquitously expressed in the mammalian immune system. IL-2, like other cytokines, chemokines, antigens and co-stimulatory molecules, are all able to recruit PI3K to the plasma membrane, whereupon PI3K phosphorylates phosphoinositides on the 3-position of the inositol ring (Merida et al., 1991), to produce important second messengers for intracellular signaling in several processes. In response to cytokine signaling, it is mainly class Ia PI3Ks that become activated. Class Ia PI3K is composed of both catalytic (p110 α , p110 β or p110 γ) and regulatory (p85 α , p55 α , p50 α , p85 α or p55 γ) subunits (Benczik and Gaffen, 2009). Class Ia PI3K activation is induced by tyrosine kinases which phosphorylate a Tyr residue within a Tyr-X-X-Met (YXXM) motif on membrane

protein receptors/adaptor proteins. This serves as a docking site for the Src-homology 2 (SH2) domain of the regulatory domain of PI3K (Songyang et al., 1993), thus bringing the catalytic subunit into proximity with the plasma membrane and its lipid substrates. However, the IL-2R does not contain sites for directly binding PI3K or a (YXXM) motif. Phosphorylation of the PI3K binding motifs occurs through Jaks or other protein tyrosine kinases. For instance, IL-2R β chain phosphorylated on Tyr392 is able to recruit the PI3K regulatory subunit (Truitt et al., 1994) and the latter can directly bind to Jak1 (Migone et al., 1998). It also has been reported that the PI3K regulatory domains can be recruited through Shc/Grb2/Gab2 via Tyr338 phosphorylation of IL-2R β (Gu et al., 2000).

Two Ser/Thr kinases, S6K1 and PKB/Akt, are activated by IL-2 in a PI3K-dependent manner in T cells (discussed in details below) (Reif et al., 1997). In addition to tyrosine kinase-dependent activation of PI3K, IL-2 also stimulates the association of PI3K with PKC ζ (Gomez et al., 1996). PKC ζ is implicated in the maintenance of cytoskeletal integrity and is required for IL-2 proliferation. Another isoform of PKC, PKC θ , promotes T cell cycle progression and also cooperates with the protein Ser/Thr phosphatase, calcineurin, in transducing signals leading to activation of several genes such as JNK and IL-2 (Werlen et al., 1998).

II.2. The PKB pathway

II.2.1. The PI3K/PKB axis

As mentioned previously, PI3K is a lipid kinase activated by growth factors and hormones that phosphorylates inositol-containing membrane lipids at the D-3 position of the inositol ring. Various forms of PI3K have been identified among which the Class I PI3Ks use phosphatidylinositol-4,5-bisphosphate (PtdIns-4,5-P₂, PIP₂) as principal substrate to produce phosphatidylinositol-3,4,5-triphosphate

(PtdIns-3,4,5-P₃, PIP₃) (Zhao and Roberts, 2006). Class I PI3Ks are divided into receptor Class Ia and Class Ib which are typically activated via protein tyrosine kinases and G protein-coupled receptors, respectively. Accumulation of PIP₃ induces the recruitment of various signaling proteins containing pleckstrin homology (PH) domains, such as the Ser/Thr kinases phosphoinositide-dependent kinase-1 (PDK1) and PKB/Akt (Cantley, 2002; Testa and Bellacosa, 1997). Association with PIP₃ at the plasma membrane allows PDK1 to phosphorylate PKB at Thr308, needed for its activation. To achieve full activation, PKB needs to be phosphorylated at Ser473 by PDK2, identified as the rictor - mammalian target of rapamycin complex 2 (mTORC2) (Alessi et al., 1996; Brazil et al., 2004). Once activated, PKB translocates to the cytosol and nucleus to phosphorylate its substrates. PKB is negatively regulated by tumor suppressor phosphatase and tensin homolog deleted on chromosome 10 (PTEN) (Stambolic et al., 1998). PTEN is a lipid phosphatase that dephosphorylates the membrane lipid products of PI3K (Maehama and Dixon, 1998; Maehama and Dixon, 1999). Decreasing of PIP₃ levels prevents PKB recruitment to the plasma membrane and thus indirectly inhibits its activation. Loss of PTEN or loss of PTEN function has been shown in many human cancers and leukaemic T cell lines, including the extensively used Jurkat T cell line. Indeed, Jurkat T cells express a nonfunctional PTEN protein due to mutations in both alleles of the *PTEN* gene, primarily leading to constitutive activation of the PI3K/PKB signaling (Freeburn and Ward, 2001; Shan et al., 2000).

II.2.2. PKB/Akt isoforms

PKB is a Ser/Thr protein kinase that belongs to the AGC (cAMP-dependent, cGMP-dependent, protein kinase C) family of protein kinases (Hanada et al., 2004). PKB displays sequence similarity with the catalytic domain of PKA and PKC. Therefore, the protein kinase was called “PKB” and “RAC-PK” (related to A

and C protein kinases) (Coffer and Woodgett, 1991; Jones et al., 1991). Another group identified the protein kinase as the product of the v-akt proto-oncogene and named it Akt (Bellacosa et al., 1991).

In mammals, there are three highly homologous isoforms of PKB: PKB α /Akt1, PKB β /Akt2 and PKB γ /Akt3. They are encoded by distinct genes located on different chromosomes. PKB α /Akt1 is ubiquitously expressed, whereas PKB β /Akt2 is predominantly expressed in insulin-sensitive tissues including liver, skeletal muscle and adipose tissue. PKB γ /Akt3 is mostly found in brain and testis (Datta et al., 1999; Manning and Cantley, 2007). Interestingly both *PKB α /Akt1* and *PKB β /Akt2* gene amplification have been reported in human gastric, ovarian, pancreatic and breast cancers (Bellacosa et al., 1995; Flier et al., 1987; Knobbe and Reifenberger, 2003; Pedrero et al., 2005; Ruggeri et al., 1998; Staal, 1987; Stal et al., 2003), however *PKB β /Akt2* gene amplification occurs more frequently. By contrast, *PKB γ /Akt3* gene amplification in cancer has not been reported.

II.2.3. Structure of PKB

With more than 80% sequence identity (Nicholson and Anderson, 2002), all PKB/Akt isoforms share a similar structure, including three functional domains: an amino-terminal pleckstrin homology (PH) domain; a central catalytic kinase domain; and a regulatory carboxyl-terminal domain containing the hydrophobic motif phosphorylation site [FxxF(S/T)Y] characteristic of all AGC-family kinases (Alessi et al., 1996; Hanada et al., 2004; Peterson and Schreiber, 1999) and phosphorylated by mTORC2. A short α -linker region is located between the PH domain and the catalytic domain, however its function is unclear. The intramolecular interaction between the PH domain and the catalytic domain is essential to keep PKB inactive. Once the PH domain binds to the lipid products of PI3K, a conformational change occurs that releases the catalytic kinase core (Manning and Cantley, 2007). Subsequently Thr308 and Ser473 are

phosphorylated within the catalytic domain and in the hydrophobic motif (Andjelkovic et al., 1997), respectively, and induce full activation of PKB (see section II.2.1.). Two constitutively phosphorylated sites have also been identified, Ser124 and Thr450, which are not needed for PKB activity, but seem to stabilize PKB and protect it from degradation.

II.2.4. Cellular functions of PKB

PKB directly phosphorylates proteins containing a consensus sequence R-X-R-X-X-S/T-B (X represents any amino acid and B is any bulky hydrophobic residue). PKB plays a key role in controlling a wide range of physiological functions, such as cell survival, protein synthesis, cell proliferation, cell growth, metabolism and angiogenesis (Carnero, 2010; Manning and Cantley, 2007).

Cell survival

Many studies have shown that PKB is essential for cell survival by directly phosphorylating pro-apoptotic proteins that inactivate pro-survival Bcl-2 family members or by directly phosphorylating transcription factors that regulate the expression of pro- and anti-apoptotic genes (Datta et al., 1999). For instance, in response to survival factors, PKB directly phosphorylates Bcl-2-associated death promoter (BAD), a protein involved in initiating apoptosis. This creates a binding site for 14-3-3 proteins, which release BAD from its target proteins (Datta et al., 2000). PKB also promotes cell survival by directly phosphorylating pro-caspase 9, which correlates with a decrease in protease activity of caspase-9 *in vitro* (Cardone et al., 1998). In addition, PKB phosphorylates transcription factors such as Forkhead box O (FOXO) proteins and tumor protein 53 (p53). PKB-mediated phosphorylation of FOXO proteins occurs in the nucleus and, as with BAD, creates a binding site for 14-3-3 proteins which remove FOXO transcription factors from target genes and trigger their export from the nucleus (Manning and Cantley,

2007). An important pro-apoptotic target of FOXO proteins is Bcl-2-like protein 11 (BIM) protein, which is an essential initiator of apoptosis in thymocyte-negative selection (Bouillet et al., 2002). PKB also phosphorylates mouse double minute 2 homolog (MDM2), an E3 ubiquitin ligase, promoting its translocation to the nucleus where it negatively regulates p53 (Mayo and Donner, 2002). PKB also activates transcription factors that upregulate anti-apoptotic genes such as IκB kinase (IKK) (Romashkova and Makarov, 1999) and cyclic-AMP response element-binding protein (CREB) (Du and Montminy, 1998).

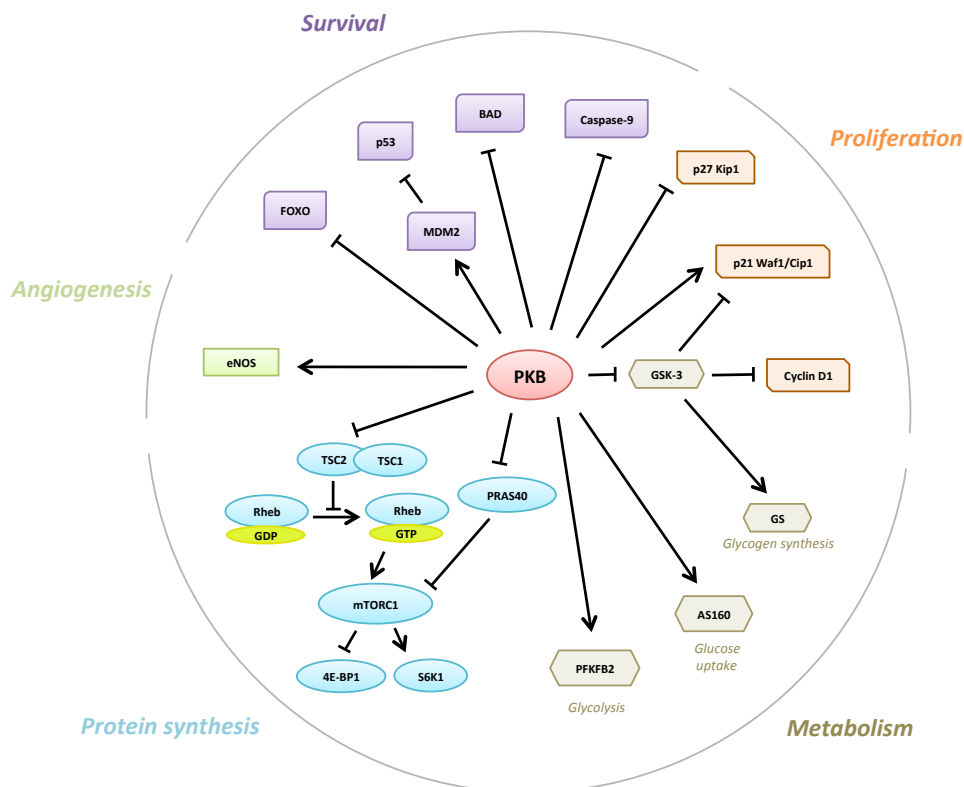


Figure 8. Cellular functions of PKB substrates. PKB-mediated phosphorylation of its targets leads to their activation (arrows) or inhibition (cross-head arrows). Regulation of PKB substrates contributes to triggering various cellular processes, such as cell survival, cell proliferation, protein synthesis, glucose metabolism, and angiogenesis.

Protein synthesis

The mammalian target of rapamycin complex 1 (mTORC1) is regulated by both nutrient availability and growth factor stimuli. mTORC1 is a critical regulator of translation initiation and ribosome biogenesis and plays an evolutionarily conserved role in stimulating cell proliferation. PKB indirectly induces mTORC1 by inhibiting tuberous sclerosis complex-2 (TSC2, also known as tuberlin), which forms a complex with its binding partner TSC1 (also known as hamartin). TSC2 acts as a GTPase-activating protein (GAP) for Ras homolog enriched in brain (Rheb), a Ras family GTPase, which strongly activates mTORC1 when in its GTP-bound active form (Inoki et al., 2003). Like TSC2, the proline-rich Akt substrate of 40 kDa (PRAS40) is also involved in mTORC1 regulation and associates with mTORC1 to negatively regulate mTORC1 signaling (Sancak et al., 2007). PKB-mediated phosphorylation of TSC2 and PRAS40 opposes their inhibitory action on mTORC1. Subsequent activation of mTORC1 stimulates protein synthesis. The two best-characterized substrates of mTORC1 proposed to mediate its effect on translation are eukaryotic translation initiation factor 4E-binding protein-1 (4E-BP1) and S6K1.

Cell proliferation and cell-cycle progression

PKB plays a crucial role in controlling proliferation by phosphorylating downstream targets involved in cell-cycle regulation. For instance, PKB directly phosphorylates cyclin-dependent kinase inhibitors p21^{Cip1/WAF1} and p27^{Kip1}, leading to their cytosolic sequestration via 14-3-3 binding and preventing their cell-cycle inhibitory effects (Manning and Cantley, 2007). PKB also controls the synthesis and stability of crucial proteins involved in cell-cycle entry via phosphorylation of glycogen synthase kinase-3 β (GSK3 β), TSC2 and PRAS40 (Manning and Cantley, 2007).

Cell metabolism

In response to growth factor stimulation, PKB regulates nutrient uptake and metabolism. PKB is known to upregulate GLUT4 translocation to the cell surface in response to insulin. This occurs via PKB-mediated phosphorylation of Akt substrate of 160 kDa (AS160, also known as TBC1 domain family member 4; TBC1D4) and TBC1D1, which decreases their Rab-GAP activity, allowing the conversion of Rab proteins to their active GTP-bound states required for insulin-stimulated GLUT4 translocation to the plasma membrane (Sano et al., 2003). Stimulated T cells also upregulate cell metabolism through a PKB-mediated pathway by increasing total expression and cell surface trafficking of GLUT1, the primary glucose transporter in hematopoietic cells (Wieman et al., 2007). PKB regulation of glucose metabolism is important during T cell development, and T cells are particularly dependent on glucose metabolism to maintain survival (Plas et al., 2001). PKB activation can also enhance glycolysis by promoting the expression of glycolytic enzymes through HIF α (Manning and Cantley, 2007). Moreover, PKB stimulates the transport and metabolism of amino acids in a mTORC1-dependent manner (Edinger and Thompson, 2002). Finally, in heart, PKB phosphorylates and activates PFK-2 activity of the PFKFB2 isoenzyme, thus leading to an increase in Fru-2,6-BP, which together with the stimulation of glucose uptake enhances the glycolysis.

Angiogenesis

In response to pro-angiogenic factors such as vascular endothelial growth factor (VEGF), PKB activation prevents endothelial cell apoptosis. Endothelial nitric oxide synthase (eNOS) is also phosphorylated and activated by PKB (Karar and Maity, 2011). This increases production of NO and stimulates vasodilation and vascular remodelling (Lamallice et al., 2007). It has also been reported that increased PKB expression induces angiogenesis (Jiang et al., 2000). PKB also

increases the translation of HIF α transcription factors, at least in part, via increased mTORC1 signaling (Karar and Maity, 2011). HIF α activation in endothelial and other cells promotes expression and subsequent secretion of VEGF and other angiogenic factors (Liu et al., 2012), thereby stimulating angiogenesis through both autocrine and paracrine signaling.

II.2.5. PKB inhibitors

Pharmacological PKB inhibitors have been developed as potential anti-cancer drugs, divided in three categories: (i) ATP-competitive inhibitors, (ii) allosteric inhibitors and (iii) inhibitors of PIP3 binding (Hers et al., 2011). ATP-competitive inhibitors inhibit PKB activity by interfering with ATP binding to the kinase, but have many off-target effects due to lack of specificity (Hers et al., 2011; Lindsley, 2010). Allosteric inhibitors are more specific, and inhibit PKB activity via binding to the PH domain and preventing PKB activation by its upstream kinases. Inhibitors of PIP3 binding prevent membrane recruitment and thus activation of PKB by PDK1 and mTORC2. Some of these inhibitors are now under clinical trial for cancer therapy. Here two PKB allosteric inhibitors will be considered, Akti-1/2 and MK-2206.

Akti-1/2

Akti-1/2 is an early generation PKB allosteric inhibitor that inhibits PKB activity *in vitro* in the nanomolar range. It has been demonstrated that Akti-1/2 inhibits glucose uptake independently of its effect of PKB, by directly inhibiting the transport activity of GLUT1 and GLUT4 (Tan et al., 2010). This side effect questions the *in vivo* specificity and clinical feasibility of using the inhibitor.

MK-2206

MK-2206 is a next generation PKB allosteric inhibitor with higher specificity and

inhibitory potency towards recombinant PKB 10-times greater than Akti-1/2 (Lindsley, 2010). In adipocytes pre-incubated with MK-2206, both insulin-stimulated PKB phosphorylation and glucose uptake were inhibited, with an IC_{50} of 0.1 – 0.2 μ M. Moreover, unlike Akti-1/2, MK-2206 did not affect the transport activity of GLUT1 or GLUT4 (Tan et al., 2011). MK-2206 can be administrated orally and is now undergoing clinical trials to treat advanced solid tumors (Yap et al., 2011).

II.3. Metabolic changes in ConA-stimulated thymocytes

Mitogenic stimulation of thymocytes triggers a drastic metabolic reprogramming needed for cell growth, cell proliferation and differentiation. This physiological response encompasses a shift from oxidative phosphorylation to aerobic glycolysis (the Warburg effect) together with stimulation of other metabolic pathways that sustain biosynthetic processes, cell proliferation and cell growth.

In vitro stimulation of thymocytes by ConA mimics the response that occurs to an antigenic challenge *in vivo*. Thymocytes cultured in the presence of ConA and growth factor IL-2 represent a unique and remarkable model to investigate the metabolic events associated with cell growth and cell proliferation (Brand et al., 1984). In ConA-stimulated thymocytes, glucose metabolism increases by at least 30-fold. About 90% of the glucose consumed is converted into lactate, whereas resting thymocytes metabolize only ~60% of glucose consumed to lactate. Other metabolic changes include a 10-fold increase in protein synthesis and a 20-fold increase in lipid biosynthesis (Wang and Green, 2012). Interestingly, glutamine is also used as a fuel and its utilization increases 8-fold in ConA-stimulated cells (Brand, 1985). Glucose consumption seems to be particularly important for cell survival, cell size, cell activation and cytokine production (Fox et al., 2005). Enhanced aerobic glycolysis not only produces ATP to meet increased energy

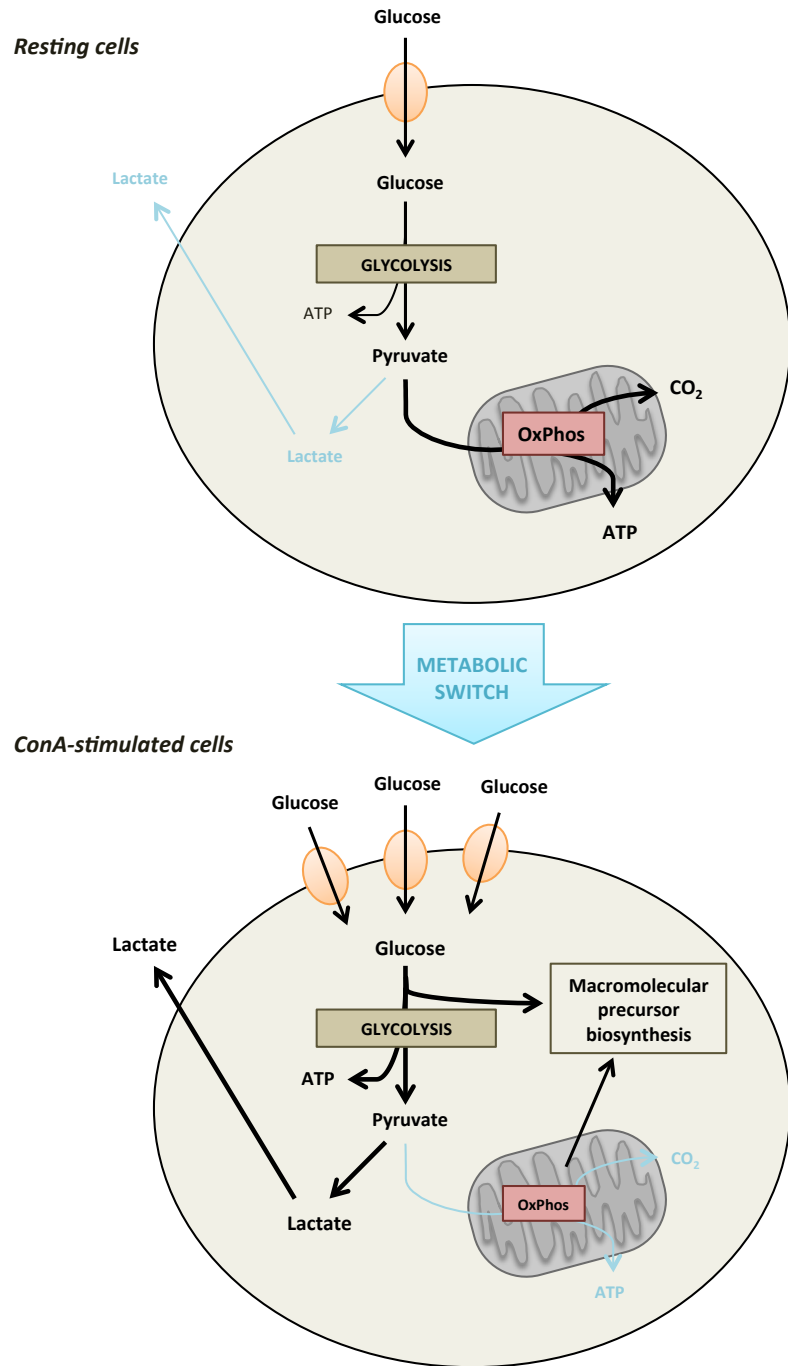


Figure 9. Summary of the metabolic switch that occurs in activated thymocytes

demand, but also provides the cell with precursors for biosynthetic processes. Regarding the molecular mechanism involved in the stimulation of glycolysis, increased GLUT1 expression is paramount. Thymocytes mainly express GLUT1 and extracellular signals, such as hormones, cytokines or growth factors, induce expression and surface localization of GLUT1 via increased PI3K/PKB signaling. PKB activation increases the expression and cell surface trafficking of GLUT1, thereby promoting glucose uptake and metabolism in stimulated cells (MacIver et al., 2008; MacIver et al., 2013). Enhanced glycolysis in proliferating thymocytes is also accompanied by induction of glycolytic enzymes which increase 4 to 10-fold following ConA stimulation and reach maximal levels after 48 h coinciding with increased DNA synthesis (Brand et al., 1988; Greiner et al., 1994). Conversely, the activities of enzymes associated with oxidative glucose and amino acid metabolism do not significantly change in proliferating thymocytes. Interestingly, using glutamine, glutamine and ribose or glutamine and uridine as alternative substrates prevents glycolytic enzyme induction and proliferation. Glucose is thus crucial to allow energy production during the G1/S transition in ConA-stimulated thymocytes (Greiner et al., 1994).

Glutamine is another key substrate for activated immune cells. In activated T cells, glucose is mainly converted to pyruvate and further reduced to lactate by lactate dehydrogenase A (LDHA). NAD^+ produced by LDHA contributes to maintain a high glycolytic rate but also to increase cytosolic malate dehydrogenase 1 (MDH1) activity to generate oxaloacetate from malate, thereby driving aspartate synthesis via glutamic oxaloacetate transaminase 1 (GOT1, also known as aspartate aminotransferase 1). The main contribution of glutamine is to provide cells with carbon and nitrogen for amino acid, nucleotide, glutathione, hexosamine and protein synthesis. In mitochondria, α -ketoglutarate is converted into succinyl-CoA and then succinate (glutamine oxidative decarboxylation), supporting anaplerosis. Interestingly, α -ketoglutarate can also be carboxylated into isocitrate to give rise to citrate (glutamine reductive carboxylation). The latter pathway also occurs in the

cytosol and represents a major source of citrate to generate acetyl-CoA and fatty acids under hypoxia, acidosis or when conventional TCA cycle is blocked (Corbet and Feron, 2017; Corbet et al., 2016)

The Crabtree effect is the inhibition of oxygen consumption by glucose and has been demonstrated in thymocytes during proliferation. Most ATP synthesis occurs during the conversion of glucose to lactate, even in the presence of both glucose and glutamine (Guppy et al., 1993). Low oxidative metabolism might be advantageous for proliferating thymocytes to reduce free radical production. In agreement, it has been demonstrated that oxidative stress decreases the expression of glycolytic enzymes in both resting and ConA-stimulated cells (Hamm-Künzelmann et al., 1997). Therefore ConA-stimulated thymocytes display certain metabolic hallmarks of cancer cells and represent an appropriate and interesting model to study metabolic changes that occur during proliferation and that are pertinent to cancer.

RESEARCH OBJECTIVES

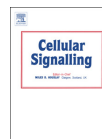
The main aim of the work was to investigate the mechanism by which ConA stimulation increases glycolysis, cell proliferation and protein synthesis in freshly isolated rat thymocytes. These cells represent a useful model to study metabolic changes resulting from the transition from the resting to the proliferating state. As mentioned previously (see section I.3.), Fru-2,6-BP content in cancer cells is 10 - 100 times higher than required to stimulate PFK-1 activity. Therefore, the potential involvement of Fru-2,6-BP in coupling glycolysis to cell proliferation and protein synthesis in ConA-stimulated thymocytes was explored. Expression of PFKFB isoenzymes and regulation of the PFKFB/Fru-2,6-BP axis were also studied. As it was previously shown that the p38/MK2 pathway was involved in PFKFB3 expression and implicated in PFK-2 activation via Ser461 phosphorylation, the questions (i) whether PKB might directly phosphorylate PFKFB3 to increase its PFK-2 activity; (ii) whether downregulation of PKB would affect PFKFB expression; and (iii) whether PFKFB3/4 isoenzymes and PKB might be involved in the control of glycolysis, cell proliferation and protein synthesis, were also addressed.

RESULTS

PAPER 1:

Role of Akt/PKB and PFKFB isoenzymes in the control of glycolysis, cell proliferation and protein synthesis in mitogen-stimulated thymocytes

Published in Cellular Signalling (2017) 34:23-37, first author.



Role of Akt/PKB and PFKFB isoenzymes in the control of glycolysis, cell proliferation and protein synthesis in mitogen-stimulated thymocytes



Amina Houddane^a, Laurent Bultot^a, Laura Novellasdemunt^b, Manuel Johanns^a, Marie-Agnès Gueuning^a, Didier Vertommen^a, Pierre G. Coulie^a, Ramon Bartrons^b, Louis Hue^a, Mark H. Rider^{a,*}

^a Université catholique de Louvain and de Duve Institute, Avenue Hippocrate 75, B-1200 Brussels, Belgium

^b Departament de Ciències Fisiològiques, IDIBELL, Campus de Ciències de la Salut, Universitat de Barcelona, L'Hospitalet de Llobregat, Barcelona E-08907, Spain

ARTICLE INFO

Article history:

Received 26 October 2016

Received in revised form 14 February 2017

Accepted 20 February 2017

Available online 22 February 2017

Keywords:

Glycolysis

Proliferation

Protein synthesis

Fru-2,6-P₂

PFKFB isoenzymes

PKB

ABSTRACT

Proliferating cells depend on glycolysis mainly to supply precursors for macromolecular synthesis. Fructose 2,6-bisphosphate (Fru-2,6-P₂) is the most potent positive allosteric effector of 6-phosphofructo-1-kinase (PFK-1), and hence of glycolysis. Mitogen stimulation of rat thymocytes with concanavalin A (ConA) led to time-dependent increases in lactate accumulation (6-fold), Fru-2,6-P₂ content (4-fold), 6-phosphofructo-2-kinase (PFK-2)/fructose-2,6-bisphosphatase isoenzyme 3 and 4 (PFKFB3 and PFKFB4) protein levels (~2-fold and ~15-fold, respectively) and rates of cell proliferation (~40-fold) and protein synthesis (10-fold) after 68 h of incubation compared with resting cells. After 54 h of ConA stimulation, PFKFB3 mRNA levels were 45-fold higher than those of PFKFB4 mRNA. Although PFKFB3 could be phosphorylated at Ser461 by protein kinase B (PKB) *in vitro* leading to PFK-2 activation, PFKFB3 Ser461 phosphorylation was barely detectable in resting cells and only increased slightly in ConA-stimulated cells. On the other hand, PFKFB3 and PFKFB4 mRNA levels were decreased (90% and 70%, respectively) by exposure of ConA-stimulated cells to low doses of PKB inhibitor (MK-2206), suggesting control of expression of the two PFKFB isoenzymes by PKB. Incubation of thymocytes with ConA resulted in increased expression and phosphorylation of the translation factors eukaryotic initiation factor-4E-binding protein-1 (4E-BP1) and ribosomal protein S6 (rpS6). Treatment of ConA-stimulated thymocytes with PFK-2 inhibitor (3PO) or MK-2206 led to significant decreases in Fru-2,6-P₂ content, medium lactate accumulation and rates of cell proliferation and protein synthesis. These data were confirmed by using siRNA knockdown of PFKFB3, PFKFB4 and PKB α/β in the more easily transfectable Jurkat E6-1 cell line. The findings suggest that increased PFKFB3 and PFKFB4 expression, but not increased PFKFB3 Ser461 phosphorylation, plays a role in increasing glycolysis in mitogen-stimulated thymocytes and implicate PKB in the upregulation of PFKFB3 and PFKFB4. The results also support a role for Fru-2,6-P₂ in coupling glycolysis to cell proliferation and protein synthesis in this model.

© 2017 Elsevier Inc. All rights reserved.

Abbreviations: 4E-BP1, eukaryotic initiation factor 4E-binding protein 1; AMPK, AMP-activated protein kinase; BSA, bovine serum albumin; ConA, concanavalin A; eEF2, eukaryotic elongation factor 2; eIF, eukaryotic initiation factor; ERK, extracellular-signal-regulated kinase; Fru-2,6-P₂, fructose 2,6-bisphosphate; p38 MAPK, p38 mitogen-activated protein kinase; MEK, mitogen-activated protein kinase/extracellular-signal-regulated kinase kinase; mTOR, mammalian target of rapamycin; Raptor, regulatory-associated protein of mTOR; PFKFB1/2/3/4, 6-phosphofructo-2-kinase/fructose-2,6-bisphosphatase isoenzyme 1, 2, 3 or 4; RSK1, 90-kDa ribosomal protein S6 kinase 1; rpS6, ribosomal protein S6; p70S6K, p70 ribosomal protein S6 kinase; TSC, tuberous sclerosis complex; PI3K, phosphatidylinositol 3-kinase; PKB, protein kinase B; PP2A, protein phosphatase-2A. * Corresponding author at: SSS/DDUV/PHOS, Avenue Hippocrate 75, bte B1.74.02, B-1200 Brussels, Belgium.

E-mail address: mark.rider@uclouvain.be (M.H. Rider).

<http://dx.doi.org/10.1016/j.cellsig.2017.02.019>

0898-6568/© 2017 Elsevier Inc. All rights reserved.

1. Introduction

Rapidly dividing cancerous and non-cancer cells require glycolysis to proliferate. In 1924, Otto Warburg found that cancer cells display increased glycolysis even in the presence of oxygen [1], a phenomenon known as "Warburg effect". Aerobic glycolysis is needed mainly to supply precursors for macromolecular synthesis rather than for ATP production [2], a feature that is not restricted to cancer cells, and increased glucose uptake and lactate production were also observed in proliferating non-cancer cells [3–7]. Fructose 2,6-bisphosphate (Fru-2,6-P₂) is the most potent positive allosteric effector of 6-phosphofructo-1-kinase (PFK-1), and hence of glycolysis. Fru-2,6-P₂ is synthesized and degraded by a bifunctional, homodimeric enzyme, called 6-phosphofructo-2-kinase (PFK-2)/fructose-2,6-bisphosphatase (FBPase-2) [8]. Four PFK-2/FBPase-2 isoenzymes, designated PFKFB1–4, have been identified in mammals encoded by four genes and each

gene generates several isoforms by alternative splicing. PFKFB3 is highly expressed in proliferating normal tissues (e.g. thymus) and many cancer cells [9] and favours glycolysis because of its high PFK-2:FBPase-2 activity ratio [8,10]. In fact Fru-2,6-P₂ concentrations in proliferating cells can reach levels 50–100 times higher than required to stimulate PFK-1 [11–13]. PFKFB3 silencing was found to decrease glycolysis and induce cell cycle arrest in HeLa cells [14,15] and inhibited vessel branching of endothelial cells [16], suggesting a link between Fru-2,6-P₂/glycolysis and cell proliferation. Interestingly an inhibitor of PFKFB3, 3-(3-pyridinyl)-1-(4-pyridinyl)-2-propen-1-one (3PO), was discovered that decreased Fru-2,6-P₂ concentrations and glycolysis in transformed cells and suppressed the growth of certain tumors in vivo [17]. PFK-2 activation of PFKFB3 was induced by phosphorylation at Ser461 by AMP-activated protein kinase (AMPK) [18] and mitogen-activated protein kinase (MAPK)-activated protein kinase 2 (MK2) [19] and PFKFB3 Ser461 phosphorylation was detected in many human tumors [20]. In addition, PFKFB4 is overexpressed in many human tumors and pharmacological targeting of its PFK-2 activity has been proposed for anti-cancer therapy [21].

Mitogen-stimulated thymocytes represent a remarkable model system for studying non-cancerous cell proliferation. Activation of resting thymocytes by concanavalin A (ConA), a mitogenic lectin, leads to both interleukin 2 receptor (IL-2R) and interleukin 2 (IL-2) production inducing progression through G1 to DNA synthesis in S phase and proliferation [3,22,23]. When thymocytes or T cells are activated, energy metabolism is amongst the first cellular processes to respond and, upon stimulation by ConA, O₂ consumption can increase by up to 40% [24]. ConA-stimulated thymocytes increase glucose metabolism by about 50-fold after mitogenic stimulation, and about 90% of glucose consumed is converted into lactate, whereas resting thymocytes metabolize about 60% of glucose to lactate. Glutamine is also used as a fuel source and its utilization increases 8-fold in ConA-stimulated cells [3, 22]. Glucose consumption seems to be particularly important for T-cell survival, T-cell activation and cytokine production [25] and is thus crucial during the G1/S transition in ConA-stimulated thymocytes [26]. Enhanced glycolysis in proliferating thymocytes is also accompanied by induction of glycolytic enzymes which increase 4- to 10-fold after ConA stimulation and reach maximal levels after 48 h, coinciding with increased DNA synthesis [22,26]. Conversely the activities of enzymes associated with oxidative glucose and amino acid metabolism do not significantly change during thymocyte proliferation [22].

Thymocyte/T cell activation results in the activation of cytosolic protein tyrosine kinases, followed by the initiation of multiple signalling cascades [27] including protein kinase C (PKC), Ca²⁺ and Ras/mitogen-activated protein kinase (MAPK) pathways [24] along with phosphatidylinositol 3-kinase (PI3K)/protein kinase B (PKB, also known as Akt) [28]. However, the precise mechanisms by which these signalling pathways impact on energy metabolism are poorly defined. In the present study, we investigated ConA stimulation of glycolysis, cell proliferation and protein synthesis in thymocytes with a particular focus on Fru-2,6-P₂/PFKFB isoenzymes and the possible roles of PKB.

2. Materials and methods

2.1. Antibodies and other reagents

MK-2206 was from Enzo Life Sciences. 3PO and rapamycin were from Merck Chemicals. PD169316 and ConA were from Sigma Aldrich. Wortmannin (WM) was from Calbiochem. All cell culture reagents were from Life Technologies. Oligonucleotide primers were synthesized by Integrated DNA Technologies. [γ -³²P] ATP, [methyl-³H] thymidine, L-[2,3,4,5,6-³H] phenylalanine and 2-deoxy-D-[1-³H]-glucose were from Perkin Elmer. Anti-total PFKFB3 (Abcam, Catalogue no. ab181861), anti-total PFKFB4 (Abcam, Catalogue no. ab137785), anti-total eukaryotic initiation factor 4E-binding protein 1 (4E-BP1) (Bioké, Catalogue no. 9644S), anti-pThr37/Thr46 4E-BP1 (Bioké, Catalogue no. 9459S),

anti-total ribosomal protein S6 (rpS6) (Bioké, Catalogue no. 2317S), anti-pSer240/Ser244 rpS6 (Cell Signaling, Catalogue no. 5364S), anti-total p70 ribosomal protein S6 kinase (p70S6K) (Bioké, Catalogue no. 9202S), anti-pThr389 p70S6K (Bioké, Catalogue no. 9205S), anti-total eukaryotic elongation factor-2 (eEF2) (Santa Cruz, Catalogue no. SC13003), anti-pThr56 eEF2 (Bioké, Catalogue no. 2331S), anti-total PKB PH domain (Millipore, Catalogue no. 05-591), anti-pSer473 PKB (Bioké, Catalogue no. 4060S), anti-total mammalian target of rapamycin (mTOR) (Cell Signaling, Catalogue no. 2983S), anti-pSer2448 mTOR (Cell Signaling, Catalogue no. 5536S), anti-total p38 MAPK (p38 MAPK) (Cell Signaling, Catalogue no. 8690S), anti-pThr180/Tyr182 p38 MAPK (Cell Signaling, Catalogue no. 4511S) and anti-protein phosphatase-2A (PP2A) [29] antibodies were obtained as indicated. A peptide surrounding Ser461 of rat PFKFB3 (CPLMRRNSVTPLAS) was synthesized with or without Ser461 phosphorylated and with a Cys (N-term) for coupling to keyhole limpet haemocyanin (KLH) or bovine serum albumin (BSA) (Inject maleimide-activated KLH/BSA kit, Thermo Fisher Scientific). The KLH-coupled phosphopeptide was injected in rabbits (Thermo Fisher Scientific) and the serum was affinity purified on both BSA-coupled phosphopeptide and BSA-coupled non-phosphopeptide linked to CH-activated Sepharose 4B (GE Healthcare). Synthetic peptides were kindly provided by Vincent Stroobant (Ludwig Institute, Brussels). Recombinant activated PKB S473D was kindly provided by Prof. D. Alessi (University of Dundee). Bacterially expressed recombinant activated AMPK α 1 β 1 γ 1 and bovine heart cyclic AMP-dependent protein kinase (PKA) catalytic subunits were prepared as described [30].

2.2. Animals

Female Wistar rats (2 months old) were obtained from the local animal house maintained at a 12:12 h light–dark cycle with free access to food and water. Animal experiments were approved by the local ethics committee and conducted within the guidelines of the “European Convention for the Protection of Vertebrate Animals used for Experimental and Other Scientific Purposes”.

2.3. Cell preparation and culture

The thymus was rapidly excised from an anaesthetized rat and thymocytes were extracted in approximately 20 ml of culture medium (RPMI Medium 1640, Fisher Scientific, Catalogue no. 11879-020) by mechanical dispersion. After filtering through a 40 μ m nylon mesh cell strainer (Fisher Scientific), thymocytes were collected by centrifugation (180g \times 5 min) and resuspended in 40 ml of culture medium for counting and seeding. Resting thymocytes were cultured at a density of 3.10⁶ cells/ml in RPMI 1640 medium supplemented with 10% (v/v) fetal bovine serum which had been dialyzed against 10 vol of phosphate-buffer saline, 11 mM glucose, 100 units/ml IL-2, 1% (v/v) penicillin/streptomycin in a humidified incubator under 5% CO₂ at 37 °C for times indicated in the figures and legends. Stimulated cells were cultured at a density of 3.10⁶ cells/ml in the same medium supplemented with 3 μ g/ml ConA for times indicated in the figures and legends. After harvesting the cells by centrifugation, incubation media were retained for lactate measurement and cell extracts were prepared for further analysis (see below). Jurkat E6-1 cells were kindly provided by Dr. S. Lucas (de Duve Institute, Université catholique de Louvain), electroporated (see below) and cultured at 37 °C in a humidified incubator under 5% CO₂ in RPMI-1640 - Glutamax™ (Catalogue no 61870-010) supplemented with 10% (v/v) fetal bovine serum and 1% (v/v) penicillin/streptomycin. Jurkat E6-1 cells were seeded at a density of 5.10⁵ cells/ml. After 48 h of incubation, the cells were harvested by centrifugation (5500g \times 15 s). Incubation media were retained for lactate measurement before washing the cells with cold phosphate-buffered saline pH 7.4 for the preparation of extracts and further analysis (see below).

2.4. siRNA electroporation of Jurkat E6-1 cells

Jurkat E6-1 cells (in 48-well plates) were electroporated with siRNA (small interfering RNA) oligonucleotides targeting PFKFB3 (Smartpool ON-TARGETplus PFKFB3 siRNA (human); Dharmacon, Catalogue no. L-006763-00-0005), PFKFB4 (Smartpool ON-TARGETplus PFKFB4 siRNA (human); Dharmacon, Catalogue no. L-006764-00-0005) or PKB α/β (SignalSilence Akt siRNA I; Cell Signaling, Catalogue no. 6211). The cells were also transfected with non-targeting siRNA (Silencer® Select Negative Control No. 2 siRNA; ThermoFisher, Catalogue no. 4390846). Cell Line Nucleofector Kit (SE Cell Line 4D-Nucleofector X kit L) was purchased from Lonza (Catalogue no. V4XC-1024 KT). Briefly cells were seeded at a density of 1.10^5 cells/ml and cultured at 37 °C in a humidified incubator under 5% CO₂ in RPMI-1640 - Glutamax™ supplemented with 10% (v/v) fetal bovine serum and 1% (v/v) penicillin/streptomycin. After 2 days, 1.10^6 cells were collected by centrifugation ($180g \times 5$ min) and carefully resuspended in 100 μ l 4D-Nucleofector™ Solution at room temperature in the presence of 4 μ M siRNA. The mixture was transferred to a Nucleocuvette™ Vessels for electroporation according to the recommended program. Pre-warmed medium (500 μ l) was added into the cuvette before carefully removing the cells. Electroporated cells were seeded equally in 2 wells containing 700 μ l of pre-warmed medium and cultured for 2 days at 37 °C in a humidified incubator under 5% CO₂ in RPMI-1640 - Glutamax™ supplemented with 10% (v/v) fetal bovine serum and 1% (v/v) penicillin/streptomycin.

2.5. Measurement of Fru-2,6-P₂ content and medium lactate concentration

Measurements of Fru-2,6-P₂ content were performed as described [31]. Briefly cells (1 ml) were harvested by centrifugation ($5500g \times 15$ s) at the indicated times, washed with cold phosphate-buffered saline, pH 7.4 and lysed with 100 μ l of 50 mM NaOH supplemented with 0.1% (w/v) Triton X-100 by heating at 80 °C for 10 min followed by cooling on ice. Incubation media were deproteinized with 100 μ l of ice-cold 45% (v/v) HClO₄ followed by neutralization with 35 μ l saturated K₂CO₃ and 2 μ l 1 M HEPES, pH 7.4 for lactate measurements as described [32]. Fru-2,6-P₂ content is expressed as pmol per mg of protein and medium lactate accumulation as mmol per mg of protein.

2.6. Measurement of glucose uptake

At the indicated times, thymocytes (2 ml in 6-well plates) or Jurkat E6-1 cells (1 ml in 48-well plates) were washed twice with warm phosphate-buffered saline, pH 7.4, to remove glucose from the culture medium. Thymocytes or Jurkat E6-1 cells were incubated in glucose-free RPMI-1640 culture medium (2 ml or 1 ml, respectively) for 20 min at 37 °C in a humidified incubator under 5% CO₂. The cells were then incubated at room temperature for 5 min prior to the addition of 2-deoxy-D-[1-³H]-glucose (0.5 μ Ci per well). After incubation for 15 min at room temperature, glucose uptake was stopped by washing rapidly with ice-cold phosphate-buffered saline followed by lysis with 100 μ l 0.5 M NaOH at room temperature. After 30 min, aliquots (85 μ l) were taken for liquid scintillation counting in 4 ml of scintillant (Ultima Gold™, PerkinElmer). Protein was estimated in an aliquot of remaining mixture (10 μ l) and rates of glucose uptake were calculated as cpm per min per mg of protein.

2.7. Measurement of rates of cell proliferation and protein synthesis

At intervals of 30 min before the indicated times, radioactive tracers [methyl-³H] thymidine (5 μ Ci/ml or 2.5 μ Ci/ml for measurements of proliferation rates in thymocytes or Jurkat E6-1 cells, respectively) or L-[2,3,4,5,6-³H] phenylalanine (10 μ Ci/ml or 5 μ Ci/ml for measurements of protein synthesis rates in thymocytes or Jurkat E6-1 cells, respectively), with 0.09 mM cold phenylalanine coming from the culture medium)

were added to 1 ml of cell suspension (see above for the cell densities of thymocytes or Jurkat E6-1 cells). After 1 h, the cell incubations were stopped by freezing in liquid N₂. Aliquots (200 μ l) of thawed cell suspension were added in triplicate to 96-well plates (MultiScreen_{HTS}-GV, 0.22 μ m Millipore) for filtration and washing twice with 50 μ l PBS. To deproteinize the cells, 200 μ l of 8% (w/v) ice-cold TCA was added for 10 min. The filters were rapidly washed three times with 100 μ l of 8% (w/v) ice-cold TCA followed by washing three times with 100 μ l of ice-cold milliQ-water and finally twice with 100 μ l of 70% (v/v) ice-cold ethanol. The plates were dried and the filters were collected using MultiScreen Disposable Punch Tips (Millipore) for liquid scintillation counting in 4 ml of scintillant (Ultima Gold™, PerkinElmer).

2.8. Cell viability

Cells (200 μ l) were seeded at a density of 3.10^6 cells/ml on 96-well cellstar suspension U-bottom plates (Greiner, Catalogue no. 650185). After incubation under 5% CO₂ at 37 °C, 50 μ l of 3-(4,5-dimethylthiazol-2-yl)-2,5-diphenyltetrazolium bromide (MTT, Sigma-Aldrich, Catalogue no. M5655) diluted in PBS was added to the cells to give a final concentration of 0.6 mg/ml. After 2 h, the cells were collected by centrifugation ($600g \times 10$ min) at 22 °C with minimal deceleration. After removing the supernatant, the pelleted cells were resuspended in 200 μ l DMSO for OD measurements at both 560 nm and 655 nm at 37 °C. Cell viability was expressed as a percentage of viable cells following incubation with or without inhibitors in the presence of 0.1% (v/v) DMSO.

2.9. Quantitative real-time PCR

Thymocytes (10 ml) were collected by centrifugation ($180g \times 5$ min) at the indicated times and washed with cold phosphate-buffered saline. TriPure™ (300 μ l) was added to the pellet and the cells were immediately frozen in liquid N₂. Total RNA was isolated using Direct-zol™ RNA MiniPrep Plus (Zymo Research, Catalogue no. R2070) according to the manufacturer's instructions. The concentration and purity of RNA samples were assessed by NanoDrop 2000c (Thermo Scientific). RNA (400 ng) was used for cDNA synthesis using the ProtoScript® First Strand cDNA Synthesis Kit (Bioké, Catalogue no. E6300) according to the manufacturer's protocol. Reverse transcription products were diluted 1:2 in nuclease-free water and an aliquot (0.6 μ l) was taken for qPCR with a Kapa Sybr Fast qPCR kit (Kapa Biosystems) in a CFX96 Real Time PCR thermocycler (Biorad). The program included 40 cycles at 95 °C for 10 s and at 60 °C for 30 s. A final melting curve was recorded to verify the presence of the desired amplicon. PCR reactions were carried out in a final volume of 10 μ l with each of the following primers at a concentration of 0.6 mM: PFKFB1, 5'-GTTTACCAGC TCGAGGCAAG-3' (forward) and 5'-TGTTGTCTGGGCGAAAGAAT-3' (reverse); PFKFB2, 5'-CCGAGGAAGTGGATCTACCA-3' (forward) and 5'-ATGTTCTGTGGGATGAG-3' (reverse); PFKFB3, 5'-CAGCGGAGAAAT GAGTACA-3' (forward) and 5'-TTCAGCTGACTGGTCCACAC-3' (reverse); PFKFB4, 5'-GGAATTCACGTGGGTCAGT-3' (forward) and 5'-CTCAGGATCCACAGATAGA-3' (reverse); PKB α /Akt1, 5'-GCTGAT GGACTCAAACGGCA-3' (forward) and 5'-CCCGAAGTCCGTTATCTGA-3' (reverse); PKB β /Akt2, 5'-CCCTCTACAACAGGACCA-3' (forward) and 5'-AGAACTGGGGAAAGTGTGTG-3' (reverse); PKB γ /Akt3, 5'-TGGGTT CAGAAGAGGGGAGAA-3' (forward) and 5'-AGGGGATAAGGTAAGT CCACATC-3' (reverse). Determinations were performed on four separate thymocyte incubations in triplicate for relative quantification as described [33].

2.10. Purification of recombinant bacterially expressed PFKFB isoenzymes

Recombinant His-tagged PFKFB1 [34] and His-tagged PFKFB2 [35] were overexpressed in *E. coli* and purified as indicated. GST-tagged PFKFB3 was expressed overnight at 18 °C in BL21 *E. coli* cells induced

with 0.5 mM IPTG. Bacteria were then collected by centrifugation (5000g × 10 min at 4 °C), resuspended in 1/10 of the culture volume of ice-cold lysis buffer (50 mM Tris-HCl, pH 7.5, 150 mM NaCl, 0.1% (v/v) 2-mercaptoethanol, 0.01% (w/v) Brij 35, 0.5 mM PMSF, 0.5 mM benzamidine Cl, 1 µg/ml leupeptin, 1 µg/ml aprotinin) and homogenized using a French press. The lysate was cleared by centrifugation (17,000g × 20 min at 4 °C) and the supernatant was passed through a 45 µm mesh filter (Millex-HA, Merck-Millipore) before loading onto a GSH-Sepharose column (10 ml, 2 × 20 cm, GE Healthcare). After extensive washing, the column was eluted with a 0–10 mM gradient of GSH. Fractions were analyzed by SDS-PAGE/Coomassie Blue staining. Fractions containing GST-tagged PFKFB3 protein were pooled and concentrated using a 50 kDa ultra-filtration unit (Amicon) while changing the buffer to enzyme storage buffer (50 mM Tris-HCl pH 7.5, 150 mM NaCl, 0.1% (v/v) 2-mercaptoethanol, 10% (v/v) glycerol).

The coding sequence of human testis PFK-2/FBPase-2 (PFKFB4) full mature mRNA in pCDNA3 [36] was transferred into pGEX6p1 by PCR with the following primers containing *EcoRI/XhoI* restriction sites: *EcoRI*_PFKFB4 (forward) 5'-AAAAGaattcATGGCGTCCCCACGGGAA-3' and *XhoI*_PFKFB4 5'-AAAActcgagTCACTGGTGAGCAGGCAC-3' (reverse). The construct was validated by Sanger DNA sequencing (Beckman Coulter Genomics). GST-tagged PFKFB4 was expressed overnight at 18 °C in BL21 *E. coli* cells induced with 0.5 mM IPTG for purification as described above for PFKFB3.

2.11. PFK-2 assay

Following phosphorylation of recombinant PFKFB3 by PKB, AMPK and PKA (see below) with non-radioactive ATP and sample dilution, aliquots of reaction mixture (20 µl) were assayed for PFK-2 activity in a final volume of 200 µl [19] except that fructose 6-phosphate (Fru-6-P) concentrations were varied up to 1 mM from a stock solution containing a mixture of 100 mM Fru-6-P/300 mM glucose 6-phosphate (Glc-6-P) to measure the K_M for Fru-6-P with an optimal concentration of MgATP (5 mM). Inhibitors were added from stock DMSO solutions directly to PFK-2 assays [19] in the presence of 2 mM Fru-6-P/6 mM Glc-6-P and 5 mM MgATP. One unit of PFK-2 activity is the amount that catalyzes the formation of 1 µmol of Fru-2,6-P₂ per min under the assay conditions.

2.12. Protein kinase assays

PKB, AMPK and PKA were assayed by measuring ³²P incorporation from 0.1 mM [γ -³²P] MgATP (specific radioactivity 1000 cpm/pmol) into 200 µM AMARA peptide (AMARAASAAALRRR) for AMPK and 200 µM MR6 (PVRMRRNSFT) for PKB and PKA as described [30]. One unit of protein kinase activity corresponds to the amount of kinase that catalyzes the incorporation of 1 nmol of ³²P/min into the peptide substrate under the assay conditions.

2.13. In vitro phosphorylation of PFKFB3 by PKB

Purified GST-tagged PFKFB3 (1 µg) was incubated without or with 200 m-units of recombinant activated PKB, 200 m-units of PKA or 200 m-units of recombinant activated AMPK in 60 µl of reaction mixture containing 10 mM MOPS, pH 7.5, 10 mM MgCl₂, 1 mM dithiothreitol, 0.5 mM EDTA supplemented with 0.1 mM [γ -³²P] MgATP (specific radioactivity 1000 cpm/pmol) at 30 °C up to 45 min to study the time-course and stoichiometry of phosphorylation [19]. Incubations were also carried out under identical conditions with non-radioactive ATP for 60 min prior to sample dilution and PFK-2 assay (see above).

2.14. Phosphorylation site identification by MS

GST-PFKFB3 (5 µg) was incubated as described above with 1 unit of PKB and 0.1 mM [γ -³²P] ATP (specific radioactivity 2000 cpm/pmol) for

60 min at 30 °C. Following tryptic digestion and separation of a single radioactive peak by HPLC, the phosphorylation site was identified by tandem MS [19].

2.15. Immunoblotting

Equal amounts of cell lysates (corresponding to approximately 15 µg of protein) were loaded into each well of a 4–15% polyacrylamide gradient gel (Bio-Rad Laboratories) for protein separation by SDS/PAGE. Proteins were transferred to polyvinylidene difluoride (PVDF) membranes and blocked in 10 mM Tris/HCl, pH 7.4, 0.15 M NaCl and 0.1% (w/v) Tween 20 (TBS-T, Tris-buffered saline plus Tween 20), containing 5% (w/v) non-fat dried skimmed milk powder for 1 h at room temperature (20 °C). After blocking, the membranes were washed briefly in TBS-T and then incubated overnight at 4 °C with primary antibodies diluted in TBS containing 0.1% (w/v) Tween and 5% (w/v) BSA. Anti-pSer461 PFKFB3 and anti-pThr56 eEF2 antibodies were used at dilutions of 1:500 and 1:7500, respectively. All other antibodies were used at dilution of 1:1000. After washing six times with TBS-T for 5 min, the membranes were incubated with appropriate secondary antibodies for 1 h at room temperature and then washed again six times for 5 min with TBS-T. Immunoreactive bands were visualized by ECL Forte substrate (Merck Millipore) for the anti-pSer461 PFKFB3 antibody or by ECL Classico substrate (Merck Millipore) for all other antibodies. Band intensities were quantified by densitometry with ImageJ (NIH) using an appropriate protein loading control. After in vitro phosphorylation of PFKFB3, 0.5 µg aliquots of PFKFB3 protein were separated for SDS-PAGE and immunoblotting with anti-pSer461 PFKFB3 and anti-total PFKFB3 antibodies at dilutions of 1:1000 and 1:10,000, respectively.

2.16. Other methods

Protein concentrations were measured using BSA as a standard [37]. Results are presented as means ± S.E.M. of at least 3 separate experiments or of at least 3 in vitro incubations of PFKFB proteins with protein kinases/inhibitors. Statistical analysis was performed using a paired Student's *t*-test and *P* < 0.05 was considered as significant. Graphs were generated using GraphPad Prism 5.0 (GraphPad software). Powerpoint software was used to process and present the images.

3. Results

3.1. In vitro phosphorylation of PFKFB3 at Ser461 by PKB causes PFK-2 activation

PFKFB3 phosphorylation by AMPK [18] and MK2 [19] was previously shown to lead to PFK-2 activation. Because of the implication of PFKFB3 in cell proliferation and the fact that PI3K signalling increases during thymocyte/T cell activation [28], we first investigated whether PFKFB3 would be targeted by PKB. Incubation with PKB or with AMPK or PKA as positive controls led to time-dependent phosphorylation of PFKFB3 reaching a maximal level of about 0.3 mol phosphate incorporated per mol of PFKFB3 enzyme subunit (Fig. 1A). Following maximal phosphorylation, effects of PKB, AMPK and PKA on PFK-2 activity were measured. Although PKA has been previously shown to phosphorylate PFKFB3 [38], its effects on the kinetic properties of PFK-2 were not fully investigated. As shown in Fig. 1B, treatment with PKB, AMPK or PKA led to PFK-2 activation reflected by an ~2.5- to 3-fold increase in V_{MAX} and 35–50% decrease in K_M for Fru-6-P. After phosphorylation by PKB for 60 min, PFKFB3 Ser461 was found to be phosphorylated by tandem MS (Fig. 1C) in a tryptic peptide purified in a single radiolabelled peak by HPLC. A phospho-specific antibody was raised in rabbit against a PFKFB3 peptide in which Ser461 was phosphorylated. The antibody recognized PFKFB3 phosphorylated by AMPK, PKA or PKB but not when PFKFB3 protein was incubated with ATP alone (Fig. 1D).

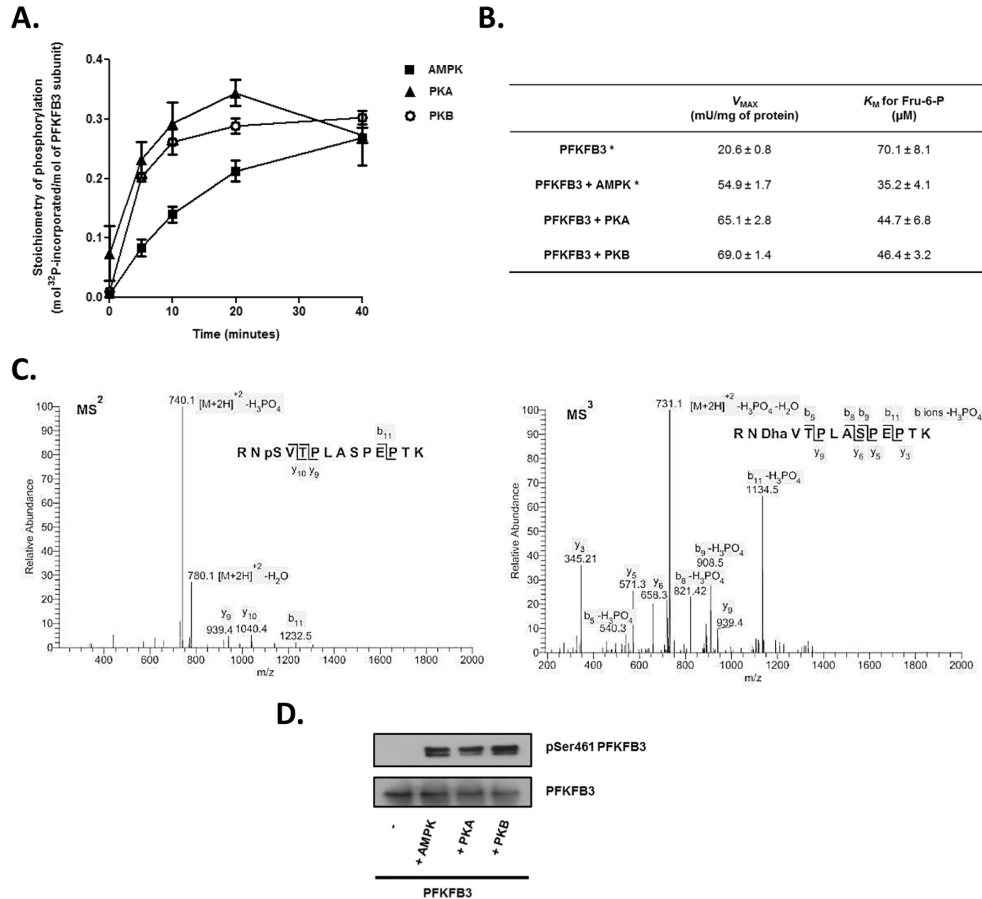
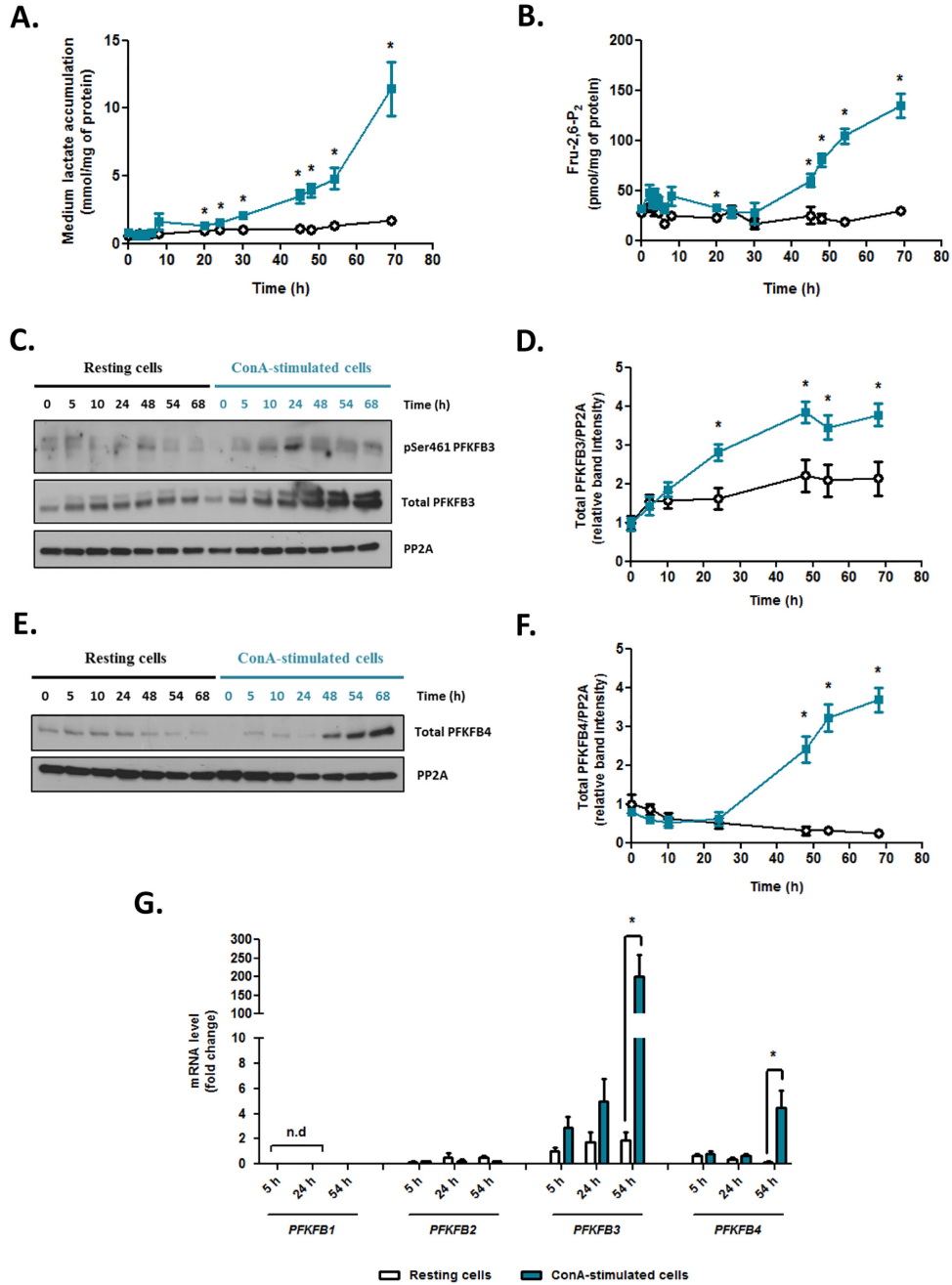


Fig. 1. In vitro phosphorylation of PFKFB3 by PKB, AMPK and PKA leads to PFK-2 activation (A) Time course of phosphorylation of purified PFKFB3 with 0.1 mM [γ - ^{32}P] MgATP and recombinant activated PKB, recombinant activated AMPK or recombinant PKA for 0, 5, 10, 20 and 40 min (see Materials and methods section). (B) Following phosphorylation with non-radioactive ATP, effects of treatment with protein kinases on K_M for Fru-6-P and V_{MAX} are shown. In (A) and (B), the results are means \pm S.E.M. for $n = 3$ –4 separate experiments. * indicates that these values are from [19] where effects of PKB and PKA treatment on the kinetic properties of PFK-2 run in the same experiments were not included. (C) Phosphorylation site identification by tandem MS after incubation for 60 min with PKB (see Materials and methods section). Left panel: MS/MS (MS^2) spectrum of the doubly charged phosphopeptide ion ($m/z = 740.1$). Neutral loss of 98 Da is observed (H_3PO_4) to produce an ion with m/z 740.1. Right panel: three-stage MS (MS^3) spectrum of the ion arising from loss of 98 Da ($m/z = 740.1$ of the doubly charged ion in the left panel). Dha denotes dehydroalanine, identifying the product of phosphoserine after losing H_3PO_4 and the b and y labels refer to ions containing the N- or C-terminal ends of the molecule respectively. The y- and b- series of ions allow exact localization of the phosphorylated residue as Ser461. (D) Purified PFKFB3 was incubated with non-radioactive ATP alone (–) or in combination with protein kinases as described above for SDS-PAGE and immunoblotting with anti-pSer461 PFKFB3 antibody (see Materials and methods section).

3.2. Time course of effects of ConA stimulation of thymocytes on Fru-2,6-P₂ content, lactate accumulation, PFKFB isoenzyme protein and mRNA expression and PFKFB3 Ser461 phosphorylation.

When isolated thymocytes in culture were incubated with ConA in the presence of IL-2, medium lactate concentrations began to increase significantly after 20 h of stimulation and continued to rise in a time-dependent manner, reaching an increase of 6-fold at 68 h compared with non-stimulated cells (Fig. 2A). Fru-2,6-P₂ concentrations fluctuated up to 30 h of stimulation, but a significant and dramatic progressive

increase was seen thereafter, reaching a 4-fold increase at 68 h compared with non-stimulated cells (Fig. 2B). PFKFB3 expression began to increase after 5–10 h of culture of both stimulated and non-stimulated thymocytes, and ConA stimulation increased PFKFB3 levels ~2-fold at 68 h compared with non-stimulated cells (Fig. 2C, D). The doublet seen by immunoblotting could correspond to the two C-terminal splice variants of the PFKFB3 gene [39] and the increase in PFKFB3 expression was based on quantification of the band intensity of the doublet in Fig. 2D. PFKFB3 Ser461 phosphorylation was barely detectable in resting cells and only increased slightly during ConA-stimulation (Fig. 2C).



PFKFB4 expression began to increase after 24 h of stimulation by ConA, reaching an ~15-fold increase at 68 h compared with non-stimulated cells (Fig. 2E, F). A comparison of PFKFB3 versus PFKFB4 protein expression during ConA stimulation cannot be assessed by immunoblotting because antigen recognition by the anti-total PFKFB3 and PFKFB4 antibodies would likely not be the same. Therefore, we measured PFKFB isoenzyme expression by quantitative real-time PCR. The data could not be quantified relative to a control mRNA because all reference mRNA levels we tested (protein phosphatase-1B, PP2A, 18S ribosomal RNA, glyceraldehyde phosphate dehydrogenase and isocitrate dehydrogenase) increased during ConA stimulation. Using the same quantity of total mRNA for quantitative real-time PCR for all conditions, mRNA levels were normalized to the level of PFKFB3 mRNA at 5 h of incubation in resting cells as reference. PFKFB3 mRNA levels increased 40-fold from 24 h to 54 h of ConA stimulation, whereas PFKFB4 mRNA content increased 7.5-fold over the same period (Fig. 2G). After 54 h of ConA stimulation, PFKFB3 mRNA levels were 45-fold higher than those of PFKFB4. PFKFB1 and PFKFB2 mRNA levels were barely detectable or very low respectively and did not increase during ConA stimulation. PFKFB3 mRNA levels were 100-fold higher in ConA-stimulated versus resting cells after 54 h of incubation whereas the increase in PFKFB4 mRNA was 25-fold (Fig. 2G).

3.3. Time course of effects of ConA stimulation of thymocytes on rates of cell proliferation and protein synthesis, expression levels/phosphorylation states of signalling proteins/translation factors and PKB isoform mRNA expression

After 20 h of stimulation of thymocytes by ConA, rates of cell proliferation measured by [³H]-thymidine incorporation and protein synthesis measured by [³H]-phenylalanine incorporation increased dramatically and significantly, reaching increases of ~40-fold and 10-fold, respectively, at 68 h compared with non-stimulated cells (Fig. 3A, B). ConA stimulation increased p38 MAPK Thr180/Tyr182 and PKB Ser473 phosphorylation, without affecting the levels of total proteins compared with non-stimulated cells (Fig. 3C). ConA stimulation also led to increased mTOR Ser2448 (PKB site) phosphorylation. Increases in phosphorylation of 4E-BP1 at the Thr37/Thr46 mTOR kinase sites and rpS6 at the Ser240/Ser244 p70S6K sites along with a decrease in phosphorylation of eEF2 Thr56 were observed after 48 h, 54 h and 68 h of stimulation by ConA and at these times significant increases in expression levels of eEF2, 4E-BP1 and rpS6 were seen (Fig. 3C). Measurements of PKB isoform mRNA levels by quantitative real-time PCR, for quantification relative to PKB α mRNA levels in resting cells after 5 h of incubation, indicated that between 24 and 54 h of ConA stimulation, PKB α and PKB β mRNA levels increased ~40-fold (Fig. 3D). After 54 h of ConA stimulation, PKB α mRNA levels were ~20-fold higher than those of PKB β (Fig. 3D). Although detectable, PKB γ mRNA levels were very low compared with the other two isoforms.

3.4. Inhibition of PFK-2 activity of PFKFB isoenzymes by 3PO

The small molecule inhibitor of PFK-2 activity of the PFKFB3 isoenzyme, 3PO, inhibits glycolysis and reduces cancer cell proliferation

[17]. Prior to testing its effects on thymocytes, we investigated its inhibitory action on PFK-2 activities of the four purified recombinant PFKFB isoenzymes after overexpression in *E. coli*. PFK-2 activity of all four PFKFB isoenzymes was inhibited by 3PO with similar IC₅₀ values and no selectivity for the PFKFB3 isoenzyme (Fig. 4).

3.5. Effects of 3PO and MK-2206 on Fru-2,6-P₂ content, lactate production and glucose uptake in ConA-stimulated thymocytes

Before testing effects of 3PO and PKB inhibitor (MK-2206) in ConA-stimulated thymocytes, effects of the inhibitors on cell viability was assessed by MTT test. After incubation of thymocytes with IL-2 and ConA for 24 h, inhibitors were added prior to measurements of cell viability after incubation for a further 30 h (total incubation time = 54 h of mitogen stimulation). Cytotoxic effects were seen at concentrations of 10 μ M 3PO (Fig. S1A) and 1 μ M MK-2206 (Fig. S1B). In thymocytes treated with non-toxic concentrations of 3 μ M 3PO, representing doses 15-times lower than the IC₅₀ for PFK-2 inhibition (Fig. 4), significant ~20%, ~35% and ~50% decreases in medium lactate, Fru-2,6-P₂ content and glucose uptake were seen, respectively (Fig. 5A, C, E), following the same protocol described above for studying cell viability. Treatment with non-toxic concentrations of 0.3 μ M MK-2206 using the same protocol led to significant ~20%, ~40% and ~50% decreases in medium lactate, Fru-2,6-P₂ content and glucose uptake, respectively (Fig. 5B, D, F). In cell free assays, incubation of purified PFKFB3 with MK-2206 up to a concentration of 30 μ M had no effect on PFK-2 activity (data not shown).

3.6. Effects of 3PO and MK-2206 on PFKFB3/4 protein/mRNA expression and phosphorylation levels of PFKFB3 Ser461 in ConA-stimulated thymocytes

Following the same protocol described above for studying cell viability, treatment with 3 μ M 3PO did not significantly affect PFKFB3/4 protein expression or PFKFB3 phosphorylation, whereas treatment with 0.3 μ M MK-2206 significantly decreased protein levels of both PFKFB3 and PFKFB4 by ~35% and ~45%, respectively, but without affecting the extent of PFKFB3 Ser461 phosphorylation (Fig. 6A, B). Measurement of PFKFB3/4 expression by quantitative real-time PCR showed that treatment with non-toxic concentrations of 0.3 μ M MK-2206 led to significant ~90% and ~70% decreases in PFKFB3 and PFKFB4 mRNA levels, respectively (Fig. 6C).

3.7. Effects of 3PO and MK-2206 on rates of proliferation and protein synthesis along with phosphorylation levels of PKB, p70S6K and 4E-BP1 in ConA-stimulated thymocytes

In ConA-stimulated thymocytes treated with non-toxic concentrations of 3 μ M 3PO using the same incubation protocol as that used to assess cytotoxicity (see above), significant ~50% and ~45% decreases in the rates of cell proliferation and protein synthesis were observed, respectively (Fig. 7A, B). Treatment with non-toxic concentrations of 0.3 μ M MK-2206 led to significant ~45% decreases in the rates of cell proliferation and of protein synthesis (Fig. 7C, D). Treatment with 0.3 μ M MK-2206 almost completely abolished PKB

Fig. 2. Time-course of effects of ConA stimulation on medium lactate accumulation (A), Fru-2,6-P₂ content (B), PFKFB3/4 protein expression (C, D, E, F), PFKFB3 phosphorylation (C) and mRNA levels of PFKFB1/2/3/4 (G). Freshly isolated rat thymocytes were cultured with 100 U/ml IL-2 without (resting cells) (○) or with 3 μ g/ml ConA (ConA-stimulated cells) (■). At the indicated times, thymocytes were harvested for measurements of Fru-2,6-P₂ content or for preparing cell extracts for immunoblotting and incubation media were retained for lactate assay. Thymocyte extracts from at least three independent experiments were immunoblotted with the indicated antibodies. Blots were quantified by calculating the ratios of band intensities obtained with anti-total PFKFB3 and anti-total PFKFB4 antibodies relative to those obtained with anti-PP2A catalytic subunit and representative blots are shown. (G) In separate experiments, total RNA was extracted for cDNA synthesis and real-time PCR using specific primers for the rat PFKFB1/2/3/4 isoenzymes (see Materials and methods section). Fold changes are relative to PFKFB3 mRNA levels in resting cells after 5 h of incubation. In (A), (B), (D), (F) and (G), the results are means \pm S.E.M. for n = 3–4 separate experiments and * indicates a significant difference compared with the resting condition ($P < 0.05$, paired *t*-test).

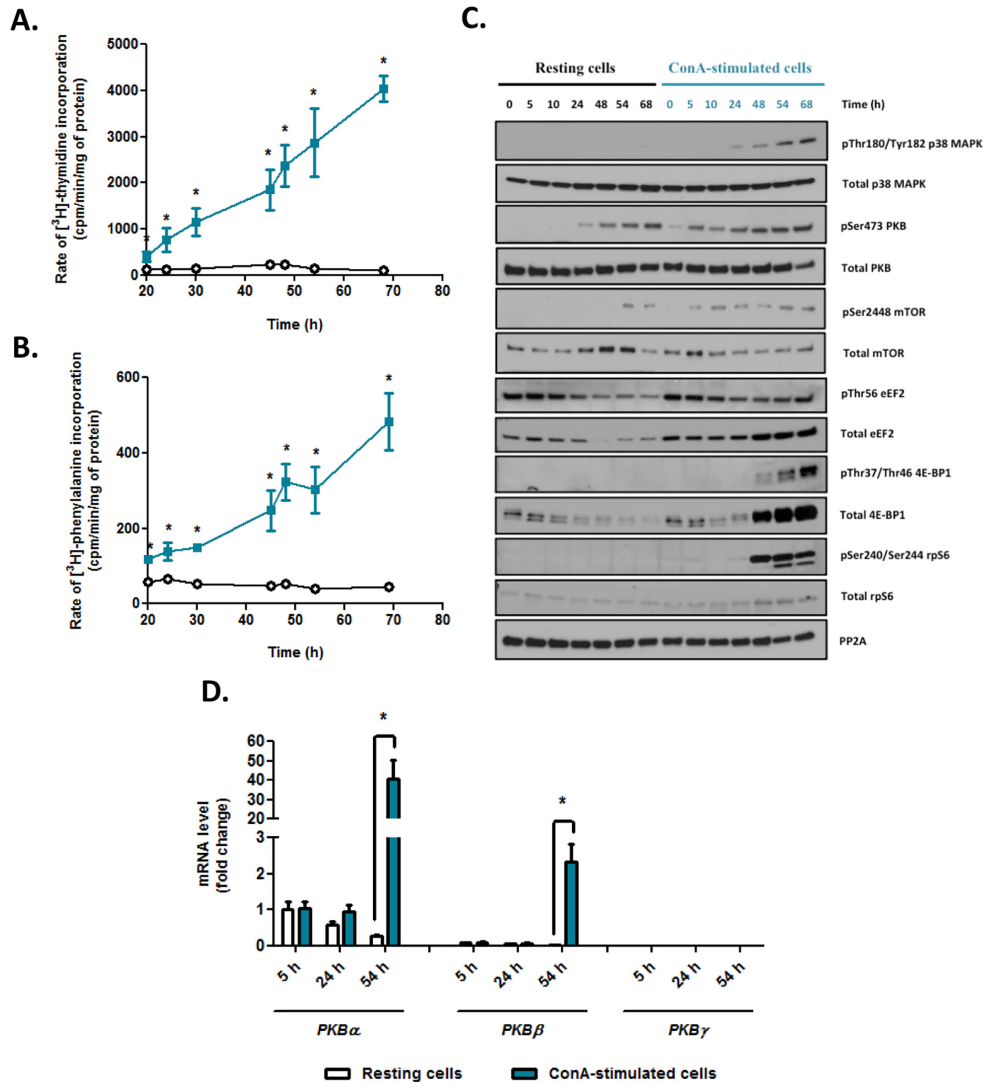


Fig. 3. Time-course of effects of ConA-stimulation on rates of cell proliferation (A) and protein synthesis (B), phosphorylation and expression levels of signalling proteins/translation factors (C) and mRNA levels of PKB isoforms (D). Rat thymocytes were incubated as described in the legend to Fig. 2. Radioactive tracers were added 30 min before the indicated times for measurements of rates of cell proliferation and protein synthesis over 1 h as described in the Materials and methods section. Alternatively, cells were freeze-stopped at the indicated times and extracts from at least three independent experiments were immunoblotted with the indicated antibodies (C). Representative blots are shown. (D) In separate experiments, total RNA was extracted for cDNA synthesis and real-time PCR using specific primers for the rat PKB isoforms (see Materials and methods section). Fold changes are relative to PKB α mRNA levels in resting cells after 5 h of incubation. The results are means \pm S.E.M. for $n = 7$ (A, B), or $n = 4$ (D) separate experiments and * indicates a significant difference compared with the resting condition ($P < 0.05$, paired t -test).

Ser473 phosphorylation and reduced levels of p70S6K Thr389 phosphorylation by ~50% and 4E-BP1 Thr37/Thr46 phosphorylation by ~40%, whereas treatment with 3 μM 3PO had no effect on PKB

Ser473 phosphorylation but slightly and significantly decreased p70S6K Thr389 and 4E-BP1 Thr37/Thr46 phosphorylation by ~20% (Fig. 7E, F).

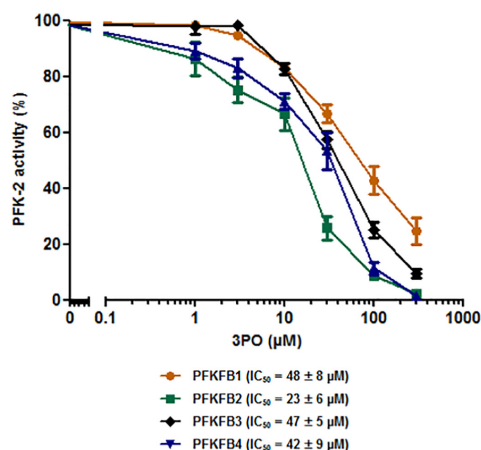


Fig. 4. Effect of 3PO on PFK-2 activity of PFKFB isoenzymes. PFK-2 activity was measured with 2 mM Fru-6-P/6 mM Glc-6-P and 5 mM MgATP with 3PO concentrations ranging from 1 to 300 μ M. The results are the means \pm S.E.M. of 4 determinations and IC_{50} values were calculated by curve fitting to each set of data using GraphPad Prism 5.0 software.

3.8. Effects of other signalling pathway inhibitors on lactate accumulation, Fru-2,6-P₂ content and rates of cell proliferation and protein synthesis in ConA-stimulated thymocytes

In thymocytes incubated for 24 h with both IL-2 and ConA prior to the addition of rapamycin (inhibitor of mTORC1) for a further 30 h, significant decreases in lactate accumulation (~20%), Fru-2,6-P₂ content (~45%) and in the rates of cell proliferation (~35%) were observed (Fig. S2A–C). Treatment with Torin (inhibitor of both mTORC1 and mTORC2) using the same protocol led to significant decreases in lactate accumulation (~25%), Fru-2,6-P₂ content (~70%) and in the rates of cell proliferation (~90%) and protein synthesis (~80%) (Fig. S2A–D). In ConA-stimulated thymocytes treated with 10 μ M PD169316 (p38 MAPK inhibitor and inhibitor of MK2 activation) using the same protocol, significant decreases in lactate accumulation (~10%), Fru-2,6-P₂ content (~65%) and in the rates of cell proliferation (~95%) and protein synthesis (~80%) were seen. Although treatment with wortmannin (PI3K inhibitor) slightly but significantly decreased lactate accumulation (~15%) and Fru-2,6-P₂ content (~20%), there was no effect on the rates of cell proliferation or protein synthesis (Fig. S2A–D).

3.9. Effects of siRNA knockdown of PFKFB3, PFKFB4 and PKB on lactate accumulation, Fru-2,6-P₂ content, glucose uptake and rates of cell proliferation and protein synthesis in constitutively proliferating Jurkat E6-1 cells

Since proliferating rat thymocytes are not amenable to transient or stable transfection, to back up the inhibitor data obtained in thymocytes we resorted to the use of siRNA knockdown in Jurkat E6-1 cells, a constitutively proliferating immortalized line of T lymphocytes deficient in phosphatase and tensin homolog (PTEN) leading to constitutive activation of PKB. Transfection of Jurkat E6-1 cells for 48 h with siRNAs directed against PFKFB3, PFKFB4 or PKB α/β isoforms led to decreases in their protein expression levels as judged by immunoblotting extracts from siRNA transfected cells versus cells transfected with scrambled siRNA

(Fig. 8A). PFKFB3 knockdown resulted in significant decreases in lactate accumulation (~45%), Fru-2,6-P₂ content (~50%) and rates of cell proliferation (~40%) and protein synthesis (~35%), respectively, compared with cells transfected with scrambled siRNA (Fig. 8B, C, E, F). PFKFB4 silencing also resulted in significant decreases in lactate accumulation (~60%), Fru-2,6-P₂ content (~40%), and rates of cell proliferation (~75%) and protein synthesis (~45%) (Fig. 8B, C, E, F). PKB α/β isoform knockdown resulted in significant decreases in lactate accumulation (~25%), Fru-2,6-P₂ content (~30%) and rates of cell proliferation (~45%) and protein synthesis (~65%) compared with cells transfected with scrambled siRNA (Fig. 8B, C, E, F). PKB α/β silencing also led to a significant ~50% decrease in glucose uptake (Fig. 8D).

4. Discussion

ConA-stimulated rat thymocytes represent a useful model to study changes in metabolism as cells undergo a transition from the resting to proliferating state. Enhanced utilization of glucose has been observed in proliferating rat thymocytes in concert with increased DNA synthesis and increased glycolytic enzyme activities [3]. Surprisingly, measurements of Fru-2,6-P₂ do not seem to have been made in this model. In the present study we show that after a lag period of about 30 h, Fru-2,6-P₂ concentrations increased during ConA stimulation reaching levels ~4-fold higher compared with non-stimulated resting cells after 68 h (Fig. 2B). Moreover, Fru-2,6-P₂ concentrations in ConA-stimulated cells rose to 150 pmol/mg of protein, similar to values measured in mitogen-stimulated or transformed cells, which would correspond to a concentration of about 50 μ M and much higher than required to stimulate PFK-1 activity [8,11]. This suggests that Fru-2,6-P₂ might have targets other than glycolysis. It has been speculated that Fru-2,6-P₂ could couple the stimulation of glycolysis to cell proliferation. Fru-2,6-P₂ addition to a HeLa cell lysate increased phosphorylation of the cell cycle inhibitor p27 at the cyclin-dependent kinase (Cdk)-specific Thr187 site [40], although it is highly unlikely that Fru-2,6-P₂ could act as phosphoryl donor. Also, ConA-induced increases in Fru-2,6-P₂ (Fig. 2B) were mirrored by increases in the rates of cell proliferation (Fig. 3A) and protein synthesis (Fig. 3B) and increases in phosphorylation states of the translation factors, rpS6 and 4E-BP1 (Fig. 3C). Results obtained with the PFK-2 inhibitor, 3PO, should be considered with caution, as the compound inhibited PFK-2 activity of all four PFKFB isoenzymes (Fig. 4). Nevertheless, consistent with previous studies [17,41,42], treatment of ConA-stimulated thymocytes with a non-toxic dose of 3 μ M 3PO led to parallel and significant decreases in lactate accumulation (Fig. 5A), Fru-2,6-P₂ concentration (Fig. 5C), glucose uptake (Fig. 5E) and rates of cell proliferation (Fig. 6A) and protein synthesis (Fig. 6B) accompanied by small (~20%) but significant decreases in p70S6K and 4E-BP1 phosphorylation (Fig. 6E).

The PFKFB3 isoenzyme has been shown to be present in proliferating and transformed cells and might be essential for tumor growth [43]. However, PFKFB4 [44,45] and PFKFB2 [46] might also be important for tumorigenesis. Our data show that PFKFB3 isoenzyme is predominantly expressed in ConA-stimulated thymocytes (Fig. 2G) and PFKFB3 protein expression increased ~2-fold after 68 h of ConA stimulation (Fig. 2C–D). PFKFB2 expression was weak by immunoblotting and did not change during incubation of ConA-stimulated or resting thymocytes (not shown). Interestingly, the profile of the increase in expression of PFKFB4 in ConA-stimulated cells after a lag period of 24–30 h (Fig. 2F) was similar to the profiles for the increases in medium lactate accumulation (Fig. 2A), Fru-2,6-P₂ content (Fig. 2B) and the rates of cell proliferation (Fig. 3A) and protein synthesis (Fig. 3B).

The lag period of ConA stimulation, before the metabolic parameters began to increase, seems to correspond to the approximate time interval needed for mitogen-induced expression of the IL-2R α [47], particularly for the expression of the IL-2R α subunit that rose after 24 h of thymocyte Con A stimulation (data not shown). PKB became activated during ConA-stimulation of thymocytes, as reflected by an increase in

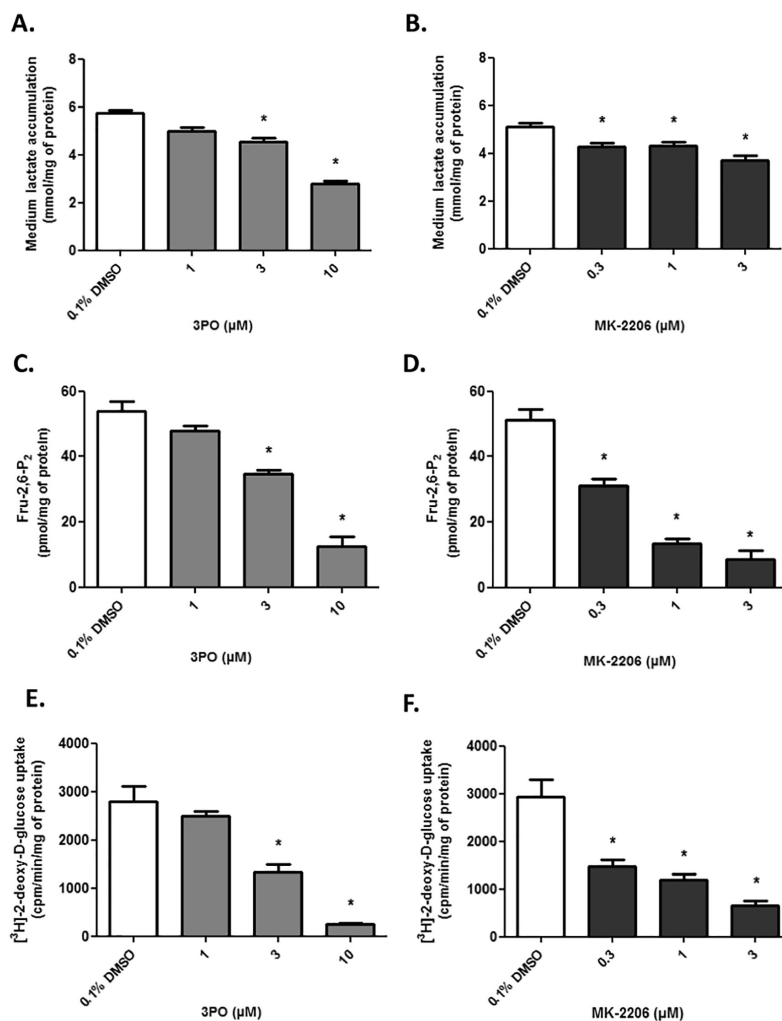


Fig. 5. Effects of 3PO and MK-2206 treatment of ConA-stimulated thymocytes on medium lactate accumulation (A, B), Fru-2,6-P₂ content (C, D) and glucose uptake (E, F). Rat thymocytes were stimulated with ConA and after 24 h inhibitors were added. After a further 30 h of incubation, the cells were harvested for measurements of medium lactate concentrations and Fru-2,6-P₂ content. In separate experiments, ConA-stimulated thymocytes treated with and without inhibitors were incubated with radioactive 2-deoxyglucose for measurements of glucose uptake. The results are means \pm S.E.M. for $n = 3-4$ separate experiments and *indicates a significant difference compared with control incubations with DMSO ($P < 0.05$, paired t -test).

PKB Ser473 and downstream mTOR Ser2448 phosphorylation (Fig. 3C). PKB was found to activate PFK-2 by phosphorylating PFKFB3 Ser461 (Fig. 1), whereas PFKFB4 was a very poor PKB substrate (data not shown). However, PFKFB3 Ser461 phosphorylation only increased slightly in ConA-stimulated cells (Fig. 2C), and was unaffected by pre-incubation of ConA-stimulated cells with low doses of the PKB inhibitor MK-2206 (Fig. 6B), that acts by interfering with its PH domain. A possible explanation is that the extent of PKB activation was not sufficient to

effectively phosphorylate PFKFB3 in ConA-stimulated thymocytes. PFKFB3 Ser461 phosphorylation thus seems not to be important for increasing Fru-2,6-P₂ levels and glycolysis during ConA stimulation. By contrast, mRNA (Fig. 6A) and protein levels (Fig. 6B, C) of PFKFB3 and PFKFB4 were decreased by exposure of ConA-stimulated cells to a non-toxic dose of 0.3 μ M MK-2206, suggesting control of expression of the two PFKFB isoenzymes by PKB (Fig. 6). It has been demonstrated that *pfkfb3* gene was hypoxia-inducible and stimulated through

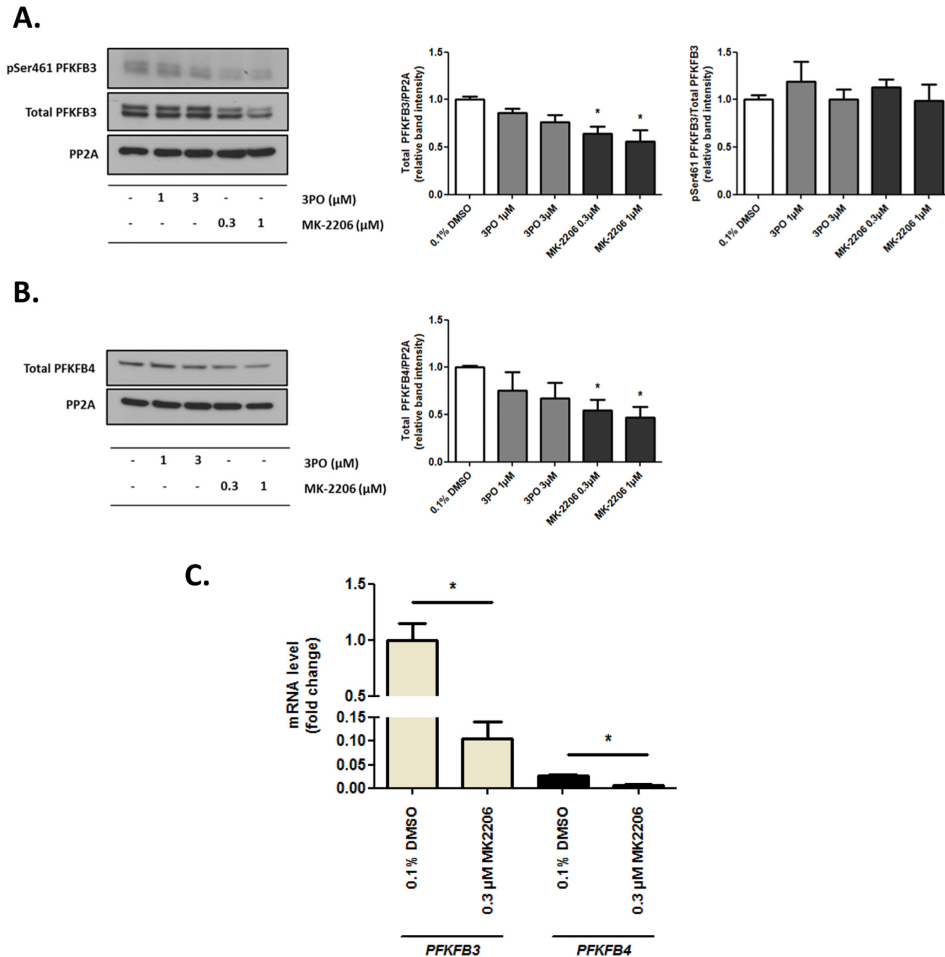
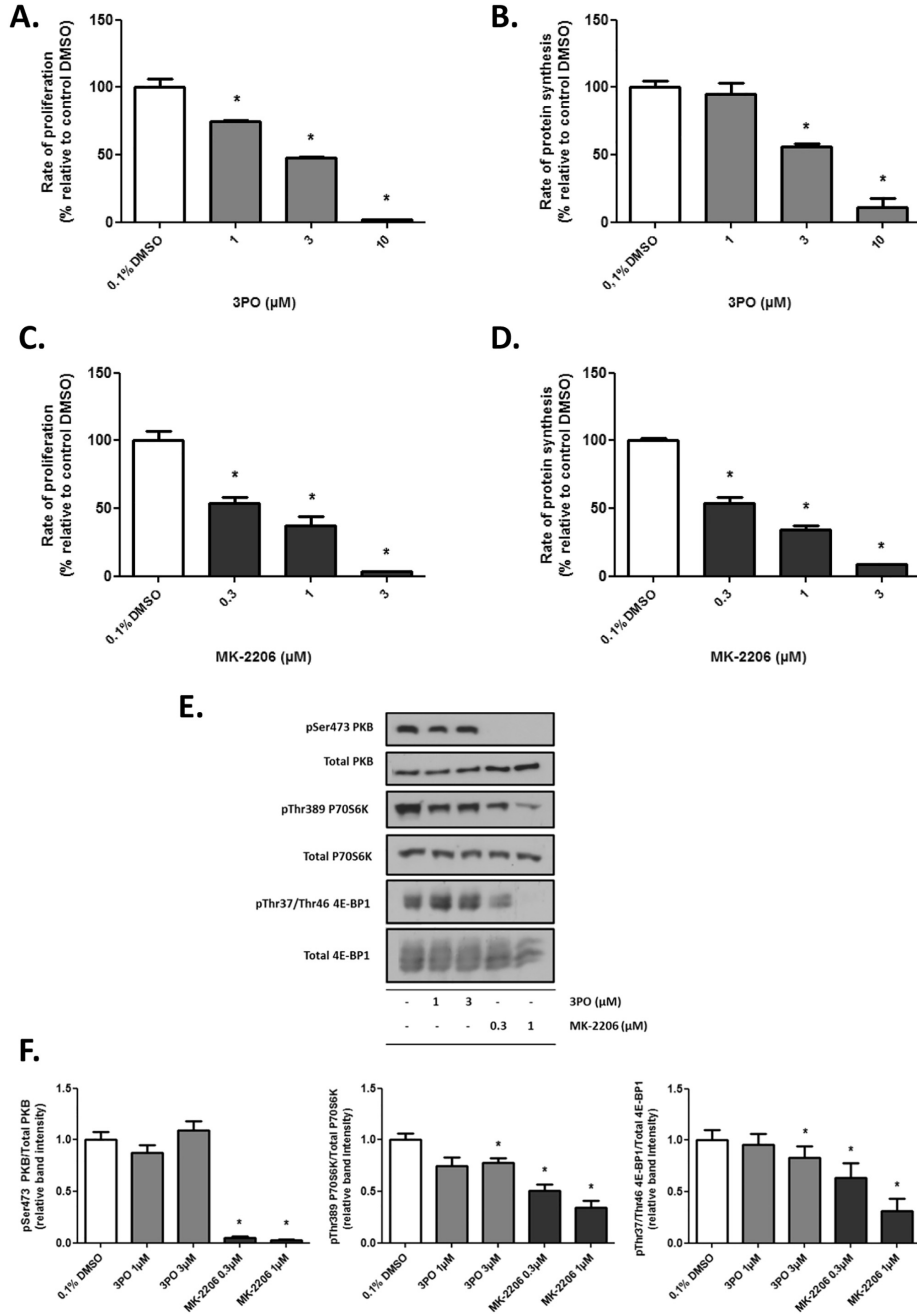


Fig. 6. Effects of 3PO and MK-2206 treatment of ConA-stimulated thymocytes on PFKFB3/4 expression and PFKFB3 Ser461 phosphorylation. Rat thymocytes were stimulated with ConA and treated with inhibitors as described in the legend to Fig. 5. The cells were harvested for RNA preparation or extracted for immunoblotting. (A, B) Thymocyte extracts were immunoblotted with the indicated antibodies and blots were quantified by calculating the ratios of band intensities obtained with anti-total PFKFB3 and anti-total PFKFB4 antibodies relative to those obtained with anti-PP2A catalytic subunit antibody. Band intensities obtained with anti-phospho PFKFB3 Ser461 antibody were calculated relative to intensities obtained with anti-total PFKFB3 antibody. Representative blots are shown. (C) Total RNA was taken for cDNA synthesis and real-time PCR using specific primers for the rat PFKFB3/4 isoenzymes. Fold changes are relative to PFKFB3 mRNA levels in control DMSO-treated thymocytes. The results are means \pm S.E.M. for $n = 3$ –4 separate experiments and * indicates a significant difference compared with control incubations with DMSO ($P < 0.05$, paired t -test).

hypoxia-inducible factor (HIF) interaction with the consensus hypoxia response element (HRE) site in its promoter region [48]. In response to ConA-stimulation, *pfkfb3* gene expression could be increased via the PI3K/PKB pathway and transcription factor HIF-1 binding to the HREs within the *pfkfb3* gene promoter. Also, p53 was recently shown to negatively regulate PFKFB4 expression by directly binding to the promoter of the *pfkfb4* gene [49]. It is also noteworthy that PKB phosphorylates and inactivates forkhead box O (FoxO) transcription factors implicated in cell survival, growth and proliferation [50]. Decreases in lactate

accumulation (Fig. 5B) and Fru-2,6-P₂ content (Fig. 5D) in ConA-stimulated cells preincubated with 0.3 μM MK-2206 were thus due to decreases in PFKFB3/4 expression (Fig. 6) rather than changes in PFKFB3 phosphorylation.

As expected, through increased mTORC1 signalling via PKB activation, treatment of ConA-stimulated thymocytes with 0.3 μM MK-2206 decreased cell proliferation (Fig. 7C), protein synthesis (Fig. 7D), severely abrogated PKB Ser473 phosphorylation and substantially reduced p70S6K and 4E-BP1 phosphorylation (Fig. 6E). Concerning the



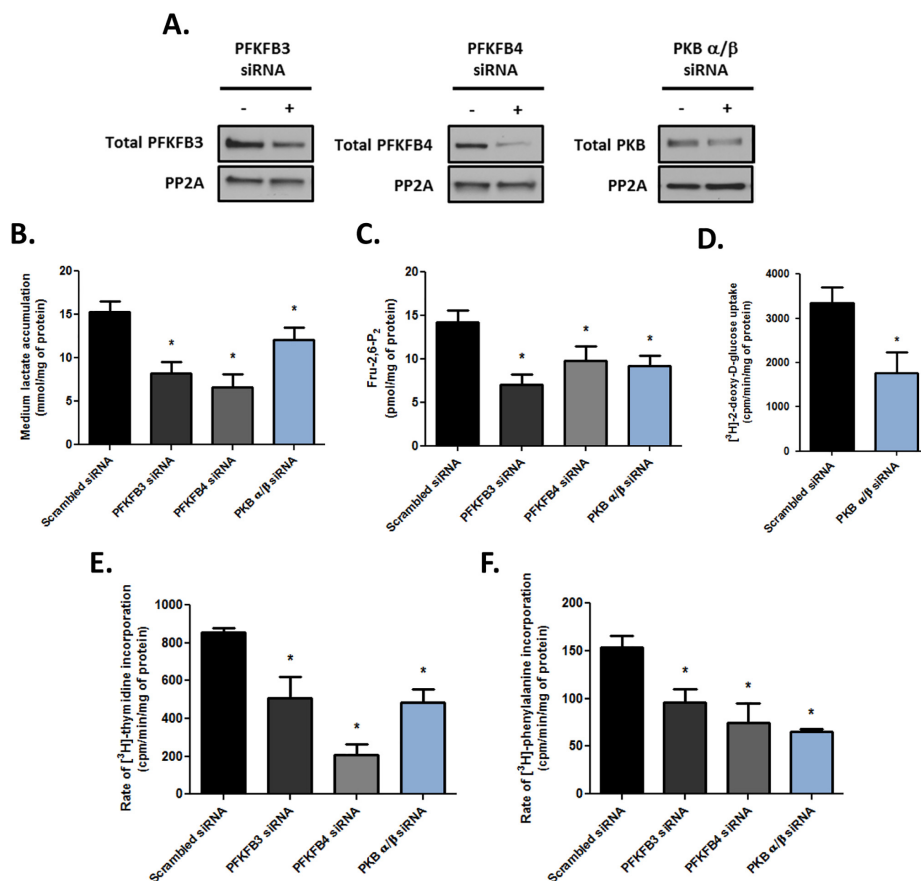


Fig. 8. Effects of PFKFB3, PFKFB4 and PKB α/β silencing (A) on lactate accumulation (B), Fru-2,6-P₂ content (C), glucose uptake (D) and rates of cell proliferation (E) and protein synthesis (F) in Jurkat E6-1 cells. Jurkat E6-1 cells were transiently transfected with scrambled siRNA or the same amounts of siRNA directed against PFKFB3, PFKFB4 or PKB α/β for 48 h as described in the Materials and methods section. The cells were harvested for immunoblotting with the indicated antibodies (A) and for measurements of medium lactate accumulation and Fru-2,6-P₂ content. In parallel, cells were incubated for measurements of glucose uptake and rates of cell proliferation and protein synthesis (see Materials and methods section). The results are means \pm S.E.M. for $n = 4-6$ separate experiments and * indicates a significant difference ($P < 0.05$, paired t -test).

signalling pathways downstream of ConA/IL-2, the inhibitor data with Torin and PD169316 (Fig. S2) suggest possible roles for mTORC1/2 and p38 MAPK/MK2 in the control of Fru-2,6-P₂ content, perhaps by decreasing PFKFB isoenzyme expression [19], and in the control of cell proliferation and protein synthesis. The increase in protein synthesis resulting from ConA stimulation would be partly due to increased expression of translation factors together with increased (4E-BP1, rpS6) or decreased (eEF2) phosphorylation (Fig. 3C).

To confirm the results obtained with inhibitors in thymocytes, we used siRNA knockdown of PFKFB3, PFKFB4 and PKB α/β in more easily transfectable Jurkat E6-1 cells. PKB α/β siRNA knockdown reduced the rates of cell proliferation and protein synthesis as expected (Fig. 8E, F) but also decreased lactate accumulation (Fig. 8B) and Fru-2,6-P₂ content (Fig. 8C) in agreement with the effects of MK-2206 to reduce medium lactate accumulation, Fru-2,6-P₂ content and PFKFB3/4 isoenzyme expression in ConA-stimulated thymocytes. As expected PFKFB3 and

Fig. 7. Effects of 3PO and MK-2206 treatment of ConA-stimulated thymocytes on the rates of cell proliferation (A, C), protein synthesis (B, D) and phosphorylation levels of PKB, p70S6K and 4E-BP1 (E, F). Rat thymocytes were stimulated with ConA and treated with inhibitors as described in the legend to Fig. 5. The cells were then incubated for measurements of rates of cell proliferation and protein synthesis. The 100% values for the rates of proliferation and protein synthesis correspond to 2324 ± 125 and 197 ± 88 cpm per min per mg of protein, respectively. In (E), thymocyte extracts were immunoblotted with the indicated antibodies and a representative blot is shown. Blots were quantified by calculating the ratios of band intensities obtained with anti-phospho antibodies relative to those obtained with anti-total protein antibodies (F). The results are means \pm S.E.M. for $n = 3-4$ separate experiments and * indicates a significant difference ($P < 0.05$, paired t -test).

PFKFB4 silencing decreased lactate accumulation (Fig. 8B) and Fru-2,6-P₂ content (Fig. 8C). Incubation of ConA-stimulated thymocytes with 3PO or MK-2206 decreased glucose uptake (Fig. 5E, F) and PKB α/β silencing in Jurkat cells also decreased glucose uptake. Therefore, reduced glucose uptake by PKB inhibition could independently contribute to reduced Fru-2,6-P₂ levels by decreased substrate availability in addition to decreases in PFKFB levels. Surprisingly, siRNA silencing of PFKFB3 and PFKFB4 significantly reduced the rates of cell proliferation and protein synthesis (Fig. 8E, F). Therefore, despite constitutive activation of PI3K/PKB signalling in Jurkat E6-1 cells, decreased expression of PFKFB3 or PFKFB4 seems to be sufficient to affect cell proliferation and protein synthesis.

In summary, the findings suggest that increased PFKFB3 and PFKFB4 expression, but not increased PFKFB3 Ser461 phosphorylation, plays a role in increasing glycolysis in mitogen-stimulated thymocytes. PKB phosphorylation and PFKFB3 expression were increased in resting cells at later time points and at certain time points similar levels of PKB Ser473 phosphorylation and PFKFB3/4 were observed in non-stimulated and ConA-stimulated thymocytes (Fig. 2C–F; Fig. 3C) yet only stimulated cells exhibit increased proliferation and protein synthesis. Therefore, increased PKB Ser473 phosphorylation and PFKFB3/4 alone would not be sufficient to induce the metabolic and proliferative effects of mitogen stimulation. However, the results implicate PKB in the up-regulation of PFKFB3 and PFKFB4 and underline its importance for cell proliferation and protein synthesis during ConA stimulation. Lastly, the data support a role for Fru-2,6-P₂ in coupling glycolysis to cell proliferation and protein synthesis.

Acknowledgements

We thank Asia El Aakchioui, Nusrat Hussain and Gaëtan Herinckx for technical assistance. We also thank Sophie Lucas for providing Jurkat E6-1 cells and Françoise Bontemps for assistance. The work was funded by the Interuniversity Poles of Attraction Belgian Science Policy (P6/28 and P7/13), by the Directorate General Higher Education and Scientific Research, French Community of Belgium, and by the Fund for Medical Scientific Research (FNRS, Belgium) grant numbers 3.4518.11 and T.0008.15 and by Instituto de Salud Carlos III - FIS (PI13/0096) and Fondo Europeo de Desarrollo Regional (FEDER) to RB.

Appendix A. Supplementary data

Supplementary data to this article can be found online at <http://dx.doi.org/10.1016/j.cellsig.2017.02.019>.

References

- [1] O. Warburg, K. Posener, E. Negelein, Ueber den Stoffwechsel der Carcinomzelle, *Biochem. Z.* 152 (1924) 309–344.
- [2] S.Y. Lunt, M.G. Vander Heiden, Aerobic glycolysis: meeting the metabolic requirements of cell proliferation, *Annu. Rev. Cell Dev. Biol.* 27 (2011) 441–464.
- [3] K. Brand, Glutamine and glucose metabolism during thymocyte proliferation. Pathways of glutamine and glutamate metabolism, *Biochem. J.* 228 (2) (1985) 353–361.
- [4] C.J. Hedeskov, Early effects of phytohemagglutinin on glucose metabolism of normal human lymphocytes, *Biochem. J.* 110 (2) (1968) 373–380.
- [5] D.A. Hume, J.L. Radik, E. Ferber, M.J. Weidemann, Aerobic glycolysis and lymphocyte transformation, *Biochem. J.* 174 (1978) 703–709.
- [6] W.H. Munyon, D.J. Merchant, The relation between glucose utilization, lactic acid production and utilization and the growth cycle of L strain fibroblasts, *Exp. Cell Res.* 17 (3) (1959) 490–498.
- [7] T. Wang, C. Marquardt, J. Foker, Aerobic glycolysis during lymphocyte proliferation, *Nature* 261 (1976) 702–705.
- [8] M.H. Rider, L. Bertrand, D. Vertommen, P.A. Michels, G.G. Rousseau, L. Hue, 6-phosphofructo-2-kinase/fructose-2,6-bisphosphatase: head-to-head with a bifunctional enzyme that controls glycolysis, *Biochem. J.* 381 (Pt 3) (2004) 561–579.
- [9] A. Yalcin, S. Telang, B. Clem, J. Chesney, Regulation of glucose metabolism by 6-phosphofructo-2-kinase/fructose-2,6-bisphosphatase in cancer, *Exp. Mol. Pathol.* 86 (3) (2009) 174–179.
- [10] D.A. Okar, A. Manzano, A. Navarro-Sabate, L. Riera, R. Bartrons, A.J. Lange, PFK-2/FBPase-2: maker and breaker of the essential biofactor fructose-2,6-bisphosphate, *Trends Biochem. Sci.* 26 (1) (2001) 30–35.
- [11] L. Bosca, G.G. Rousseau, L. Hue, Phorbol 12-myristate 13-acetate and insulin increase the concentration of fructose 2,6-bisphosphate and stimulate glycolysis in chicken embryo fibroblasts, *Proc. Natl. Acad. Sci. U. S. A.* 82 (19) (1985) 6440–6444.
- [12] L. Hue, M.H. Rider, Role of fructose 2,6-bisphosphate in the control of glycolysis in mammalian tissues, *Biochem. J.* 245 (2) (1987) 313–324.
- [13] L. Hue, G.G. Rousseau, Fructose 2,6-bisphosphate and the control of glycolysis by growth factors, tumor promoters and oncogenes, *Adv. Enzym. Regul.* 33 (1993) 97–110.
- [14] M.N. Calvo, R. Bartrons, E. Castano, J.C. Perales, A. Navarro-Sabate, A. Manzano, PFKFB3 gene silencing decreases glycolysis, induces cell-cycle delay and inhibits anchorage-independent growth in HeLa cells, *FEBS Lett.* 580 (13) (2006) 3308–3314.
- [15] A. Yalcin, B.F. Clem, Y. Imbert-Fernandez, S.C. Ozcan, S. Peker, J. O'Neal, A.C. Klarer, A.L. Clem, S. Telang, J. Chesney, 6-Phosphofructo-2-kinase (PFKFB3) promotes cell cycle progression and suppresses apoptosis via Cdk1-mediated phosphorylation of p27, *Cell Death Dis.* 5 (2014), e1337.
- [16] K. De Bock, M. Georgiadou, S. Schoors, A. Kuchnio, B.W. Wong, A.R. Cantelmo, A. Quaegebeur, B. Ghesquiere, S. Cauwenberghs, G. Eelen, L.K. Phng, I. Betz, B. Tembuysse, K. Brepoels, J. Welts, I. Geudens, I. Segura, B. Cruys, F. Bifari, I. Decimo, R. Blanco, S. Wyns, J. Vangindertael, S. Rocha, R.T. Collins, S. Munck, D. Daelemaans, H. Imamura, R. Devlieger, M. Rider, P.P. Van Veldhoven, F. Schuit, R. Bartrons, J. Hofkens, P. Fraisi, S. Telang, R.J. Deberardinis, L. Schoonjans, S. Vincicker, J. Chesney, H. Gerhardt, M. Dewerchin, P. Carmeliet, Role of PFKFB3-driven glycolysis in vessel sprouting, *Cell* 154 (3) (2013) 651–663.
- [17] B. Clem, S. Telang, A.L. Clem, A. Yalcin, J. Meier, A. Simmons, M.A. Rasku, S. Arumugam, W.L. Dean, J. Eaton, A. Lane, J.O. Trent, J. Chesney, Small-molecule inhibition of 6-phosphofructo-2-kinase activity suppresses glycolytic flux and tumor growth, *Mol. Cancer Ther.* 7 (1) (2008) 110–120.
- [18] A.S. Marsin, C. Bouzin, L. Bertrand, L. Hue, The stimulation of glycolysis by hypoxia in activated monocytes is mediated by AMP-activated protein kinase and inducible 6-phosphofructo-2-kinase, *J. Biol. Chem.* 277 (34) (2002) 30778–30783.
- [19] L. Novellasdemunt, L. Bultot, A. Manzano, F. Ventura, J.L. Rosa, D. Vertommen, M.H. Rider, A. Navarro-Sabate, R. Bartrons, PFKFB3 activation in cancer cells by the p38/MK2 pathway in response to stress stimuli, *Biochem. J.* 452 (3) (2013) 531–543.
- [20] H. Bando, T. Atsumi, T. Nishio, H. Niwa, S. Mishima, C. Shimizu, N. Yoshioka, R. Bucala, T. Koike, Phosphorylation of the 6-phosphofructo-2-kinase/fructose 2,6-bisphosphatase/PFKFB3 family of glycolytic regulators in human cancer, *Clin. Cancer Res.* 11 (16) (2005) 5784–5792.
- [21] J. Chesney, J. Clark, L. Lanceta, J.O. Trent, S. Telang, Targeting the sugar metabolism of tumors with a first-in-class 6-phosphofructo-2-kinase (PFKFB4) inhibitor, *Oncotarget* 6 (20) (2015) 18001–18011.
- [22] K. Brand, S. Aichinger, S. Forster, S. Kupper, B. Neumann, W. Nürnberg, G. Ohirsch, Cell-cycle-related metabolic and enzymatic events in proliferating rat thymocytes, *Eur. J. Biochem.* 172 (3) (1988) 695–702.
- [23] A. Weiss, R. Shields, M. Newton, B. Manger, J. Imboden, Ligand-receptor interactions required for commitment to the activation of the interleukin 2 gene, *J. Immunol.* 138 (7) (1987) 2169–2176.
- [24] S. Krauss, M.D. Brand, F. Buttgeriet, Signaling takes a breath—new quantitative perspectives on bioenergetics and signal transduction, *Immunity* 15 (4) (2001) 497–502.
- [25] C.J. Fox, P.S. Hammerman, C.B. Thompson, Fuel feeds function: energy metabolism and the T-cell response, *Nat. Rev. Immunol.* 5 (11) (2005) 844–852.
- [26] E.F. Greiner, M. Guppy, K. Brand, Glucose is essential for proliferation and the glycolytic enzyme induction that provokes a transition to glycolytic energy production, *J. Biol. Chem.* 269 (50) (1994) 31484–31490.
- [27] B.A. Judd, G.A. Koretzky, Antigen specific T lymphocyte activation, *Rev. Immunogenet.* 2 (2) (2000) 164–174.
- [28] E. Fayard, G. Moncayo, B.A. Hemmings, G.A. Holländer, Phosphatidylinositol 3-kinase signaling in thymocytes: the need for stringent control, *Sci. Signal.* 3 (135) (2010) re5.
- [29] S. Horman, N. Hussain, S.M. Dilworth, K.B. Storey, M.H. Rider, Evaluation of the role of AMP-activated protein kinase and its downstream targets in mammalian hibernation, *Comp. Biochem. Physiol. B Biochem. Mol. Biol.* 142 (4) (2005) 374–382.
- [30] L. Bultot, B. Guigas, A. Von Wilamowitz-Moellendorff, L. Maisin, D. Vertommen, N. Hussain, M. Beullens, J.J. Guinovart, M. Foretz, B. Viollet, K. Sakamoto, L. Hue, M.H. Rider, AMP-activated protein kinase phosphorylates and inactivates liver glycogen synthase, *Biochem. J.* 443 (1) (2012) 193–203.
- [31] E. Van Schalfingen, B. Lederer, R. Bartrons, H.G. Hers, A kinetic study of pyrophosphate: fructose-6-phosphate phosphotransferase from potato tubers. Application to a microassay of fructose 2,6-bisphosphate, *Eur. J. Biochem.* 129 (1) (1982) 191–195.
- [32] I. Gutmann, A. Wahlefeld, L-(+)-lactate determination with lactate dehydrogenase and NAD, *Methods of Enzymatic Analysis*, second ed. 1974, pp. 1464–1468.
- [33] M.W. Pfaffl, A new mathematical model for relative quantification in real-time RT-PCR, *Nucleic Acids Res.* 29 (9) (2001), e45.
- [34] D. Vertommen, L. Bertrand, B. Sontag, A. Di Pietro, M.P. Louckx, H. Vidal, L. Hue, M.H. Rider, The ATP-binding site in the 2-kinase domain of liver 6-phosphofructo-2-kinase/fructose-2,6-bisphosphatase. Study of the role of Lys-54 and Thr-55 by site-directed mutagenesis, *J. Biol. Chem.* 271 (30) (1996) 17875–17880.
- [35] J. Deprez, D. Vertommen, D.R. Alessi, L. Hue, M.H. Rider, Phosphorylation and activation of heart 6-phosphofructo-2-kinase by protein kinase B and other protein kinases of the insulin signaling cascades, *J. Biol. Chem.* 272 (28) (1997) 17269–17275.
- [36] A. Manzano, J.X. Pérez, M. Nadal, X. Estivill, A. Lange, R. Bartrons, Cloning, expression and chromosomal localization of a human testis 6-phosphofructo-2-kinase/fructose-2,6-bisphosphatase gene, *Gene* 229 (1–2) (1999) 83–89.

- [37] M.M. Bradford, A rapid and sensitive method for the quantification of microgram quantities of protein utilizing the principle of protein-dye binding, *Anal. Biochem.* 72 (1976) 248–254.
- [38] N. Okamura, R. Sakakibara, A common phosphorylation site for cyclic AMP-dependent protein kinase and protein kinase C in human placental 6-phosphofructo-2-kinase/fructose-2,6-bisphosphatase, *Biosci. Biotechnol. Biochem.* 62 (10) (1998) 2039–2042.
- [39] A. Navarro-Sabate, A. Manzano, L. Riera, J.L. Rosa, F. Ventura, R. Bartrons, The human ubiquitous 6-phosphofructo-2-kinase/fructose-2,6-bisphosphatase gene (PFKFB3): promoter characterization and genomic structure, *Gene* 264 (1) (2001) 131–138.
- [40] A. Yalcin, B.F. Clem, A. Simmons, A. Lane, K. Nelson, A.L. Clem, E. Brock, D. Siow, B. Wattenberg, S. Telang, J. Chesney, Nuclear targeting of 6-phosphofructo-2-kinase (PFKFB3) increases proliferation via cyclin-dependent kinases, *J. Biol. Chem.* 284 (36) (2009) 24223–24232.
- [41] A.C. Klarer, J. O'Neal, Y. Imbert-Fernandez, A. Clem, S.R. Ellis, J. Clark, B. Clem, J. Chesney, S. Telang, Inhibition of 6-phosphofructo-2-kinase (PFKFB3) induces autophagy as a survival mechanism, *Cancer Metab.* 2 (1) (2014) 2.
- [42] S. Telang, B.F. Clem, A.C. Klarer, A.L. Clem, J.O. Trent, R. Bucala, J. Chesney, Small molecule inhibition of 6-phosphofructo-2-kinase suppresses T cell activation, *J. Transl. Med.* 10 (2012) 95.
- [43] J. Chesney, R. Mitchell, F. Benigni, M. Bacher, L. Spiegel, Y. Al-Abed, J.H. Han, C. Metz, R. Bucala, An inducible gene product for 6-phosphofructo-2-kinase with an AU-rich instability element: role in tumor cell glycolysis and the Warburg effect, *Proc. Natl. Acad. Sci. U. S. A.* 96 (6) (1999) 3047–3052.
- [44] J. Chesney, J. Clark, A.C. Klarer, Y. Imbert-Fernandez, A.N. Lane, S. Telang, Fructose-2,6-bisphosphate synthesis by 6-phosphofructo-2-kinase/fructose-2,6-bisphosphatase 4 (PFKFB4) is required for the glycolytic response to hypoxia and tumor growth, *Oncotarget* 5 (16) (2014) 6670–6686.
- [45] S. Ros, C.R. Santos, S. Moco, F. Baenke, G. Kelly, M. Howell, N. Zamboni, A. Schulze, Functional metabolic screen identifies 6-phosphofructo-2-kinase/fructose-2,6-bisphosphatase 4 as an important regulator of prostate cancer cell survival, *Cancer Discov.* 2 (4) (2012) 328–343.
- [46] J.S. Moon, W.J. Jin, J.H. Kwak, H.J. Kim, M.J. Yun, J.W. Kim, S.W. Park, K.S. Kim, Androgen stimulates glycolysis for de novo lipid synthesis by increasing the activities of hexokinase 2 and 6-phosphofructo-2-kinase/fructose-2,6-bisphosphatase 2 in prostate cancer cells, *Biochem. J.* 433 (1) (2011) 225–233.
- [47] G.H. Reem, N.H. Yeh, D.L. Urdal, P.L. Kilian, J.J. Farrar, Induction and upregulation by interleukin 2 of high-affinity interleukin 2 receptors on thymocytes and T cells, *Proc. Natl. Acad. Sci. U. S. A.* 82 (24) (1985) 8663–8666.
- [48] M. Obach, A. Navarro-Sabate, J. Caro, X. Kong, J. Duran, M. Gomez, J.C. Perales, F. Ventura, J.L. Rosa, R. Bartrons, 6-Phosphofructo-2-kinase (pfkfb3) gene promoter contains hypoxia-inducible factor-1 binding sites necessary for transactivation in response to hypoxia, *J. Biol. Chem.* 279 (51) (2004) 53562–53570.
- [49] S. Ros, J. Floter, I. Kaymak, C. Da Costa, A. Houddane, S. Dubuis, B. Griffiths, R. Mitter, S. Walz, S. Blake, A. Behrens, K.M. Brindle, N. Zamboni, M.H. Rider, A. Schulze, 6-Phosphofructo-2-kinase/fructose-2,6-bisphosphatase 4 is essential for p53-null cancer cells, *Oncogene* (2017) (in press).
- [50] X. Zhang, N. Tang, T.J. Hadden, A.K. Rishi, Akt, FoxO and regulation of apoptosis, *Biochim. Biophys. Acta* 1813 (11) (2011) 1978–1986.

SUPPLEMENTARY DATA

Fig.S1

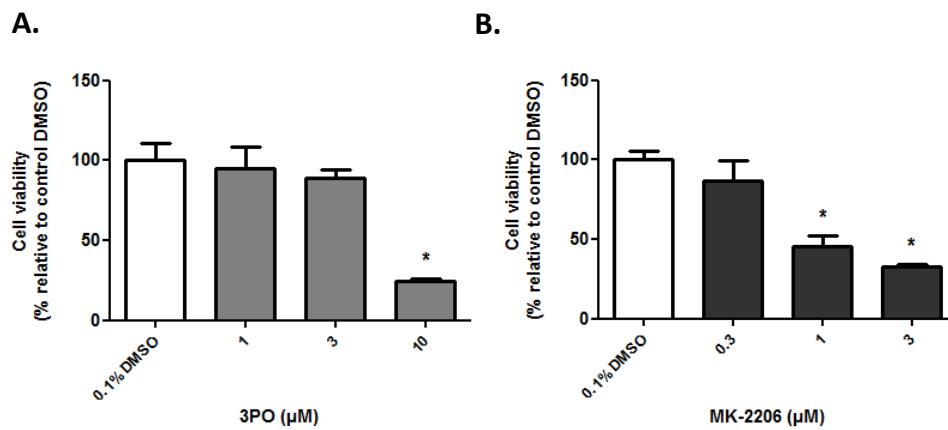


Fig. S1 Effects of 3PO and MK-2206 treatment of ConA-stimulated thymocytes on cell viability. Rat thymocytes were stimulated with ConA and treated with inhibitors as described in the legend to Fig. 5 of the main paper. Cell viability was then measured (see Methods section). The results are means \pm S.E.M. (n = 7-8) and * indicates a significant difference ($P < 0.05$, paired t -test).

Fig.S2

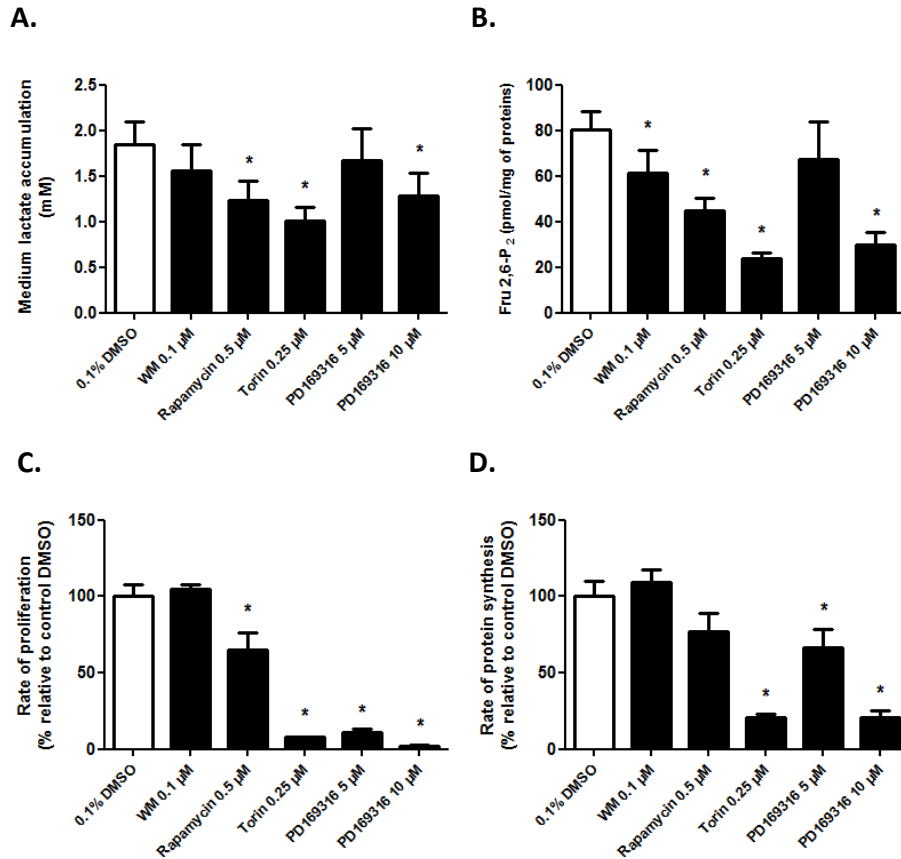


Fig. S2 Effects of treatment of ConA-stimulated thymocytes with signalling pathway inhibitors on lactate accumulation (A), Fru-2,6-P₂ content (B) and rates of cell proliferation (C) and protein synthesis (D). Rat thymocytes were stimulated with ConA and treated with inhibitors as described in the legend to Fig. 5 of the main paper. The cells were then harvested for measurements of medium lactate accumulation (A), Fru-2,6-P₂ content (B) or rates of cell proliferation (C) and protein synthesis (D). The 100% values for the rates of proliferation and protein synthesis correspond to 2548 ± 248 and 217 ± 26 cpm per min per mg of protein, respectively. The results are means \pm S.E.M. ($n = 5-10$) and * indicates a significant difference ($P < 0.05$, paired t -test).

DISCUSSION

Activated T cells need to generate energy for converting available supplies into biosynthetic macromolecules. This metabolic reprogramming is rapidly observed in activated T cells prior to the first cell division, at approximately 24 h post activation, during which protein and lipid synthesis is dramatically increased. In spite of energy requirements for biosynthesis, ATP levels rise, indicating enhanced metabolism. Glucose uptake, glycolysis, glutaminolysis and oxygen consumption are also elevated, and a decrease in uptake and catabolism of free fatty acids by β -oxidation occurs in parallel (Wang and Green, 2012).

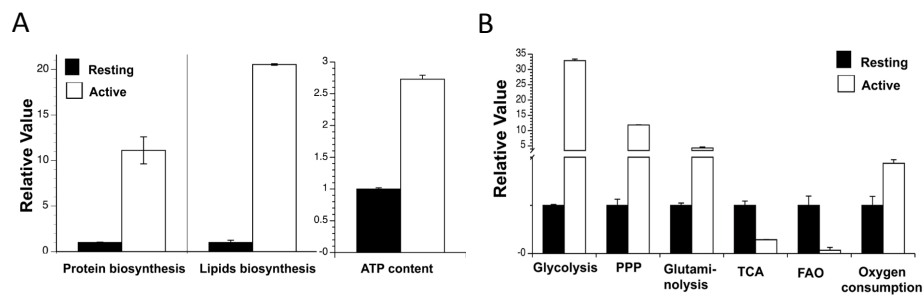


Figure 10. (A) Increased biosynthesis and energy production upon T-cell activation. (B) Metabolic reprogramming in activated T cells. (Wang and Green, 2012)

ConA-stimulated thymocytes represent a useful model to study these metabolic changes that occur during the transition from the resting to the proliferating state. Surprisingly, although enhanced glycolysis has been demonstrated in ConA-stimulated thymocytes in concert with increased DNA synthesis and glycolytic enzyme activities (Brand, 1985), measurements of Fru-2,6-BP content have not been made in this model. Therefore we investigated the role of Fru-2,6-BP in the control of glycolysis, and the possibility that protein synthesis and cell proliferation might also be controlled via Fru-2,6-BP in mitogen-stimulated thymocytes.

- 1. Fru-2,6-BP.** In ConA-stimulated cells, Fru-2,6-BP concentrations dramatically increased. Indeed, after a lag period of about 30 h, Fru-2,6-BP content increased by ConA stimulation reaching levels ~4-fold higher compared with resting cells after 68 h (paper 1, Fig. 2B). Increased expression of PFKFB3 and PFKFB4 proteins, but not of PFKFB2, was also observed. PFKFB2 expression was barely detectable by immunoblotting and did not change during incubation of ConA-stimulated or resting thymocytes (data not shown), while PFKFB3 expression increased ~2-fold after 68 h of ConA stimulation. Interestingly, the profile of the increase in expression of PFKFB4 in ConA-stimulated cells after a lag period of 24-30 h (paper 1, Fig.2F) was similar to the time-courses of the increases in medium lactate accumulation (paper 1, Fig.2A), Fru-2,6-BP content (paper 1, Fig.2B) and the rates of cell proliferation (paper 1, Fig.3A) and protein synthesis (paper 1, Fig.3B). It is noteworthy that, although the expression of PFKFB3 and PFKFB4 isoenzymes are co-expressed in ConA-stimulated thymocytes, PFKFB3 isoenzyme is predominant. PFKFB3 mRNA levels are ~45-fold higher compared with PFKFB4 after 54 h of ConA-stimulation (paper 1, Fig.2G). Fru-2,6-BP concentrations increase to a level of about 150 pmol per mg of protein which would correspond to a concentration of about 50 μ M which would be 50 times higher than required to stimulate PFK-1. The study was extended to investigate the potential relationships between the Fru-2,6-BP/PFKFB axis and PKB (see below).
- 2. Interleukin 2.** It is noteworthy that the lag period of ConA stimulation, before metabolic parameters began to increase, seems to correspond to the approximate time interval needed for mitogen-induced expression of the IL-2R, particularly for the expression of the IL-2R α subunit that increased after 24h of thymocyte ConA stimulation (see Figure 11).

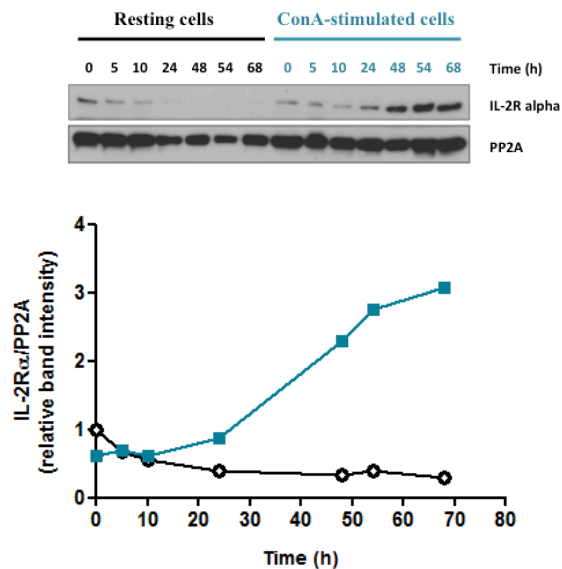


Figure 11. Time-course of ConA stimulation on IL-2R α expression. Freshly isolated rat thymocytes were cultured with 100 U/mL IL-2 without (Resting cells) (○) or with 3 μ g/mL ConA (ConA-stimulated cells) (■).

3. PKB and PFKFB3 phosphorylation. During ConA-stimulation of thymocytes, PKB became activated, as reflected by an increase in PKB Ser473 and downstream mTOR Ser2448 phosphorylation (paper 1, Fig.3C). PKB was found to phosphorylate PFKFB3 *in vitro*, resulting in an increase in V_{MAX} of PFK-2 and a decrease in K_M for Fru-6-P. Mass spectrometric analysis identified the phosphorylated residue as Ser461 (paper 1, Fig.1). However, only a slight increase in PFKFB3 Ser461 phosphorylation was observed in ConA-stimulated cells (paper 1, Fig.2C), and it was unaffected by pre-incubation of ConA-stimulated cells with low doses of the PKB inhibitor MK-2206 (paper 1, Fig.6A). A possible explanation is that the extent of PKB activation might not be sufficient to effectively phosphorylate PFKFB3 in ConA-stimulated thymocytes. Thus the importance of PFKFB3 Ser461

phosphorylation remains unclear. As expected, PFKFB4 was a very poor PKB substrate *in vitro* (data not shown).

- 4. Effects of PKB inhibition.** In ConA-stimulated cells, treatment with a non-toxic dose (0.3 μ M) MK-2206 reduced mRNA levels of PFKFB3 and PFKFB4 isoenzymes (paper 1, Fig. 6C), suggesting that PFKFB3/4 expression is controlled by PKB. It has been shown that *pfkfb3* gene was hypoxia-inducible and stimulated through HIF interaction with the consensus hypoxia response element (HRE) site in its promoter region (Obach et al., 2004). In response to ConA-stimulation, *pfkfb3* gene expression could be increased via the PI3K/PKB pathway and transcription factor HIF-1 binding to the HREs within the *pfkfb3* gene promoter. Also, a recent study reported that p53 negatively regulates PFKFB4 expression by directly binding to the promoter of the *pfkfb4* gene. Loss of p53 function either by deletion or mutation reduced the expression of PFKFB4 in cancer cells, which could explain the decrease in content of the PFKFB4 protein (Ros et al., 2017). It is also noteworthy that PKB phosphorylates and inactivates forkhead box O (FoxO) transcription factors implicated in cell survival, growth and proliferation (Zhang et al., 2011). Treatment with low doses of MK-2206 (0.3 μ M) induced a fall in lactate accumulation (paper 1, Fig.5B) and Fru-2,6-BP content (paper 1, Fig.5D), which were probably due to decreases in PFKFB3/4 expression and were not due to changes in PFKFB3 phosphorylation (paper 1, Fig.6A-B). However, we also demonstrated that MK-2206 (0.3 μ M) significantly decreased glucose uptake (paper 1, Fig.5F). It has been reported that, unlike Akti-1/2, MK-2206 did not affect transport activity of GLUT1 or GLUT4 (Tan et al., 2011). As expected, because of increased mTORC1 signalling via PKB activation, treatment of ConA-stimulated thymocytes with 0.3 μ M MK-2206 decreased cell proliferation, protein synthesis, severely abrogated PKB Ser473 phosphorylation and substantially reduced p70S6K and 4E-BP1

phosphorylation. Concerning the signalling pathways downstream of ConA/IL-2, the inhibitor data with Torin (inhibitor of both mTORC1 and mTORC2) and PD169316 (p38MAPK inhibitor) (paper 1, Fig.S2) suggest possible roles for mTORC1/2 and p38MAPK/MK2 in the control of Fru-2,6-BP content, perhaps by decreasing PFKFB isoenzyme expression, and in the control of cell proliferation and protein synthesis. Interestingly, a recent study reported that, in acute myeloid leukemia, only the PFKFB3 isoenzyme was a novel downstream substrate of mTOR signaling pathway. It was shown that PFKFB3 expression was upregulated by mTORC1 and was dependent on HIF1 α , a positive regulator of glycolysis (Feng and Wu, 2017).

5. ***Cell proliferation and protein synthesis.*** It has been speculated that Fru-2,6-BP could couple glycolysis to cell proliferation. Fru-2,6-BP addition to a HeLa cell lysate increased phosphorylation of the cell cycle inhibitor p27 at the cyclin-dependent kinase (Cdk)-specific Thr187 site (Yalcin et al., 2009), although it is highly unlikely that Fru-2,6-BP could act as phosphoryl donor. In this study we show that ConA-induced increases in Fru-2,6-BP were mirrored by increases in the rates of cell proliferation (paper 1, Fig.3A) and protein synthesis (paper 1, Fig.3B), which would be partly due to increased expression of translation factors together with increased (4E-BP1, rpS6) or decreased (eEF2) phosphorylation (paper 1, Fig.3C).
6. ***Inhibition of PFK-2.*** The results obtained with the PFK-2 inhibitor, 3PO, should be considered with caution, as the compound inhibited PFK-2 activity of all four PFKFB isoenzymes (paper 1, Fig.4). Nevertheless, treatment of ConA stimulated thymocytes with a non-toxic dose of 3 μ M 3PO led to parallel and significant decreases in lactate accumulation (paper 1, Fig.5A), Fru-2,6-BP concentration (paper 1, Fig.5C), and rates of cell proliferation (paper 1, Fig.7A) and protein synthesis (paper 1, Fig.7B) accompanied by

small (~20%) but significant decreases in S6K1 and 4E-BP1 phosphorylation (paper 1, Fig.7E-F).

7. Knockdown of PKB α/β and PFKFB3/4 in Jurkat cells. We confirmed results obtained with MK-2206 in ConA-stimulated thymocytes by using siRNA knockdown of PKB α/β in more easily transfectable Jurkat E6-1 cells. siRNA silencing of PKB α/β reduced the rates of cell proliferation and protein synthesis (paper 1, Fig.8E-F) as expected but also decreased lactate accumulation (paper 1, Fig.8B), Fru-2,6-BP content (paper 1, Fig.8C) and glucose uptake (paper 1, Fig.8D). Therefore the data support a role for PKB in the regulation of PFKFB3/4 expression and glucose uptake in ConA-stimulated cells. As expected, PFKFB3 and PFKFB4 silencing decreased lactate accumulation (paper 1, Fig.8B) and Fru-2,6-BP content (paper 1, Fig.8C). Surprisingly, siRNA silencing of PFKFB3 or PFKFB4 significantly reduced the rates of cell proliferation and protein synthesis (paper 1, Fig.8E-F). Therefore, despite constitutive activation of the PI3K/PKB signaling in Jurkat E6-1 cells, reduced expression of PFKFB3 or PFKFB4 proteins is sufficient to affect cell proliferation and protein synthesis.

CONCLUSION

Taken together, the findings suggest that the increase in PFKFB3 and PFKFB4 expression, but not PFKFB3 Ser461 phosphorylation, plays a role in increasing glycolysis in mitogen-stimulated thymocytes. PKB phosphorylation and PFKFB3 expression were increased in resting cells at later time points and similar levels of PKB Ser473 phosphorylation and PFKFB3/4 were observed at certain time points in both resting and ConA-stimulated thymocytes (paper 1, Fig. 2C-F; Fig. 3C). However, only ConA-stimulated cells display increases in cell proliferation and

protein synthesis. Thus, increased PKB Ser473 phosphorylation and PFKFB3 alone would not be sufficient to induce the metabolic changes occurring during mitogen stimulation. The results implicate PKB in the upregulation of PFKFB3 and PKBFB4 and underline its importance for cell proliferation and protein synthesis during ConA stimulation. Rates of amino acid incorporation might be an underestimation of protein synthesis, since some proteins have a relatively short lifetime and protein degradation could also be occurring. However, we used a short window of phenylalanine incorporation, and hence the rates of amino acid incorporation that were measured mainly reflect net protein synthesis rather than total protein synthesis. Alternatively, an inhibitor of the ubiquitin-proteasome system or autophagy (such as compound SBI-0206965 or Spautin-1) could have been added a few minutes before adding the radioactive tracer. Concerning siRNA transfection, a difference in their efficacy should also take in account. However, immunoblotting does not allow to measure protein expression levels (due to different antibodies, different sensitivities, exposure time, different secondary antibodies, etc.). It might have been preferable to check mRNA expression quantitatively by qPCR. Therefore, comparing effects of siRNA knockdowns on glycolysis, cell proliferation and protein synthesis should be exercised with caution. Lastly, the data support a role for Fru-2,6-BP in coupling glycolysis to cell proliferation and protein synthesis.

ANNEXES

PAPER 2:

A conserved phosphatase destroys toxic glycolytic side products in mammals and yeast.

Published in Nature Chemical Biology (2016) 12(8):601-7, co-author, contributed to expression and purification of PFKFB4 isoenzyme.

A conserved phosphatase destroys toxic glycolytic side products in mammals and yeast

François Collard^{1,2,6}, Francesca Baldin^{1,2,6}, Isabelle Gerin^{1,2}, Jennifer Bolsée^{1,2}, Gaëtane Noël^{1,2}, Julie Graff^{1,2}, Maria Veiga-da-Cunha^{1,2}, Vincent Stroobant³, Didier Vertommen⁴, Amina Houddane⁴, Mark H Rider⁴, Carole L Linster⁵, Emile Van Schaftingen^{1,2,7*} & Guido T Bommer^{1,2,7*}

Metabolic enzymes are very specific. However, most of them show weak side activities toward compounds that are structurally related to their physiological substrates, thereby producing side products that may be toxic. In some cases, 'metabolite repair enzymes' eliminating side products have been identified. We show that mammalian glyceraldehyde 3-phosphate dehydrogenase and pyruvate kinase, two core glycolytic enzymes, produce 4-phosphoerythronate and 2-phospho-L-lactate, respectively. 4-Phosphoerythronate strongly inhibits an enzyme of the pentose phosphate pathway, whereas 2-phospho-L-lactate inhibits the enzyme producing the glycolytic activator fructose 2,6-bisphosphate. We discovered that a single, widely conserved enzyme, known as phosphoglycolate phosphatase (PGP) in mammals, dephosphorylates both 4-phosphoerythronate and 2-phospho-L-lactate, thereby preventing a block in the pentose phosphate pathway and glycolysis. Its yeast ortholog, Pho13, similarly dephosphorylates 4-phosphoerythronate and 2-phosphoglycolate, a side product of pyruvate kinase. Our work illustrates how metabolite repair enzymes can make up for the limited specificity of metabolic enzymes and permit high flux in central metabolic pathways.

© 2016 Nature America, Inc. All rights reserved.



It is generally assumed that enzymes of intermediary metabolism are perfectly specific. The reality is somewhat different; most enzymes have some action on substrates that structurally resemble their physiological substrate (or substrates)^{1,2}, albeit with a much lower affinity and at a much lower rate. In rare cases, the resulting side products may be useful³ or allow organisms to adapt to modified metabolic demands^{4,5}. In other cases, the side products are potentially toxic^{1,2}, as shown by the fact that some of them are destroyed by dedicated enzymes and that deficiency in such 'metabolite repair' enzymes may lead to disease. For example, a side activity of mitochondrial L-malate dehydrogenase, representing less than 1/10⁷ of its normal activity in terms of catalytic efficiency, leads to the formation of L-2-hydroxyglutarate. If the latter is not degraded by the metabolite repair enzyme L-2-hydroxyglutarate dehydrogenase, it accumulates in tissues to concentrations in the millimolar range, thereby causing a neurological disease known as L-2-hydroxyglutaric aciduria in humans^{2,6,7}. This example also illustrates that, even at very low production rates, some side products may accumulate to high concentrations if they are not eliminated by dedicated enzymes^{2,8}.

A few metabolite repair enzymes have been identified (~15 are mentioned in ref. 2), but presently it is not known whether a similar repair mechanism applies to glycolysis, one of the most ancient metabolic pathways. As a starting point for the present study, we reasoned that the formation of side products might be particularly important in glycolysis because even very small side activities could lead to the formation of substantial amounts of side products at the high concentration of the enzymes involved in this pathway⁹. Hence, we decided to investigate whether a core enzyme of glycolysis can produce a potentially toxic side product that would need to be eliminated by an as-yet-undefined metabolite repair enzyme.

These investigations led to the discovery of a single highly conserved enzyme that eliminates side products made by two central glycolytic enzymes, glyceraldehyde 3-phosphate dehydrogenase and pyruvate kinase.

RESULTS

PGP eliminates 4-P-erythronate, a side product of GAPDH

The glycolytic enzyme GAPDH catalyzes the oxidative phosphorylation of the three-carbon substrate glyceraldehyde 3-phosphate to 1,3-bisphosphoglycerate, which is further metabolized by phosphoglycerate kinase to 3-phosphoglycerate (3-P-glycerate; Fig. 1a and Supplementary Results, Supplementary Fig. 1). GAPDH also has some activity on erythrose-4-phosphate¹⁰, a four-carbon analog of its physiological substrate that is present in nearly all cells as an intermediate of the pentose phosphate pathway (Fig. 1a and Supplementary Fig. 1). The problem of this side activity (the mechanism of which is further investigated below) is that it eventually leads to the formation of 4-phosphoerythronate (4-P-erythronate), a potent inhibitor of 6-phosphogluconate dehydrogenase^{10,11}. Hence, accumulation of this side product could reach concentrations susceptible to inhibit the pentose phosphate pathway unless an enzyme existed that serves to destroy it (Fig. 1a). We therefore hypothesized that living cells contain a 4-P-erythronate phosphatase and that this enzyme is needed for the coexistence of glycolysis and the pentose phosphate pathway.

Using radiolabeled 4-P-erythronate as substrate, we indeed found that mammalian tissue extracts show substantial phosphatase activity on this phosphate ester. The phosphatase was partially purified from human erythrocytes (Fig. 1b) and displayed kinetic properties shared by phosphatases of the haloacid dehalogenase family (Supplementary Fig. 2a)¹². Furthermore, the 4-P-erythronate

¹Wallon Excellence in Lifesciences and Biotechnology (WELBIO), Brussels, Belgium. ²Laboratory of Physiological Chemistry, de Duve Institute, Université Catholique de Louvain, Brussels, Belgium. ³Ludwig Institute for Cancer Research, Brussels, Belgium. ⁴Protein Phosphorylation Unit, de Duve Institute, Université Catholique de Louvain, Brussels, Belgium. ⁵Luxembourg Centre for Systems Biomedicine, University of Luxembourg, Esch-sur-Alzette, Luxembourg. ⁶These authors contributed equally to this work. ⁷These authors jointly supervised this work. *e-mail: emile.vanschaftingen@uclouvain.be or guido.bommer@uclouvain.be

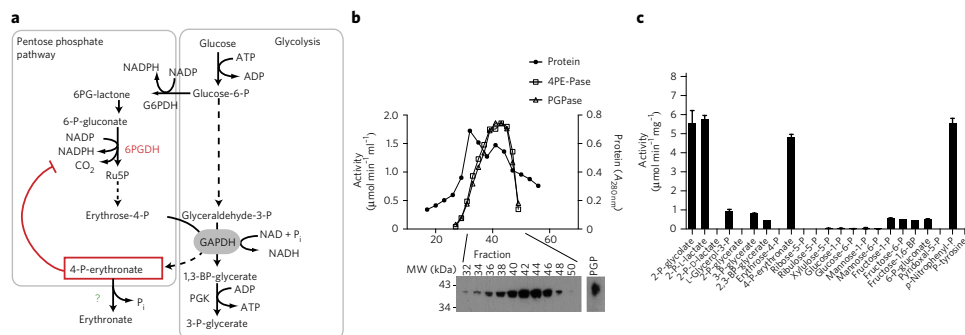


Figure 1 | Elimination of the GAPDH side product 4-P-erythronate by PGP. (a) Working hypothesis of the present paper. Schematic representation of the canonical and side reactions of GAPDH and of the inhibitory effect of the side product 4-P-erythronate (4PE) on 6-P-gluconate dehydrogenase (6PGDH). PGK, phosphoglycerate kinase; 6PG-lactone, 6-P-gluconolactone; Ru5P, ribulose-5-P; MW, molecular weight. (b) 4-P-erythronate phosphatase activity copurifies with PGP. Fractions from a gel filtration column were analyzed for 4PE phosphatase activity (4PE-Pase, open squares), 2-P-glycolate phosphatase activity (PGPase, open triangles) and protein concentration (A_{280} , filled circles) and were subjected to western blot analysis with anti-PGP. (c) Activity of recombinant mouse PGP toward the indicated substrates (1 mM) was assessed by measuring P_i release and is expressed per min and mg of protein. Values are shown as mean \pm s.e.m. of three independent experiments. Uncropped gel images are available in **Supplementary Figure 15**.

phosphatase activity copurified with (Fig. 1b) and showed a similar tissue distribution to (Supplementary Fig. 2b,c) phosphoglycolate phosphatase (PGP), a haloacetal dehalogenase family member that is particularly active in erythrocytes^{13,14}.

To confirm that PGP is responsible for the 4-P-erythronate phosphatase activity, we overexpressed and purified recombinant mouse PGP. Among several potentially physiological phosphate esters, 4-P-erythronate, 2-phosphoglycolate (2-P-glycolate) and 2-phospho-L-lactate (2-P-L-lactate) were by far the best substrates, with comparable catalytic efficiencies (Fig. 1c and Supplementary Fig. 3a). An almost identical substrate specificity profile was observed for the *Saccharomyces cerevisiae* homolog Pho13 (Supplementary Fig. 3a,b). At first sight, their substrate spectra might suggest lack of specificity of PGP and Pho13. However, we noted that, despite close structural similarity to 2-P-glycolate and 4-P-erythronate, the canonical glycolytic intermediates 3-P-glycerate and 2-P-glycerate were poor substrates (Fig. 1c and Supplementary Fig. 3b,c), indicating that PGP and Pho13 spare these important metabolites and show a 'negative' specificity that has been maintained during evolution.

4-P-erythronate inhibits 6-P-gluconate dehydrogenase

To investigate the role of PGP in cellular metabolism, we inactivated the *PGP* gene in the human colorectal cancer cell line HCT116 using the CRISPR/Cas9 system (subsequently referred to as PGP KO cells)¹⁵. Biallelic inactivation was confirmed by sequencing and by showing that the PGP protein was absent (Supplementary Fig. 4a,b and Supplementary Table 1). We then measured metabolite concentrations by targeted GC/MS analysis. In wild-type cells, 4-P-erythronate was barely detectable. In contrast, knockout cells showed at least a ten-fold increase in 4-P-erythronate concentration that reached 20–30 μ M (PGP KO clone no. 3) and was reduced to normal levels upon reexpression of PGP (Fig. 2a and Supplementary Fig. 4c). 2-P-glycolate could not be detected reliably, suggesting that its production is minimal in our experimental system (i.e., $<2 \mu$ M). However, we did observe a strong increase in 2-phospholactate (2-P-lactate) concentrations (reaching 2–4 mM; Fig. 2b and Supplementary Fig. 4d).

Previous studies had identified 4-P-erythronate as an extremely potent inhibitor of 6-phosphogluconate dehydrogenase (6-P-gluconate dehydrogenase), most likely because of its structural resemblance

to the ene-diolate intermediate occurring during the reaction of 6-P-gluconate dehydrogenase (Supplementary Fig. 4g). This indicated that accumulation of 4-P-erythronate might lead to disturbances in the oxidative pentose phosphate pathway (Fig. 1a).

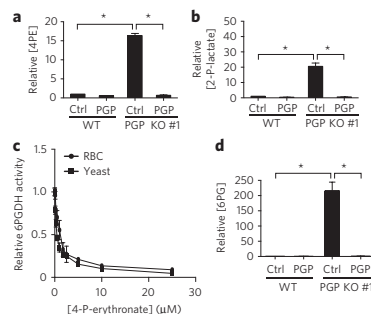


Figure 2 | Accumulation of 4-P-erythronate in PGP KO cells leads to inhibition of the pentose phosphate pathway. (a,b) Targeted GC/MS analysis of 4-P-erythronate (4PE) (a) and 2-P-lactate (b) was performed in parental HCT116 (WT) and a phosphoglycerate kinase (PGK) knockout clone (PGP KO #1) after infection with a retrovirus driving expression of PGP or an empty vector (Ctrl). (c) Activity of 6-P-gluconate dehydrogenase (6PGDH) from human red blood cells (RBCs) and yeast was measured in the presence of the indicated concentrations of 4-P-erythronate. Values presented are mean \pm s.d. ($n = 3$ independent experiments) and are normalized to the activity of the enzyme in the absence of 4-P-erythronate. (d) Targeted GC/MS analysis of 6-P-gluconate in the same samples as described in a. Metabolite measurements (a,b,d) represent mean \pm s.e.m. of four independent experiments performed in triplicates and are normalized to concentrations in wild-type control (WT ctrl) cells within each experiment. Asterisks indicate multiplicity-adjusted P values ($P < 0.05$) obtained from Dunnett's multiple-comparisons test performed on log-transformed values. Complementary data to this figure are available in **Supplementary Figure 4**.



To our surprise, in these studies, 4-P-erythronate was found to inhibit 6-P-gluconate dehydrogenase from *Trypanosoma brucei* with a K_i of 0.13 μM , whereas the sheep liver enzyme was 83-fold less sensitive¹¹. For both human and yeast 6-P-gluconate dehydrogenase, we observed a half-maximum inhibitory concentration (IC_{50}) of $<1 \mu\text{M}$ for 4-P-erythronate (Fig. 2c). The concentration of this compound in PGP KO cells was at least 20 times higher (i.e., $>20 \mu\text{M}$). Thus, we anticipated that these cells would accumulate 6-P-gluconate. Indeed, we observed a more than 100-fold increase in the concentrations of 6-P-gluconate and its dephosphorylation product gluconate in PGP KO cells (Fig. 2d and Supplementary Fig. 4e,f). These observations indicate that PGP eliminates the GAPDH side product 4-P-erythronate, which would otherwise inhibit 6-P-gluconate dehydrogenase.

The oxidative pentose phosphate pathway is a major source of NADPH. Hence, inhibition of 6-P-gluconate dehydrogenase activity by 4-P-erythronate could be expected to reduce the cellular NADPH/NADP⁺ ratio. However, in our experimental system, loss of PGP did not affect this ratio in cells (Supplementary Fig. 5a) and only slightly slowed down cellular growth (Supplementary Fig. 5b,c). This is consistent with recent observations indicating that NADPH production in certain cancer cells largely relies on other sources¹⁶.

Increase of 2-P-L-lactate and decrease of fructose 2,6-BP

To our surprise, glucose consumption and lactate production in PGP KO cells were reduced by about 40% (Fig. 3a,b and Supplementary Fig. 6a,b), indicating a reduction in glycolytic flux, whereas cellular oxygen consumption was increased (Supplementary Fig. 6d). Intracellular concentrations of several glycolytic intermediates downstream of phosphofruktokinase-1 (dihydroxyacetone phosphate, 3-P-glycerate, phosphoenolpyruvate (P-enolpyruvate), lactate and pyruvate) were reduced, but levels of hexose-6-phosphate, which is upstream of phosphofruktokinase-1, were not (Supplementary Tables 2 and 3). These findings suggested that glycolysis was inhibited at the level of phosphofruktokinase-1 (PFK-1), an enzyme influenced by many different allosteric regulators¹⁷. One of the most important activators of phosphofruktokinase-1 is fructose 2,6-bisphosphate (fructose-2,6-BP), a purely regulatory molecule synthesized by the enzyme phosphofruktokinase-2 (PFK-2)^{18,19} (Fig. 3c). Measurements of fructose-2,6-BP showed that the concentration of this potent effector of phosphofruktokinase-1 was in fact decreased by 80% in PGP KO cells (Fig. 3d and Supplementary Fig. 6c).

PFK-2 is inhibited by P-enolpyruvate. Given the structural similarity between 2-P-lactate and P-enolpyruvate, we wondered whether the 2-P-lactate accumulating in PGP KO cells might inhibit PFK-2 (Fig. 3c). To test this hypothesis, we measured PFK-2 activity in crude lysates obtained from wild-type HCT116 cells and observed 70% inhibition when 100 μM 2-P-L-lactate was added (Fig. 3e). Cellular PFK-2 activity is contributed by several bifunctional enzymes that have both PFK-2 and fructose-2,6-bisphosphatase activities. These isozymes are produced from four different genes (*PFKFB1*–*PFKFB4*) and differ in organ-specific expression, ratio of kinase to phosphatase activity and regulation by allosteric regulators

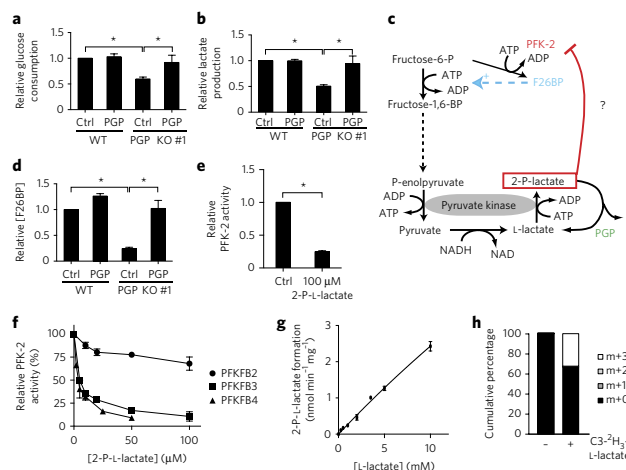


Figure 3 | 2-P-lactate accumulating in PGP KO cells can inhibit the production of fructose-2,6-BP. (a,b) Glucose consumption (a) and lactate production (b) were measured in the cell lines described in Figure 2a. (c) Schematic representation of the formation of 2-P-lactate and of the hypothesis about its metabolic function. (d) Fructose-2,6-BP concentrations were determined in cell lines described in Figure 2. (e,f) PFK-2 activity was measured in crude lysates of HCT116 cells in the presence of 0.5 mM fructose-6-P (e) or with partially purified PFKFB2, PFKFB3 or PFKFB4 in the presence of 100 μM fructose-6-P (f). Values were normalized to the activity in the absence of 2-P-lactate within each experiment. (g) Activity of recombinant human pyruvate kinase M2 on L-lactate was assayed in the presence of 2.5 mM ATP. (h) Mass isotopomer distribution of 2-P-L-lactate in PGP KO cells upon treatment with 3 mM C3-²H₃-L-lactate for 6 h. Values represent mean \pm s.e.m. of four (a,b) or three (d-g) independent experiments and were normalized to values measured in wild-type control cells (a,b,d) or in the condition without 2-P-lactate (e,f). Asterisks indicate multiplicity-adjusted P values ($P < 0.05$) obtained from Dunnett's multiple-comparisons test (a,b,d) or Student's t -test (e). Complementary data are available in Supplementary Figure 6.

and covalent modifications¹⁸. To test which isoforms are inhibited by 2-P-L-lactate, we generated recombinant partially purified PFKFB2, PFKFB3 and PFKFB4 proteins. The effect of 2-P-L-lactate on the PFK-2 activity of each of these isoenzymes was markedly different, ranging from an $\text{IC}_{50} <10 \mu\text{M}$ for PFKFB4 and PFKFB3 (the two major isoforms expressed in HCT116 cells) to hardly any inhibition in PFKFB2, the form expressed mainly in the heart (Fig. 3f). This indicates that the cell-specific expression pattern of PFKFB isoenzymes most likely determines the degree of PFK-2 inhibition by 2-P-L-lactate.

Given that cellular 2-P-L-lactate concentrations reach more than 1 mM in PGP KO cells, 2-P-L-lactate most likely contributes to the reduction in fructose-2,6-BP levels observed in PGP KO cells. In turn, by reducing levels of this important glycolytic regulator, 2-P-L-lactate accumulation might contribute to the observed reduction in glucose consumption (Fig. 3a,b).

Previous *in vitro* studies had suggested that 2-P-lactate can be produced when pyruvate kinase acts on L-lactate, an end product of glycolysis²⁰. Indeed, incubation of recombinant pyruvate kinase M2 with L-lactate and ATP led to the formation of 2-P-L-lactate, albeit at a very slow rate (for example, 1.3 $\text{nmol min}^{-1} \text{mg}^{-1}$ at 5 mM L-lactate) and with an estimated K_m of more than 30 mM (compared to the forward reaction with a K_m of 142 μM and a V_{max} of 100 $\mu\text{mol min}^{-1} \text{mg}^{-1}$; Fig. 3g). To test whether direct phosphorylation of lactate occurs in cells, we incubated PGP KO cells with lactate in which all three hydrogen atoms on carbon 3 were replaced with

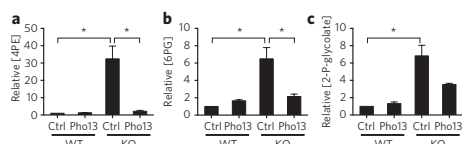


Figure 4 | The metabolite repair system is conserved in *S. cerevisiae*. (a–c) 4-P-Erythronate (4PE) (a), 6-P-gluconate (6PG) (b) and 2-P-glycolate (c) concentrations were determined in wild-type (WT) or *pho13* (KO) strains where the *PHO13* cDNA (Pho13) or an empty vector (Ctrl) had been reintroduced. Concentrations were normalized to values measured in wild-type control (WT ctrl) cells within each experiment and are shown as mean \pm s.e.m. of three independent experiments. Asterisks indicate multiplicity-adjusted *P* values ($P < 0.05$) obtained from Dunnett's multiple-comparisons test performed on log-transformed values. Complementary data are available in **Supplementary Figure 7**.

deuterium (C3-²H₃-l-lactate). As we would have expected if lactate had been directly phosphorylated, we observed almost exclusively m+3 isotopomers of 2-P-lactate (Fig. 3h). In contrast, we almost observed no m+2 and m+1 isotopomers, which would be present if P-lactate were formed indirectly, for example, by a hypothetical enzyme that would reduce P-enolpyruvate. Although these data indicate that pyruvate kinase contributes to 2-P-lactate production, a role for other kinases in this process cannot be excluded.

Collectively, our findings indicate that suppression of PGP activity causes increases in the concentration of 4-P-erythronate and 2-P-l-lactate, which in turn inhibit 6-P-gluconate dehydrogenase and PFK-2, respectively. These changes profoundly affect glucose metabolism through the pentose phosphate pathway and glycolysis.

The metabolite repair system is conserved in yeast

S. cerevisiae Pho13 has a similar specificity to PGP (Supplementary Fig. 3b). Hence, we predicted that *PHO13*-deficient cells would display similar metabolic perturbations to mammalian PGP KO cells. Using targeted GC/MS analysis, we confirmed that 4-P-erythronate and 6-P-gluconate accumulated in *PHO13*-deficient yeasts more than 20-fold and more than 5-fold, respectively (Fig. 4a,b and Supplementary Fig. 7a,b,d). In contrast, we did not observe any 2-P-lactate, consistent with the fact that l-lactate, the metabolite from which 2-P-l-lactate is made, is absent from yeast. In comparison to mammalian PGP KO cells, *PHO13*-deficient yeast cells showed a more modest increase in 6-P-gluconate levels (10-fold versus 100-fold). We therefore investigated the hypothesis that a transcriptional response may partially mask the effect of 6-P-gluconate dehydrogenase inhibition caused by 4-P-erythronate in yeast. As shown in Supplementary Figure 8a and as independently found by others²¹, *PHO13*-deficient cells markedly upregulated a series of genes encoding enzymes of the pentose phosphate pathway and of gluconate metabolism, an effect that might partially prevent an increase in 6-P-gluconate concentrations (Supplementary Fig. 8b). Notably, 2-P-glycolate levels were increased eight-fold in Pho13 mutant cells (Fig. 4c and Supplementary Fig. 7c), consistent with the previous observation that this metabolite can be formed by yeast pyruvate kinase from glycolate²².

Hence, our data indicate that elimination of the GAPDH side product 4-P-erythronate by PGP and Pho13 has been conserved between yeast and humans. In this context, it is important to mention that dephosphorylation of 2-P-glycolate by PGP homologs is also highly conserved and serves a well-defined function in plants, where 2-P-glycolate is formed in a side reaction of the photosynthesis enzyme ribulose-1,5-bisphosphate carboxylase^{3,23}. In contrast, a previously described weak protein phosphatase activity

for Pho13 and PGP is not conserved, as in these studies PGP acted on phosphotyrosine and Pho13 acted on phosphoserine and phosphothreonine^{24,25}.

Mechanism of 4-P-erythronate formation

Although our data demonstrate that PGP and Pho13 are responsible for 4-P-erythronate degradation, the molecular details of the formation of 4-P-erythronate by GAPDH are still unclear. To test whether GAPDH contributes to the formation of 4-P-erythronate in cells, we knocked down this enzyme in two PGP KO clones using shRNAs (Fig. 5a). Concentrations of 4-P-erythronate in GAPDH knockdown cells were significantly decreased ($P < 0.05$; Fig. 5b, Supplementary Fig. 9a), suggesting that this metabolite is indeed produced by this enzyme (Fig. 5b, Supplementary Fig. 9b). This decrease was paralleled by a decrease in 6-P-gluconate concentrations (Fig. 5c), consistent with the model in which 6-P-gluconate accumulates because of the inhibitory action of 4-P-erythronate on 6-P-gluconate dehydrogenase (Fig. 1a).

GAPDH catalyzes the oxidative phosphorylation of glyceraldehyde-3-phosphate (glyceraldehyde-3-P) to 1,3-bisphosphoglycerate (Fig. 1a), which contains a high-energy acyl-phosphate bond needed to make ATP from ADP in the reaction catalyzed by phosphoglycerate kinase. By analogy, we reasoned that GAPDH might convert erythrose-4-phosphate (erythrose-4-P) to 1,4-bisphosphoerythronate (1,4-BP-erythronate; Fig. 5d), which would then be dephosphorylated to 4-P-erythronate by phosphoglycerate kinase (Fig. 5d) or another enzyme able to sever the acyl-phosphate bond (Fig. 5d). Alternatively, 4-P-erythronate could be directly formed by GAPDH if the thioacyl-intermediate formed during the catalytic cycle is directly hydrolyzed (Fig. 5d), as previously shown for the bacterial enzyme erythrose-4-P dehydrogenase²⁶. The experiments reported in the following paragraphs indicate that GAPDH converts erythrose-4-P mainly to 1,4-BP-erythronate.

When GAPDH was incubated with glyceraldehyde-3-P, inorganic phosphate and P_i, the concentration of NADH increased and rapidly reached a plateau (after ~2 min in Fig. 5e) because the reaction had reached its thermodynamic equilibrium. Accordingly, the reaction resumed upon either the addition of phosphoglycerate kinase and ADP or of recombinant acylphosphatase 1, a mammalian enzyme that hydrolyzes different acyl phosphates²⁷ (Fig. 5e). The reaction also resumed upon addition of arsenate because this structural analog of phosphate leads to the formation of an extremely unstable acyl-arsenate intermediate (Fig. 5e) that spontaneously hydrolyzes²⁸.

The reaction catalyzed by GAPDH on erythrose-4-P is much slower than the one it catalyzes on glyceraldehyde-3-P and therefore requires much higher (~100-fold) enzyme concentrations to be studied. As observed with glyceraldehyde-3-P, the formation of NADH catalyzed by GAPDH with erythrose-4-P slowed down with time and was accelerated by the addition of phosphoglycerate kinase (+ADP), acyl-phosphatase or arsenate, indicating that 1,4-BP-erythronate was formed. However, the reaction performed in the absence of arsenate, acyl-phosphatase or phosphoglycerate kinase did not reach a plateau in the rather long (up to 50 min) time frame that we investigated, suggesting that part of the erythrose-4-P might be directly converted to 4-P-erythronate.

Acylphosphatase 1 was much better than phosphoglycerate kinase at using 1,4-BP-erythronate as it led to a comparable acceleration of the GAPDH reaction on erythrose-4-P at much lower enzyme concentrations (Fig. 5f). Still, as phosphoglycerate kinase is present in cells at much higher concentrations than acylphosphatase 1 (ref. 9), both enzymes most likely contribute to the formation of 4-P-erythronate *in vivo*. In contrast, phosphoglycerate kinase was much better than acylphosphatase 1 at using 1,3-bisphosphoglycerate (Fig. 5e). Hence, in cells, acylphosphatase 1 is not expected to represent a relevant bypass for the phosphoglycerate kinase reaction.



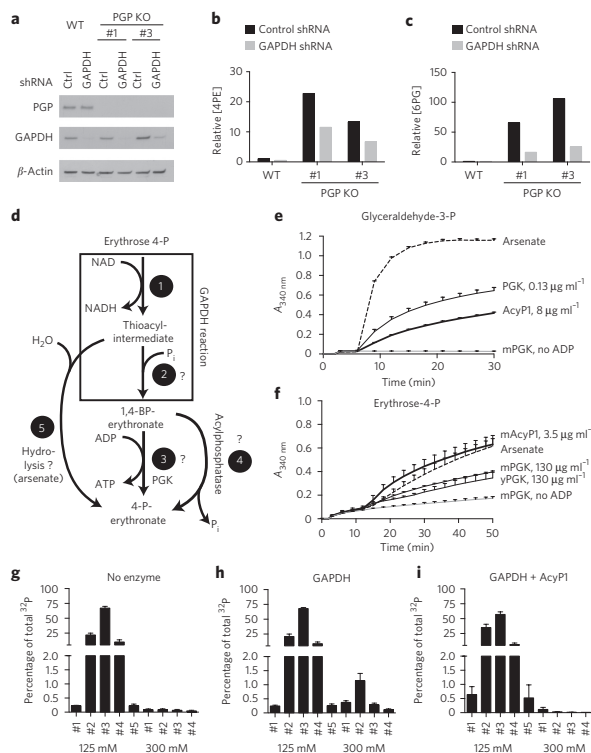


Figure 5 | 4-P-erythronate is formed by GAPDH via a 1,4-BP-erythronate intermediate, which is dephosphorylated by acylphosphatase or phosphoglycerate kinase. (a–c) Western blot analysis (a) and targeted GC/MS analysis of 4-P-erythronate (4PE) (b) and 6-P-gluconate (6PG) (c) of two PGP KO clones (1 and 3) expressing GAPDH or nonsilencing control (Ctrl) shRNAs. PGK, phosphoglycerate kinase. Values are the mean of three samples from one representative experiment and are normalized to values obtained in wild-type control shRNA cells. Results from four independent experiments are shown in **Supplementary Figure 9a, b**. (d) Schematic representation of potential mechanisms of 4-P-erythronate formation by GAPDH, leading to the formation of a thioacyl intermediate (reaction 1) and 1,4-BP-erythronate (reaction 2), which can be further metabolized via phosphoglycerate kinase (reaction 3) or acylphosphatase (reaction 4). Alternatively, the thioacyl intermediate could be directly hydrolyzed (reaction 5). (e, f) Progression of the reaction of GAPDH on 0.2 mM glyceraldehyde-3-P (e) or 0.2 mM erythrose-4-P (f) was measured spectrophotometrically in the presence of 5 mM inorganic phosphate (P_i) by following the absorption at 340 nm. Arrows indicate addition of 5 mM arsenate, mouse (mPGK) or yeast PGK (yPGK) \pm 1 mM ADP or mouse acylphosphatase 1 (mAcyP1). (g–i) Incorporation of [^{32}P]P_i into 1,4-BP-erythronate upon incubation of erythrose-4-P with [^{32}P]P_i and GAPDH. The reaction mixtures were chromatographed on an anion exchanger. P_i elutes at 125 mM NaCl, and the peak of radioactivity eluting with 300 mM NaCl depends on the presence of GAPDH (h) and is destroyed by acylphosphatase (i). Values in e–i are mean \pm s.e.m. of three independent experiments. Uncropped gels are available in **Supplementary Figure 15**.

To estimate the relative rate of the side reaction catalyzed by GAPDH, we compared its activities on erythrose-4-P and glyceraldehyde-3-P in the presence of arsenate, which stimulates both reactions. This revealed that GAPDH has a 3,500-fold lower catalytic

efficiency for erythrose-4-P than for glyceraldehyde-3-P (**Supplementary Fig. 10a, b**).

Confirmation of the involvement of 1,4-BP-erythronate

To confirm the formation of 1,4-BP-erythronate by GAPDH, we incubated erythrose-4-P with this enzyme and ^{32}P -labeled P_i (in the presence of lactate dehydrogenase and pyruvate to consume the formed NADH and thereby favor the oxidation of erythrose-4-P). We next chromatographed the reaction mixture on an anion exchanger to separate [^{32}P]1,4-BP-erythronate from radiolabeled P_i (eluting at 125 mM NaCl). A peak of radioactivity eluting at a higher salt concentration than P_i was indeed observed (**Fig. 5g, h**). This peak was suppressed when acylphosphatase 1 was present in the incubation mixture (**Fig. 5i**), indicating that it corresponded to 1,4-BP-erythronate.

If 4-P-erythronate formation from erythrose-4-P involves 1,4-BP-erythronate as an intermediate, we expected that, conversely, 4-P-erythronate would be converted to erythrose-4-P in the combined presence of phosphoglycerate kinase, GAPDH, ATP and NADH (i.e., the reverse of reactions 1–3 in **Fig. 5d**). Indeed, incubation of 4-P-erythronate led to the formation of a compound that was reduced by GAPDH in the presence of NADH (**Supplementary Fig. 11**). The decrease in the concentrations of NADH corresponded to the concentration of 4-P-erythronate added to the assay, indicating that the observed activity was not due to a minor contaminant potentially present in the 4-P-erythronate preparation.

Finally, to ensure that PGP was able to act on the 4-P-erythronate formed as a result of GAPDH's action, we incubated this enzyme with NAD⁺ and erythrose-4-P with or without PGP and/or acylphosphatase 1. In the absence of PGP, erythrose-4-P was partially converted to 4-P-erythronate, and this conversion was enhanced by acylphosphatase 1, confirming that part of the erythrose-4-P is converted to 1,4-BP-erythronate (**Supplementary Fig. 12**). When PGP was also present, 4-P-erythronate was almost completely converted to erythronate. The fact that acylphosphatase 1 stimulated the formation of 4-P-erythronate in the absence of PGP and stimulated the formation of erythronate in its presence confirmed that the oxidation of erythrose-4-P by GAPDH largely proceeds through 1,4-BP-erythronate.

DISCUSSION

With few exceptions, little attention has been paid to side reactions catalyzed by major enzymes of intermediary metabolism. Yet detailed characterization of enzymes in the past has disclosed side activities on substrates that are present in cells. In fact, the reason some expected side products are absent from cells is that they are destroyed by metabolite repair enzymes². PGP, conserved in yeast as Pho13, is remarkable in this 'sanitizing' function. It acts best on three abnormal metabolites but does not act substantially on 'classical' phosphate esters belonging to major metabolic pathways (**Fig. 6**). Its role in destroying 4-P-erythronate and 2-P-L-lactate in mammalian cells is supported by the finding

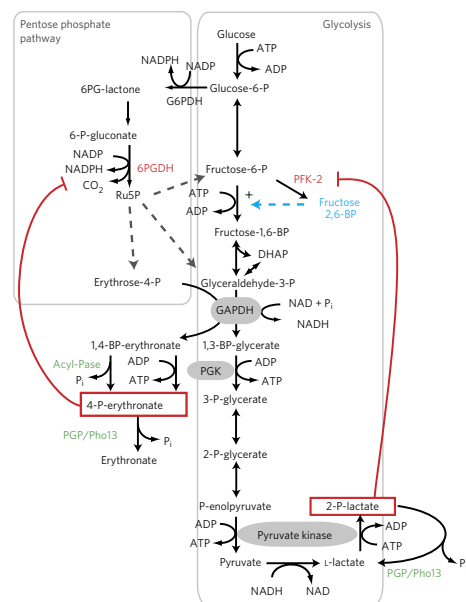


Figure 6 | Schematic representation of the metabolite repair function of PGP in central carbon metabolism. New metabolite repair activities and inhibitory interferences discovered or characterized in this paper are highlighted in green and red, respectively. The action of the known glycolytic activator fructose-2,6-BP is highlighted in blue. 6PGDH, 6-P-gluconate dehydrogenase; PGK, phosphoglycerate kinase; 6PG-lactone, 6-P-gluconolactone; Ru5P, ribulose-5-P. The potential direct formation of 4-P-erythronate by GAPDH is not represented in this schematic.

that these two compounds accumulate if PGP is knocked out. Concentrations of 4-P-erythronate in PGP KO cells are then more than 20 times higher than the IC_{50} for 6-P-gluconate dehydrogenase, leading to a marked accumulation of 6-P-gluconate. The 10- to 40-fold increase in the concentration of 2-P-L-lactate most likely inhibits fructose-2,6-BP production and thereby might contribute to the reduction of glycolytic flux observed in PGP KO cells.

These findings indicate that the absence of the metabolite repair enzyme PGP in mammalian cells induces major perturbations in central carbohydrate metabolism. Glycolysis is an archetypical high-flux pathway, and pyruvate kinase and GAPDH are among the most abundant proteins in cells⁹. Our data suggest the price of this high flux is the formation of side products that need to be eliminated to prevent negative interferences.

The catalytic efficiency of the action of GAPDH on erythrose-4-P is 3,500-fold lower than that on glyceraldehyde-3-P (Supplementary Fig. 6a,b). Likewise, the activity of pyruvate kinase on lactate is several orders of magnitude lower than the physiological pyruvate kinase reaction. Hence, both side reactions represent negligible fractions of the overall activity of these enzymes. Nevertheless, in the absence of PGP, the side products accumulated to levels similar to or even above those of regular metabolites (20–30 μ M for 4-P-erythronate; 2–4 mM for 2-P-L-lactate). Though this accumulation may seem surprising, it is not unexpected as a similar accumulation was indeed previously observed in the case of L-2-hydroxyglutarate⁶.

Even if the production rate is very low, side products will continue to accumulate in the absence of the dedicated repair enzyme until nonspecific mechanisms of degradation (or export) reach a rate that matches the production rate. If, for instance, these nonspecific mechanisms are 200-fold less efficient than the specific metabolite repair enzyme (for example, their K_m is 200-fold higher and the V_{max} is the same), the steady-state concentration of side product is expected to be 200-fold higher in the absence than in the presence of the specific repair enzyme. Side products may also accumulate until the reaction that produces them reaches its thermodynamic equilibrium, but again, this may occur at side product concentrations that are orders of magnitude higher than the level normally maintained by the metabolite repair enzyme.

Advances in metabolomics have revealed that the cellular metabolome is considerably more complex than that expected on the basis of our knowledge of canonical metabolic pathways²⁹. A considerable part of this complexity may result from side activities that form a kind of ‘underground metabolism’. This underground metabolism may be advantageous because it offers a repertoire of enzymatic reactions useful for microorganisms when they need to adjust to particular metabolic situations^{4,5}. In contrast, some side products may need to be eliminated because they are inhibitors of enzymes of intermediary metabolism, as it is in the case for 4-P-erythronate, 2-P-L-lactate (this work), L-2-hydroxyglutarate⁶ and 1,5-BP-xylulose⁸. Furthermore, the formation of some side products may cause ‘metabolite loss’. For example, formation of P-glycolate by a side reaction of Rubisco would lead to major carbon loss and inefficiency of photosynthesis were it not for the existence of a series of reactions allowing reconversion of P-glycolate to useful compounds^{3,23}. Lastly, side product accumulation may lead to osmotic problems if they are not destroyed or extruded from cells.

Molecules such as fructose-2,6-BP and cyclic AMP are purely regulatory molecules; i.e., they exert a regulatory role without being intermediates in any known metabolic pathway. Similarly, both 4-P-erythronate and 2-P-L-lactate are not intermediates in any known metabolic pathway in vertebrates, and they both modulate the activity of potentially rate-limiting enzymes. One may therefore wonder whether they could also have a regulatory role in cells, rather than just being unnecessary side products.

A major difference between fructose-2,6-BP and cyclic AMP, on the one hand, and 4-P-erythronate and 2-P-L-lactate, on the other hand, relates to their synthesis and breakdown. The former two compounds are synthesized and destroyed by dedicated enzymes, allowing their levels to be tightly controlled by many effectors. By contrast, 4-P-erythronate and 2-P-L-lactate are synthesized by enzymes whose main function is different, and because they are destroyed by a single enzyme their level cannot be independently controlled.

Other differences relate to the targets of 4-P-erythronate and 2-P-L-lactate; i.e., to the enzymes they regulate. The target of 4-P-erythronate, 6-P-gluconate dehydrogenase, is not an ideal target to control metabolism as it catalyzes a reaction downstream of a regulated step (the reaction catalyzed by glucose-6-phosphate dehydrogenase) in a linear sequence of reactions³⁰. Furthermore, blocking its activity leads to accumulation of 6-P-gluconate and to some wasteful dephosphorylation of the latter to gluconate.

The situation is different for 2-P-L-lactate, which can inhibit the production of fructose-2,6-BP. As 2-P-L-lactate is formed from lactate, an end product of glycolysis, it might serve as a feedback inhibitor that slows down glycolysis when L-lactate accumulates. Although this speculation is tempting, it will be difficult to test for several reasons. First, 2-P-L-lactate most likely acts on PFK-2 via the same site as P-enolpyruvate, and these effects are not expected to be simply additive but rather dependent on many other regulators of this enzyme. Second, we do not have the ability to selectively changing the 2-P-L-lactate levels in cells. Third, the cellular response of

PFK-2 depends on the presence of different isoforms that strongly differ in their regulation by 2-P-lactate and other regulators⁸.

In conclusion, our work illustrates that the coexistence of different metabolic pathways in cells causes major problems due to the many side reactions that are likely to occur. We demonstrate that metabolite repair enzymes can have an important role in preventing inhibitory interferences between metabolic pathways operating in parallel. Our work also suggests that the search for metabolite repair enzymes is an important strategy that will help to unravel the function of many remaining orphan enzymes in the human genome, including enzymes that provide key support for major metabolic pathways.

Received 1 June 2015; accepted 28 March 2016;
published online 13 June 2016

METHODS

Methods and any associated references are available in the [online version of the paper](#).

References

1. Tawfik, D.S. Accuracy-rate tradeoffs: how do enzymes meet demands of selectivity and catalytic efficiency? *Curr. Opin. Chem. Biol.* **21**, 73–80 (2014).
2. Linster, C.L., Van Schaftingen, E. & Hanson, A.D. Metabolite damage and its repair or pre-emption. *Nat. Chem. Biol.* **9**, 72–80 (2013).
3. Bauwe, H., Hagemann, M. & Fernie, A.R. Photorespiration: players, partners and origin. *Trends Plant Sci.* **15**, 330–336 (2010).
4. Notebaart, R.A. *et al.* Network-level architecture and the evolutionary potential of underground metabolism. *Proc. Natl. Acad. Sci. USA* **111**, 11762–11767 (2014).
5. Tawfik, D.S. Messy biology and the origins of evolutionary innovations. *Nat. Chem. Biol.* **6**, 692–696 (2010).
6. Rzem, R. *et al.* A mouse model of L-2-hydroxyglutaric aciduria, a disorder of metabolite repair. *PLoS ONE* **10**, e0119540 (2015).
7. Van Schaftingen, E. *et al.* Metabolite proofreading, a neglected aspect of intermediary metabolism. *J. Inher. Metab. Dis.* **36**, 427–434 (2013).
8. Bracher, A., Sharma, A., Starling-Windhof, A., Hartl, F.U. & Hayer-Hartl, M. Degradation of a potent Rubisco inhibitor by selective sugar phosphatase. *Nat. Plants* **1**, 14002 (2015).
9. Wiśniewski, J.R., Hein, M.Y., Cox, J. & Mann, M.A. 'Proteomic ruler' for protein copy number and concentration estimation without spike-in standards. *Mol. Cell. Proteomics* **13**, 3497–3506 (2014).
10. Ishii, Y., Hashimoto, T., Minakami, S. & Yoshikawa, H. The formation of erythronic acid 4-phosphate from erythrose 4-phosphate by glyceraldehyde-3-phosphate dehydrogenase. *J. Biochem.* **56**, 111–112 (1964).
11. Pasti, C. *et al.* Sugar derivatives as new 6-phosphogluconate dehydrogenase inhibitors selective for the parasite *Trypanosoma brucei*. *Bioorg. Med. Chem.* **11**, 1207–1214 (2003).
12. Maliekal, P., Vertommen, D., Delpierre, G. & Van Schaftingen, E. Identification of the sequence encoding N-acetylneuraminic-9-phosphate phosphatase. *Glycobiology* **16**, 165–172 (2006).
13. Ndubuisi, M.I. *et al.* Characterization of a novel mammalian phosphatase having sequence similarity to *Schizosaccharomyces pombe* PHO2 and *Saccharomyces cerevisiae* PHO13. *Biochemistry* **41**, 7841–7848 (2002).
14. Rose, Z.B., Grove, D.S. & Seal, S.N. Mechanism of activation by anions of phosphoglycolate phosphatases from spinach and human red blood cells. *J. Biol. Chem.* **261**, 10996–11002 (1986).
15. Ran, F.A. *et al.* Genome engineering using the CRISPR-Cas9 system. *Nat. Protoc.* **8**, 2281–2308 (2013).
16. Fan, J. *et al.* Quantitative flux analysis reveals folate-dependent NADPH production. *Nature* **510**, 298–302 (2014).
17. Schöneberg, T., Kloos, M., Bruser, A., Kirchberger, J. & Sträter, N. Structure and allosteric regulation of eukaryotic 6-phosphofructokinases. *Biol. Chem.* **394**, 977–993 (2013).
18. Rider, M.H. *et al.* 6-phosphofructo-2-kinase/fructose-2,6-bisphosphatase: head-to-head with a bifunctional enzyme that controls glycolysis. *Biochem. J.* **381**, 561–579 (2004).

19. Van Schaftingen, E., Hue, L. & Hers, H.G. Fructose 2,6-bisphosphate, the probable structure of the glucose- and glucagon-sensitive stimulator of phosphofructokinase. *Biochem. J.* **192**, 897–901 (1980).
20. Ash, D.E., Goodhart, P.J. & Reed, G.H. ATP-dependent phosphorylation of α -substituted carboxylic acids catalyzed by pyruvate kinase. *Arch. Biochem. Biophys.* **228**, 31–40 (1984).
21. Kim, S.R. *et al.* Deletion of *PHO13*, encoding haloacid dehalogenase type IIA phosphatase, results in upregulation of the pentose phosphate pathway in *Saccharomyces cerevisiae*. *Appl. Environ. Microbiol.* **81**, 1601–1609 (2015).
22. Leblond, D.J. & Robinson, J.L. Secondary kinase reactions catalyzed by yeast pyruvate kinase. *Biochim. Biophys. Acta* **438**, 108–118 (1976).
23. Schwarte, S. & Bauwe, H. Identification of the photorespiratory 2-phosphoglycolate phosphatase, PGLP1, in *Arabidopsis*. *Plant Physiol.* **144**, 1580–1586 (2007).
24. Kaneko, Y., Toh-e, A., Banno, I. & Oshima, Y. Molecular characterization of a specific *p*-nitrophenylphosphatase gene, *PHO13*, and its mapping by chromosome fragmentation in *Saccharomyces cerevisiae*. *Mol. Gen. Genet.* **220**, 133–139 (1989).
25. Seifried, A. *et al.* Evolutionary and structural analyses of mammalian haloacid dehalogenase-type phosphatases AUM and chronophin provide insight into the basis of their different substrate specificities. *J. Biol. Chem.* **289**, 3416–3431 (2014).
26. Corbier, C., Della Seta, F. & Branlant, G. A new chemical mechanism catalyzed by a mutated aldehyde dehydrogenase. *Biochemistry* **31**, 12532–12535 (1992).
27. Stefani, M., Taddei, N. & Ramponi, G. Insights into acylphosphatase structure and catalytic mechanism. *Cell. Mol. Life Sci.* **53**, 141–151 (1997).
28. Dixon, H.B.F. The biochemical action of arsenic acids especially as phosphate analogues. *Adv. Inorg. Chem.* **44**, 191–227 (1996).
29. Fiehn, O., Barupal, D.K. & Kind, T. Extending biochemical databases by metabolomic surveys. *J. Biol. Chem.* **286**, 23637–23643 (2011).
30. Stincone, A. *et al.* The return of metabolism: biochemistry and physiology of the pentose phosphate pathway. *Biol. Rev. Camb. Philos. Soc.* **90**, 927–963 (2014).

Acknowledgments

Funding was provided from WELBIO (CR-2015A-09 to E.V.S.), the Belgian National Science Fund (T0120.14 to E.V.S. and J0044.14 to G.T.B.), the Training Fund for Research in Industry and Agriculture (to E.B. and J.B.), the Belgian Cancer Foundation (2010-155 to G.T.B. and 2014-298 to E.V.S.), the Interuniversity Attraction Pole (IAP-P7.43 to E.V.S.), the European Union Seventh Framework Programme (FP7/2007–2013 grant no. 276814 to C.L.L. and EURO-CDG to E.V.S.) and Horizon 2020 (E-RARE-3: EURO-CDG2 to E.V.S.), the de Duve Institute and the Université Catholique de Louvain. We would like to thank E.R. Fearon (University of Michigan), F. Zhang (Massachusetts Institute of Technology), V. Delcenserie (University of Liège), G. Daube (University of Liège), L. Novellasedumant and R. Bartrons (University of Barcelona) for reagents, R. Gemayel (Catholic University of Leuven) for help with yeast experiments, C. Jäger and C. Singh (University of Luxembourg) for help with the GC/MS analysis, P. Sonveaux (Université Catholique de Louvain) and P.E. Porporato (Université Catholique de Louvain) for help with the Seahorse XF bioanalyzer (grant F.R.S.-FNRS FRFC 2.5025.12) and A.D. Hanson, L. Hue, J.-F. Collet and A. Peracchi for critical reading of the manuscript.

Author contributions

The study was mainly designed and written by G.T.B., E.V.S., F.C. and F.B. G.T.B. and E.V.S. supervised the work and are equally contributing corresponding authors. All authors contributed to the interpretation of the results, participated in the writing of the manuscript and approved the final version. F.C. identified and purified PGP and ACYP1. F.C., E.B. and I.G. performed enzymatic analysis. E.B., I.G., G.T.B., J.G. and C.L.L. performed GC/MS analysis. G.T.B., I.G., J.B., M.V. and F.B. generated and analyzed mammalian cell lines. J.B. measured oxygen consumption rate. F.B. generated and analyzed yeast strains. G.N., E.V.S. and I.G. performed PFK-2 analysis. A.H. and M.H.R. cloned and produced PFKFB proteins. D.V. and V.S. performed MS analysis.

Competing financial interests

The authors declare no competing financial interests.

Additional information

Any supplementary information, chemical compound information and source data are available in the [online version of the paper](#). Reprints and permissions information is available online at <http://www.nature.com/reprints/index.html>. Correspondence and requests for materials should be addressed to E.V.S. or G.T.B.

ONLINE METHODS

Unless otherwise stated, chemicals were obtained from Sigma at the highest degree of purity.

Synthesis of erythrose-4-P. D-Erythrose-4-P was produced enzymatically by phosphoketolase (E.C.4.1.2.22 from *Bifidus crudilactis*, described below³¹) from fructose-6-P. Fructose-6-P (5 mM) was incubated in a mixture (5 ml) containing 25 mM MES, pH 6.0, 5 mM inorganic phosphate (or 0.1 mM arsenate), 1 mM MnCl₂, 0.1 mM thiamine pyrophosphate, and 50 μg of phosphoketolase for 2 h at 30 °C. Because of its chemical instability, erythrose-4-P was not purified. Syntheses of [¹⁴C]erythrose-4-P and [¹⁴C]erythrose-4-P were performed similarly, starting with [¹⁴C]fructose-6-P or [¹⁴C]fructose-6-P. [¹⁴C]Fructose-6-P was obtained by phosphorylation of [¹⁴C]fructose (25 μmol; Cortecnet, France) upon incubation (1 h at 30 °C) in a reaction mixture (5 ml) containing 25 mM MES, pH 6.0, 5 mM ATP-Mg, 5 mM MgCl₂ and 50 μg yeast hexokinase (Roche). [¹⁴C]Fructose-6-P was prepared from [¹⁴C]glucose (Amersham), which was incubated with hexokinase under the conditions described above in the presence of 5 μg yeast phosphoglucose isomerase (Sigma). For spectrophotometric assays, D-erythrose-4-P was obtained from Sigma.

Synthesis of 4-P-erythronate. U-¹⁴C-labeled, U-¹⁴C-labeled and nonlabeled 4-P-erythronate were produced enzymatically from erythrose-4-P and the NAD-dependent erythrose-4-P dehydrogenase (gapB) from *Escherichia coli* K12 (ref. 32). Erythrose-4-P (5 mM) was incubated for 3 h at 30 °C in the presence of 100 μg purified recombinant erythrose-4-P dehydrogenase in a mixture (final volume 5 ml) containing 25 mM Hepes, pH 7.5, 0.1 mM NAD, 10 μg lactate dehydrogenase from rabbit muscle (Roche) and 5 mM pyruvate. The reaction was stopped by heating 10 min at 80 °C, and the reaction mixture was diluted in 20 ml water and loaded on a 25 ml AG1-X8 Dowex column (Cl⁻ form). The column was washed with 100 ml of water, a linear gradient of NaCl (0 to 1 M in 300 ml) was applied, and fractions (4 ml) were collected. For the detection of nonradioactive 4-P-erythronate, 50 μl of the fractions were incubated with 1 μg of alkaline phosphatase for 30 min at 30 °C in a mixture (100 μl) containing 25 mM Tris, pH 8.0, 1 mM MgCl₂ and 0.1 mM ZnCl₂. The reaction was stopped by heating for 5 min at 80 °C, and inorganic phosphate was measured³³. GC/MS analysis suggested >90% purity for 4-P-erythronate. For the purification of radiolabeled [¹⁴C]₄-P-erythronate, an aliquot (5 μl) of each fraction was counted for radioactivity in the presence of Ultima Gold (Perkin Elmer) in a liquid scintillation counter. Fractions containing 4-P-erythronate were lyophilized and freed from NaCl by filtration on a Bio-Gel P2 (Bio-Rad) column (50 cm × 1.0 cm) equilibrated with water.

Synthesis of 2-P-lactate. 2-P-lactate was synthesized as described previously³⁴. Briefly, 0.5 ml of methyl-L-lactate or methyl-D-lactate were phosphorylated with a ten-fold molar excess of POCl₃ in 5 ml of trimethylphosphate overnight at 0 °C. The reaction mixture was poured over 50 g of ice and immediately titrated to pH 9.5 with a saturated solution of lithium hydroxide. This solution was kept at pH 9.5 by repeated addition of lithium hydroxide for 3 h at room temperature (until the pH remained stable). The supernatant resulting from a centrifugation of 30 min at 5,000g and 4 °C was washed with two volumes of chloroform and saponified overnight at room temperature by addition of sodium hydroxide to a final concentration of 1 M. After adjusting the pH to 9.5 with HCl, two volumes of acetone were added, and the resulting mixture was incubated for 2 h at 0 °C. The pellet obtained after centrifugation for 30 min at 5,000g and 4 °C was washed with acetone and dried; 0.5 g of this pellet was resuspended in 100 ml of water and loaded on an anion exchange column (AG1-X8, Cl⁻ form, 200–400 mesh size, 15 × 1.9 cm). After washing with water (50 ml) and 10 mM HCl (25 ml), fractions were collected during an elution with 50 mM HCl. Fractions containing 2-P-lactate, as identified by measuring the phosphate released in the presence of alkaline phosphatase³⁵, were lyophilized, pooled and analyzed by GC/MS, suggesting >70% purity.

Purification and identification of 4-P-erythronate phosphatase from human erythrocytes. A hemolysate was prepared starting from 300 ml packed human erythrocytes as described³⁵. The supernatant (800 ml) was diluted with 800 ml

Buffer A (25 mM Hepes, pH 7.1, 1 mM DTT, 1 μg/ml leupeptin and antipain) and loaded onto a 75-ml DEAE Sepharose column equilibrated with the same buffer. The column was washed, a linear gradient (0–0.5 M NaCl in 2 × 250 ml buffer A) was applied, and fractions (5 ml) were collected. 4-P-erythronate and 2-P-glycolate phosphatase activities were measured in fractions (described below). Fractions containing 2-P-glycolate/4-P-erythronate phosphatase activity were pooled, diluted five-fold in Buffer B (25 mM Tris, pH 8.0, 1 mM DTT, 1 μg/ml leupeptin and antipain) and loaded onto a 25-ml Q-Sepharose column equilibrated with Buffer B. A linear NaCl gradient (0–0.5 M NaCl in 2 × 125 ml Buffer C) was applied. Fractions containing 4-P-erythronate phosphatase activity were pooled and concentrated to 2 ml in an Amicon Ultra 30-kDa concentration unit (Millipore) and loaded onto a Superdex S-200 gel filtration column (GE Healthcare) in the presence of markers of molecular mass, as described previously³⁶.

Fractions containing 2-P-glycolate/4-P-erythronate phosphatase activity were loaded on a 10% (w/v) polyacrylamide-SDS gel. After electrophoresis, the gel was stained with colloidal Coomassie Blue (Fermentas). The bands of interest were cut out and digested with trypsin. Peptides were analyzed by capillary LC/tandem MS in a LTQ XL ion trap mass spectrometer (ThermoScientific) fitted with a microelectrospray source. The data were analyzed with the ProteomeDiscoverer software (ThermoScientific), and the proteins were identified with SEQUEST against a target-decoy nonredundant human protein database obtained from NCBI. The false discovery rate was below 5%. In parallel, fractions were analyzed by Western Blot analysis using an anti-PGP antibody (Santa-Cruz Biotechnology, described below).

Cloning and preparation of expression vectors. *B. crudilactis* phosphoketolase (PKT; WP_034252558.1), *Mus musculus* PGP (PGP; GenBank reference sequence NM_025954), glyceraldehyde-3-phosphate dehydrogenase (GAPDH; GenBank reference sequence NM_001289726), acylphosphatase 1 (ACYP; GenBank reference sequence NM_001107.4), phosphoglycerate kinase 1 (PGK; GenBank reference sequence NM_008828), *Homo sapiens* pyruvate kinase M2 (PKM2; GenBank reference sequence NM_002654) and *S. cerevisiae* S288c *PHO13* (GenBank reference sequence NM_001180296) were PCR amplified from *B. crudilactis* genomic DNA (kind gift from V. Delcenserie and G. Daube, University of Liège), mouse liver cDNA, human cDNA obtained from the colorectal cancer cell line HT29 or yeast genomic DNA, using 5′ primers (PKT: GTC CAT GGC CAT ATG ACC GAT TTC ACC TGG TCT GAA CTG GAC G; PGP: GTCC GAT CGC CAT ATG GCA GAG GCG GAA GCC GGT GGC; GAPDH: CGC GGG ATC CAT ATG GTG AAG GTC GGT GTG AAC G; ACYP: GTC CAT GGC CAT ATG GCA GAA GGG GAC ACC TTG; PGK: ATT CAA CAT ATG TCG CTT TCC AAC AAG CTG A; *PHO13*: GTC CAT GGC CAT ATG ACT GCT CAA CAA GGT GTA; PKM2: ATA CAA ACA TAT GTC GAA GCC CCA TAG TGA AG) containing a NdeI restriction site (in bold) and 3′ primers containing a BamHI site (PKT: GTTA GCA GCC GGA TCC TCA GGC CTT GGC TTC GGC GAT GGA GGC C; PGP: GTTA GCA GGC GGA TCC TTA ACC TTG AAG GGC AGG CAA GAG CTC GGC; ACYP: GCC ATG GAC GGA TCC TTA TTT TAC AAT TTG GAA GTC TGA ATA ATC C; PGK: ATA TTA GGA TCC CTA AAC ATT GCT GAG AGC ATC; *PHO13*: GCC ATG GAC GGA TCC CTA TAA CTC ATT ATT GGT TAA GGT) or containing an XhoI site (GAPDH: GAG CTC CTC GAG CTC CTT GGA GGC CAT GTA GGC; PKM2: TTA TAT CTC GAG CCA TCA CCG CAC AGG AAC AAC A). The resulting PCR products were inserted in the pET15b bacterial expression vector at the NdeI-BamHI or NdeI-XhoI sites. The expression vector for *E. coli* GapB (NP_417402.1) was obtained from the ASKA collection³⁷.

Human PFKFB4 cDNA in the vector pCDNA3 was generously provided by R. Bartrons (University of Barcelona)³⁸. The protein-coding sequence was amplified by PCR (EcoRI_PFKFB4 (forward) 5′-AAA AGA ATT CAT GGC GTC CCC ACG GGA A-3′ and XhoI_PFKFB4 5′-AAA ACT CGA GTC ACT GGT GAG CAG GCA C-3′ (reverse)) and inserted into the EcoRI and XhoI restriction sites of the vector pGEX-6P-1 (GE Healthcare). The expression vector for GST-tagged PFKFB2 was previously described³⁹, and that used for GST-tagged PFKFB3 was a generous gift from L. Novellademunt (Francis Crick Institute)⁴⁰.

To generate a retroviral vector for expression of murine PGP, we performed a PCR with primers mPGP_s ATA CAT TGT ACA CAC CAT GGC AGA GGC

GGA AG and mPGP_as TTA TAT GCG GCCGCC CAG AGA TTA AAG ACA CTA GAT CT on mouse liver cDNA using Pfu polymerase. This PCR product was initially inserted in a lentiviral vector via the restriction sites NotI and BsrGI and subsequently shuttled into the BamHI and EcoRI sites of the retroviral vector pBABE-PURO as a PCR product obtained with the primers mPGP_s2 ATA CAT GGA TCC CAC CAT GGC AGA GGC GGA AG and mPGP_as2 TTA TAT GAA TTC CCA GAG ATT AAA GAC ACT AGA TCT.

CRISPR-Cas9 constructs were generated by ligating two different annealed primer pairs (CRISP_PGP_s1 CAC CGG CAG CGG GCG TCG TCG CCA C and CRISP_PGP_as1 AAA CGT GGC GAC GAC GCC GCG TGC C, CRISP_PGP_s2 CAC CGG CGG GCG TCA GCC GCA CGC AG and CRISP_PGP_as2 AAA CCT GCG TGC GGC TGA GCG CCG CC) into the vector pSpCas9(BB)-2A-Puro (PX459) (a gift from F. Zhang, Massachusetts Institute of Technology; Addgene plasmid no. 48139)¹⁵. All constructs were validated by sequencing (Beckman Coulter Genomics).

Expression and purification of recombinant proteins. His-tagged proteins were produced in BL21*pLysS* carrying the appropriate expression plasmid as previously described¹⁵. The expression of PKT was carried out at 16 °C for 24 h, and the expression of PGP, GAPDH, ACYP1, PGK, PKM2, Pho13 and GapB was carried out at 37 °C for 4 h. The preparation of bacterial extracts and the purification of recombinant proteins on His-trap columns and subsequent desalting on PD-10 columns was performed as described before¹². Purity was estimated to be at least 80%, based on SDS-PAGE analysis using Coomassie Blue staining (Supplementary Fig. 14).

GST-tagged PFKFB2, PFKFB3 and PFKFB4 were expressed overnight at 18 °C in BL21 *E. coli* cells induced with 0.5 mM IPTG. Bacteria were collected by centrifugation (5,000g × 10 min at 4 °C), resuspended in one-tenth of the culture volume of ice-cold lysis buffer (50 mM Tris-HCl pH 7.5, 150 mM NaCl, 0.1% (v/v) 2-mercaptoethanol, 0.01% (w/v) Brij 35, 0.5 mM PMSE, 0.5 mM benzamidine Cl, 1 μg/ml leupeptin and 1 μg/ml aprotinin) and homogenized using a French press. The lysate was cleared by centrifugation (17,000g × 20 min at 4 °C), and the supernatant was passed through a 45-μm mesh filter (Millex-HA, Merck-Millipore) before loading onto a GSH-Sepharose column (0.5 × 20 cm, GE Healthcare). After extensive washing, the column was eluted with a 0–10 mM gradient of GSH. Fractions were analyzed by SDS-PAGE followed by Coomassie Blue staining. Fractions containing GST-tagged PFKFB protein were pooled and concentrated using a 50-kDa ultra-filtration unit (Amicon) while changing the buffer to enzyme storage buffer (50 mM Tris-HCl pH 7.5, 150 mM NaCl, 0.1% (v/v) 2-mercaptoethanol and 10% (v/v) glycerol).

Tissue distribution of 4-P-erythronate phosphatase. Mouse (male, C57BL/6) tissues were homogenized with 3 ml/g Buffer A (25 mM Hepes, pH 7.1, 120 mM NaCl) and centrifuged for 30 min at 18,000g. The supernatants were used for the measurements of 4-P-erythronate phosphatase activity using radiolabeled substrate. Protein was assayed with the method of Bradford using bovine γ globulin as a standard (Bio-Rad). A relative quantification of 4-P-erythronate/2-P-glycolate phosphatase (PGP) was performed by quantitative western blot on an Odyssey Infrared Imager (Licor) using anti-PGP antibodies (Sigma Aldrich, diluted 1:2,000) and IRdye 680 anti-goat secondary antibodies (Licor, diluted 1:5,000).

Enzymatic assays. Phosphatase activity assays were performed at 30 °C in a mixture (usually 100 μl) containing 25 mM Tris, pH 7.1, 1 mM MgCl₂ and various concentrations of substrate and the appropriate amount of enzyme and incubation time to remain below 20% substrate consumption. The incubation was stopped (typically after 20–30 min) by heating 5 min at 80 °C. The denatured proteins were removed by centrifugation (15 min at 15,000g at 4 °C) and the released inorganic phosphate was measured according to the method described in ref. 33.

A more sensitive 4-P-erythronate phosphatase assay was also performed using radiolabeled [U-¹⁴C]4-P-erythronate in a mixture (200 μl final volume) comprising, unless otherwise stated, 25 mM Hepes, pH 7.1, 5 mM glucose-6-P, 1 mM MgCl₂, 30,000 c.p.m. radiolabeled 4-P-erythronate and unlabeled 4-P-erythronate in concentrations ranging from 0 mM to 1 mM. After

30 min at 30 °C, the reaction was stopped by heating 5 min at 80 °C and centrifuged (15 min at 15,000g at 4 °C). The resulting supernatant was diluted with 0.8 ml 10 mM Hepes, pH 7.1 (buffer C) and applied onto a 1-ml Dowex AG1-X8 column (Cl⁻ form, 100–200 mesh, Acros Organics) prepared in a Pasteur capillary pipette. The resin was washed with 4 ml of buffer C, followed by 8 ml of 75 mM NaCl in buffer C to elute [U-¹⁴C]erythronate and then 8 ml of 150 mM NaCl in buffer C to elute [U-¹⁴C]4-P-erythronate. Fractions (2 ml) were collected and counted for radioactivity in the presence of Ultima Gold (Perkin Elmer) in a liquid scintillation counter.

Fructose-2,6-BP concentrations were determined in cellular lysates obtained by lysis in 0.1 M NaOH as described before¹⁴ and normalized to protein concentrations. PFK-2 activity was assessed by measuring the fructose-2,6-BP formation in a 500-μl reaction containing 25 mM Hepes, pH 7.1, 2 mM MgCl₂, 25 mM KCl, 1 mM P_i, 500 μM fructose-6-P, 1,750 μM glucose-6-P and 5 mM ATP/Mg after incubation for 30 min at 30 °C in the presence of 25 μl of crude lysate (10 μg/μl) and without or with 100 μM 2-P-lactate. Crude lysates from HCT116 cells were obtained in three freeze-thaw cycles in a buffer containing 50 mM Hepes, pH 7.5, 0.2% Triton X-100, 50 mM KF, 1 mM P_i, 5 mM EDTA, 5 mM EGTA, 1 mM Na₂VO₄, 15 mM mercaptoethanol, 1 mM PMSE, 1 μg/ml leupeptin and 2 mM DTT.

Kinase activities of PFKFB2, PFKFB3 and PFKFB4 were assessed in a similar reaction except for the presence of 100 μM fructose-6-P, 350 μM glucose-6-P and 0.62 μg/ml of enzyme in the presence of the indicated concentrations of 2-P-lactate (Fig. 3f). Phosphofruktokinase-2 reactions were stopped by addition of an equal volume of 0.2 M NaOH, and fructose-2,6-BP concentrations were measured as described before¹⁴.

Activity of pyruvate kinase was assessed by incubating sodium l-lactate (pH 8) (at the indicated concentrations; Fig. 3g) for 5 h at 30 °C in a mixture containing 25 mM Tris, pH 8, 5 mM MgCl₂, 20 mM KCl, 2.5 mM ATP and 0.1 mM fructose-1,6-BP. The reaction was stopped by heating for 5 min at 95 °C and was centrifuged to remove denatured proteins; 100 μl of the supernatant were analyzed by HPLC on a strong anion exchange column (Partisphere SAX, 125 × 4.6 mm) using an Agilent 1100 HPLC system with a diode array detector. Elution was performed with a gradient of ammonium phosphate buffer at pH 3.7 (10–500 mM) at a flow rate of 2 ml/min, and absorptions at 220 nm were followed. Concentrations of 2-P-lactate were determined by comparing the peak areas with those obtained from purified standards of defined concentration.

To follow the progression of the oxidative phosphorylation activity of GAPDH on erythrose-4-P and glyceraldehyde-3-P, we measured the absorption of NADH at 340 nm (Fig. 5e,f). Substrates were tested at a fixed concentration of 0.2 mM in a mixture containing 25 mM Hepes, pH 7.4, 1 mM MgCl₂, 0.5 mM NAD⁺, 1 mM DTT, 5 mM P_i and 0.1 mM BSA. Approximately 0.3 mg/ml of rabbit muscle GAPDH were used in the tests with erythrose-4-P, and 100 times less enzyme was used for glyceraldehyde-3-P. Where indicated, mouse acylphosphatase-1, mouse or yeast phosphoglycerate kinase, ADP or arsenate were added.

To investigate the formation of 1,4-BP-erythronate in the presence of ³²P (Fig. 5g–i), we incubated erythrose-4-P (1 mM) in a reaction mixture (2 ml) containing 25 mM Hepes, pH 7.4, 10⁶ c.p.m. of [³²P]P_i, 0.1 mM of cold P_i, 0.5 mM NAD⁺, 0.05 mg/ml lactate dehydrogenase (LDH) and 2 mM pyruvate in the presence or absence of 0.15 mg/ml GAPDH and/or 0.0025 mg/ml acylphosphatase 1 (ACYPI) for 90 min at 30 °C. Pyruvate and LDH were incorporated in this reaction to keep concentrations of NADH low. The pH of the mixture was lowered to ~5 by addition of 50 mM acetic acid to stabilize the acyl-phosphate formed during the reaction, and the resulting sample was loaded onto a 1-ml AG1-X8 Dowex column (Cl⁻ form). The column was washed with 1 ml of water. Five milliliters of 125 mM NaCl in 10 mM acetic acid and 4 ml of 300 mM NaCl in 10 mM acetic acid were successively applied, and fractions (1 ml) were collected. ³²P was assayed by counting an aliquot (250 μl) of each fraction in a liquid scintillation counter in the presence of Ultima Gold (Perkin Elmer) scintillation cocktail.

The combined action of phosphoglycerate kinase and GAPDH on 4-P-erythronate (i.e., the reverse reaction of Fig. 5d) was assessed (Supplementary Fig. 11) by incubating 4-P-erythronate (0–75 μM) in a reaction mixture containing 25 mM Hepes, pH 7.4, 1 mM MgCl₂, 1 mM ATP and 0.1 mM

NADH in the presence or absence of 0.10 mg/ml phosphoglycerate kinase and 0.15 mg/ml GAPDH in this order. NADH consumption was followed spectrophotometrically at 340 nm.

To detect the formation of 4-P-erythronate and erythronate by GAPDH (Supplementary Fig. 12), 1 mM erythrose-4-P was incubated in a mixture containing 25 mM Hepes, pH 7.4, 1 mM MgCl₂, 0.5 mM NAD⁺, 1 mM DTT, 5 mM P_i and 0.1 mM BSA in the presence of GAPDH (8 μg/ml), 8 μg/ml ACYP1 and/or 10 μg/ml PGP. Reactions were quenched with an equivalent volume of cold methanol containing 25 μM ribitol. Metabolites were extracted, derivatized and analyzed by GC/MS as described below. Integrated peak intensities were normalized to those obtained for ribitol.

6-P-gluconate dehydrogenase inhibition assay. 6-P-gluconate dehydrogenase inhibition by 4-P-erythronate was measured in the presence of the indicated concentrations of this metabolite (Fig. 2c) in an assay mixture comprising 20 mM Hepes, pH 7.1, 0.1 mM 6-P-gluconate, 0.5 mM NADP⁺, 1 mM MgCl₂ and 25 mM KCl. NADPH formation was followed spectrophotometrically at 340 nm. Human 6-P-gluconate dehydrogenase was partially purified from human erythrocytes. Briefly, a hemolysate was prepared starting from 100 ml packed human erythrocytes as described³⁵. The supernatant (250 ml) was diluted with 250 ml Buffer A (25 mM Hepes, pH 7.1, 1 mM DTT, 1 mM MgCl₂, 1 μg/ml leupeptin and antipain) and loaded onto an 80-ml Blue Sepharose (GE Healthcare) column equilibrated with the same buffer. The column was washed, a linear gradient (0–1 M NaCl in 2 × 250 ml buffer A) was applied, and fractions (5 ml) were collected. Fractions containing 6-P-gluconate dehydrogenase activity were pooled and used for the assays. Yeast 6-P-gluconate dehydrogenase was purchased from Sigma-Aldrich (P4553).

Yeast strain construction and culture conditions. The *S. cerevisiae* strains used in this study were generated from the BY4742 strain (MATα; his3Δ 1; leu2Δ 0; lys2Δ 0; ura3Δ 0) derived from *S. cerevisiae* S288C from EUROSCARF⁴². Strains were grown in YPD medium (1% Bacto yeast extract, 2% Bacto peptone and 2% glucose) at 30 °C. For metabolite analysis, yeasts were grown in supplemented minimal medium (0.67% Bacto yeast nitrogen base without amino acids and 2% carbon source) to which we added 20 mg/l uracil, 20 mg/l l-histidine, 30 mg/l l-leucine and 30 mg/l l-lysine.

The deletion strains were generated by replacing the gene *PHO13* with an antibiotic-resistance cassette by homologous recombination. A PCR product encompassing a kanamycin resistance cassette (KanMX) was amplified from the pUG6 plasmid⁴³ with the primers 5'-AGC CAA ATC ACA AAA AAA GCC TTA TAG CTT GCC CTG ACA AAG AAT ATA CAA CTC GGG AAA CAG GTC GAC AAC CCT TAA T-3' and 5'-AAA CCT GAA TAT TTT TCC TTT TCA AAA AGT AAT TCT ACC CCT AGA TTT TGC ATT GCT CCT GTG GAT CTG ATA TCA CCT A-3' using PfuI polymerase.

To generate a plasmid vector for expression of yeast Pho13, we performed a PCR with primers Pho13_s_GTC CAT GGC GGT ACC ATG ACT GCT CAA CAA GGT GTA and Pho13_as GCC ATG GAC GGA TCC CTA TAA CTC ATT ATT GGT TAA GGT on *S. cerevisiae* cDNA using Pfu polymerase. The resulting PCR product was inserted in the plasmid pRS426 via the restriction sites KpnI and BamHI. Transformed yeasts were selected in synthetic complete medium without uracil. Yeasts transformed with an empty vector served as control.

Yeast transformations were performed by the lithium acetate procedure⁴⁴ and correctly targeted clones were identified by PCR and verified by sequencing. A commercial *PHO13*-deficient strain obtained from EUROSCARF (ID: Y13933)⁴² was also used, and similar results were obtained.

Extraction of metabolites from yeast after methanol quenching. Yeast cell cultures in mid-exponential phase (OD₆₀₀ 1.0) were quenched according to the method described in ref. 45 with the following adaptations. Samples (5 ml) were quickly released into a 25-ml methanol-water solution (60% v/v) at –20 °C, resulting in a final methanol concentration of 50% (v/v). Biomass was separated from the quenching solution by centrifugation at 3,900g for 3 min at –10 °C. Extraction was initiated by resuspending the pellet in 1 ml of methanol-water solution (50% v/v) at –20 °C with 45 nmol of [¹³C]erythronate-4-P (as internal standard) and 500 mg of acid-washed glass beads (150–212 μm;

Sigma-Aldrich). Cells were homogenized on a rotary shaker at 2,200 r.p.m. for 15 min at 4 °C (IKA Vibrax VXR). One milliliter of chloroform was added, and samples were shaken for 1 min using a vortex mixer. Phase separation was induced by centrifugation (13,200 r.p.m., 3 min, 4 °C). The upper aqueous phase, containing the polar metabolites, was collected, dried and stored at –80 °C. Samples were derivatized and analyzed as described below for mammalian samples. Protein concentration in parallel cultures was determined with the bicinchoninic acid method (BCA assay, Thermo Scientific).

Analysis of intracellular metabolites in mammalian cell lines. Metabolite extraction, derivatization and GC/MS analysis were performed using modifications of methods described previously^{46,47}. Cells were plated at 700,000 cells per well of a six-well plate 18 h before harvesting (Fig. 5a–c). Alternatively, 400,000 cells per well were plated 40 h before harvesting, and medium was replaced 16 h before harvesting by medium containing dialyzed FCS and 10 mM D-glucose (Figs. 2 and 3). Where indicated, 5 mM C³-H₂-l-lactate (Cambridge Isotope Laboratories) was added 6 h before harvesting.

After briefly rinsing with 2 ml of ice-cold 0.9% NaCl, we sequentially added 0.5 ml of –80 °C cold methanol and 0.5 ml of ice-cold water (containing 3 μM [U-¹³C]₄P-erythronate as an internal standard). Cells were collected with a scraper, transferred into a tube containing 1 ml of chloroform and vigorously vortexed for 30 min at 4 °C. The upper aqueous phase, obtained after centrifugation at 22,000g for 5 min at 4 °C, was dried down under vacuum.

Dried samples were dissolved in 15 μl 4% methoxyamine in pyridine and incubated for 90 min at 30 °C. Trimethylsilylation was performed by adding 30 μl of MSTFA (Covachem) and incubating at 37 °C for 30 min. GC/MS analysis was performed using an Agilent 7890A GC equipped with a 30-m DB-5 ultra inert capillary column connected to an Agilent 5977 mass-sensitive detector operating under electron impact ionization at 70 eV. One microliter of sample was injected in splitless mode at 270 °C, using helium as the carrier gas at a flow rate of 1 ml min^{–1}. The GC oven temperature was held at 100 °C for 3 min and increased to 300 °C at 3.5 °C min^{–1} (ref. 46). The MS source and quadrupole detector were held at 230 °C and 150 °C, respectively. Data were acquired in combined selected-ion monitoring and scanning mode (68–700 *m/z*). Compounds were identified on the basis of their retention time and characteristic ions (Supplementary Fig. 13 and ref. 47). Selected-ion monitoring (SIM) chromatograms were integrated using Masshunter software (Agilent), and areas were normalized to total ion current⁴⁷. GC/MS experiments were performed three or four times on separate days over a time frame of six weeks. In each experiment, for each condition three tissue-culture wells were quenched, extracted and derivatized separately. Each sample was then analyzed separately (i.e., the samples were not pooled) by GC/MS. Peak areas of selected quantifier ion chromatograms were integrated and normalized to total ion current⁴⁷ (Supplementary Data Sets 1 and 2, panel 1, #1). To facilitate the comparison between experiments, we then divided the values by the average of the values obtained in the control cell line (Supplementary Data Sets 1 and 2). In each experiment, the mean values for the normalized metabolite concentrations were calculated (Supplementary Data Sets 1 and 2, panel 1, #3). The resulting three or four mean values (depending on the number of experiments) were then used to calculate mean values and s.e.m. (Supplementary Data Sets 1 and 2, panel 1, #4), which are shown in the figures. Because metabolite concentrations are log-normal distributed, we log-transformed normalized metabolite concentrations (Supplementary Data Sets 1 and 2, panel 1, #3) before calculations of confidence intervals (Supplementary Tables 2 and 3 and Supplementary Data Sets 1 and 2, panel 2). Calculations based on the peak area obtained with a known amount of [U-¹³C]₄-P-erythronate spiked into the cell extracts allowed us to determine the absolute amount of 4-P-erythronate per mg protein. Cellular concentrations were then estimated on the basis of a cellular water content of 4 μl per mg protein⁴⁸. Concentrations of 2-P-l-lactate in PGP KO clone #1 were estimated by linear regression of the peak areas extracted from SIM chromatograms from samples, where different amounts of purified 2-P-l-lactate had been spiked in. Mass isotopomer distributions of 2-P-lactate (*m/z* 371–376) were extracted from SIM chromatograms and corrected for natural isotope distributions using the program IsoCor⁴⁹.

Determination of metabolite concentrations in culture medium. To 0.2 ml of clarified medium we added perchloric acid to a final concentration of 5%. Samples were centrifuged for 10 min at 12,000 r.p.m. and 4 °C, and the resulting supernatant was neutralized by addition of 2 M K₂CO₃. Concentrations of metabolites were determined at 30 °C by monitoring the change in absorbance at 340 nm using a DU 800 UV/Vis Beckman Coulter spectrophotometer. Glucose concentration measurement was performed in a reaction mixture (1 ml) containing 50 mM Tris, pH 7.6, 1 mM NADP⁺, 5 mM MgCl₂, 2 mM ATP, 0.1% BSA using yeast hexokinase and glucose-6-phosphate-dehydrogenase as coupling enzymes. For the measurement of l-lactate, lactate dehydrogenase from rabbit muscle (Roche) was added to a reaction mixture (1 ml) containing 2.5 mM NAD⁺ and 300 mM glycine/hydrazine sulfate buffer at pH 9.0.

Lentiviral and retroviral transduction. HCT116 cells, a gift from E. Fearon (University of Michigan, Ann Arbor), were cultured in DMEM (Dulbecco's modified Eagle's medium) containing 10% FBS, 2 mM l-glutamine and penicillin/streptomycin (Life Technologies). CRISPR constructs were transfected using Lipofectamine 2000. After 24 h, cells were passaged into medium containing 2 µg/ml puromycin. Medium was changed to medium without puromycin 48 h later to avoid selection of cell lines with genomic integration of the CRISPR construct. Colonies were picked 14 d later, expanded and analyzed using western blot for PGP protein expression. Sequencing of PCR products encompassing the targeted sites was used to validate that the analyzed clones are derived from distinct targeting events (**Supplementary Table 1**). Comparable results were obtained with clones obtained by cotransfection of two CRISPR/Cas9 constructs (clones #1, #2 and #4) or single CRISPR/Cas9 (clone #3 and #5) constructs. A lentiviral shRNA construct targeting human glyceraldehyde-3-phosphate dehydrogenase (GAPDH) was obtained from GE Healthcare Life Sciences in the vector pGIPZ (allowing expression of shRNA, GFP and puromycin resistance from the same transcript). Lentivirus production was performed as described previously, and cell lines were transduced in the presence of 8 µg/ml polybrene (Sigma)[®]. Selection was performed with 2 µg/ml of puromycin for 4 d.

Recombinant retroviruses expressing mouse PGP were produced by cotransfection of the retroviral vector (pBABE-PURO and pBABE-PURO-mPGP, respectively) and the packaging plasmid pCL-ampho (Promega) into HEK293T cells using the calcium phosphate precipitation method⁴⁰. Supernatants were used to infect target cells three times at 12-h intervals. Selection with puromycin was performed as above.

Measurement of oxygen consumption rate. Cells were plated at 15,000 cells per well of a XF96 cell plate (Seahorse) 24 h before the experiment. Just before the assay, medium was replaced by DME base medium (Sigma, D5030) supplemented with 4.5 g/l glucose, 0.584 g/l l-glutamine, 0.11 g/l sodium pyruvate, 0.015 g/l phenol red and 1.85 g/l NaCl, and cells were incubated for 1 h in a non-CO₂ incubator. A mitochondrial stress test was then performed using the different compounds of the Mitostress kit (Seahorse) at the following concentrations: 1 µM oligomycin, 0.45 µM FCCP, 1 µM antimycin A and 1 µM rotenone. Oxygen consumption rate was normalized to protein concentration.

Alamar Blue. Cell proliferation was assessed using the Alamar Blue assay⁵¹. Cells were plated in 96-well microtiter plates. Cell viability was assessed 24 h and 96 h after plating by adding one-tenth the volume of a 560-µM solution of resazurin (prepared in 0.9% NaCl solution from a 10-mM stock solution in DMSO), incubating for 4 h at 37 °C and measuring fluorescence upon excitation at 540 nm and emission at 590 nm. To exclude the influence of different plating efficiencies, we normalized the results obtained after 96 h to the results obtained after 24 h.

NADPH/NADP⁺ assay. NADPH and NADP⁺ concentrations were determined by modifying a previously described method⁵². 500,000 cells were plated in each well of a six-well plate. After 24 h, cells were washed once with ice-cold PBS and lysed in 200 µl of a 1:1 mixture of alkaline lysis buffer (100 mM Na₂CO₃, 20 mM NaHCO₃, 0.05% (v/v) Triton X-100, 10 mM nicotinamide, 1% dodecyltrimethylammonium bromide (DTAB)) and PBS. Lysates were clarified by centrifugation for 1 min at 12,000g and 4 °C. The resulting supernatant

was divided in three portions of 50 µl. To measure both NADP⁺ and NADPH, portion A was neutralized by adding 45 µl of a 1:1:1 mixture of 1 M HCl, 1 M NaOH and 1 M bicine. To destroy NADPH, we heated portion B for 20 min at 60 °C after addition of 15 µl of 1 M HCl. To destroy NADP⁺, portion C was directly heated for 20 min at 60 °C. Portions B and C were neutralized by addition of 30 µl of a 1:1 mixture of 1 M NaOH and 1 M bicine or by addition of 45 µl of a 1:1:1 mixture of 1 M HCl, 1 M NaOH and 1 M bicine, respectively. The concentrations of NADPH and NADP⁺ were determined in a cycling assay (total volume 120 µl) containing 50 µl of the treated lysates, 0.1 M bicine, 50 mM EDTA, 50 µM resazurin, 5 mM glucose 6-phosphate, 1 U/ml of yeast glucose 6-phosphate dehydrogenase (Roche) and 10 µg/ml diaphorase from *Clostridium kluyveri* (Sigma D2197). The increase of fluorescence resulting from the reduction of resazurin to resorufin (excitation 530 nm, excitation 590 nm) was measured over time using a temperature-controlled (30 °C) multiwell plate fluorescence reader (Spectramax XS, Molecular Devices) and compared to standards.

Statistical analysis. Statistical analysis was performed with GraphPad Prism. When two conditions were compared, a two-sided Student's *t*-test was performed. When multiple groups were compared, two-way ANOVA was performed followed by a comparison of groups using Dunnett's test for multiple comparisons (when comparing to a single control group) or the Tukey's test (when performing several pairwise comparisons). Metabolite concentrations were log-transformed before statistical analysis. In all cases, a multiplicity adjusted *P* value of < 0.05 was considered significant and is indicated by an asterisk.

- Delcenserie, V. *et al.* Description of a new species, *Bifidobacterium crudilactis* sp. nov., isolated from raw milk and raw milk cheeses. *Syst. Appl. Microbiol.* **30**, 381–389 (2007).
- Boschi-Muller, S., Azza, S., Pollastro, D., Corbier, C. & Branlant, G. Comparative enzymatic properties of GapB-encoded erythrose-4-phosphate dehydrogenase of *Escherichia coli* and phosphorylating glyceraldehyde-3-phosphate dehydrogenase. *J. Biol. Chem.* **272**, 15106–15112 (1997).
- Itaya, K. & Ui, M. A new micromethod for the colorimetric determination of inorganic phosphate. *Clin. Chim. Acta* **14**, 361–366 (1966).
- Nowak, T. & Mildvan, A.S. Stereoselective interactions of phosphoenolpyruvate analogues with phosphoenolpyruvate-utilizing enzymes. *J. Biol. Chem.* **245**, 6057–6064 (1970).
- Delpierre, G. *et al.* Identification, cloning, and heterologous expression of a mammalian fructosamine-3-kinase. *Diabetes* **49**, 1627–1634 (2000).
- Collard, F. *et al.* Molecular identification of *N*-acetylaspartylglutamate synthase and β-citrylglutamate synthase. *J. Biol. Chem.* **285**, 29826–29833 (2010).
- Kitagawa, M. *et al.* Complete set of ORF clones of *Escherichia coli* ASKA library (a complete set of *E. coli* K-12 ORF archive): unique resources for biological research. *DNA Res.* **12**, 291–299 (2005).
- Manzano, A. *et al.* Cloning, expression and chromosomal localization of a human testis 6-phosphofructo-2-kinase/fructose-2,6-bisphosphatase gene. *Gene* **229**, 83–89 (1999).
- Deprez, J., Vertommen, D., Alessi, D.R., Hue, L. & Rider, M.H. Phosphorylation and activation of heart 6-phosphofructo-2-kinase by protein kinase B and other protein kinases of the insulin signaling cascades. *J. Biol. Chem.* **272**, 17269–17275 (1997).
- Novellademunt, L. *et al.* PFKFB3 activation in cancer cells by the p38/MK2 pathway in response to stress stimuli. *Biochem. J.* **452**, 531–543 (2013).
- Van Schaftingen, E., Lederer, B., Bartrons, R. & Hers, H.G. A kinetic study of pyrophosphate: fructose-6-phosphate phosphotransferase from potato tubers. Application to a microassay of fructose 2,6-bisphosphate. *Eur. J. Biochem.* **129**, 191–195 (1982).
- Brachmann, C.B. *et al.* Designer deletion strains derived from *Saccharomyces cerevisiae* S288C: a useful set of strains and plasmids for PCR-mediated gene disruption and other applications. *Yeast* **14**, 115–132 (1998).
- Güldener, U., Heck, S., Fielder, T., Beinhauer, J. & Hegemann, J.H. A new efficient gene disruption cassette for repeated use in budding yeast. *Nucleic Acids Res.* **24**, 2519–2524 (1996).
- Amberg, D., Burke, D. & Straethern, J. *Methods in Yeast Genetics* (CSHL Press, 2005).
- de Koning, W. & van Dam, K. A method for the determination of changes of glycolytic metabolites in yeast on a subsecond time scale using extraction at neutral pH. *Anal. Biochem.* **204**, 118–123 (1992).



46. Metallo, C.M. *et al.* Reductive glutamine metabolism by IDH1 mediates lipogenesis under hypoxia. *Nature* **481**, 380–384 (2012).
47. Jaeger, C. *et al.* The mouse brain metabolome: region-specific signatures and response to excitotoxic neuronal injury. *Am. J. Pathol.* **185**, 1699–1712 (2015).
48. Feijó Delgado, F. *et al.* Intracellular water exchange for measuring the dry mass, water mass and changes in chemical composition of living cells. *PLoS ONE* **8**, e67590 (2013).
49. Millard, P., Letisse, F., Sokol, S. & Portais, J.C. IsoCor: correcting MS data in isotope labeling experiments. *Bioinformatics* **28**, 1294–1296 (2012).
50. Gerin, I. *et al.* Identification of TP53-induced glycolysis and apoptosis regulator (TIGAR) as the phosphoglycolate-independent 2,3-bisphosphoglycerate phosphatase. *Biochem. J.* **458**, 439–448 (2014).
51. O'Brien, J., Wilson, I., Orton, T. & Pognan, F. Investigation of the Alamar Blue (resazurin) fluorescent dye for the assessment of mammalian cell cytotoxicity. *Eur. J. Biochem.* **267**, 5421–5426 (2000).
52. Zhu, C.T. & Rand, D.M. A hydrazine coupled cycling assay validates the decrease in redox ratio under starvation in *Drosophila*. *PLoS ONE* **7**, e47584 (2012).



PAPER 3:

6-phosphofructo-2-kinase/fructose-2,6-bisphosphatase 4 is essential for p53-null cancer cells

Published in *Oncogene* (2017) 1–13, co-author, contributed to Fru-2,6-BP measurements.

ORIGINAL ARTICLE

6-Phosphofructo-2-kinase/fructose-2,6-biphosphatase 4 is essential for p53-null cancer cells

S Ros^{1,2}, J Flöter³, I Kaymak³, C Da Costa⁴, A Houddane⁵, S Dubuis⁶, B Griffiths¹, R Mitter⁷, S Walz⁸, S Blake⁴, A Behrens^{4,9}, KM Brindle², N Zamboni⁶, MH Rider⁵ and A Schulze^{1,3}

The bifunctional enzyme 6-phosphofructo-2-kinase/fructose-2,6-biphosphatase-4 (PFKFB4) controls metabolic flux through allosteric regulation of glycolysis. Here we show that p53 regulates the expression of PFKFB4 and that p53-deficient cancer cells are highly dependent on the function of this enzyme. We found that p53 downregulates PFKFB4 expression by binding to its promoter and mediating transcriptional repression via histone deacetylases. Depletion of PFKFB4 from p53-deficient cancer cells increased levels of the allosteric regulator fructose-2,6-bisphosphate, leading to increased glycolytic activity but decreased routing of metabolites through the oxidative arm of the pentose-phosphate pathway. PFKFB4 was also required to support the synthesis and regeneration of nicotinamide adenine dinucleotide phosphate (NADPH) in p53-deficient cancer cells. Moreover, depletion of PFKFB4-attenuated cellular biosynthetic activity and resulted in the accumulation of reactive oxygen species and cell death in the absence of p53. Finally, silencing of PFKFB4-induced apoptosis in p53-deficient cancer cells *in vivo* and interfered with tumour growth. These results demonstrate that PFKFB4 is essential to support anabolic metabolism in p53-deficient cancer cells and suggest that inhibition of PFKFB4 could be an effective strategy for cancer treatment.

Oncogene advance online publication, 16 January 2017; doi:10.1038/onc.2016.477

INTRODUCTION

Cancer cells need to generate large amounts of metabolic precursors to support macromolecule biosynthesis during cell growth and proliferation. Cancer cell metabolism is characterized by enhanced nutrient uptake and increased activity of many biosynthetic processes, including protein and lipid biosynthesis. Nicotinamide adenine dinucleotide phosphate (NADPH) is a cofactor for anabolic reactions and required for the regeneration of reduced glutathione for the detoxification of reactive oxygen species (ROS). The enhanced demand for biosynthetic processes and control of oxidative stress makes NADPH synthesis and regeneration an essential process in cancer.¹

The tumour suppressor p53 counteracts many of the metabolic alterations observed in cancer cells.² Indeed, modulation of metabolic activity was shown to be a major component of the tumour suppressor activity of p53.³ Loss of p53 function leads to enhanced glucose uptake⁴ but decreased mitochondrial oxidative metabolism.⁵ Activation of p53 by DNA damage induces the expression of TIGAR, a fructose-2,6-bisphosphatase domain containing protein, which reduces glycolytic activity and increases the flux of metabolites to the oxidative pentose-phosphate pathway (PPP)⁶ to facilitate nucleotide synthesis for DNA repair. Seemingly contradictory to this, loss of p53 in cancer cells enhances oxidative PPP activity by increasing the activity of glucose-6-phosphate dehydrogenase (G6PD) and 6-phosphogluconate dehydrogenase (6PGD), the two NADPH-generating enzymes of this pathway.^{7,8} p53 also regulates the expression of malic enzymes 1 and 2 (ME1 and ME2),

two additional NADPH producing metabolic enzymes.⁹ It can therefore be concluded that deletion of p53 overall increases the synthesis and regeneration of NADPH to support biosynthetic processes in cancer cells.

We have previously shown that 6-phosphofructo-2-kinase/fructose-2,6-biphosphatase-4 (PFKFB4) supports the survival of prostate cancer cells *in vitro* and *in vivo* by reducing the generation of the allosteric regulator fructose-2,6-bisphosphate (Fru-2,6-BP), thereby inhibiting glycolytic flux and promoting the production of NADPH for lipid synthesis and regeneration of glutathione.¹⁰ Silencing of PFKFB4 blocked acetate-dependent lipid synthesis and resulted in the accumulation of ROS in cancer cells.¹⁰ However, it was not known whether loss of p53 function alters the dependency of cancer cells on allosteric regulation of glycolysis by PFKFB4, thereby postulating a potential biomarker for therapeutic targeting strategies.

We now demonstrate that p53 negatively regulates PFKFB4 expression by directly binding to the promoter of the gene. Conversely, loss of p53 function either by deletion or mutation increases the expression of PFKFB4 in cancer cells. Cancer cells that have lost p53 function are also highly sensitive to PFKFB4 depletion. Allosteric regulation of glycolysis by PFKFB4 is required for the routing of metabolites to the oxidative PPP to maintain NADPH synthesis and regeneration. Depletion of PFKFB4 in p53-deficient cancer cells increases oxidative stress and results in the induction of apoptosis. This dependence was also observed in xenograft tumours, where silencing of PFKFB4 caused more efficient blockade of tumour growth of p53-negative cancer cells.

¹Gene Expression Analysis Laboratory, Cancer Research UK London Research Institute, London, UK; ²Cancer Research UK Cambridge Institute, University of Cambridge, Cambridge, UK; ³Theodor-Boveri-Institute, Biocenter, Am Hubland, Würzburg, Germany; ⁴Adult Stem Cell Laboratory, The Francis Crick Institute, London, UK; ⁵Protein Phosphorylation Unit, de Duve Institute, Université Catholique de Louvain, Brussels, Belgium; ⁶Institute of Molecular Systems Biology, ETH Zurich, Zurich, Switzerland; ⁷Bioinformatics and Biostatistics, The Francis Crick Institute, London, UK; ⁸Comprehensive Cancer Center, Core Unit Bioinformatics, Biocenter, Würzburg, Germany and ⁹Faculty of Life Sciences and Medicine, King's College London, Guy's Campus, London, UK. Correspondence: Professor A Schulze, Theodor-Boveri-Institute, Biocenter, Am Hubland, 97074 Würzburg, Bavaria, Germany.

E-mail: almut.schulze@uni-wuerzburg.de

Received 29 July 2015; revised 8 November 2016; accepted 15 November 2016

2

Our results reveal that inhibition of PFKFB4 interacts in a synthetic lethal manner with loss of function of p53 in cancer cells and provide a rationale for targeting allosteric regulation of glycolysis for pharmaceutical intervention in cancers that are defective in *TP53*.

RESULTS

p53 negatively regulates PFKFB4 expression

To investigate whether PFKFB4 is regulated by p53, we analysed expression of the four human PFKFB isoforms in isogenic p53^{+/+} and p53^{-/-} HCT116 colon cancer cells. mRNA levels of *PFKFB4*, but not any of the other *PFKFB* isoforms, were markedly increased in

p53^{-/-} cells compared to their wild-type counterparts (Figure 1a). This induction was similar to the increased expression of *malic enzyme 1 (ME1)* and *malic enzyme 2 (ME2)*, which were previously identified as negative targets of p53,⁹ while expression of *TIGAR* was not altered between p53^{+/+} and p53^{-/-} cells (Figure 1b). In agreement with altered mRNA levels, we also detected increased expression of PFKFB4 protein in HCT116 p53^{-/-} cells (Figure 1c), whereas the other PFKFB isoforms showed no differential expression (Supplementary Figure 1a). Moreover, CRE-mediated deletion of p53 in primary embryonic fibroblasts (MEF) derived from *tpr53^{fl/fl}* mice also resulted in increased *Pfkfb4* expression (Figure 1d). Silencing of *TP53* in HCT116 p53^{+/+} cells, using a lentiviral vector for the doxycycline-inducible expression of short hairpin RNA (shRNA) targeting p53, efficiently reduced the

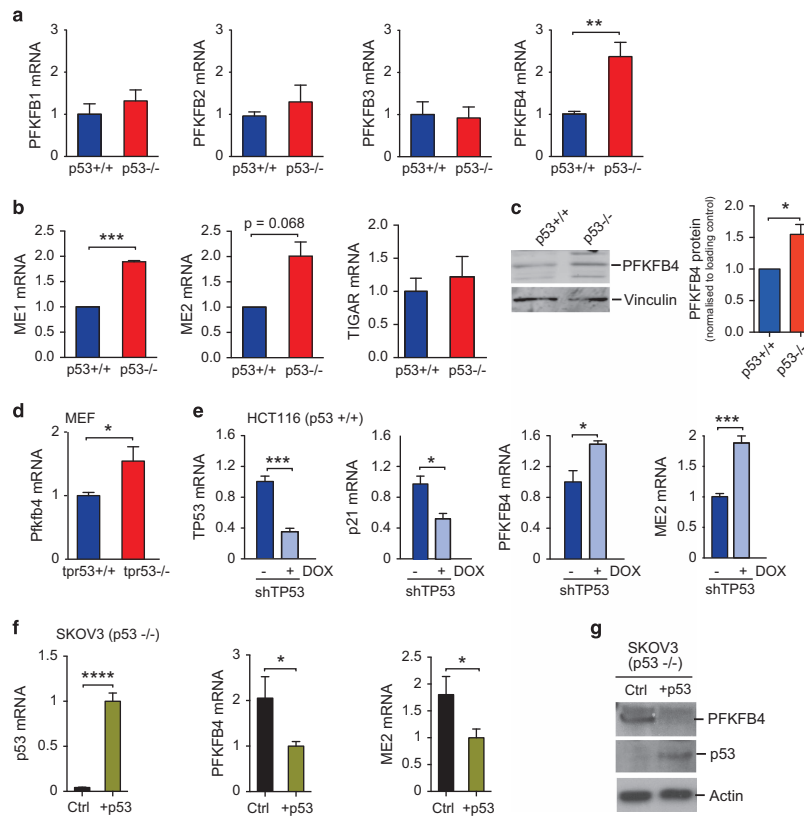


Figure 1. Differential expression of PFKFB4 in p53-deficient cells. **(a)** HCT116 p53^{+/+} or p53^{-/-} cells were cultured in full medium for 24 h. Expression of *PFKFB1*, *PFKFB2*, *PFKFB3* and *PFKFB4* was determined by qPCR and normalized to *B2M*. Data are presented as mean \pm s.e.m. ($n=6$). **(b)** Levels of *ME1*, *ME2* and *TIGAR* in p53^{+/+} or p53^{-/-} HCT116 cells. Data are presented as mean \pm s.e.m. ($n=6$). **(c)** Expression of PFKFB4 protein in HCT116 p53^{+/+} and p53^{-/-} cells. Vinculin was used as loading control. Bar graph shows the mean \pm s.e.m. of three replicate experiments. **(d)** MEFs from *tpr53^{fl/fl}* mice were infected with Adeno-CRE-GFP to excise the floxed allele. mRNA from selected cells was analysed for expression of *Pfkfb4*. Data are presented as mean \pm s.e.m. (*tpr53^{+/+}* $n=7$, *tpr53^{-/-}* $n=8$). **(e)** HCT116 p53^{+/+} cells were transduced with lentiviral vectors expressing inducible shRNA targeting p53. Cells were treated with 1 μ g/ml doxycycline (Dox) or solvent for 8 days. Expression of *Pfkfb4*, *ME2*, *TP53* and *p21* was determined by qPCR. Data are presented as mean \pm s.e.m. ($n=4$). **(f)** SKOV3 cells were transduced with a lentiviral vector expressing wild-type p53 or a control vector. Expression of *TP53*, *PFKFB4* and *ME2* was determined by qPCR in monoclonal populations. Data are presented as mean \pm s.d. ($n=3$). **(g)** Expression of PFKFB4 and p53 protein in cells as **f**. Actin was used as loading control.

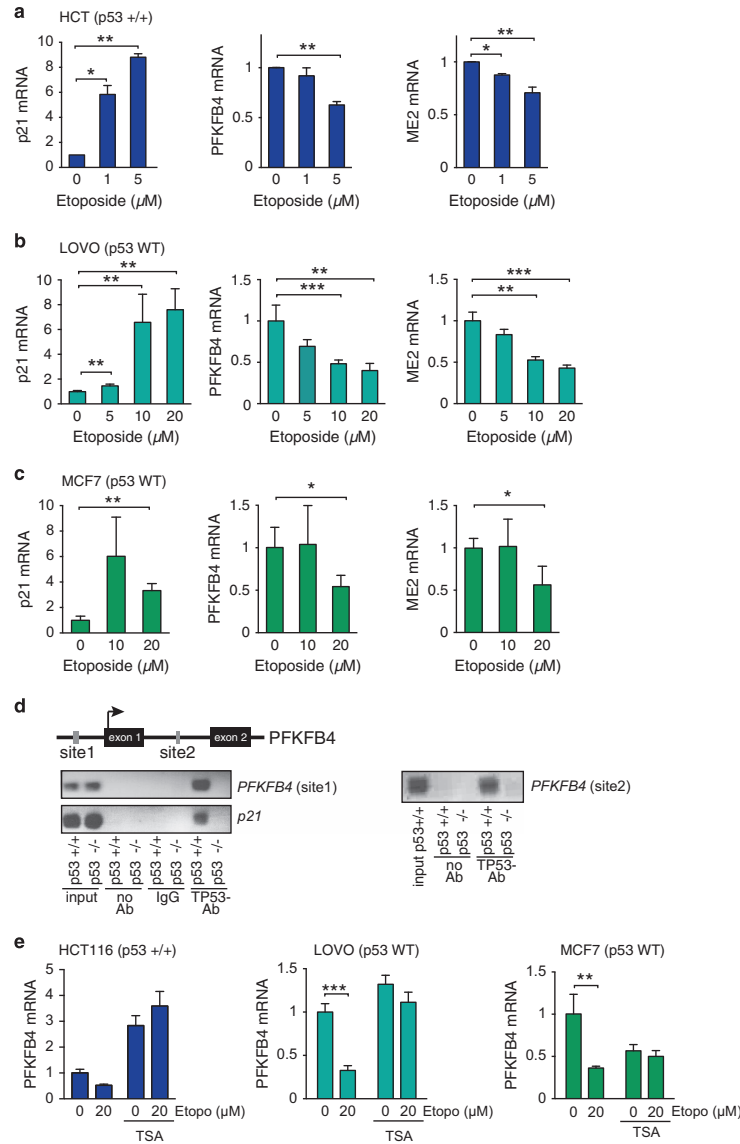


Figure 2. p53 represses PFKFB4 expression in cancer cells. **(a)** HCT116 p53^{+/+} cells were treated with different concentrations of etoposide for 24 h. Expression of *PFKFB4*, *p21* (*CDKN1A*) and *ME2* was determined by qPCR. Data are presented as mean \pm s.e.m. ($n = 3$). **(b)** Regulation of *p21*, *PFKFB4* and *ME2* in p53 wild-type LOVO colon cancer cells after etoposide treatment. Data are presented as mean \pm s.d. ($n = 3$). **(c)** Regulation of *p21*, *PFKFB4* and *ME2* in p53 wild-type MCF7 breast cancer cells after etoposide treatment. Data are presented as mean \pm s.d. ($n = 3$). **(d)** Overview of the structure of the human *PFKFB4* promoter. Sequences corresponding to putative p53 response elements are indicated. (B4-site 1: position chr3:48598858-48598880; B4-site 2: position: chr3:48592906-48592928; GRCh37/hg19). HCT116 cells (p53^{+/+} and p53^{-/-}) were subjected to chromatin immunoprecipitation assays using p53-specific antibodies (TP53 Ab), isotype-matched controls (IgG) or no antibody (no Ab). Promoter regions corresponding to p53-site 1 (left panel) or p53-site2 (right panel) of the *PFKFB4* promoter were amplified using qPCR. A p53-site in the p21 promoter was used as positive control. **(e)** HCT116 p53^{+/+} cells, LOVO and MCF7 cancer cells were treated with 20 μ M etoposide in the presence or absence of 100 nM trichostatin A. Expression of *p21*, *PFKFB4* and *ME2* mRNA was determined by qPCR. HCT p53^{+/+} cells data are presented as mean \pm s.e.m. ($n = 2$). LOVO and MCF7 data are presented as mean \pm s.d. ($n = 3$).

expression of *p53* and *p21* but increased expression of *PFKFB4* and *ME2* (Figure 1e). Conversely, expression of *p53* in the p53-deficient ovarian cancer cell line SKOV3 caused a marked decrease in the expression of *PFKFB4* mRNA and protein (Figures 1f and g).

The normally short-lived p53 protein is stabilized in response to DNA damage.¹¹ We therefore treated p53^{+/+} and p53^{-/-} HCT116 cells with the genotoxic agent etoposide and monitored changes in expression of p53 target genes. Etoposide caused a dose-dependent induction in *p21* expression only in p53^{+/+} but not in p53^{-/-} cells (Figure 2a; Supplementary Figure 1b, left graphs). In the same cells, expression of *PFKFB4* was reduced in response to etoposide treatment only in the presence of p53^{+/+} (Figure 2a; Supplementary Figure 1b, middle graphs). This was similar to the regulation of *ME2* (Figure 2a; Supplementary Figure 1b, right graphs). Similar results were also obtained in a second p53 wild-type colon cancer cell line, LOVO (Figure 2b), and a p53 wild-type breast cancer cell line, MCF7 (Figure 2c).

Analysis of the human *PFKFB4* promoter revealed several putative p53 response elements. Chromatin immunoprecipitation (ChIP) experiments showed specific binding of p53 to two of these sites (Figure 2d), confirming that p53 regulates *PFKFB4* expression by binding to its promoter. Negative regulation of transcription by p53 frequently involves the recruitment of histone deacetylases to the promoter regions of target genes.^{12,13} We therefore investigated whether inhibition of histone deacetylases by trichostatin A prevents the negative effect of p53 on *PFKFB4* expression. Trichostatin A treatment efficiently blocked *PFKFB4* downregulation in the presence of etoposide in HCT116 p53^{+/+} and LOVO colon cancer cells, as well as in MCF7 breast cancer cells (Figure 2e).

Taken together, these results demonstrate that p53 negatively regulates expression of *PFKFB4*, both at basal levels and when p53 is activated in response to DNA damage. To confirm the link between *PFKFB4* expression and p53 also in human cancer, we interrogated public data sets from the Gene Expression Omnibus (GEO). We retrieved expression data of cancer samples with differential p53 status from a study investigating somatic mutations in lung adenocarcinoma.¹⁴ Comparative analysis revealed that *PFKFB4* expression is significantly increased in p53^{-/-} lung adenocarcinomas when compared to p53^{+/+} tissues of the same cancer type (Supplementary Figure 1c).

PFKFB4 is essential for the viability of p53-null cancer cells

PFKFB proteins are homodimeric bifunctional enzymes that control the rate of glycolysis by modulating levels of Fru-2,6-BP, an allosteric activator of phosphofruktokinase 1 and inhibitor of fructose-1,6-bisphosphatase (FBPase-1).¹⁵ Allosteric regulation by *PFKFB4* regulates the distribution of metabolites between glycolysis and the oxidative PPP and is required for the generation of NADPH for anabolic reactions and antioxidant synthesis in cancer cells.^{10,16}

To investigate whether the increased expression of *PFKFB4* is linked to the altered metabolic demand of p53^{-/-} cancer cells, we

performed silencing experiments using inducible expression of shRNAs targeting *PFKFB4*. Depletion of *PFKFB4* using two independent shRNA hairpins only slightly reduced the cell number in p53^{+/+} cells. In contrast, depletion of *PFKFB4* caused a substantial reduction of viability in p53^{-/-} cells (Figure 3a). Efficient depletion of *PFKFB4* was confirmed in both HCT116 p53^{+/+} and p53^{-/-} cell lines, with sequence #68 achieving an 80% reduction in mRNA while expression of sequence #64 resulted in a 50% reduction (Figure 3b). We also controlled that depletion of *PFKFB4* did not cause any changes in the expression of *PFKFB1*, *PFKFB2* or *PFKFB3* (Supplementary Figure 2a). Furthermore, to establish specificity of silencing, we generated shRNA-insensitive expression constructs by introducing silent mutations within the *PFKFB4* coding sequence. These constructs were expressed in p53^{+/+} and p53^{-/-} HCT116 colon cancer cells, which were subsequently infected with the lentiviral shRNA expression constructs targeting endogenous *PFKFB4*. We confirmed that the expression of exogenous *PFKFB4* mRNA was not changed upon doxycycline treatment (Supplementary Figures 2b and c). Importantly, reduced viability of HCT116 p53^{-/-} cells in response to shRNA induction was completely rescued by re-expression of *PFKFB4* (Figure 3c).

We next investigated the wider applicability of these findings using a panel of colon cancer cell lines. These included three additional p53 wild-type colon cancer cell lines (RKO, LOVO and LS174T) and two colon cancer cell lines (SW680 and SW620) expressing a mutant form of p53 carrying a mutation within the DNA binding domain (R273H). This mutant exerts a dominant negative effect by blocking DNA binding of the wild-type protein.¹⁷ Wild-type cell lines expressed significantly lower levels of *PFKFB4*, with RKO cells expressing nearly undetectable levels (Figures 3d and e). We next transduced two p53 wild-type and p53-mutant cell lines with lentiviral shRNA constructs targeting *PFKFB4*. Depletion of *PFKFB4* reduced the viability of both p53-mutant cell lines, while not affecting viability of cells expressing wild-type p53 (Figures 3e and f). Conclusively, these results confirm that *PFKFB4* is selectively required for the viability of p53-deficient cancer cells.

PFKFB4 maintains balance of metabolite flux between glycolysis and PPP in p53-deficient cancer cells

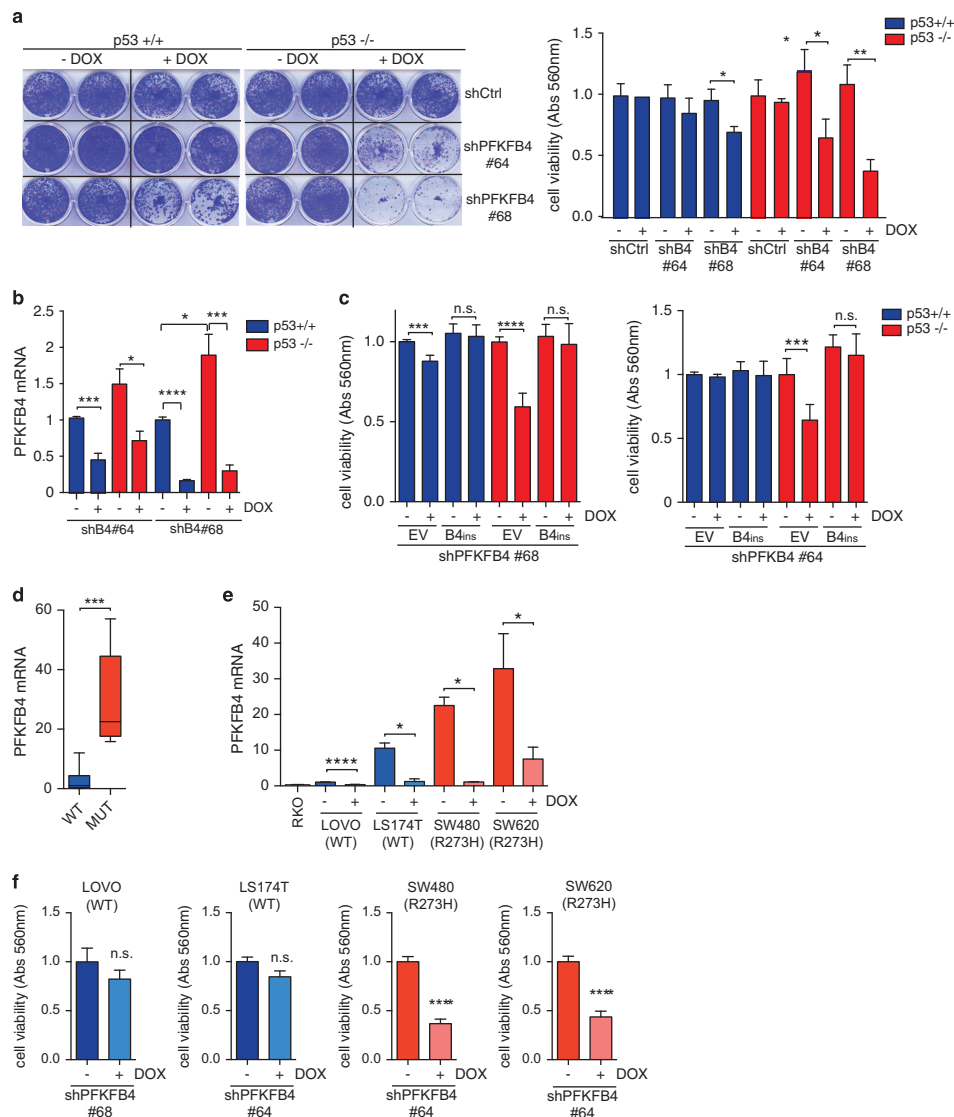
We next asked which catalytic activity of *PFKFB4* mediates the survival of p53^{-/-} cells. We first established the efficiency and timing of *PFKFB4* protein depletion in response to shRNA expression. Although mRNA levels were already efficiently reduced after 2 days of doxycycline treatment in cells expressing sequence #68, substantial amounts of protein were still detectable after 3 days of shRNA induction (Supplementary Figures 3a and b). Moreover, p53-deficient cells showed a larger increase in *PFKFB4* protein expression at the later time point (Figure 4a; Supplementary Figure 3d). We next determined the levels of Fru-2,6-BP, the substrate of the fructose-2,6-bisphosphatase activity of *PFKFB4* at 3 and 6 days

Figure 3. *PFKFB4* is required for viability of p53-deficient cancer cells. (a) HCT116 p53^{+/+} and p53^{-/-} cells were transduced with lentiviral vectors expressing inducible shRNA targeting *PFKFB4* (shPFKFB4 #68 or #64). Cells were seeded at low density, treated with 1 µg/ml doxycycline (Dox) or solvent for 8 days and stained with crystal violet. Left: representative images. Right: quantification. Data are presented as mean ± s.e.m. (n = 5) and are relative to HCT116 p53^{+/+} shCtrl cells treated with solvent. (b) Cells were treated with 1 µg/ml doxycycline (Dox) or solvent for 6 days and expression of *PFKFB4* was determined by qPCR and normalized to *B2M*. Data are presented as mean ± s.e.m. (n = 5) and are relative to HCT116 p53^{+/+} shPFKFB4 cells treated with solvent. (c) HCT116 cells (p53^{+/+} and p53^{-/-}) expressing inducible shRNAs targeting *PFKFB4* were stably transfected with pBabe-vectors expressing shRNA-insensitive versions of *PFKFB4* (*PFKFB4*_m). Cells were seeded at low density and treated with doxycycline (Dox) for 8 days. Cultures were fixed and analysed by crystal violet staining. Data are presented as mean ± s.e.m. (n = 6). (d) Expression of *PFKFB4* in p53 wild-type cells (RKO, LOVO, LS174T) or p53-mutant cells (SW480 and SW620) was determined by qPCR relative to *B2M*. Box plot represents the differential expression of *PFKFB4* between both groups of cell lines. (e) LOVO, LS174Tm SW480 and SW460 cells were transduced with lentiviral vectors expressing inducible shRNA targeting *PFKFB4* (shPFKFB4 #68 or #64). Silencing of *PFKFB4* was confirmed by qPCR. (f) Cells in e were seeded at low density, treated with 1 µg/ml doxycycline (Dox) or solvent for 8 days and stained with crystal violet. Data are presented as mean ± s.e.m. (n = 3) and are relative to cells treated with solvent.

after PFKFB4 depletion in both cell types. At the earlier time point, depletion of PFKFB4 caused an increase in Fru-2,6-BP in both p53^{+/+} and p53^{-/-} cells (Supplementary Figure 3c). However, at the later time point, where p53^{-/-} cells show increased expression of the protein, no changes in metabolite levels were observed in p53^{+/+} cells. In contrast, depletion of PFKFB4 for 6 days caused a significant increase in Fru-2,6-BP levels in p53-deficient cells (Figure 4b). Induction of the second, less effective, shRNA sequence only caused partial ablation of PFKFB4 protein after

6 days, which also increased the levels of Fru-2,6-BP only in p53^{-/-} cells, although the data failed to reach statistical significance (Supplementary Figure 3e).

To further investigate the consequences of PFKFB4 depletion on cellular metabolism, we examined changes in glucose uptake using 2-[N-(7-nitrobenz-2-oxa-1,3-diazol-4-yl) amino]-2-deoxy-D-glucose (2-NBDG), a fluorescent derivative of 2-deoxyglucose. p53 inhibits glucose uptake by downregulating the expression of glucose transporters GLUT1 and GLUT4.¹⁸ Moreover, activation of



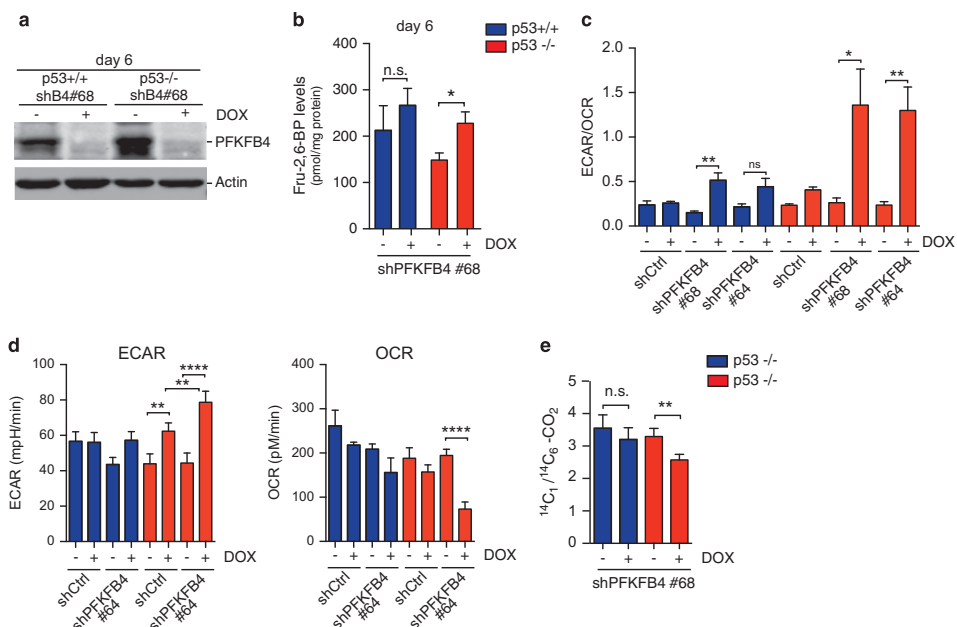


Figure 4. PFKFB4 maintains balance between glycolysis and pentose-phosphate pathway in p53-deficient cancer cells. **(a)** Downregulation of PFKFB4 protein in HCT116 p53^{+/+} and p53^{-/-} cells after 6 days of shRNA-mediated silencing. Actin was used as loading control. **(b)** HCT116 p53^{+/+} and p53^{-/-} cells expressing inducible shRNAs targeting PFKFB4 were treated with 1 μg/ml doxycycline (Dox) or solvent for 6 days. Intracellular levels of fructose-2,6-biphosphate (Fru-2,6-BP) were determined. Data are presented as mean ± s.e.m. (n = 5). **(c)** Extracellular acidification rates (ECAR) and oxygen consumption rates (OCR) were determined in cells treated as in **a**. Graph displays ECAR/OCR and data are presented as mean ± s.e.m. **(d)** Changes in ECAR and OCR in HCT116 p53^{+/+} and p53^{-/-} cells after silencing of PFKFB4. Data are presented as mean ± s.e.m. (n = 5). **(e)** HCT116 p53^{+/+} and p53^{-/-} cells were treated with doxycycline (Dox) for 6 days and the labelled with either ¹⁴C₁ or ¹⁴C₆ glucose. Relative production of CO₂ from both substrates was determined. Data are presented as mean ± s.e.m. (n = 4).

p53 suppresses NF-κB activation and reduces glucose uptake and glycolysis by blocking the expression of GLUT3.⁴ However, we observed no major differences in 2-NBDG uptake between p53^{+/+} and p53^{-/-} cells. Depletion of PFKFB4 caused a moderate increase in 2-NBDG uptake in both cell lines, which was significant only in p53^{-/-} cells (Supplementary Figure 3f).

To provide further detail of the metabolic response to PFKFB4 depletion, we also performed mass isotopomer distribution (MID) analysis after exposing cells to [1,2-¹³C]-glucose that allows us to estimate the relative contribution of the PPP to the metabolite pool in glycolysis. Specifically, molecules with one ¹³C atom (M+1) indicate that they transited through the oxidative PPP, whereas molecules with two ¹³C atoms (M+2) came directly from glycolysis (Supplementary Figure 3g). We analysed the mass isotopomer fractions of FBP and phosphoenolpyruvate, and found that silencing of PFKFB4 in p53^{-/-} HCT116 cells leads to an increased fraction of M+1 over the M+2 fraction for both FBP and phosphoenolpyruvate (Supplementary Figure 3h), that means a relative increase in the fraction of pentose phosphates that is routed back to glycolysis through the non-oxidative PPP. The most plausible explanation for this result is that PFKFB4 depletion causes a difference in the outflow of pentose phosphate for purine biosynthesis, which is the major biosynthetic sink for PPP intermediates. Hence, depletion of PFKFB4 from p53^{-/-} cells induces a reduction in the net flux through the oxidative PPP from

glucose-6-phosphate to the pentose-phosphate pool, but the latter is seemingly channelled back because of a reduced outflow to purine synthesis.

MID analysis is not able to provide any estimation of the rate at which metabolites pass through a metabolic pathway. We next investigated the effect of PFKFB4 depletion on glycolytic flux (extracellular acidification rates (ECAR)) and oxygen consumption (oxygen consumption rates (OCR)) using the Seahorse Bioanalyzer. Both cell lines showed similar ECAR/OCR ratios in the basal state and depletion of PFKFB4 had only a minor effect in p53^{+/+} cancer cells (Figure 4c). In contrast, p53^{-/-} cells showed a strong increase in the ECAR/OCR ratio upon PFKFB4 depletion (Figure 4c). This was caused by an increase in glycolysis and a decrease in respiration (Figure 4d), confirming that PFKFB4 is required to limit glycolytic flux in these cells.

Increased glycolysis affects metabolite flux towards the oxidative and non-oxidative arm of the PPP. We therefore analysed the activity of the oxidative PPP by comparing the production of ¹⁴CO₂ from 1-¹⁴C-glucose relative to that from 6-¹⁴C-glucose. We observed a significant reduction of this ratio in HCT116 p53^{-/-} cells after silencing of PFKFB4 (Figure 4e). In contrast, silencing of PFKFB4 had no effect on PPP flux in p53^{+/+} cells (Figure 4e). This confirms that PFKFB4 is required to maintain the activity of the oxidative arm of the PPP in p53-deficient cancer cells.

PFKFB4 maintains NADPH production for biosynthetic activity and antioxidant production

The metabolic outputs of the PPP include the synthesis of riboses for nucleotide biosynthesis and the regeneration of NADPH. We therefore investigated whether PFKFB4 influences NADPH levels and oxidation status in cancer cells. Interestingly, we found that levels of NADPH as well as the total amount of this coenzyme (NADPH+NADP⁺) were reduced following PFKFB4 silencing only in p53^{-/-} cells (Figure 5a, left graph). In contrast, the ratio between the reduced and oxidized forms of the coenzyme was not altered (Figure 5a, right graph). Moderate depletion of PFKFB4 protein achieved by the second, less efficient sequence also reduced NADPH levels (Supplementary Figure 4a). This effect was only detectable at the later time point, when efficient depletion of PFKFB4 protein was achieved (Supplementary Figure 4a), while short-term silencing had no effect (Supplementary Figure 4b). We additionally determined expression of *ME1* and *ME2* after PFKFB4 knockdown and observed no compensation by these genes (Supplementary Figure 4c). In agreement with the results of the MID analysis, this result suggests that PFKFB4 is required to maintain NADPH regeneration through the oxidative arm of the PPP and also facilitates the synthesis of the coenzyme by providing riboses via the biosynthetic output of this pathway.

NADPH provides reducing power for biosynthetic reactions, including lipid biosynthesis, leading us to investigate whether inhibition of PFKFB4 affects the activity of this process in cancer cells. We first established that p53^{-/-} cells display a higher rate of acetate-dependent lipid biosynthesis compared to p53^{+/+} cells (Figure 5b). Moreover, p53-deficient cells also showed increased activity of a reporter containing a fragment of the human HMG-CoA synthase promoter carrying an intact sterol regulatory element (SRE) (Figure 5c). This activity depends on the SRE-binding proteins (SREBP), a family of transcription factors controlling genes involved in fatty acid and cholesterol biosynthesis.¹⁹ This is in agreement with previous reports showing that SREBP is activated by loss or mutation of p53.^{20,21} It is therefore possible that p53-deficient cancer cells have a higher demand for NADPH than their p53 proficient counterparts, which is aided by the induction of PFKFB4. In agreement with this hypothesis, silencing of PFKFB4 caused a stronger reduction in acetate-dependent lipid synthesis in p53^{-/-} cells compared with p53^{+/+} cells (Figure 5d).

Increased NADPH demand also compromises the availability of this coenzyme for the production of antioxidants, leading to oxidative damage and ROS generation. We therefore investigated the effect of PFKFB4 depletion on cellular ROS levels in the two cell lines. Although silencing of PFKFB4 had no effect on ROS in p53^{+/+} cells, it caused a strong increase in ROS levels in p53^{-/-} cells (Figure 5e). Furthermore, treatment with the antioxidant N-acetylcysteine blocked the induction of apoptosis in response to PFKFB4 depletion in p53^{-/-} cells (Figure 5f), indicating that ROS accumulation is the cause of the reduced viability observed in these cells.

Taken together, these results confirm the role of PFKFB4 in promoting the routing of metabolites from glycolysis into the PPP for the synthesis and regeneration of NADPH to support anabolic reactions and maintain cellular redox balance. This function is essential to fulfil the increased NADPH demand of p53-deficient cancer cells to drive biosynthetic processes including lipid synthesis (Figure 5g).

PFKFB4 silencing inhibits spheroid and tumour growth in the absence of p53

Metabolic reprogramming in cancer supports cell growth under oxygen and nutrient limited conditions, such as those found in hypo-vascularized tumour regions.^{22,23} The environmental conditions found in tumours can generate specific metabolic

constraints and reveal sensitivities of cancer cells that could be exploited for therapy.

To investigate the contribution of PFKFB4 to the viability of p53-deficient cancer cells under nutrient limited conditions, we employed tumour spheroid culture conditions. These multi-layered three-dimensional structures recreate nutrient and oxygen gradients found in live tumours.²⁴ Silencing of PFKFB4-induced a reduction in spheroid volume in both p53^{+/+} and p53^{-/-} HCT116 colon cancer cells (Supplementary Figure 5a), indicating that the metabolically compromised conditions present in this culture system could sensitize p53^{+/+} cells towards PFKFB4 inhibition. However, depletion of PFKFB4 caused a further reduction in spheroid growth in p53^{-/-} cells, confirming the increased dependency of the cells on this enzyme in the absence of the tumour suppressor.

We next investigated the importance of PFKFB4 for tumour growth using a xenograft tumour model. For this, we first generated p53^{+/+} and p53^{-/-} HCT116 cells expressing luciferase and used these for expression of inducible shRNA constructs targeting PFKFB4 or scrambled shRNA controls. Efficient PFKFB4 silencing and inhibition of cell proliferation was confirmed in these cells (Supplementary Figures 5b and c). Cells were then injected subcutaneously into nude mice and tumour growth was followed over time in control and doxycycline treated cohorts. As control, we established that PFKFB4 silencing had no effect on the size of tumours generated by HCT116 cells expressing a scrambled shRNA control (Supplementary Figures 5d and e).

Interestingly, we found that *PFKFB4* mRNA levels were higher in p53^{-/-} tumours, confirming that the differential expression of this gene is also maintained *in vivo*, and that doxycycline treatment efficiently depleted *PFKFB4* mRNA from both types of tumours (Supplementary Figure 5f). Strong silencing of PFKFB4 by sequence #68 slowed the growth of p53^{+/+} tumours, with a plateau being reached after 15 days of doxycycline treatment. Induction of the less efficient sequence (#64) did not impair growth of p53^{+/+} tumours (Figure 6a, left graphs). In contrast, expression of either shRNA sequences efficiently blocked tumour growth in the p53^{-/-} background. Indeed, strong silencing by sequence #68 caused a reduction of the initial tumour mass and a 17-fold reduction of tumour size compared with untreated controls at the end of the experiment (Figure 6a, right graphs). Consequently, the effects of PFKFB4 depletion on bioluminescence detection (Figure 6b), tumour weight (Supplementary Figure 5d) and tumour size (Supplementary Figure 5e) were more pronounced in p53^{-/-} background.

Histological analysis showed that tumour regression was accompanied by the appearance of apoptotic areas (Figure 6c), while minor changes in proliferation were detected (Figure 6d; Supplementary Figure 5g). We also analysed transcriptional changes associated with PFKFB4 inhibition in these tumours using whole-genome RNA sequencing (RNAseq). Interestingly, both p53^{+/+} and p53^{-/-} tumours showed downregulation of genes associated with ribosome synthesis, assembly of the ternary translation complex and rapamycin sensitivity (Figure 6e; Supplementary Figure 6a). However, only p53^{-/-} tumours showed regulation of genes linked to apoptosis and oxidative stress (Supplementary Figure 6a). Finally, analysis of public gene expression data revealed that high expression of the glycolytic enzyme PFKFB4 is a predictor of reduced survival in breast and non-small cell lung cancer patients (Supplementary Figures 6b and c).

In conclusion, our study demonstrates that p53 represses PFKFB4 expression, and that allosteric regulation of glycolytic flux by PFKFB4 supports lipid synthesis and prevents oxidative stress in p53-deficient cancer cells to support cell proliferation and tumour growth.

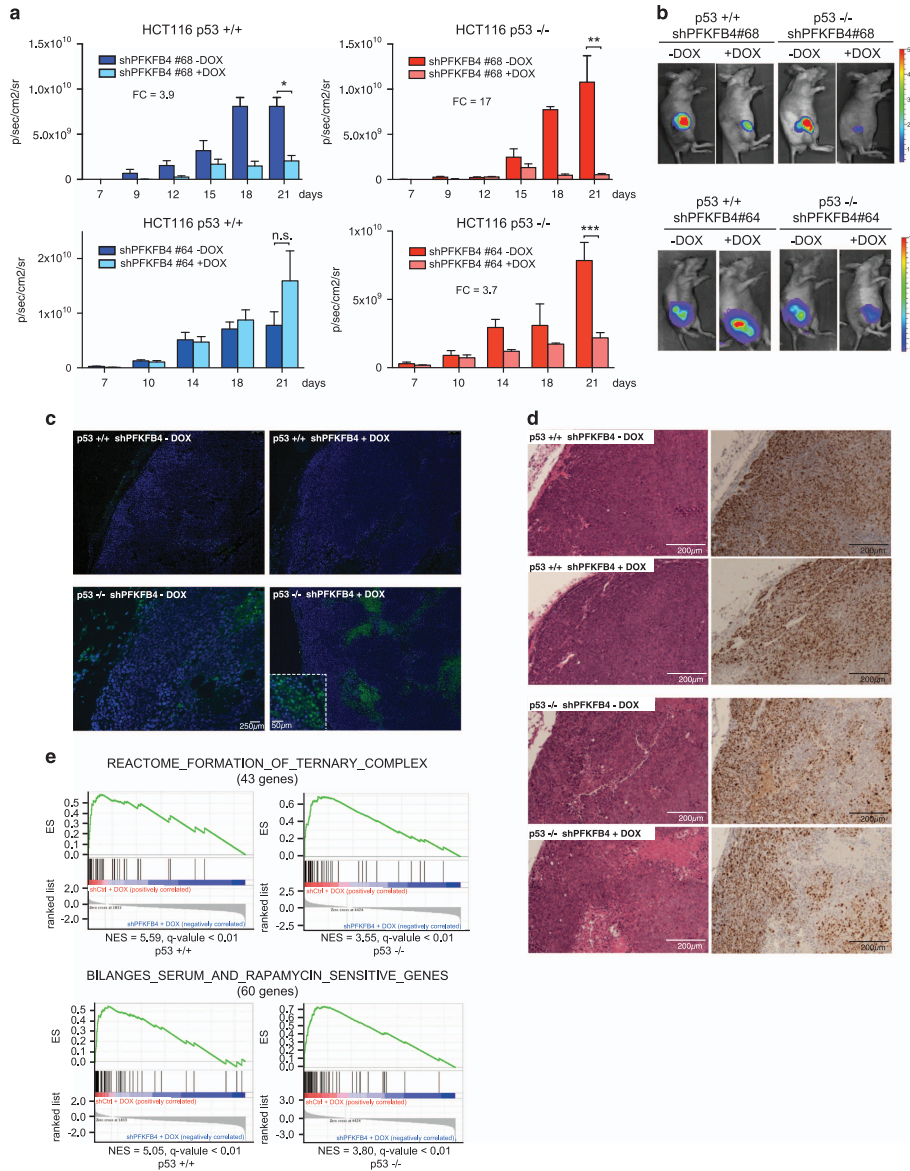


Figure 6. PFKFB4 supports tumour growth in p53-deficient cancer cells. **(a)** HCT116_{luc} p53^{+/+} and p53^{-/-} cells expressing inducible shRNAs targeting PFKFB4 (shPFKFB4#68 above and shPFKFB4 #64 below) were injected subcutaneously into nude mice. Mice were divided into two cohorts with equal tumour burden and one cohort received doxycycline in their food (DOX) started one day after implantation. Tumour growth was monitored by *in vivo* quantification of luciferase. Graphs show mean bioluminescence (p/s/cm²/sr) ± s.e.m. for each group. **(b)** Representative mice for each group at day 21 are shown. **(c)** Analysis of fragmented DNA in apoptotic cells using TUNEL assays in tumours recovered at day 21, representative images. **(d)** Analysis of proliferation using histological staining for the Ki-67 marker in tumours recovered at day 21, representative images. **(e)** Selected gene sets showing decreased expression in tumours depleted of PFKFB4 compared with controls by gene set enrichment analysis (GSEA).

DISCUSSION

Loss of p53 in cancer cells inactivates important DNA damage and cell cycle checkpoints but has also multiple effects on cellular metabolism.²⁵ Indeed, the metabolic effects of p53 may be sufficient to explain its functions as a tumour suppressor.³ In normal cells, p53 regulates metabolism on multiple levels.² For example, p53 reduces glucose uptake by lowering NF- κ B dependent expression of GLUT3.⁴ Induction of p53 in response to DNA damage inhibits glycolysis through the induction of TIGAR.⁶ It also reduces the expression of several glycolytic enzymes via a microRNA-dependent mechanism²⁶ and increases mitochondrial activity by inducing the expression of cytochrome c oxidase 2 (SCO2).⁵ At the same time, p53 also increases the ability of cells to respond to nutrient starvation, by facilitating cell cycle arrest, autophagy or the use of alternative energy source, such as lipids.² Cancer cells deficient in p53 can therefore be more sensitive towards perturbations within the metabolic network and these selective vulnerabilities can be exploited for cancer therapy.²⁷

Enhanced macromolecule biosynthesis increases the cellular demand for NADPH, the reducing coenzyme for anabolic reaction. Cancer cells therefore need to upregulate mechanisms that increase NADPH synthesis and regeneration to maintain rapid proliferation and prevent excess oxidative stress. We demonstrate that p53 negatively regulates expression of PFKFB4, while loss of p53 increases the expression of PFKFB4, an enzyme that controls cellular levels of the allosteric regulator Fru-2,6-BP. Through this regulation, p53 alters the routing of metabolites between glycolysis and the PPP, which is critical for NADPH synthesis and regeneration. Depletion of PFKFB4 impairs the ability of cancer cells to generate sufficient amounts of reducing cofactors to fulfil the demand generated by increased lipid synthesis. As a result, inhibition of PFKFB4 selectively increases oxidative stress in p53-deficient cancer cells, leading to reduced viability *in vitro* and tumour regression *in vivo*.

Several mechanisms have been proposed for the negative regulation of gene expression by p53. These include competition for DNA binding or transactivation function of positive regulators of transcription.²⁸ We found that p53 directly binds to two p53 response elements within the PFKFB4 promoter. Moreover, we found that activation of p53 by DNA damaging agents reduced PFKFB4 expression, which was blocked by addition of trichostatin A, suggesting that p53 represses transcription by recruiting histone deacetylases. Loss of p53 relieves this inhibition and allows increased expression of PFKFB4.

Allosteric regulation of glycolytic activity by PFKFB proteins is an important principle for the control of metabolic flux in cancer cells.²⁹ PFKFB proteins have two independent catalytic centres and it is important to establish the exact role of PFKFB4 within the metabolic network of cancer cells. We have previously shown that PFKFB4 limits Fru-2,6-BP levels and induce the routing of metabolites into the PPP to support NADPH production and ROS detoxification in prostate cancer cells.¹⁰ In contrast, a recent study observed that PFKFB4 promotes the synthesis of Fru-2,6-BP to increase glycolytic flux in cancer cells grown under hypoxic conditions or as xenograft tumours.³⁰ Here we show that depletion of PFKFB4 increases the levels of Fru-2,6-BP in p53-deficient colon cancer cells. Mass isotopomer distribution analysis confirmed that depletion of PFKFB4 increases the relative fraction of pentose phosphates that are routed back to glycolysis from the non-oxidative PPP. We also found that PFKFB4 depletion increases glycolytic rate and decreased activity of the oxidative arm of the PPP. Together, these metabolic changes results in reduced availability of PPP intermediates for biosynthetic processes, such as the production of NADPH, an essential cofactor for biosynthetic reaction. Indeed, NADPH levels were markedly reduced following PFKFB4 depletion. This resulted in the selective induction of oxidative stress and cell death in p53-deficient cancer cells.

There are several factors that contribute to the exquisite sensitivity of p53-deficient cancer cells towards PFKFB4 depletion. One is the increased biosynthetic demand of p53-deficient cancer cells. p53 was shown to decrease the expression of lipogenic genes in adipocytes of obese mice.²¹ Loss of p53 increases the activity of mTORC1,³¹ which drives both protein and lipid biosynthesis.³² As lipid biosynthesis requires large amounts of NADPH, regulatory mechanisms that support the production of this coenzyme must be upregulated when lipid biosynthesis is high. Another explanation could be that p53-deficient cancer cells fail to undergo cell cycle arrest under metabolic starvation conditions, such as the absence of exogenous serine.²⁷ It is therefore likely that p53-deficient cells are unable to adapt to the altered metabolite flux following PFKFB4 depletion by efficiently downregulating NADPH-consuming biosynthetic processes. This would cause further NADPH depletion, leading to oxidative stress and cell death. In line with this hypothesis, the reduction in tumour growth observed after strong PFKFB4 depletion in p53 proficient cancers was not associated with the induction of cell death. Remarkably, p53 proficient cancer cells were not affected in their ability to form xenograft tumours when PFKFB4 was partially depleted using a less efficient shRNA sequence. In contrast, p53-deficient cancer cells were highly dependent on PFKFB4, as both partial and efficient silencing blocked tumour growth. Moreover, depletion of PFKFB4 from p53-deficient tumours resulted in the induction of apoptosis and tumour regression.

Dynamic regulation of carbohydrate flux is essential to counteract oxidative stress in yeast.³³ In cancer, the control of NADPH synthesis and regeneration to maintain anabolic metabolism and antioxidant production is an essential function of drivers of oncogenic transformation. The results of this study demonstrate that allosteric regulation of the glycolytic flux by PFKFB4 is essential for the survival of p53-deficient cancer cells. This synthetic lethality suggests that targeting PFKFB4 could be an effective strategy for the treatment of tumours that have lost the function of this important tumour suppressor.

MATERIALS AND METHODS

Cell culture and reagents

HCT116 p53^{+/+} and p53^{-/-}³⁴ were a gift of B. Vogelstein (Johns Hopkins University, Baltimore, MD, USA). HEK 293T, MCF7, LOVO, LS174T, SW480 and SW620 cells were from LRI Cell Services (London, UK). SKOV3, and also MCF7, LOVO were from CRUK-CI Biorepository Services (Cambridge, UK). All cell lines were authenticated by STR profiling and used at low passage. All cell lines were confirmed to be free from mycoplasma throughout the experiments by regular testing. Cells were cultured at 37 °C in a humidified incubator at 5% CO₂ in Dulbecco's modified Eagle's medium (DMEM; Life Technologies, Carlsbad, CA, USA) with 10% foetal bovine serum (FBS, Sigma-Aldrich, St Louis, MO, USA) and 2 mM L-glutamine. Primary MEF were derived from embryonic day 12.5 (E12.5) embryos and were cultured in DMEM supplemented with 10% FBS at 37 °C with 5% CO₂ and 3% O₂. For Cre-mediated deletion of p53 floxed alleles, MEF from tp53^{fl/fl} mice were infected with Adeno-Cre-green fluorescent protein (GFP) or Adeno-GFP virus (Gene Transfer Vector Core, Iowa University) for 48 h. Virus was removed and the cells were allowed 48 h to recover before passaging.

Antibodies for PFKFB1 (SAB1408617) and PFKFB2 (SAB1406248) were from Sigma-Aldrich, for PFKFB3 (H00005209-A01) from Abnova (Taipei City, Taiwan) and PFKFB4 (ab137785) from Abcam (Cambridge, UK) or from Abgent (Center, AP815c; San Diego, CA, USA). Antibodies for p53 (DO-1, sc-126 x) were from Santa Cruz Biotechnology (Dallas, TX, USA). All other reagents were from Sigma-Aldrich. The HMGCS promoter constructs pGL3-SYNwt-luc and pGL3-SYNmutSRE1 were a gift from J. Swinnen (Catholic University, Leuven).

RNA extraction, reverse transcription and RT-qPCR

Total RNA was isolated using an RNeasy kit (Qiagen, Hilden, Germany). Two micrograms of total RNA was used for first strand cDNA synthesis with SuperScript II Reverse Transcriptase and oligo-dT primers (Invitrogen, Carlsbad, CA, USA). Real time PCR was performed with SYBR Green PCR Master Mix (Applied Biosystems, Carlsbad, CA, USA) using Quantitect primers (Qiagen) in

an ABI PRISM 7900 Sequence Detection System (Applied Biosystems). The relative amount of all mRNAs was calculated using the comparative CT method after normalization to *B2M* and/or *Bactin*.

Protein analysis

Cells were lysed in Triton lysis buffer (1% Triton X-100, 50 mM Tris pH 7.5, 300 mM NaCl, 1 mM EGTA, 1 mM DTT, 1 mM NaVO₄, Protease-Inhibitor-Cocktail and Phosphatase-Inhibitor-Cocktail (Roche, Burgess Hill, UK)). Proteins were separated on SDS-PAGE and blotted onto PVDF membrane (Immobilon, Merck Millipore, Watford, UK). Membranes were blocked with 3% bovine serum albumin, incubated with antibody solutions and signals were detected using ECL-reagent.

Generation of doxycycline-inducible shRNA cell lines and expression of p53 in SKOV3 cells

Lentiviral vectors containing short hairpin RNA sequences targeting PFKFB4 were described previously.¹⁰ shRNA sequences targeting p53 were cloned into the TetOnPLKO lentiviral vector using the following oligonucleotides: forward 5'- CCGGCACCATCACTCAACTACATCTCGAGATGTAGTTGATGGATGGTGT TTT and reverse 5'- AATTAATAACACCATCCACTCAACTACATCTCGAGATGTA GTTGTAGTGGATGGT. Lentiviruses were produced by co-transfecting HEK 293T with shRNA plasmids and the packaging plasmids pCMVΔR8.91 (gag-pol) and pMD.G (VSV-G glycoprotein).³⁵ Supernatants containing lentiviruses were collected 48 h after transfection, mixed with polybrene (8 μg/ml) and used for infection. Fresh medium containing puromycin (2 μg/ml) was added after 24 h and cells were selected for at least 48 h before use.

The coding sequence of human *TP53* was excised from pCMV-Neo-Bam p53 wt (Addgene, 16434) and inserted into the lentiviral vector pBOBI (a gift from the Verma laboratory, Salk Institute, La Jolla to K.M.Brindle). In the resulting vector, mStrawberry is separated from *TP53* by an E2A sequence (EF1-5-p53_WT), which results in expression from a single mRNA transcript in equimolar concentrations. After lentiviral transduction, SKOV3 cells displaying similar levels of fluorescence were single cell sorted using a cell sorter BD FACSAria (Flow Cytometry, CRUK-CI), and a homogenous population was established.

ChIP assay

TP53 binding sites were predicted in the promoter of the human *PFKFB4* gene using the MatInspector tool from Genomatix. For ChIP assays, cells were washed with phosphate-buffered saline (PBS) and crosslinked with 1% formaldehyde for 15 min at 37 °C. The reaction was stopped by the addition of glycine to 125 mM final concentration. Samples were sonicated to generate DNA fragments with an average size below 1000 base pairs, followed by immunoprecipitation with the indicated antibodies. Bound DNA fragments were eluted and amplified by PCR using the following primer pairs: *PFKFB4_p53-site1* 5'-CGTCCACTGCCTGGAAA-3', 5'-CAGC CCAACTCCATTGC-3'; *PFKFB4_p53-site2* 5'-TGAGCATGTGCGGAAGGA-3', 5'-AAAGGAACCCATGAGGGAAAGT-3'; *p21_p53-site* 5'-CTGAAAACAGGCAGCC AAG-3', 5'-GTGGCTCTGATTGGCTTTCTG-3'

Cell viability assays

Cells were seeded on 12-well plates. After incubation, cells were fixed with 70% ethanol, stained with 0.01% crystal violet, washed and dried. For quantification, dye was extracted with 10% acetic acid and OD was measured at 560 nm.

Generation of PFKFB4 constructs

The Hs_PFKFB4 cDNA was obtained from Origene and used as template for cloning into pBabe-blast using the BD In Fusion PCR Cloning kit (Clontech, Takara, Mountain View, CA, USA) and the following primers: (forward 5'- TCTAGGCGCCGGCCGATGGCGTCCCAACGG and reverse 5'-CTGTGCTGGC GAATTCATCTGGTGGAGCAGG). shRNA-insensitive constructs were generated by site-directed mutagenesis using the following primers: (PFKFB4_{m166S}: forward 5'- GGCCAGTATCGCCGGATGTCGTGAACAGGTATAAATCTTTTG and reverse 5'- CAAAAGATTATACGTGTTCCAGCATCCCGGCATACTGGCC; PFKFB4_{m164}: forward 5'-CCTGAGGTCATAGCTGCGAATATAGTCCAGGTCAA ACTGGGACGCC and reverse 5'- GGCTGCCAGTTTGACCTGGACTATATTCGC AGCTATGACCTCAGG).

Determination of Fru-2,6-BP

Cells were homogenized in 50 mM NaOH and 0.1% Triton X-100, heated to 80 °C for 5 min, and centrifuged for 5 min. The supernatant was

neutralized with acetic acid in 20 mM N-(2-Hydroxyethyl)piperazine-N'-(2-ethanesulfonic acid). Fru-2,6-BP was determined as previously described.³⁶ Protein concentration was used for normalization.

2-NBDG uptake

Cells were treated with 1 μg/ml doxycycline for 6 days, washed with PBS and incubated in media with 100 μM of 2-[N-(7-nitrobenz-2-oxa-1,3-diazol-4-yl) amino]-2-deoxy-D-glucose (2-NBDG, Sigma-Aldrich), a fluorescent derivative of 2-deoxyglucose, for 20 min. Medium was removed and cells were washed twice in PBS followed by fluorescence-activated cell sorting (FACS) analysis. 4',6-diamidine-2'-phenylindole dihydrochloride was added before analysis to exclude dead cells.

Analysis of cellular respiration

Cells were treated with 1 μg/ml doxycycline for 5 days. Cells (4 × 10⁵) were plated in sextuplets in a 96-well XF culture plate. Twenty-four hours later, medium was changed to assay medium (Seahorse Biosciences/Agilent Technologies, Santa Clara, CA, USA) supplemented with 1 mM sodium pyruvate and 10 mM glucose with pH adjusted to 7.4. Cells were incubated in a CO₂-free atmosphere for 1 h and oxygen consumption (OCR) and extracellular acidification (ECAR) rates were determined using a XF96 Extracellular Flux Analyser (Software Version 1.4, Seahorse Biosciences/Agilent Technologies). During the experiment, 1 μM oligomycin A, 0.4 μM FCCP and 1 μM antimycin A (all Sigma-Aldrich) were injected. Rates were normalized to total protein content determined by sulforhodamine B staining.

¹⁴C-glucose incorporation into CO₂

Cells were cultivated in the presence or absence of doxycycline for 6 days and then treated with 1 μCi ¹⁻¹⁴C or 6-¹⁴C-glucose and incubated at 37 °C for 90 min. To release ¹⁴CO₂, 150 μl perchloric acid was added to each well, immediately covered with phenylethylamine saturated paper and incubated at room temperature for 24 h. The paper was then analysed by scintillation counting.

Mass isotopomer distribution analysis

Cells were labelled with 17.5 mM 1,2-¹³C-glucose (Cambridge Isotope Laboratories, Tewksbury, MA, USA) for 24 h and extracted using acetonitrile/methanol/water (40/40/20). Dried cell extracts were resuspended in 100 μl deionized water, 10 μl of which were injected into a Waters Acquity UPLC with a Waters T3 column (150 × 2.1 mm × 1.8 μm; Waters Corporation, Milford, MA, USA) coupled to a Thermo TSQ Quantum Ultra triple quadrupole instrument (Thermo Fisher Scientific, Waltham, MA, USA) with electrospray ionization. Compound separation was achieved by a gradient of two mobile phases (i) 10 mM tributylamine, 15 mM acetic acid, 5% (v/v) methanol and (ii) 2-propanol³⁷ and MIDs of intact and fragmented carbon backbones were acquired as described in Ruhl *et al.*³⁸ and correct for natural isotopic abundance.

Determination of NADPH levels

For detection of NADPH, cells were lysed in buffer containing 20 mM nicotinamide, 20 mM NaHCO₃ and 100 mM Na₂CO₃. Scraped cells were sonicated and 150 μl cleared supernatants were incubated for 30 min at 60 °C. Twenty microlitre of heated or not heated supernatant were then mixed with 160 μl NADP-cycling buffer (100 mM Tris-Cl pH 8.0, 0.5 mM thiazolyl blue, 2 mM phenazine ethosulfate, 5 mM EDTA and 1.3 IU glucose-6-phosphate dehydrogenase). After 1 min incubation in the dark at 30 °C, 1 mM glucose-6-phosphate was added and the change in absorbance at 570 nm was measured every 30 s for 4 min at 30 °C. Protein concentration was used for normalization.

Determination of acetate-dependent lipid synthesis

Cells were incubated in medium containing 10 μCi/ml [¹⁻¹⁴C] acetate (85 μM final concentration, Perkin Elmer) for 3 h. After washing three times with PBS, cells were lysed in 0.5% Triton X-100/PBS. Lipids were extracted by successive addition of 2 ml methanol, 2 ml chloroform, and 1 ml dH₂O. Phases were separated by centrifugation before the organic phase was dried and used for scintillation counting. Results were normalized to total protein content determined by sulforhodamine B staining.

Reporter assays

Cells were transfected with 0.5 µg pGL3-SYNwt-luc or pGL3-SYNmutSRE1³⁹ and 0.5 µg pRL-SV40 using Lipofectamine 2000. Cells were lysed and activity was determined using a Dual Luciferase assay (Promega, Madison, WI, USA).

Determination of ROS levels

ROS levels were determined by incubating cells for 30 min at 37 °C in medium with 1.6 µM CM-H₂-DCFDA (Molecular Probes, Eugene, OR, USA) followed by FACS analysis. 4',6-Diamidino-2'-phenylindole dihydrochloride was added prior to analysis to exclude dead cells.

Apoptosis assay

Cells were trypsinized and stained with Annexin V-pacific blue and propidium iodide. Apoptotic cells were determined by FACS analysis.

Induction of spheroid growth

For spheroid formation, cells were trypsinized, counted and placed in 96-well ultralow attachment plates (Corning/Costar, Sigma-Aldrich). Spheroid formation was initiated by centrifugation at 650 g for 10 min and cultures were incubated for 13 days. Spheroid size was determined by imaging on an inverted microscope (Axiovert 100 M, Carl Zeiss, Oberkochen, Germany) and images were processed in ImageJ.

Xenograft experiments

To generate luciferase expressing cells, a pBabe-Luciferase retroviral vector (a gift from J. Downward) was packaged in Phoenix-Ampho cells and used to infect HCT116 p53^{+/+} and p53^{-/-} cells. After selection, cells were transduced with lentiviral vectors and selected as in Generation of doxycycline-inducible shRNA cell lines section. Cells (1 × 10⁶) were subcutaneously injected into the dorsal flank of male nude mice (ICRF nude). Animals were randomly assigned to two cohorts. For induction of shRNA expression, one animal cohort received doxycycline (Doxycycline diet, 0.2 g/kg food pellet, Harlan D.98186) starting 1 day after implantation, and tumour growth was followed over 21 days. HCT116_{luc}p53^{+/+}shCtrl (*n* = 6), HCT116_{luc}p53^{+/+}shB4#68 (*n* = 5), HCT116_{luc}p53^{+/+}shB4#68 DOX (*n* = 4), HCT116_{luc}p53^{-/-}shCtrl (*n* = 5), HCT116_{luc}p53^{-/-}shCtrl DOX (*n* = 6), HCT116_{luc}p53^{-/-}shB4#68 (*n* = 4), HCT116_{luc}p53^{-/-}shB4#68 DOX (*n* = 6), HCT116_{luc}p53^{-/-}shB4#64 (*n* = 6), HCT116_{luc}p53^{+/+}shB4#64 DOX (*n* = 5), HCT116_{luc}p53^{-/-}shB4#68 (*n* = 5), HCT116_{luc}shB4#68 DOX (*n* = 5). Mice were anaesthetized, intraperitoneally injected with Luciferin (Promega) and imaged using an IVIS Spectrum imaging system. Investigators were blinded to group allocation. Images were analysed using the IVIS Living Image software. Criteria for the exclusion of animal from the analysis were pre-defined based on morbidity unrelated to experimental treatment. This was not observed during the experiment and no animals were excluded. All animal experiments were performed according to UK Home Office guidelines.

Histology

Four-micrometer thick tissue sections were mounted, dewaxed and rehydrated. Antigen retrieval was performed with citrate buffer (pH 6.0) in a microwave oven for 30 min. Endogenous peroxidase activity was blocked by incubating sections in 3% (v/v) hydrogen peroxide for 10 min. Sections were blocked with 3% (w/v) bovine serum albumin for 30 min and incubated with the monoclonal mouse anti-human Ki-67 antibody (9106, Thermo Scientific, Waltham, MA, USA), diluted 1:200 over night at 4 °C in a humidified chamber. Sections were washed in PBS and incubated with biotinylated secondary antibody followed by streptavidin-horseradish-peroxidase assay (Vector Labs, Dako). Reaction was developed using 3,3'-diaminobenzidine (Cell Signaling Technologies, Danvers, MA, USA). Slides were counterstained with Gilmore 3 hematoxylin, dehydrated, cleared and mounted with coverslips. TUNEL assay was performed according to the manufacturer's instructions (In Situ Cell Death Detection Kit, Roche no. 11684795910).

RNAseq analysis

Total RNA from three tumours in each treatment group (HCT116_{luc}p53^{+/+}shCtrl, HCT116_{luc}p53^{+/+}shB4#68, HCT116_{luc}p53^{-/-}shCtrl and HCT116_{luc}p53^{-/-}shB4#68 all treated with DOX) was extracted using RNeasy mini columns (Qiagen) with on column DNase I digestion. PolyA+ RNA was extracted using the NEBNext Poly(A) mRNA Magnetic Isolation Module (NEB, Ipswich, MA, USA). For library

preparation, the NEBNext Ultra RNA Library Prep Kit for Illumina (NEB) was used. Quantification and quality control was performed using the Experion Automated Electrophoresis System (BioRad, Hercules, CA, USA). Sequencing was performed using an Illumina NextSeq500 System (Illumina, San Diego, CA, USA).

Fastq files were mapped to the human genome assembly hg19 using TopHat v2.0.7 (Johns Hopkins University, Center for Computational Biology, Baltimore, MD, USA) with default parameters and subsequently normalized to the number of mapped reads in the smallest sample. Reads per gene were counted using the countOverlaps function from the R package (Genomic Ranges). Weakly expressed genes were removed (threshold: mean read count over all samples < 1) and differentially expressed genes were called using EdgeR (www.bioconductor.org). GSE analyses⁴⁰ were performed with signal2noise metric, 1000 permutations and the C2 gene set. Pathway analysis of differentially expressed genes (logFC ≤ 0.7, q ≤ 0.05) was performed using the DAVID tool^{41,42} with default settings. RNAseq data was deposited in GEO with accession number GSE89110.

Analysis of patient data and survival analysis

Lung cancer data were downloaded from the Gene Expression Omnibus (GSE12667) and MAS 5.0 processed signals were generated on Affymetrix Human Genome U133 Plus 2.0. Normalized data were log₂ transformed. A Wilcoxon rank sum test was used to assess significant changes in expression between p53^{+/+} and p53^{-/-} groups for probeset detecting the PFKFB4 gene. Analysis of survival data from public data sets for breast cancer⁴³ and non-small cell lung cancer⁴⁴ was performed using PROGene.⁴⁵ Patients were divided based on median PFKFB4 expression and relapse-free survival was analysed. Expression data for PFKFB4 in lung adenocarcinoma were extracted from public data sets.⁴⁴

Statistical analysis

Graphs were generated using GraphPad Prism 5.0 (GraphPad Software, La Jolla, CA, USA). All experiments were performed with three biologically independent replicates unless stated otherwise. Sample sizes are calculated to allow significance to be reached. Statistical significance of magnitude of changes between different conditions was calculated using the parametric two-tailed unpaired Student *t*-tests. Statistical significance was defined as a *P*-value of < 0.05. *P*-values are depicted as follows: **P* < 0.05, ***P* < 0.01, ****P* < 0.001 and *****P* < 0.0001. NS = not significant.

CONFLICT OF INTEREST

The authors declare no conflict of interest.

ACKNOWLEDGEMENTS

We thank C. Esnault (LRI) for advice on ChIP and H. Miess for help with Seahorse Analysis, C. Watkins and J. Bee (LRI, BRU) for help with animal experimentation, F. Lassailli, P. Johnson and T. Snoeks (In vivo imaging facility, LRI) for assistance with *in vivo* imaging and the LRI research services for technical support. We also thank C. Ade and Barbara Bauer (Theodor-Boveri-Institute, Würzburg) for help with RNAseq analysis and histology, Beatrice Dankworth for help with cell line generation and W. Schmitz for insightful discussions. Cancer Research UK, the German Cancer Aid (grant 111917), the German Research Foundation (FOR 2314), and the CRUK-EP SRC Imaging Centre in Cambridge and Manchester (grant 16465) supported this work.

AUTHOR CONTRIBUTIONS

SR and AS conceived the project and wrote the manuscript. SR, JF, IK, CD, AH, SD, BG and SB performed experiments and analysis of results. RM and SW performed the bioinformatic analysis. AB, KMB, NZ and MHR contributed to the study design and data analysis. All authors commented on the manuscript.

REFERENCES

- Lunt SY, Vander Heiden MG. Aerobic glycolysis: meeting the metabolic requirements of cell proliferation. *Annu Rev Cell Dev Biol* 2011; **27**: 441–464.
- Kruiswijk F, Labuschagne CF, Voudsen KH. p53 in survival, death and metabolic health: a lifeguard with a licence to kill. *Nat Rev Mol Cell Biol* 2015; **16**: 393–405.
- Li T, Kon N, Jiang L, Tan M, Ludwig T, Zhao Y *et al*. Tumor suppression in the absence of p53-mediated cell-cycle arrest, apoptosis, and senescence. *Cell* 2012; **149**: 1269–1283.

- 4 Kawauchi K, Araki K, Tobiume K, Tanaka N. p53 regulates glucose metabolism through an IKK-NF-kappaB pathway and inhibits cell transformation. *Nat Cell Biol* 2008; **10**: 611–618.
- 5 Matoba S, Kang JG, Patino WD, Wragg A, Boehm M, Gavrilova O *et al*. p53 regulates mitochondrial respiration. *Science* 2006; **312**: 1650–1653.
- 6 Bensaad K, Tsuruta A, Selak MA, Vidal MN, Nakano K, Bartrons R *et al*. TIGAR, a p53-inducible regulator of glycolysis and apoptosis. *Cell* 2006; **126**: 107–120.
- 7 Hitosugi T, Zhou L, Elf S, Fan J, Kang HB, Seo JH *et al*. Phosphoglycerate mutase 1 coordinates glycolysis and biosynthesis to promote tumor growth. *Cancer Cell* 2012; **22**: 585–600.
- 8 Jiang P, Du W, Wang X, Mancuso A, Gao X, Wu M *et al*. p53 regulates biosynthesis through direct inactivation of glucose-6-phosphate dehydrogenase. *Nat Cell Biol* 2011; **13**: 310–316.
- 9 Jiang P, Du W, Mancuso A, Wellen KE, Yang X. Reciprocal regulation of p53 and malic enzymes modulates metabolism and senescence. *Nature* 2013; **493**: 689–693.
- 10 Ros S, Santos CR, Moco S, Baenke F, Kelly G, Howell M *et al*. Functional metabolic screen identifies 6-phosphofructo-2-kinase/fructose-2,6-bisphosphatase 4 as an important regulator of prostate cancer cell survival. *Cancer Discov* 2012; **2**: 328–343.
- 11 Lavin MF, Gueven N. The complexity of p53 stabilization and activation. *Cell Death Differ* 2006; **13**: 941–950.
- 12 Ho J, Benchimol S. Transcriptional repression mediated by the p53 tumour suppressor. *Cell Death Differ* 2003; **10**: 404–408.
- 13 Murphy M, Ahn J, Walker KK, Hoffman WH, Evans RM, Levine AJ *et al*. Transcriptional repression by wild-type p53 utilizes histone deacetylases, mediated by interaction with mSin3a. *Genes Dev* 1999; **13**: 2490–2501.
- 14 Ding L, Getz G, Wheeler DA, Mardis ER, McLellan MD, Cibulskis K *et al*. Somatic mutations affect key pathways in lung adenocarcinoma. *Nature* 2008; **455**: 1069–1075.
- 15 Okar DA, Manzano A, Navarro-Sabate A, Riera L, Bartrons R, Lange AJ. PFK-2/FBPase-2: maker and breaker of the essential biofactor fructose-2,6-bisphosphate. *Trends Biochem Sci* 2001; **26**: 30–35.
- 16 Strohecker AM, Joshi S, Possemato R, Abraham RT, Sabatini DM, White E. Identification of 6-phosphofructo-2-kinase/fructose-2,6-bisphosphatase as a novel autophagy regulator by high content shRNA screening. *Oncogene* 2015; **34**: 5662–5676.
- 17 Willis A, Jung EJ, Wakefield T, Chen X. Mutant p53 exerts a dominant negative effect by preventing wild-type p53 from binding to the promoter of its target genes. *Oncogene* 2004; **23**: 2330–2338.
- 18 Schwartzberg-Bar-Yoseph F, Armoni M, Karnieli E. The tumor suppressor p53 down-regulates glucose transporters GLUT1 and GLUT4 gene expression. *Cancer Res* 2004; **64**: 2627–2633.
- 19 Bengoechea-Alonso MT, Ericsson J. SREBP in signal transduction: cholesterol metabolism and beyond. *Curr Opin Cell Biol* 2007; **19**: 215–222.
- 20 Freed-Pastor WA, Mizuno H, Zhao X, Langerod A, Moon SH, Rodriguez-Barrueco R *et al*. Mutant p53 disrupts mammary tissue architecture via the mevalonate pathway. *Cell* 2012; **148**: 244–258.
- 21 Yahagi N, Shimano H, Matsuzaka T, Najima Y, Sekiya M, Nakagawa Y *et al*. p53 Activation in adipocytes of obese mice. *J Biol Chem* 2003; **278**: 25395–25400.
- 22 Denko NC. Hypoxia, HIF1 and glucose metabolism in the solid tumour. *Nat Rev Cancer* 2008; **8**: 705–713.
- 23 Mayers JR, Vander Heiden MG. Famine versus feast: understanding the metabolism of tumors in vivo. *Trends Biochem Sci* 2015; **40**: 130–140.
- 24 Casciari JJ, Sotirchos SV, Sutherland RM. Variations in tumor cell growth rates and metabolism with oxygen concentration, glucose concentration, and extracellular pH. *J Cell Physiol* 1992; **151**: 386–394.
- 25 Maddocks OD, Vouden KH. Metabolic regulation by p53. *J Mol Med* 2011; **89**: 237–245.
- 26 Kim HR, Roe JS, Lee JE, Cho EJ, Youn HD. p53 regulates glucose metabolism by miR-34a. *Biochem Biophys Res Commun* 2013; **437**: 225–231.
- 27 Maddocks OD, Berkens CR, Mason SM, Zheng L, Blyth K, Gottlieb E *et al*. Serine starvation induces stress and p53-dependent metabolic remodelling in cancer cells. *Nature* 2013; **493**: 542–546.
- 28 Rinn JL, Huarte M. To repress or not to repress: this is the guardian's question. *Trends Cell Biol* 2011; **21**: 344–353.
- 29 Ros S, Schulze A. Balancing glycolytic flux: the role of 6-phosphofructo-2-kinase/fructose 2,6-bisphosphatases in cancer metabolism. *Cancer Metab* 2013; **1**: 8.
- 30 Chesney J, Clark J, Klarer AC, Imbert-Fernandez Y, Lane AN, Telang S. Fructose-2,6-bisphosphate synthesis by 6-phosphofructo-2-kinase/fructose-2,6-bisphosphatase 4 (PFKFB4) is required for the glycolytic response to hypoxia and tumor growth. *Oncotarget* 2014; **5**: 6670–6686.
- 31 Feng Z, Hu W, de Stanchina E, Teresky AK, Jin S, Lowe S *et al*. The regulation of AMPK beta1, TSC2, and PTEN expression by p53: stress, cell and tissue specificity, and the role of these gene products in modulating the IGF-1-AKT-mTOR pathways. *Cancer Res* 2007; **67**: 3043–3053.
- 32 Laplante M, Sabatini DM. An emerging role of mTOR in lipid biosynthesis. *Curr Biol* 2009; **19**: R1046–R1052.
- 33 Ralser M, Wamelink MM, Kowald A, Gerisch B, Heeren G, Struys EA *et al*. Dynamic rerouting of the carbohydrate flux is key to counteracting oxidative stress. *J Biol Chem* 2007; **282**: 1497–1501.
- 34 Bunz F, Dutriaux A, Lengauer C, Waldman T, Zhou S, Brown JP *et al*. Requirement for p53 and p21 to sustain G2 arrest after DNA damage. *Science* 1998; **282**: 1497–1501.
- 35 Zufferey R, Nagy D, Mandel RJ, Naldini L, Trono D. Multiply attenuated lentiviral vector achieves efficient gene delivery in vivo. *Nat Biotechnol* 1997; **15**: 871–875.
- 36 Van Schaftingen E, Lederer B, Bartrons R, Hers HG. A kinetic study of pyrophosphate: fructose-6-phosphate phosphotransferase from potato tubers. Application to a microassay of fructose 2,6-bisphosphate. *Eur J Biochem* 1982; **129**: 191–195.
- 37 Buescher JM, Moco S, Sauer U, Zamboni N. Ultrahigh performance liquid chromatography-tandem mass spectrometry method for fast and robust quantification of anionic and aromatic metabolites. *Anal Chem* 2010; **82**: 4403–4412.
- 38 Ruhl M, Rupp B, Noh K, Wiechert W, Sauer U, Zamboni N. Collisional fragmentation of central carbon metabolites in LC-MS/MS increases precision of (1)(3)C metabolic flux analysis. *Biotechnol Bioeng* 2012; **109**: 763–771.
- 39 Swinnen JV, Heemers H, Deboel L, Foufelle F, Heyns W, Verhoeven G. Stimulation of tumor-associated fatty acid synthase expression by growth factor activation of the sterol regulatory element-binding protein pathway. *Oncogene* 2000; **19**: 5173–5181.
- 40 Subramanian A, Tamayo P, Mootha VK, Mukherjee S, Ebert BL, Gillette MA *et al*. Gene set enrichment analysis: a knowledge-based approach for interpreting genome-wide expression profiles. *Proc Natl Acad Sci USA* 2005; **102**: 15545–15550.
- 41 Huang, da W, Sherman BT, Lempicki RA. Systematic and integrative analysis of large gene lists using DAVID bioinformatics resources. *Nat Protoc* 2009; **4**: 44–57.
- 42 Huang DW, Sherman BT, Tan Q, Kir J, Liu D, Bryant D *et al*. DAVID Bioinformatics resources: expanded annotation database and novel algorithms to better extract biology from large gene lists. *Nucleic Acids Res* 2007; **35**: W169–W175.
- 43 Ivshina AV, George J, Senko O, Mow B, Putti TC, Smeds J *et al*. Genetic reclassification of histologic grade delineates new clinical subtypes of breast cancer. *Cancer Res* 2006; **66**: 10292–10301.
- 44 Lee ES, Son DS, Kim SH, Lee J, Jo J, Han J *et al*. Prediction of recurrence-free survival in postoperative non-small cell lung cancer patients by using an integrated model of clinical information and gene expression. *Clin Cancer Res* 2008; **14**: 7397–7404.
- 45 Goswami CP, Nakshatri H. PROGene: gene expression based survival analysis web application for multiple cancers. *J Clin Bioinform* 2013; **3**: 22.

Supplementary Information accompanies this paper on the Oncogene website (<http://www.nature.com/onc>)

SUPPLEMENTARY FIGURE LEGENDS

Supplementary Figure 1 (related to Figure 1 and 2)

- a) Expression of PFKFB1, PFKFB2, PFKFB3 and p53 protein in HCT116 p53^{+/+} and p53^{-/-} cells. Actin was used as loading control.
- b) HCT116 p53^{-/-} cells were treated with different concentrations of etoposide for 24 hours. Expression of *PFKFB4*, *p21 (CDKN1A)* and *ME2* was determined by qPCR, and normalised to *B2M*. Data are presented as mean ± SEM (n=3)
- c) Differential expression of *PFKFB4* in p53^{+/+} or p53^{-/-} human lung adenocarcinoma.

Supplementary Figure 2 (related to Figure 3)

- a) HCT116 p53^{+/+} and p53^{-/-} cells expressing inducible shRNAs targeting PFKFB4 were treated with 1µg/ml doxycycline (DOX) or solvent for 6 days. Expression of PFKFB1, PFKFB2 and PFKFB3 protein was determined by Western blot using vinculin as loading control.
- b) HCT116 p53^{+/+} and p53^{-/-} cells expressing inducible shRNAs targeting PFKFB4 (shPFKFB4 #68) were stably transfected with pBabe-vectors expressing shRNA-insensitive versions of PFKFB4 (PFKFB4_{ins}) for this sequence. Silencing of endogenous *PFKFB4* and expression of shRNA-insensitive exogenous *PFKFB4* was determined by qPCR. Data are presented as mean ± SD (n=4).
- c) Cells expressing inducible shRNAs targeting PFKFB4 (shPFKFB4 #64) were stably transfected with pBabe-vectors expressing shRNA-insensitive versions of PFKFB4 (PFKFB4_{ins}) for this sequence. Silencing of endogenous *PFKFB4* and expression of shRNA-insensitive exogenous *PFKFB4* was determined by qPCR. Data are presented as mean ± SD (n=4).

Supplementary Figure 3 (related to Figure 4)

a) HCT116 p53^{+/+} and p53^{-/-} cells expressing inducible shRNA targeting PFKFB4 (shPFKFB4 #68) were treated with 1µg/ml doxycycline (Dox) or solvent for 2 days. Expression of *PFKFB4* was determined by qPCR and normalised to *B2M*. Data are presented as mean ± SEM (n=4).

b) Expression of PFKFB4 protein was determined after 3 days of doxycycline treatment. Actin expression was used as a loading control.

c) HCT116 p53^{+/+} and p53^{-/-} cells expressing inducible shRNAs targeting PFKFB4 (shPFKFB4 #68) were treated with 1µg/ml doxycycline (Dox) or solvent for 3 days. Intracellular levels of fructose 2,6-biphosphate (Fru-2,6-BP) were determined. Data are presented as mean ± SEM (n=5).

d) HCT116 p53^{+/+} and p53^{-/-} cells expressing inducible shRNA targeting PFKFB4 (shPFKFB4 #64) were treated with 1µg/ml doxycycline (Dox) or solvent for 6 days. Expression of PFKFB4 protein was determined. Actin is shown as a loading control.

e) HCT116 p53^{+/+} and p53^{-/-} cells expressing inducible shRNAs targeting PFKFB4 (shPFKFB4 #64) were treated with 1µg/ml doxycycline (Dox) or solvent for 6 days. Intracellular levels of fructose 2,6-biphosphate (Fru-2,6-BP) were determined. Data are presented as mean ± SEM (n=3).

f) HCT116 p53^{+/+} and p53^{-/-} cells expressing inducible shRNAs targeting PFKFB4 (shPFKFB4 #68) were treated with 1µg/ml Dox or solvent for 6 days. Uptake of 2-NBDG was measured after 20 minutes incubation. Data are presented as mean ± SEM (n=2).

g) Mass isotopomer distribution in cells exposed to [1,2-¹³C]-glucose. The diagram shows the differential labelling of glycolytic metabolites depending on whether they are generated via glycolysis or the PPP.

h) HCT116 p53^{-/-} cells were treated with doxycycline (Dox) for 6 days and exposed to 17.5mM [1,2-¹³C]-glucose for 24h. Mass isotopomer analysis (MID) was performed using mass spectrometry. The relative fraction of M+0, M+1 and

M+2 isotopomers of FBP and PEP are displayed. Data are presented as mean \pm SEM (n=3).

Supplementary Figure 4 (related to Figure 5)

a) HCT116 p53^{+/+} and p53^{-/-} cells expressing inducible shRNA targeting PFKFB4 (shPFKFB4 #64) were treated with 1 μ g/ml doxycycline (Dox) or solvent for 6 days. Levels of NADP⁺ and NADPH were determined and normalised to total protein content. Values are presented relative to solvent controls. Data are presented as mean \pm SEM (n=5).

b) HCT116_{luc} p53^{+/+} or p53^{-/-} cells expressing inducible shRNA targeting PFKFB4 (shPFKFB4 #68) were treated with 1 μ g/ml doxycycline (DOX) or solvent for 3 days. Levels of NADP⁺ and NADPH were determined and normalised to total protein content. Values are presented relative to solvent controls. Data are presented as mean \pm SEM (n=5).

c) HCT116 p53^{+/+} and p53^{-/-} cells expressing inducible shRNA targeting PFKFB4 (shPFKFB4 #68) were treated with 1 μ g/ml doxycycline (Dox) or solvent for 6 days. Expression of *ME1* and *ME2* was determined by qPCR and normalised to *B2M*. Data are presented as mean \pm SEM (n=3) and are relative to HCT116 p53^{+/+} cells treated with solvent.

Supplementary Figure 5 (related to Figure 6)

a) HCT116 p53^{+/+} and p53^{-/-} cells expressing shRNAs targeting PFKFB4 (shPFKFB4#68) were seeded in spheroid cultures and treated with 1 μ g/ml doxycycline (Dox) or solvent. Spheroid size was determined over 13 days. Data represent median \pm SEM (n=4).

b) HCT116_{luc} p53^{+/+} or p53^{-/-} cells expressing inducible shRNA targeting PFKFB4 (shPFKFB4 #68) were treated with 1 μ g/ml Dox or solvent for 6 days. Expression of *PFKFB4* was determined by qPCR and normalised to *B2M*. Data are presented as mean \pm SEM (n=3).

- c) HCT116_{luc} p53^{+/+} or p53^{-/-} cells expressing inducible shRNA targeting PFKFB4 (shPFKFB4 #68) were seeded at low density, treated with Dox or solvent for 8 days and stained with crystal violet. Left: representative images. Right: Quantitation of results. Graphs show means \pm SEM (n=5)
- d) HCT116_{luc} p53^{+/+} and p53^{-/-} cells expressing inducible shRNAs targeting PFKFB4 (shPFKFB4 #68 or shPFKFB4 #64) were injected subcutaneously into nude mice. Mice were divided into two cohorts and one cohort received doxycycline in their food (Dox). Tumours from the PFKFB4 (shPFKFB4 #68) or control (shCtrl) xenograft were excised on day 21 and tumour weight was determined. Data are presented as mean \pm SEM. n.s = not significant.
- e) Representative images of tumours from the different cohorts.
- f) Expression of *PFKFB4* in excised tumours (shPFKFB4 #68 or shPFKFB4 #64) was determined in triplicates by qPCR and normalised to *B2M* (for shPFKFB4 #68) and the geomean of *B2M* and *Bactin* (for shPFKFB4 #68).
- g) Tumours from the PFKFB4 (shPFKFB4 #64) xenograft were stained for Ki67 and H&E. Images are taken from the animals represented in Fig. 6A.

Supplementary Figure 6 (related to Figure 6)

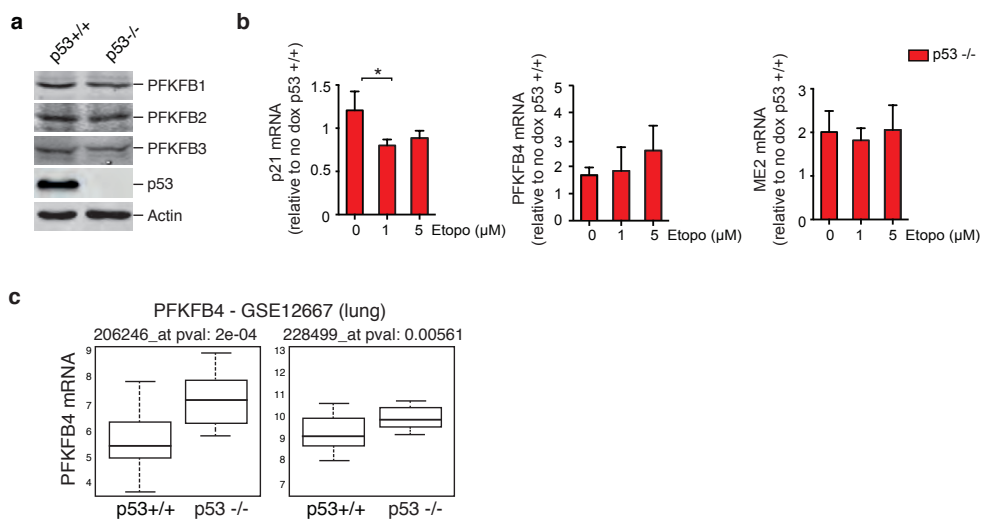
- a) Pathway analysis (DAVID) of genes downregulated in HCT116 p53^{+/+} or p53^{-/-} tumours following silencing of PFKFB4.
- b) Kaplan-Meier curves for breast cancer patients (Ivshina et al., 2006) displaying low or high levels of PFKFB4 expression. Patients were divided based on median PFKFB4 expression and relapse-free survival was analysed.
- c) Kaplan-Meier curves for non-small cell lung cancer patients (Lee et al., 2008) displaying low or high levels of PFKFB4 expression. Patients were divided based on median PFKFB4 expression and relapse-free survival was analysed.

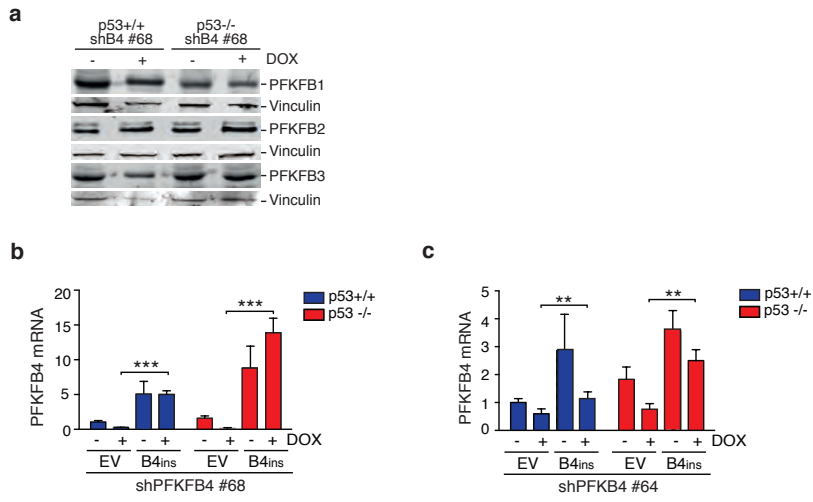
SUPPLEMENTARY REFERENCES:

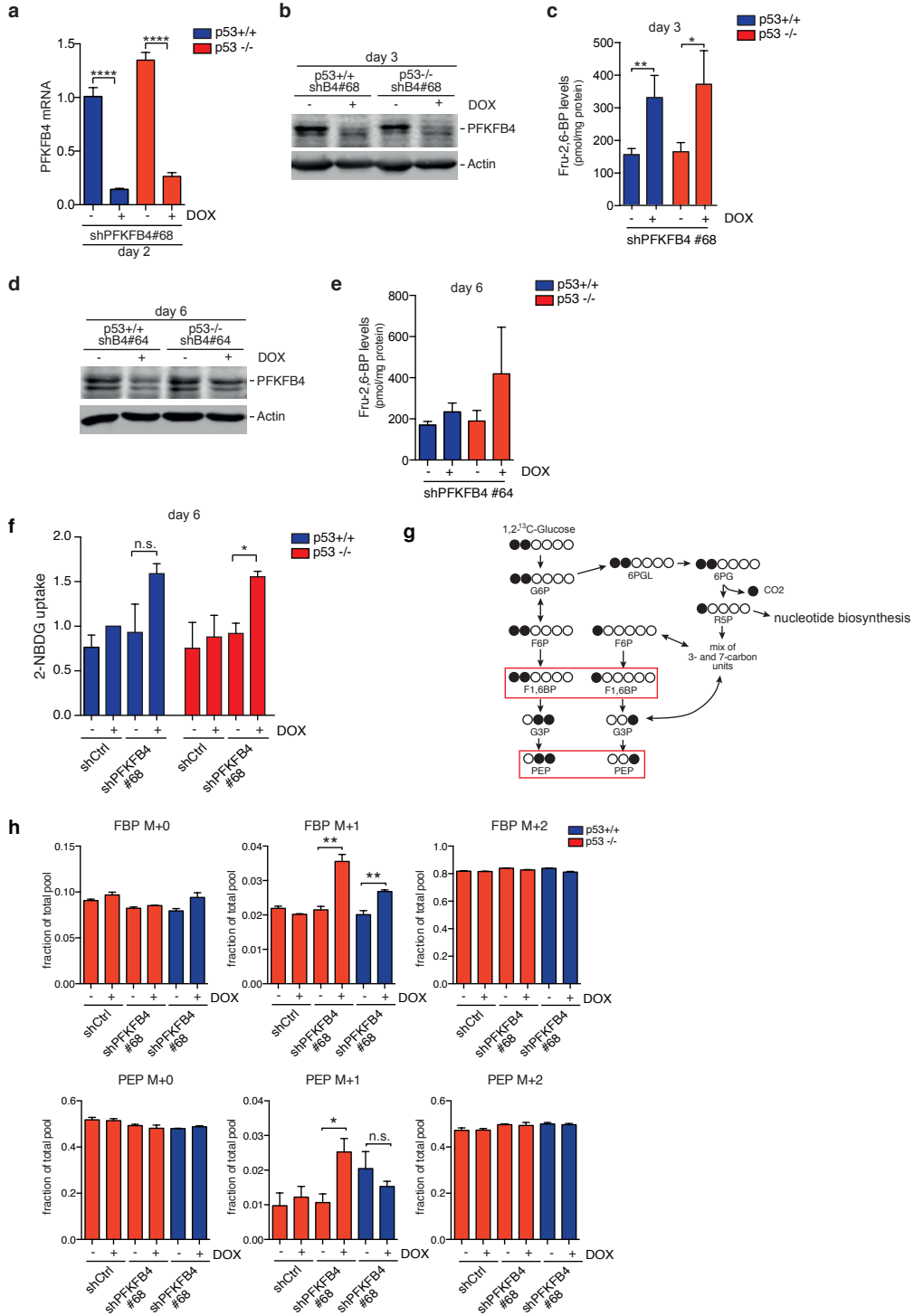
Ivshina, A.V., George, J., Senko, O., Mow, B., Putti, T.C., Smeds, J., Lindahl, T., Pawitan, Y., Hall, P., Nordgren, H., *et al.* (2006). Genetic reclassification of histologic grade delineates new clinical subtypes of breast cancer. *Cancer research* 66, 10292-10301.

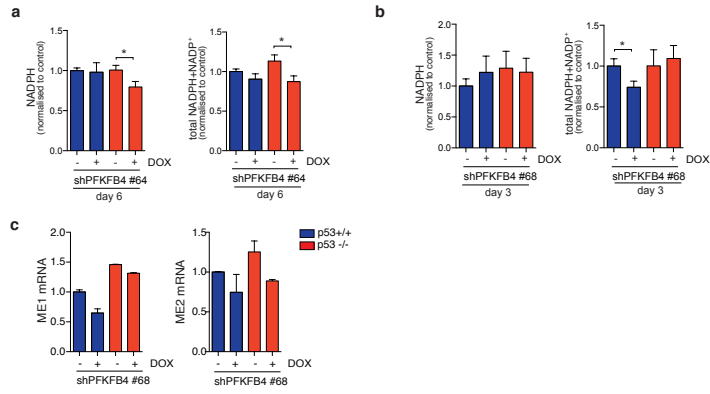
Lee, E.S., Son, D.S., Kim, S.H., Lee, J., Jo, J., Han, J., Kim, H., Lee, H.J., Choi, H.Y., Jung, Y., *et al.* (2008). Prediction of recurrence-free survival in postoperative non-small cell lung cancer patients by using an integrated model of clinical information and gene expression. *Clinical cancer research : an official journal of the American Association for Cancer Research* 14, 7397-7404.

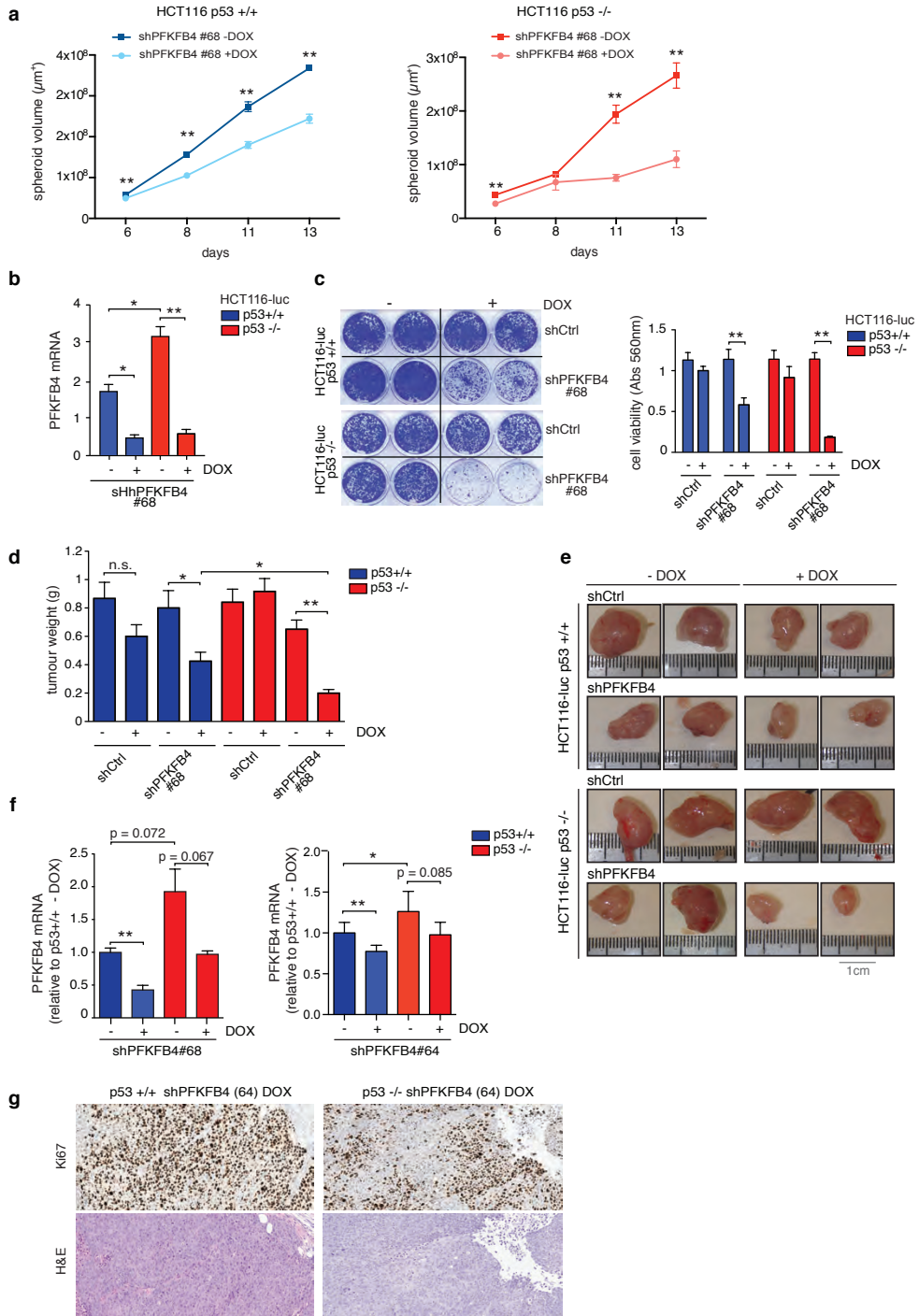
Ros et al. Supplementary Figure 1











a

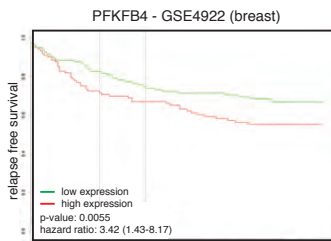
Functional annotation of genes downregulated in response to PFKFB4 depletion in HCT116 p53 WT

| Term | Pvalue | Genes |
|--|--------|-----------------------------------|
| GO:0022627~cytosolic small ribosomal subunit | 0.0132 | RPS28, FTLP2, HBA2, HBA1 |
| GO:0015935~small ribosomal subunit | 0.0310 | RPS28, FTLP2, HBA2, HBA1 |
| GO:0005840~ribosome | 0.0680 | RPS17P5, RPS28, FTLP2, HBA2, HBA1 |

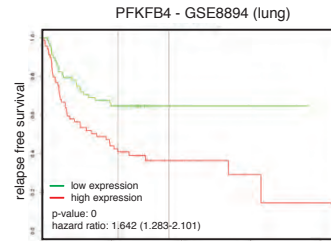
Functional annotation of genes downregulated in response to PFKFB4 depletion in HCT116 p53 NULL

| Term | Pvalue | Genes |
|---|----------|---|
| GO:0003735~structural constituent of ribosome | 2.15E-18 | RPL18, MRPL41, RPL8P2, RPL37A9, RPS9, RPLP0P2, RPL35P2, RPS5, RPL35P1, RPL28, RPL13AP5, RPS3, RPS28, MRPL28, RPL18A, RPS15, RPL8, RPS7P4, RPL37A, RPS11, RPS21, RPS23, RPL36AL |
| hsa03010.Ribosome | 2.40E-18 | RPL18, RPL8P2, RPS9, RPLP0P2, RPL35P2, RPS5, RPL35P1, RPL28, RPL13AP5, RPS3, RPS28, RPL18A, RPS15, RPL8, RPS7P4, RPL37A, RPS11, RPS21, RPS23, RPL36AL |
| GO:0005840~ribosome | 8.07E-17 | RPL18, MRPL41, RPL8P2, FTLP2, RPL37A9, RPS9, RPLP0P2, RPL35P2, RPS5, RPL35P1, RPL28, RPL13AP5, RPS3, RPS28, MRPL28, RPL18A, RPS15, RPL8, RPS7P4, RPL37A, RPS11, RPS21, RPS23, RPL36AL |
| ribosomal protein | 9.06E-17 | RPL18, MRPL41, RPL8P2, RPS9, RPLP0P2, RPL35P2, RPS5, RPL35P1, RPL28, RPL13AP5, RPS3, RPS28, MRPL28, RPL18A, RPS15, RPL8, RPS7P4, RPL37A, RPS11, RPS21, RPS23, RPL36AL |
| GO:0022626~cytosolic ribosome | 1.68E-16 | RPL18, RPL8P2, FTLP2, RPS9, RPLP0P2, RPL35P2, RPS5, RPL35P1, RPL28, RPS3, RPS28, RPL18A, RPS15, RPL8, RPS7P4, RPS11, RPS21, RPS23 |
| GO:0033279~ribosomal subunit | 4.96E-16 | RPL18, MRPL41, RPL8P2, FTLP2, RPS9, RPLP0P2, RPL35P2, RPS5, RPL35P1, RPL28, RPL13AP5, RPS3, RPS28, RPL18A, RPS15, RPL8, RPS7P4, RPS11, RPS21, RPS23 |
| REACT_1762.3~UTR-mediated translational regulation | 7.19E-15 | RPL18, RPL8P2, RPS9, RPLP0P2, RPL35P2, RPS5, RPL35P1, RPL28, RPL13AP5, RPS3, RPS28, RPL18A, RPS15, RPL8, RPS7P4, RPL37A, RPS11, RPS21, RPS23 |
| GO:0006412~translation | 1.57E-14 | RPL18, RPL8P2, MRPL41, RPL37A9, RPLP0P2, RPL13AP5, RPS3, RPS28, RPL8, RPS7P4, RPS21, RPS23, RPL36AL, EEF1A2, RPS9, RPS5, RPL35P2, RPL35P1, SARS2, RPL28, RPL18A, MRPL28, RPS15, RPL37A, RPS11 |
| ribonucleoprotein | 1.38E-13 | RPL18, MRPL41, RPL8P2, RPS9, RPLP0P2, RPL35P2, RPS5, RPL35P1, RPL28, RPL13AP5, RPS3, RPS28, MRPL28, RPL18A, RPS15, RPL8, RPS7P4, RPL37A, RPS11, RPS21, RPS23, RPL36AL |
| protein biosynthesis | 4.31E-13 | RPL18, RPL8P2, EEF1A2, RPS9, RPLP0P2, RPS5, RPL13AP5, SARS2, RPS3, RPS28, RPL18A, RPS15, RPL8, RPS7P4, RPS11, RPS21, RPS23, RPL36AL |
| GO:0022627~cytosolic small ribosomal subunit | 3.74E-11 | RPS28, FTLP2, RPS15, RPS7P4, RPS9, RPS11, RPS21, RPS5, RPS23, RPS3 |
| REACT_17015.Metabolism of proteins | 3.85E-11 | RPL18, RPL8P2, SPHK1, RPS9, RPLP0P2, RPL35P2, RPS5, RPL35P1, RPL28, RPL13AP5, RPS3, RPS28, RPL18A, RPS15, RPL8, RPS7P4, RPL37A, RPS11, RPS21, RPS23 |
| GO:0030529~ribonucleoprotein complex | 3.07E-10 | RPL18, RPL8P2, MRPL41, FTLP2, RPL37A9, RPLP0P2, RPL13AP5, RPS3, RPS28, RPL8, RPS7P4, RPS21, RPS23, RPL36AL, RPS9, RPS5, RPL35P2, RPL35P1, RPL28, RPL18A, MRPL28, RPS15, RPL37A, RPS11, POP7 |
| REACT_71.Gene Expression | 1.10E-09 | RPL18, RPL8P2, POLR21, RPS9, RPLP0P2, RPL35P2, RPS5, RPL35P1, RPL28, RPL13AP5, SARS2, RPS3, RPS28, RPL18A, RPS15, RPL8, TCEB2, RPS7P4, RPL37A, RPS11, RPS21, RPS23 |
| GO:0015935~small ribosomal subunit | 2.75E-09 | RPS28, FTLP2, RPS15, RPS7P4, RPS9, RPS11, RPS21, RPS5, RPS23, RPS3 |
| GO:0015934~large ribosomal subunit | 1.54E-06 | RPL18, RPL8P2, MRPL41, RPL18A, RPL8, RPLP0P2, RPL35P2, RPL35P1, RPL28, RPL13AP5 |
| GO:0022625~cytosolic large ribosomal subunit | 1.65E-05 | RPL18, RPL8P2, RPL18A, RPL8, RPLP0P2, RPL35P2, RPL35P1, RPL28 |
| GO:0034569~cellular response to oxidative stress | 3.82E-04 | GPX1, GPXD, GPX4, ROMO1, PRDX5 |
| GO:0034614~cellular response to reactive oxygen species | 0.0018 | GPX1, GPX4, ROMO1, PRDX5 |
| GO:0043066~negative regulation of apoptosis | 0.0022 | GPX1, MSX1, CEBPB, EEF1A2, SPHK1, TNFRSF18, HSPB1, PRDX5, PDE3A, GSTP1 |
| GO:0043069~negative regulation of programmed cell death | 0.0024 | GPX1, MSX1, CEBPB, EEF1A2, SPHK1, TNFRSF18, HSPB1, PRDX5, PDE3A, GSTP1 |
| GO:0060548~negative regulation of cell death | 0.0025 | GPX1, MSX1, CEBPB, EEF1A2, SPHK1, TNFRSF18, HSPB1, PRDX5, PDE3A, GSTP1 |
| GO:0000302~response to reactive oxygen species | 0.0031 | GPX1, UCP2, GPX4, ROMO1, PRDX5 |
| GO:0042274~ribosomal small subunit biogenesis | 0.0034 | RPS28, RPS15, RPS7P4 |
| GO:0042981~regulation of apoptosis | 0.0051 | PLEKHF1, GPX1, EPHA7, MSX1, CEBPB, EEF1A2, LGALS1, SPHK1, TNFRSF18, HSPB1, PRDX5, PDE3A, ID3, GSTP1, RPS3 |
| GO:0043067~regulation of programmed cell death | 0.0056 | PLEKHF1, GPX1, EPHA7, MSX1, CEBPB, EEF1A2, LGALS1, SPHK1, TNFRSF18, HSPB1, PRDX5, PDE3A, ID3, GSTP1, RPS3 |
| GO:0010941~regulation of cell death | 0.0057 | PLEKHF1, GPX1, EPHA7, MSX1, CEBPB, EEF1A2, LGALS1, SPHK1, TNFRSF18, HSPB1, PRDX5, PDE3A, ID3, GSTP1, RPS3 |
| GO:0006916~anti-apoptosis | 0.0064 | GPX1, CEBPB, EEF1A2, SPHK1, TNFRSF18, HSPB1, GSTP1 |
| GO:0006979~response to oxidative stress | 0.0105 | GPX1, G6PD, UCP2, GPX4, ROMO1, PRDX5 |
| GO:0042254~ribosome biogenesis | 0.0170 | RPS28, EXOSC4, RPS15, RPS7P4, RPLP0P2 |
| selenocysteine | 0.0171 | GPX1, DIO3, GPX4 |
| GO:0042743~hydrogen peroxide metabolic process | 0.0212 | GPX1, G6PD, GPX4 |
| GO:0006749~glutathione metabolic process | 0.0244 | HYAL1, KRTR8, ACVRL1, CRIP2, SPHK1, IGFBP6, RPS9, ROMO1, SPARC, GPX1, MSX1, PTGES, FGFBP1 |
| GO:004127~regulation of cell proliferation | 0.0381 | RPS28, EXOSC4, RPS15, RPS7P4 |
| GO:0006364~RNA processing | 0.0643 | PLEKHF1, HYAL1, GPX1, MRPL41, SLC25A6, LGALS1, TNFRSF18, HSPB1, CGB7, PHLDA2, RPS3 |
| GO:0008219~cell death | 0.0667 | PLEKHF1, HYAL1, GPX1, MRPL41, SLC25A6, LGALS1, TNFRSF18, HSPB1, CGB7, PHLDA2, RPS3 |
| GO:0016265~death | 0.0667 | PLEKHF1, HYAL1, GPX1, MRPL41, SLC25A6, LGALS1, TNFRSF18, HSPB1, CGB7, PHLDA2, RPS3 |
| GO:0004602~glutathione peroxidase activity | 0.0839 | GPX1, GPX4 |

b



c



REFERENCES

Alessi, D.R., M. Andjelkovic, B. Caudwell, P. Cron, N. Morrice, P. Cohen, and B.A. Hemmings. 1996. Mechanism of activation of protein kinase B by insulin and IGF-1. *EMBO J.* 15(23):6541-6551.

Almeida, A., J.P. Bolanos, and S. Moncada. 2010. E3 ubiquitin ligase APC/C-Cdh1 accounts for the Warburg effect by linking glycolysis to cell proliferation. *Proc Natl Acad Sci U S A.* 107(2):738-741.

Almeida, A., S. Moncada, and J.P. Bolanos. 2004. Nitric oxide switches on glycolysis through the AMP protein kinase and 6-phosphofructo-2-kinase pathway. *Nat Cell Biol* 6(1):45-51.

Andjelkovic, M., D.R. Alessi, R. Meier, A. Fernandez, N.J. Lamb, M. Frech, P. Cron, P. Cohen, J.M. Lucocq, and B.A. Hemmings. 1997. Role of translocation in the activation and function of protein kinase B. *J Biol Chem.* 272(50):31515-31524.

Atsumi, T., J. Chesney, C. Metz, L. Leng, S. Donnelly, Z. Makita, R. Mitchell, and R. Bucala. 2002. High expression of inducible 6-phosphofructo-2-kinase/fructose-2,6-bisphosphatase (iPFK-2; PFKFB3) in human cancers. *Cancer Res.* 62(20):5881-5887.

Bando, H., T. Atsumi, T. Nishio, H. Niwa, S. Mishima, C. Shimizu, N. Yoshioka, R. Bucala, and T. Koike. 2005. Phosphorylation of the 6-phosphofructo-2-kinase/fructose 2,6-bisphosphatase/PFKFB3 family of glycolytic regulators in human cancer. *Clin Cancer Res.* 11:5784-5792.

Bartrons, R., L. Hue, E. Van Schaftingen, and H.G. Hers. 1983. Hormonal control of fructose 2,6-bisphosphate concentration in isolated rat hepatocytes. *Biochem J.* 214(3):829-837.

Bazan, J.F., R.J. Fletterick, and S.J. Pilgis. 1989. Evolution of a bifunctional enzyme: 6-phosphofructo-2-kinase/fructose-2,6-bisphosphatase. *Proc Natl Acad Sci U S A.* 86(24):9642-9646.

Beauloye, C., A.S. Marsin, L. Bertrand, J.L. Vanoverschelde, M.H. Rider, and L. Hue. 2002. The stimulation of heart glycolysis by increased workload does not require AMP-activated protein kinase but a wortmannin-sensitive mechanism. *FEBS Lett.* 531(2):324-328.

Bellacosa, A., D. de Feo, A.K. Godwin, D.W. Bell, J.Q. Cheng, D.A. Altomare, M. Wan, L. Dubeau, G. Scambia, V. Masciullo, G. Ferrandina, P. Benedetti Panici, S. Mancuso, G. Neri, and J.R. Testa. 1995. Molecular alterations of the AKT2 oncogene in ovarian and breast carcinomas. *Int J Cancer.* 64(4):280-285.

Bellacosa, A., J.R. Testa, S.P. Staal, and P.N. Tsichlis. 1991. A retroviral oncogene, akt, encoding a serine-threonine kinase containing an SH2-like region. *Science*. 254(5029):274-277.

Benczik, M., and S.L. Gaffen. 2009. The Interleukin (IL) - 2 Family Cytokines: Survival and Proliferation Signaling Pathways in T Lymphocytes. *Immunological Investigations*. 33:109-142.

Bensaad, K., A. Tsuruta, M.A. Selak, M.N. Vidal, K. Nakano, R. Bartrons, E. Gottlieb, and K.H. Vousden. 2006. TIGAR, a p53-inducible regulator of glycolysis and apoptosis. *Cell*. 126(1):107-120.

Bensaad, K., and K.H. Vousden. 2007. p53: new roles in metabolism. *Trends Cell Biol*. 17:286-291.

Bertrand, L., D. Vertommen, E. Depiereux, L. Hue, M.H. Rider, and E. Feytmans. 1997. Modelling the 2-kinase domain of 6-phosphofructo-2-kinase/fructose-2,6-bisphosphatase on adenylate kinase. *Biochem J*. 321(Pt 3):615-621.

Bertrand, L., D. Vertommen, P.M. Freeman, J. Wouters, E. Depiereux, A. Di Pietro, L. Hue, and M.H. Rider. 1998. Mutagenesis of the fructose-6-phosphate-binding site in the 2-kinase domain of 6-phosphofructo-2-kinase/fructose-2,6-bisphosphatase. *Eur J Biochem*. 254(3):490-496.

Binétruy, B., T. Smeal, and K. M. 1991. Ha-Ras augments c-Jun activity and stimulates phosphorylation of its activation domain. *Nature*. 351(6322):122-127.

Bobarykina, A.Y., D.O. Minchenko, I.L. Opentanova, M. Moenner, J. Caro, H. Esumi, and O.H. Minchenko. 2006. Hypoxic regulation of PFKFB-3 and PFKFB-4 gene expression in gastric and pancreatic cancer cell lines and expression of PFKFB genes in gastric cancers. *Acta Biochim Pol*. 53(4):789-799.

Bosca, L., G.G. Rousseau, and L. Hue. 1985. Phorbol 12-myristate 13-acetate and insulin increase the concentration of fructose 2,6-bisphosphate and stimulate glycolysis in chicken embryo fibroblasts. *Proc Natl Acad Sci U S A*. 82(19):6440-6444.

Bouillet, P., J.F. Purton, D.I. Godfrey, L.C. Zhang, L. Coultas, H. Puthalakath, M. Pellegrini, S. Cory, J.M. Adams, and A. Strasser. 2002. BH3-only Bcl-2 family member Bim is required for apoptosis of autoreactive thymocytes. *Nature*. 415(6874):922-926.

- Brand, K. 1985. Glutamine and glucose metabolism during thymocyte proliferation. Pathways of glutamine and glutamate metabolism. *Biochem J.* 228(2):353-361.
- Brand, K., S. Aichinger, S. Forster, S. Kupper, B. Neumann, W. Nürnberg, and G. Ohrisch. 1988. Cell-cycle-related metabolic and enzymatic events in proliferating rat thymocytes. *Eur J Biochem.* 172(3):695-702.
- Brand, K., J.F. Williams, and M.J. Weidemann. 1984. Glucose and glutamine metabolism in rat thymocytes. *Biochem J.* 221:471-475.
- Brazil, D.P., Z.Z. Yang, and B.A. Hemmings. 2004. Advances in protein kinase B signalling: AKTion on multiple fronts. *Trends Biochem Sci.* 29(5):233-242.
- Brown, R.S., and R.L. Wahl. 1993. Overexpression of Glut-1 glucose transporter in human breast cancer. An immunohistochemical study. *Cancer* 72(10):2979-2985.
- Bruni, P., P. Vandoolaeghe, G.G. Rousseau, L. Hue, and M.H. Rider. 1999. Expression and regulation of 6-phosphofructo-2-kinase/fructose-2,6-bisphosphatase isozymes in white adipose tissue. *Eur J Biochem.* 259(3):756-761.
- Calvo, M.N., R. Bartrons, E. Castano, J.C. Perales, A. Navarro-Sabate, and A. Manzano. 2006. PFKFB3 gene silencing decreases glycolysis, induces cell-cycle delay and inhibits anchorage-independent growth in HeLa cells. *FEBS Lett.* 580(13):3308-3314.
- Cantley, L.C. 2002. The phosphoinositide 3-kinase pathway. *Science.* 296(5573):1655-1657.
- Cardone, M.H., N. Roy, H.R. Stennicke, G.S. Salvesen, T.F. Franke, E. Stanbridge, S. Frisch, and J.C. Reed. 1998. Regulation of cell death protease caspase-9 by phosphorylation. *Science.* 282(5392):1318-1321.
- Carnero, A. 2010. The PKB/AKT pathway in cancer. *Curr Pharm Des.* 16(1):34-44.
- Cavalier, M.C., S.G. Kim, D. Neau, and Y.H. Lee. 2012. Molecular basis of the fructose-2,6-bisphosphatase reaction of PFKFB3: transition state and the C-terminal function. *Proteins.* 80(4):1143-1153.
- Chaneton, B., and E. Gottlieb. 2012. Rocking cell metabolism: revised functions of the key glycolytic regulator PKM2 in cancer. *Trends Biochem Sci.* 37:309-316.

Chesney, J., R. Mitchell, F. Benigni, M. Bacher, L. Spiegel, Y. Al-Abed, J.H. Han, C. Metz, and R. Bucala. 1999. An inducible gene product for 6-phosphofructo-2-kinase with an AU-rich instability element: role in tumor cell glycolysis and the Warburg effect. *Proc Natl Acad Sci U S A*. 96(6):3047-3052.

Chikri, M., and G.G. Rousseau. 1995. Rat gene coding for heart 6-phosphofructo-2-kinase/fructose-2,6-bisphosphatase: characterization of an unusual promoter region and identification of four mRNAs. *Biochemistry*. 34(27):8876-8884.

Christofk, H.R., M.G. Vander Heiden, M.H. Harris, A. Ramanathan, R.E. Gerszten, R. Wei, M.D. Fleming, S.L. Schreiber, and L.C. Cantley. 2008. The M2 splice isoform of pyruvate kinase is important for cancer metabolism and tumour growth. *Nature*. 452:230-233.

Clem, B., S. Telang, A.L. Clem, A. Yalcin, J. Meier, A. Simmons, M.A. Rasku, S. Arumugam, W.L. Dean, J. Eaton, A. Lane, J.O. Trent, and J. Chesney. 2008. Small-molecule inhibition of 6-phosphofructo-2-kinase activity suppresses glycolytic flux and tumor growth. *Mol Cancer Ther*. 7(1):110-120.

Coffer, P.J., and J.R. Woodgett. 1991. Molecular cloning and characterisation of a novel putative protein-serine kinase related to the cAMP-dependent and protein kinase C families. *Eur J Biochem*. 201(2):475-481.

Corbet, C., and O. Feron. 2017. Cancer cell metabolism and mitochondria: Nutrient plasticity for TCA cycle fueling. *Biochim Biophys Acta*. 1868(1):7-15.

Corbet, C., A. Pinto, R. Martherus, J.P. Santiago de Jesus, F. Polet, and O. Feron. 2016. Acidosis Drives the Reprogramming of Fatty Acid Metabolism in Cancer Cells through Changes in Mitochondrial and Histone Acetylation. *Cell Metab*. 24:311-323.

Crawley, J.B., L. Rawlinson, F.V. Lali, T.H. Page, J. Saklatvala, and B.M. Foxwell. 1997. T cell proliferation in response to interleukins 2 and 7 requires p38MAP kinase activation. *J Biol Chem*. 272(23):15023-15027.

Darville, M.I., I.V. Antoine, and G.G. Rousseau. 1992. Characterization of an enhancer upstream from the muscle-type promoter of a gene encoding 6-phosphofructo-2-kinase/fructose-2,6-bisphosphatase. *Nucleic Acids Res*. 20(14):3575-3583.

Darville, M.I., M. Chikri, E. Lebeau, L. Hue, and G.G. Rousseau. 1991. A rat gene encoding heart 6-phosphofructo-2-kinase/fructose-2,6-bisphosphatase. *FEBS Lett*. 288(1-2):91-94.

Darville, M.I., K.M. Crepin, L. Hue, and G.G. Rousseau. 1989. 5' flanking sequence and structure of a gene encoding rat 6-phosphofructo-2-kinase/fructose-2,6-bisphosphatase. *Proc Natl Acad Sci U S A.* 86(17):6543-6547.

Datta, S.R., A. Brunet, and M.E. Greenberg. 1999. Cellular survival: a play in three Akts. *Genes Dev.* 13(22):2905-2927.

Datta, S.R., A. Katsov, L. Hu, A. Petros, S.W. Fesik, M.B. Yaffe, and M.E. Greenberg. 2000. 14-3-3 proteins and survival kinases cooperate to inactivate BAD by BH3 domain phosphorylation. *Mol Cell.* 6(1):41-51.

de Vries-Smits, A.M., B.M. Burgering, S.J. Leever, C.J. Marshall, and J.L. Bos. 1992. Involvement of p21ras in activation of extracellular signal-regulated kinase 2. *Nature.* 357(6379):602-604.

Depré, C., M.H. Rider, and L. Hue. 1998. Mechanisms of control of heart glycolysis. *Eur J Biochem.* 258(2):277-290.

Depré, C., M.H. Rider, K. Veitch, and L. Hue. 1993. Role of fructose 2,6-bisphosphate in the control of heart glycolysis. *J Biol Chem.* 268(18):13274-13279.

Deprez, J., D. Vertommen, D.R. Alessi, L. Hue, and M.H. Rider. 1997. Phosphorylation and activation of heart 6-phosphofructo-2-kinase by protein kinase B and other protein kinases of the insulin signaling cascades. *J Biol Chem.* 272(28):17269-17275.

Du, K., and M. Montminy. 1998. CREB is a regulatory target for the protein kinase Akt/PKB. *J Biol Chem.* 273(49):32377-32379.

Dupriez, V.J., M.I. Darville, I.V. Antoine, A. Gegonne, J. Ghysdael, and G.G. Rousseau. 1993. Characterization of a hepatoma mRNA transcribed from a third promoter of a 6-phosphofructo-2-kinase/fructose-2,6-bisphosphatase-encoding gene and controlled by ets oncogene-related products. *Proc Natl Acad Sci U S A.* 90(17):8224-8228.

Dutton, R.W. 1972. Inhibitory and stimulatory effects of concanavalin A on the response of mouse spleen cell suspensions to antigen. I. Characterization of the inhibitory cell activity. *J Exp Med.* 136(6):1445-1460.

Edinger, A.L., and C.B. Thompson. 2002. Akt maintains cell size and survival by increasing mTOR-dependent nutrient uptake. *Mol Biol Cell.* 13:2276-2288.

Eigenbrodt, E., S. Leib, W. Kramer, R. Friis, and W. Schoner. 1983. Structural and kinetic differences between the M2 type pyruvate kinases from lung and various tumors. *Biomed Biochim Acta*. 42(11-12):S278-282.

Fantin, V.R., and P. Leder. 2006. Mitochondriotoxic compounds for cancer therapy. *Oncogene*. 25:4787-4797.

Feng, Y., and L. Wu. 2017. mTOR up-regulation of PFKFB3 is essential for acute myeloid leukemia cell survival. *Biochem Biophys Res Commun*.

Flier, J.S., M.M. Mueckler, P. Usher, and H.F. Lodish. 1987. Elevated levels of glucose transport and transporter messenger RNA are induced by ras or src oncogenes. *Science*. 235(4795):1492-1495.

Fox, C.J., P.S. Hammerman, and C.B. Thompson. 2005. Fuel feeds function: energy metabolism and the T-cell response. *Nat Rev Immunol*. 5:844-852.

Frank, D.A., M.J. Robertson, A. Bonni, J. Ritz, and M.E. Greenberg. 1995. Interleukin 2 signaling involves the phosphorylation of Stat proteins. *Proc Natl Acad Sci U S A*. 92(17):7779-7783.

Freeburn, R.W., and S.G. Ward. 2001. The Jurkat cell line has constitutively active PI3K/PKB signalling: effect of inducible expression of a membrane-localised SHIP construct. *Biochem Soc Trans*. 29(5):A128.

Gao, X., H. Wang, J.J. Yang, X. Liu, and Z.R. Liu. 2012. Pyruvate kinase M2 regulates gene transcription by acting as a protein kinase. *Mol Cell*. 45(5):598-609.

Garrison, J.C., D.E. Johnsen, and C.P. Campanile. 1984. Evidence for the role of phosphorylase kinase, protein kinase C, and other Ca²⁺-sensitive protein kinases in the response of hepatocytes to angiotensin II and vasopressin. *J Biol Chem*. 259(5):3283-3292.

Gerin, I., G. Noël, J. Bolsée, O. Haumont, E. Van Schaftingen, and G.T. Bommer. 2014. Identification of TP53-induced glycolysis and apoptosis regulator (TIGAR) as the phosphoglycolate-independent 2,3-bisphosphoglycerate phosphatase. *Biochem J*. 458(3):439-448.

Gesbert, F., M. Delespine-Carmagnat, and J. Bertoglio. 1998. Recent advances in the understanding of interleukin-2 signal transduction. *J Clin Immunol*. 18:307-320.

- Gilmour, K.C., R. Pine, and N.C. Reich. 1995. Interleukin 2 activates STAT5 transcription factor (mammary gland factor) and specific gene expression in T lymphocytes. *Proc Natl Acad Sci U S A*. 92(23):10772-10776.
- Goidts, V., J. Bageritz, L. Puccio, S. Nakata, M. Zapatka, S. Barbus, G. Toedt, B. Campos, A. Korshunov, S. Momma, E. Van Schaftingen, G. Reifenberger, C. Herold-Mende, P. Lichter, and B. Radlwimmer. 2012. RNAi screening in glioma stem-like cells identifies PFKFB4 as a key molecule important for cancer cell survival. *Oncogene*. 31(27):3235-3243.
- Gomez, J., C. Martinez-A., A. Garcia, and A. Rebollo. 1996. Association of phosphatidylinositol 3 kinase to protein kinase C zeta during interleukin-2 stimulation. *Eur. J. Immunol*. 26:1781-1787.
- Gottlob, K., N. Majewski, S. Kennedy, E. Kandel, R.B. Robey, and N. Hay. 2001. Inhibition of early apoptotic events by Akt/PKB is dependent on the first committed step of glycolysis and mitochondrial hexokinase. *Genes Dev*. 15:1406-1418.
- Greiner, E.F., M. Guppy, and K. Brand. 1994. Glucose is essential for proliferation and the glycolytic enzyme induction that provokes a transition to glycolytic energy production. *J Biol Chem*. 269(50):31484-31490.
- Gu, H., H. Maeda, J.J. Moon, J.D. Lord, M. Yoakim, B.H. Nelson, and B.G. Neel. 2000. New role for Shc in activation of the phosphatidylinositol 3-kinase/Akt pathway. *Mol Cell Biol*. 20(19):7109-7120.
- Guppy, M., E. Greiner, and K. Brand. 1993. The role of the Crabtree effect and an endogenous fuel in the energy metabolism of resting and proliferating thymocytes. *Eur J Biochem*. 212(1):95-99.
- Hamilton, J.A., M.J. Callaghan, R.L. Sutherland, and C.K. Watts. 1997. Identification of PRG1, a novel progestin-responsive gene with sequence homology to 6-phosphofructo-2-kinase/fructose-2,6-bisphosphatase. *Mol Endocrinol*. 11(4):490-502.
- Hamm-Künzelmann, B., D. Schäfer, C. Weigert, and K. Brand. 1997. Redox-regulated expression of glycolytic enzymes in resting and proliferating rat thymocytes. *FEBS Letters*. 403:87-90.
- Hanada, M., J. Feng, and B.A. Hemmings. 2004. Structure, regulation and function of PKB/AKT: a major therapeutic target. *Biochim Biophys Acta*. 1697(1-2):3-16.

- Hasemann, C.A., E.S. Istvan, K. Uyeda, and J. Deisenhofer. 1996. The crystal structure of the bifunctional enzyme 6-phosphofructo-2-kinase/fructose-2,6-bisphosphatase reveals distinct domain homologies. *Structure*. 4(9):1017-1029.
- Hedekov, C.J. 1968. Early effects of phytohaemagglutinin on glucose metabolism of normal human lymphocytes. *Biochem J*. 110(2):373-380.
- Heine-Suner, D., M.A. Diaz-Guillen, A.J. Lange, and S. Rodriguez de Cordoba. 1998. Sequence and structure of the human 6-phosphofructo-2-kinase/fructose-2,6-bisphosphatase heart isoform gene (PFKFB2). *Eur J Biochem*. 254(1):103-110.
- Hers, H.G., and L. Hue. 1983. Gluconeogenesis and related aspects of glycolysis. *Annu Rev Biochem*. 52:617-653.
- Hers, I., E.E. Vincent, and J.M. Tavaré. 2011. Akt signalling in health and disease. *Cell Signal*. 23:1515-1527.
- Higuchi, M., H. Asao, N. Tanaka, K. Oda, T. Takeshita, M. Nakamura, J. Van Snick, and K. Sugamura. 1996. Dispensability of Jak1 tyrosine kinase for interleukin-2-induced cell growth signaling in a human T cell line. *Eur J Immunol*. 26(6):1322-1327.
- Hoshino, A., J.A. Hirst, and H. Fujii. 2007. Regulation of cell proliferation by interleukin-3-induced nuclear translocation of pyruvate kinase. *J Biol Chem*. 282(24):17706-17711.
- Hue, L. 1982. Role of fructose 2,6-bisphosphate in the stimulation of glycolysis by anoxia in isolated hepatocytes. *Biochem J*. 206(2):359-365.
- Hue, L., C. Beauloye, A.S. Marsin, L. Bertrand, S. Horman, and M.H. Rider. 2002. Insulin and ischemia stimulate glycolysis by acting on the same targets through different and opposing signaling pathways. *J Mol Cell Cardiol*. 34(9):1091-1097.
- Hue, L., and M.H. Rider. 1987. Role of fructose 2,6-bisphosphate in the control of glycolysis in mammalian tissues. *Biochem J*. 245(2):313-324.
- Hue, L., and G.G. Rousseau. 1993. Fructose 2,6-bisphosphate and the control of glycolysis by growth factors, tumor promoters and oncogenes. *Adv Enzyme Regul*. 33:97-110.
- Hume, D.A., J.L. Radik, E. Ferber, and M.J. Weidemann. 1978. Aerobic glycolysis and lymphocyte transformation. *Biochem J*. 174:703-709.

- Imamura, K., and T. Tanaka. 1972. Multimolecular forms of pyruvate kinase from rat and other mammalian tissues. I. Electrophoretic studies. *J Biochem.* 71(6):1043-1051.
- Imamura, K., K. Taniuchi, and T. Tanaka. 1972. Multimolecular forms of pyruvate kinase. II. Purification of M₂-type pyruvate kinase from Yoshida ascites hepatoma 130 cells and comparative studies on the enzymological and immunological properties of the three types of pyruvate kinases, L, M₁, and M₂. *J Biochem.* 72(4):1001-1015.
- Inoki, K., Y. Li, T. Xu, and K.L. Guan. 2003. Rheb GTPase is a direct target of TSC2 GAP activity and regulates mTOR signaling. *Genes Dev.* 17:1829-1834.
- Iqbal, M.A., V. Gupta, P. Gopinath, S. Mazurek, and R.N. Bamezai. 2014. Pyruvate kinase M2 and cancer: an updated assessment. *FEBS Lett.* 588(16):2685-2692.
- Ivshina, A.V., J. George, O. Senko, B. Mow, T.C. Putti, J. Smeds, T. Lindahl, Y. Pawitan, P. Hall, H. Nordgren, J.E. Wong, E.T. Liu, J. Bergh, V.A. Kuznetsov, and L.D. Miller. 2006. Genetic reclassification of histologic grade delineates new clinical subtypes of breast cancer. *Cancer research.* 66:10292-10301.
- Jenkins, C.M., J. Yang, H.F. Sims, and R.W. Gross. 2011. Reversible high affinity inhibition of phosphofructokinase-1 by acyl-CoA: a mechanism integrating glycolytic flux with lipid metabolism. *J Biol Chem.* 286:11937-11950.
- Ji, D., Z.T. Lu, Y.Q. Li, Z.Y. Liang, P.F. Zhang, C. Li, J.L. Zhang, X. Zheng, and Y.M. Yao. 2014. MACC1 expression correlates with PFKFB2 and survival in hepatocellular carcinoma. *Asian Pac J Cancer Prev.* 15(2):999-1003.
- Jiang, B.H., J.Z. Zheng, M. Aoki, and P.K. Vogt. 2000. Phosphatidylinositol 3-kinase signaling mediates angiogenesis and expression of vascular endothelial growth factor in endothelial cells. *Proc Natl Acad Sci U S A.* 97(4):1749-1753.
- Jones, J.F., T. Jakubowicz, F.J. Pitossi, F. Maurer, and B.A. Hemmings. 1991. Molecular cloning and identification of a serine/threonine protein kinase of the second-messenger subfamily. *Proc Natl Acad Sci U S A.* 88(10):4171-4175.
- Joost, H.-G., and B. Thorens. 2009. The extended GLUT-family of sugar/polyol transport facilitators: nomenclature, sequence characteristics, and potential function of its novel members. *Molecular Membrane Biology.* 18:247-256.
- Karar, J., and A. Maity. 2011. PI3K/AKT/mTOR Pathway in Angiogenesis. *Front Mol Neurosci.* 4:51.

- Kessler, R., and K. Eschrich. 2001. Splice isoforms of ubiquitous 6-phosphofructo-2-kinase/fructose-2,6-bisphosphatase in human brain. *Brain Res Mol Brain Res.* 87(2):190-195.
- Kim, H.P., J. Imbert, and W.J. Leonard. 2006a. Both integrated and differential regulation of components of the IL-2/IL-2 receptor system. *Cytokine Growth Factor Rev.* 17:349-366.
- Kim, S.G., N.P. Manes, M.R. El-Maghrabi, and Y.H. Lee. 2006b. Crystal structure of the hypoxia-inducible form of 6-phosphofructo-2-kinase/fructose-2,6-bisphosphatase (PFKFB3): a possible new target for cancer therapy. *J Biol Chem.* 281(5):2939-2944.
- Kitamura, K., K. Kangawa, H. Matsuo, and K. Uyeda. 1988. Phosphorylation of myocardial fructose-6-phosphate,2-kinase: fructose-2,6-bisphosphatase by cAMP-dependent protein kinase and protein kinase C. Activation by phosphorylation and amino acid sequences of the phosphorylation sites. *J Biol Chem.* 263(32):16796-16801.
- Knobbe, C.B., and G. Reifenberger. 2003. Genetic alterations and aberrant expression of genes related to the phosphatidylinositol-3'-kinase/protein kinase B (Akt) signal transduction pathway in glioblastomas. *Brain Pathol.* 13(4):507-518.
- Lamallice, L., F. Le Boeuf, and J. Huot. 2007. Endothelial cell migration during angiogenesis. *Circ Res.* 100:782-794.
- Lee, E.S., D.S. Son, S.H. Kim, J. Lee, J. Jo, J. Han, H. Kim, H.J. Lee, H.Y. Choi, Y. Jung, M. Park, Y.S. Lim, K. Kim, Y. Shim, B.C. Kim, K. Lee, N. Huh, C. Ko, K. Park, J.W. Lee, Y.S. Choi, and J. Kim. 2008. Prediction of recurrence-free survival in postoperative non-small cell lung cancer patients by using an integrated model of clinical information and gene expression. *Clinical cancer research : an official journal of the American Association for Cancer Research.* 14:7397-7404.
- Lefebvre, V., M.C. Méchin, M.P. Louckx, M.H. Rider, and L. Hue. 1996. Signaling pathway involved in the activation of heart 6-phosphofructo-2-kinase by insulin. *J Biol Chem.* 271(37):22289-22292.
- Leonard, W.J. 2001. Role of Jak kinases and STATs in cytokine signal transduction. *Int J Hematol.* 73(3):271-277.
- Leonard, W.J., J.M. Depper, G.R. Crabtree, S. Rudikoff, J. Pumphrey, R.J. Robb, M. Krönke, P.B. Svetlik, N.J. Pfeffer, T.A. Waldmann, and W.C. Greene. 1984. Molecular cloning and expression of cDNAs for the human interleukin-2 receptor. *Nature.* 311(5987):626-631.

- Liao, W., J.X. Lin, and W.J. Leonard. 2011. IL-2 family cytokines: new insights into the complex roles of IL-2 as a broad regulator of T helper cell differentiation. *Curr Opin Immunol.* 23:598-604.
- Lin, J.X., and W.J. Leonard. 1997. Signaling from the IL-2 receptor to the nucleus. *Cytokine Growth Factor Rev.* 8(4):313-332.
- Lin, J.X., and W.J. Leonard. 2000. The role of Stat5a and Stat5b in signaling by IL-2 family cytokines. *Oncogene.* 19(21):2566-2576.
- Lindsley, C.W. 2010. The Akt/PKB family of protein kinases: a review of small molecule inhibitors and progress towards target validation: a 2009 update. *Curr Top Med Chem.* 10(4):458-477.
- Liu, W., S.M. Shen, X.Y. Zhao, and G.Q. Chen. 2012. Targeted genes and interacting proteins of hypoxia inducible factor-1. *Int J Biochem Mol Biol.* 3(2):165-178.
- MacIver, N.J., S.R. Jacobs, H.L. Wieman, J.A. Wofford, J.L. Coloff, and J.C. Rathmell. 2008. Glucose metabolism in lymphocytes is a regulated process with significant effects on immune cell function and survival. *J Leukoc Biol.* 84(4):949-957.
- MacIver, N.J., R.D. Michalek, and J.C. Rathmell. 2013. Metabolic regulation of T lymphocytes. *Annu Rev Immunol.* 31:259-283.
- Maehama, T., and J.E. Dixon. 1998. The tumor suppressor, PTEN/MMAC1, dephosphorylates the lipid second messenger, phosphatidylinositol 3,4,5-trisphosphate. *J Biol Chem.* 273(22):13375-13378.
- Maehama, T., and J.E. Dixon. 1999. PTEN: a tumour suppressor that functions as a phospholipid phosphatase. *Trends Cell Biol.* 9(4):125-128.
- Majewski, N., V. Nogueira, P. Bhaskar, P.E. Coy, J.E. Skeen, K. Gottlob, N.S. Chandel, C.B. Thompson, R.B. Robey, and N. Hay. 2004. Hexokinase-mitochondria interaction mediated by Akt is required to inhibit apoptosis in the presence or absence of Bax and Bak. *Mol Cell.* 16:819-830.
- Manning, B.D., and L.C. Cantley. 2007. AKT/PKB signaling: navigating downstream. *Cell.* 129(7):1261-1274.
- Manzano, A., J.X. Pérez, M. Nadal, X. Estivill, A. Lange, and R. Bartrons. 1999. Cloning, expression and chromosomal localization of a human testis 6-phosphofructo-2-kinase/fructose-2,6-bisphosphatase gene. *Gene.* 229(1-2):83-89.

- Marshall, M.J., D.M. Goldberg, F.E. Neal, and D.R. Millar. 1978. Enzymes of glucose metabolism in carcinoma of the cervix and endometrium of the human uterus. *Br J Cancer*. 37(6):990-1001.
- Marsin, A.S., L. Bertrand, M.H. Rider, J. Deprez, C. Beauloye, M.F. Vincent, G. Van den Berghe, D. Carling, and L. Hue. 2000. Phosphorylation and activation of heart PFK-2 by AMPK has a role in the stimulation of glycolysis during ischaemia. *Curr Biol*. 10(20):1247-1255.
- Marsin, A.S., C. Bouzin, L. Bertrand, and L. Hue. 2002. The stimulation of glycolysis by hypoxia in activated monocytes is mediated by AMP-activated protein kinase and inducible 6-phosphofructo-2-kinase. *J Biol Chem*. 277(34):30778-30783.
- Massie, C.E., A. Lynch, A. Ramos-Montoya, J. Boren, R. Stark, L. Fazli, A. Warren, H. Scott, B. Madhu, N. Sharma, H. Bon, V. Zecchini, D.M. Smith, G.M. DeNicola, N. Mathews, M. Osborne, J. Hadfield, S. Macarthur, B. Adryan, S.K. Lyons, K.M. Brindle, J. Griffiths, M.E. Gleave, P.S. Rennie, D.E. Neal, and I.G. Mills. 2011. The androgen receptor fuels prostate cancer by regulating central metabolism and biosynthesis. *EMBO J*. 30(13):2719-2733.
- Mathupala, S.P., A. Rempel, and P.L. Pedersen. 2001. Glucose catabolism in cancer cells: identification and characterization of a marked activation response of the type II hexokinase gene to hypoxic conditions. *J Biol Chem*. 276:43407-43412.
- Mayo, L.D., and D.B. Donner. 2002. The PTEN, Mdm2, p53 tumor suppressor-oncoprotein network. *Trends Biochem Sci*. 27(9):462-467.
- Mazurek, S. 2011. Pyruvate kinase type M2: a key regulator of the metabolic budget system in tumor cells. *Int J Biochem Cell Biol*. 43:969-980.
- Merida, I., E. Diez, and G.N. Gaulton. 1991. IL-2 binding activates a tyrosine-phosphorylated phosphatidylinositol-3-kinase. *J Immunol*. 147(7):2202-2207.
- Migone, T.S., S. Rodig, N.A. Cacalano, M. Berg, R.D. Schreiber, and W.J. Leonard. 1998. Functional cooperation of the interleukin-2 receptor beta chain and Jak1 in phosphatidylinositol 3-kinase recruitment and phosphorylation. *Mol Cell Biol*. 18(11):6416-6422.
- Minchenko, D.O., V.G. Mykhalchenko, K. Tsuchihara, S. Kanehara, O.P. Yavorovsky, I.V. Zavgorodny, Y.O. Paustovsky, S.V. Komisarenko, H. Esumi, and O.H. Minchenko. 1999a. Alternative splice variants of rat 6-phosphofructo-2-kinase/ fructose-2,6-bisphosphatase-4 mRNA. *Ukr Biokhim Zh*. 80(4):66-73.

- Minchenko, O.H., T. Ogura, I.L. Opentanova, D.O. Minchenko, A. Ochiai, J. Caro, S.V. Komisarenko, and H. Esumi. 1999b. 6-Phosphofructo-2-kinase/fructose-2,6-bisphosphatase gene family overexpression in human lung tumor. *Ukr Biokhim Zh.* 77(6):46-50.
- Minchenko, O.H., I.L. Opentanova, T. Ogura, D.O. Minchenko, S.V. Komisarenko, J. Caro, and H. Esumi. 2005. Expression and hypoxia-responsiveness of 6-phosphofructo-2-kinase/fructose-2,6-bisphosphatase 4 in mammary gland malignant cell lines. *Acta Biochim Pol.* 52(4):881-888.
- Miyatake, K., T. Enomoto, and S. Kitaoka. 1986. Fructose-2,6-bisphosphate Activates Pyrophosphate:d-Fructose 6-Phosphate 1-Phosphotransferase from *Euglena gracilis*. *Agricultural and Biological Chemistry.* 50:2417-2418.
- Moon, J.S., W.J. Jin, J.H. Kwak, H.J. Kim, M.J. Yun, J.W. Kim, S.W. Park, and K.S. Kim. 2011. Androgen stimulates glycolysis for de novo lipid synthesis by increasing the activities of hexokinase 2 and 6-phosphofructo-2-kinase/fructose-2,6-bisphosphatase 2 in prostate cancer cells. *Biochem J.* 433(1):225-233.
- Moreno-Sanchez, R., S. Rodriguez-Enriquez, A. Marin-Hernandez, and E. Saavedra. 2007. Energy metabolism in tumor cells. *FEBS J.* 274:1393-1418.
- Morgan, D.A., F.W. Ruscetti, and R. Gallo. 1976. Selective in vitro growth of T lymphocytes from normal human bone marrows. *Science.* 193(4257):1007-1008.
- Mouton, V., L. Toussaint, D. Vertommen, M.A. Gueuning, L. Maisin, X. Havaux, C. Sanchez-Canedo, L. Bertrand, F. Dequiedt, B.A. Hemmings, L. Hue, and M.H. Rider. 2010. Heart 6-phosphofructo-2-kinase activation by insulin requires PKB (protein kinase B), but not SGK3 (serum- and glucocorticoid-induced protein kinase 3). *Biochem J.* 431(2):267-275.
- Munyon, W.H., and D.J. Merchant. 1959. The relation between glucose utilization, lactic acid production and utilization and the growth cycle of L strain fibroblasts. *Exp Cell Res.* 17(3):490-498.
- Nakamura, Y., S.M. Russell, S.A. Mess, M. Friedmann, M. Erdos, C. Francois, Y. Jacques, S. Adelstein, and W.J. Leonard. 1994. Heterodimerization of the IL-2 receptor beta- and gamma-chain cytoplasmic domains is required for signalling. *Nature.* 369(6478):330-333.
- Navarro-Sabate, A., A. Manzano, L. Riera, J.L. Rosa, F. Ventura, and R. Bartrons. 2001. The human ubiquitous 6-phosphofructo-2-kinase/fructose-2,6-bisphosphatase gene (PFKFB3): promoter characterization and genomic structure. *Gene* 264(1):131-138.

- Nelson, B.H., J.D. Lord, and P.D. Greenberg. 1994. Cytoplasmic domains of the interleukin-2 receptor beta and gamma chains mediate the signal for T-cell proliferation. *Nature*. 369(6478):333-336.
- Netzker, R., E. Greiner, E. Eigenbrodt, T. Noguchi, T. Tanaka, and K. Brand. 1992. Cell cycle-associated expression of M2-type isozyme of pyruvate kinase in proliferating rat thymocytes. *J Biol Chem*. 267(9):6421-6424.
- Nicholson, K.M., and N.G. Anderson. 2002. The protein kinase B/Akt signalling pathway in human malignancy. *Cell Signal*. 14(5):381-395.
- Nielsen, M., A. Svejgaard, S. Skov, and N. Odum. 1994. Interleukin-2 induces tyrosine phosphorylation and nuclear translocation of stat3 in human T lymphocytes. *Eur J Immunol*. 24(12):3082-3086.
- Nikaido, T., A. Shimizu, N. Ishida, H. Sabe, K. Teshigawara, M. Maeda, T. Uchiyama, J. Yodoi, and T. Honjo. 1984. Molecular cloning of cDNA encoding human interleukin-2 receptor. *Nature*. 311(5987):631-635.
- Noguchi, T., H. Inoue, and T. Tanaka. 1986. The M1- and M2-type isozymes of rat pyruvate kinase are produced from the same gene by alternative RNA splicing. *J Biol Chem*. 261(29):13807-13812.
- Noguchi, T., K. Yamada, H. Inoue, T. Matsuda, and T. Tanaka. 1987. The L- and R-type isozymes of rat pyruvate kinase are produced from a single gene by use of different promoters. *J Biol Chem*. 262(29):14366-14371.
- Noguchi, Y., A. Saito, Y. Miyagi, S. Yamanaka, D. Marat, C. Doi, T. Yoshikawa, A. Tsuburaya, T. Ito, and S. Satoh. 2000. Suppression of facilitative glucose transporter 1 mRNA can suppress tumor growth. *Cancer Lett*. 154(2):175-182.
- Novellademunt, L., L. Bultot, A. Manzano, F. Ventura, J.L. Rosa, D. Vertommen, M.H. Rider, A. Navarro-Sabate, and R. Bartrons. 2013. PFKFB3 activation in cancer cells by the p38/MK2 pathway in response to stress stimuli. *Biochem J*. 452:531-543.
- Novellademunt, L., M. Obach, L. Millan-Arino, A. Manzano, F. Ventura, J.L. Rosa, A. Jordan, A. Navarro-Sabate, and R. Bartrons. 2012. Progestins activate 6-phosphofructo-2-kinase/fructose-2,6-bisphosphatase 3 (PFKFB3) in breast cancer cells. *Biochem J*. 442(2):345-356.
- Nowell, P.C. 1960. Phytohemagglutinin: an initiator of mitosis in cultures of normal human leukocytes. *Cancer Res*. 20:462-466.

- Obach, M., A. Navarro-Sabate, J. Caro, X. Kong, J. Duran, M. Gomez, J.C. Perales, F. Ventura, J.L. Rosa, and R. Bartrons. 2004. 6-Phosphofructo-2-kinase (pfkfb3) gene promoter contains hypoxia-inducible factor-1 binding sites necessary for transactivation in response to hypoxia. *J Biol Chem.* 279:53562-53570.
- Okamura, N., and R. Sakakibara. 1998. A common phosphorylation site for cyclic AMP-dependent protein kinase and protein kinase C in human placental 6-phosphofructo-2-kinase/fructose-2,6-bisphosphatase. *Biosci Biotechnol Biochem.* 62(10):2039-2042.
- Okar, D.A., and A.J. Lange. 1999. Fructose-2,6-bisphosphate and control of carbohydrate metabolism in eukaryotes. *Biofactors.* 10(1):1-14.
- Okar, D.A., A. Manzano, A. Navarro-Sabate, L. Riera, R. Bartrons, and A.J. Lange. 2001. PFK-2/FBPase-2: maker and breaker of the essential biofactor fructose-2,6-bisphosphate. *Trends Biochem Sci.* 26(1):30-35.
- Pedrero, J.M., D.G. Carracedo, C.M. Pinto, A.H. Zapatero, J.P. Rodrigo, C.S. Nieto, and M.V. Gonzalez. 2005. Frequent genetic and biochemical alterations of the PI 3-K/AKT/PTEN pathway in head and neck squamous cell carcinoma. *Int J Cancer.* 114(2):242-248.
- Perkins, G.R., J. Marvel, and M.K. Collins. 1993. Interleukin 2 activates extracellular signal-regulated protein kinase 2. *J Exp Med.* 178(4):1429-1434.
- Pessin, J.E., D.C. Thurmond, J.S. Elmendorf, K.J. Coker, and S. Okada. 1999. Molecular basis of insulin-stimulated GLUT4 vesicle trafficking. *J Biol Chem.* 274(5):2593-2596.
- Peterson, R.T., and S.L. Schreiber. 1999. Kinase phosphorylation: Keeping it all in the family. *Curr Biol.* 9(14):R521-524.
- Pilkis, S.J., T.H. Claus, I.J. Kurland, and A.J. Lange. 1995. 6-Phosphofructo-2-kinase/fructose-2,6-bisphosphatase: a metabolic signaling enzyme. *Annu Rev Biochem.* 64:799-835.
- Plas, D.R., S. Talapatra, A.L. Edinger, J.C. Rathmell, and C.B. Thompson. 2001. Akt and Bcl-xL promote growth factor-independent survival through distinct effects on mitochondrial physiology. *J Biol Chem.* 276:12041-12048.
- Postic, C., M. Shiota, and M.A. Magnuson. 2001. Cell-specific roles of glucokinase in glucose homeostasis. *Recent Prog Horm Res.* 56:195-217.

- Pozuelo Rubio, M., M. Peggie, B.H. Wong, N. Morrice, and C. MacKintosh. 2003. 14-3-3s regulate fructose-2,6-bisphosphate levels by binding to PKB-phosphorylated cardiac fructose-2,6-bisphosphate kinase/phosphatase. *EMBO J.* 22(14):3514-3523.
- Ravichandran, K.S., and S.J. Burakoff. 1994. The adapter protein Shc interacts with the interleukin-2 (IL-2) receptor upon IL-2 stimulation. *J Biol Chem.* 269(3):1599-1602.
- Reif, K., B.M. Burgering, and D.A. Cantrell. 1997. Phosphatidylinositol 3-kinase links the interleukin-2 receptor to protein kinase B and p70 S6 kinase. *J Biol Chem.* 272(22):14426-14433.
- Rich, R.R., and S. Rich. 1975. Biological expressions of lymphocyte activation IV. Concanavalin A-activated suppressor cells in mouse mixed lymphocyte reactions. *J Immunol.* 114(3):1112-1115.
- Rider, M.H., L. Bertrand, D. Vertommen, P.A. Michels, G.G. Rousseau, and L. Hue. 2004. 6-phosphofructo-2-kinase/fructose-2,6-bisphosphatase: head-to-head with a bifunctional enzyme that controls glycolysis. *Biochem J.* 381(Pt 3):561-579.
- Rider, M.H., K.M. Crepin, M. De Cloedt, L. Bertrand, and L. Hue. 1994. Site-directed mutagenesis of rat muscle 6-phosphofructo-2-kinase/fructose-2,6-bisphosphatase: role of Asp-130 in the 2-kinase domain. *Biochem J.* 300(Pt 1):111-115.
- Rider, M.H., and L. Hue. 1984. Activation of rat heart phosphofructokinase-2 by insulin in vivo. *FEBS Lett.* 176(2):484-488.
- Rider, M.H., J. van Damme, D. Vertommen, A. Michel, J. Vandekerckhove, and L. Hue. 1992. Evidence for new phosphorylation sites for protein kinase C and cyclic AMP-dependent protein kinase in bovine heart 6-phosphofructo-2-kinase/fructose-2,6-bisphosphatase. *FEBS Lett.* 310(2):139-142.
- Robb, R.J. 1984. Interleukin 2: the molecule and its function. *Immunol Today.* 5(7):203-209.
- Robb, R.J., W.C. Greene, and C.M. Rusk. 1984. Low and high affinity cellular receptors for interleukin 2. Implications for the level of Tac antigen. *J Exp Med.* 160(4):1126-1146.
- Robb, R.J., A. Munck, and K.A. Smith. 1981. T cell growth factor receptors. Quantitation, specificity, and biological relevance. *J Exp Med.* 154(5):1455-1474.

- Robb, R.J., C.M. Rusk, J. Yodoi, and W.C. Greene. 1987. Interleukin 2 binding molecule distinct from the Tac protein: analysis of its role in formation of high-affinity receptors. *Proc Natl Acad Sci U S A*. 84(7):2002-2006.
- Robey, R.B., and N. Hay. 2006. Mitochondrial hexokinases, novel mediators of the antiapoptotic effects of growth factors and Akt. *Oncogene*. 25:4683-4696.
- Romashkova, J.A., and S.S. Makarov. 1999. NF-kappaB is a target of AKT in antiapoptotic PDGF signalling. *Nature*. 401(6748):86-90.
- Ros, S., J. Floter, I. Kaymak, C. Da Costa, A. Houddane, S. Dubuis, B. Griffiths, R. Mitter, S. Walz, S. Blake, A. Behrens, K.M. Brindle, N. Zamboni, M.H. Rider, and A. Schulze. 2017. 6-Phosphofructo-2-kinase/fructose-2,6-biphosphatase 4 is essential for p53-null cancer cells. *Oncogene*.
- Ros, S., C.R. Santos, S. Moco, F. Baenke, G. Kelly, M. Howell, N. Zamboni, and A. Schulze. 2012. Functional metabolic screen identifies 6-phosphofructo-2-kinase/fructose-2,6-biphosphatase 4 as an important regulator of prostate cancer cell survival. *Cancer Discov*. 2(4):328-343.
- Ros, S., and A. Schulze. 2013. Balancing glycolytic flux: the role of 6-phosphofructo-2-kinase/fructose 2,6-bisphosphatases in cancer metabolism. *Cancer Metab*. 1(1):8.
- Rosa, J.L., F. Ventura, J. Carreras, and R. Bartrons. 1990. Fructose 2,6-bisphosphate and 6-phosphofructo-2-kinase during liver regeneration. *Biochem J*. 270(3):645-649.
- Ruggeri, B.A., L. Huang, M. Wood, J.Q. Cheng, and J.R. Testa. 1998. Amplification and overexpression of the AKT2 oncogene in a subset of human pancreatic ductal adenocarcinomas. *Mol Carcinog*. 21(2):81-86.
- Russell, R.R., R. Bergeron, and G.I. Shulman. 1999. Translocation of myocardial GLUT-4 and increased glucose uptake through activation of AMPK by AICAR. *Am J Physiol*. 277(2 Pt 2):H643-649.
- Sabularse, D.C., and R.L. Anderson. 1981. D-Fructose 2,6-bisphosphate: a naturally occurring activator for inorganic pyrophosphate:D-fructose-6-phosphate 1-phosphotransferase in plants. *Biochem Biophys Res Commun*. 103(3):848-855.
- Sakai, A., M. Kato, M. Fukasawa, M. Ishiguro, E. Furuya, and R. Sakakibara. 1996. Cloning of cDNA encoding for a novel isozyme of fructose 6-phosphate, 2-kinase/fructose 2,6-bisphosphatase from human placenta. *J Biochem*. 119(3):506-511.

- Sakata, J., Y. Abe, and K. Uyeda. 1991. Molecular cloning of the DNA and expression and characterization of rat testes fructose-6-phosphate,2-kinase:fructose-2,6-bisphosphatase. *J Biol Chem.* 266(24):15764-15770.
- Sancak, Y., C.C. Thoreen, T.R. Peterson, R.A. Lindquist, S.A. Kang, E. Spooner, S.A. Carr, and D.M. Sabatini. 2007. PRAS40 is an insulin-regulated inhibitor of the mTORC1 protein kinase. *Mol Cell.* 25:903-915.
- Sano, H., S. Kane, E. Sano, C.P. Miinea, J.M. Asara, W.S. Lane, C.W. Garner, and G.E. Lienhard. 2003. Insulin-stimulated phosphorylation of a Rab GTPase-activating protein regulates GLUT4 translocation. *J Biol Chem.* 278:14599-14602.
- Seo, M., J.D. Kim, D. Neau, I. Sehgal, and Y.H. Lee. 2011. Structure-based development of small molecule PFKFB3 inhibitors: a framework for potential cancer therapeutic agents targeting the Warburg effect. *PLoS One.* 6(9):e24179.
- Shan, X., M.J. Czar, S.C. Bunnell, P. Liu, Y. Liu, P.L. Schwartzberg, and R.L. Wange. 2000. Deficiency of PTEN in Jurkat T cells causes constitutive localization of Itk to the plasma membrane and hyperresponsiveness to CD3 stimulation. *Mol Cell Biol.* 20(18):6945-6957.
- Shinohara, Y., K. Yamamoto, K. Kogure, J. Ichihara, and H. Terada. 1994. Steady state transcript levels of the type II hexokinase and type 1 glucose transporter in human tumor cell lines. *Cancer Lett.* 82(1):27-32.
- Simon-Molas, H., M.N. Calvo-Vidal, E. Castano, A. Rodriguez-Garcia, A. Navarro-Sabate, R. Bartrons, and A. Manzano. 2016. Akt mediates TIGAR induction in HeLa cells following PFKFB3 inhibition. *FEBS Lett.* 590(17):2915-2926.
- Smeal, T., B. Binetruy, D.A. Mercola, M. Birrer, and M. Karin. 1991. Oncogenic and transcriptional cooperation with Ha-Ras requires phosphorylation of c-Jun on serines 63 and 73. *Nature.* 354(6353):494-496.
- Songyang, Z., S.E. Shoelson, M. Chaudhuri, G. Gish, T. Pawson, W.G. Haser, F. King, T. Roberts, S. Ratnofsky, R.J. Lechleider, B.G. Neel, R.B. Birge, J.E. Fajardo, M.M. Chou, H. Hanafusa, B. Schaffhausen, and L.C. Cantley. 1993. SH2 domains recognize specific phosphopeptide sequences. *Cell.* 72(5):767-778.
- Staal, S.P. 1987. Molecular cloning of the akt oncogene and its human homologues AKT1 and AKT2: amplification of AKT1 in a primary human gastric adenocarcinoma. *Proc Natl Acad Sci U S A.* 84(14):5034-5037.

- Stal, O., G. Pérez-Tenorio, L. Akerberg, B. Olsson, B. Nordenskjöld, L. Skoog, and L.E. Rutqvist. 2003. Akt kinases in breast cancer and the results of adjuvant therapy. *Breast Cancer Res.* 5(2):R37-44.
- Stambolic, V., A. Suzuki, J.L. de la Pompa, G.M. Brothers, C. Mirtsos, T. Sasaki, J. Ruland, J.M. Penninger, D.P. Siderovski, and T.W. Mak. 1998. Negative regulation of PKB/Akt-dependent cell survival by the tumor suppressor PTEN. *Cell.* 95(1):29-39.
- Stauber, D.J., E.W. Debler, P.A. Horton, K.A. Smith, and I.A. Wilson. 2006. Crystal structure of the IL-2 signaling complex: paradigm for a heterotrimeric cytokine receptor. *Proc Natl Acad Sci U S A.* 103(8):2788-2793.
- Tamada, M., M. Suematsu, and H. Saya. 2012. Pyruvate kinase M2: multiple faces for conferring benefits on cancer cells. *Clin Cancer Res.* 18:5554-5561.
- Tan, S., Y. Ng, and D.E. James. 2011. Next-generation Akt inhibitors provide greater specificity: effects on glucose metabolism in adipocytes. *Biochem J.* 435:539-544.
- Tan, S.X., Y. Ng, and D.E. James. 2010. Akt inhibitors reduce glucose uptake independently of their effects on Akt. *Biochem J.* 432:191-197.
- Taniguchi, T., H. Matsui, T. Fujita, C. Takaoka, N. Kashima, R. Yoshimoto, and J. Hamuro. 1983. Structure and expression of a cloned cDNA for human interleukin-2. *Nature.* 302(5906):305-310.
- Telang, S., A. Yalcin, A.L. Clem, R. Bucala, A.N. Lane, J.W. Eaton, and J. Chesney. 2006. Ras transformation requires metabolic control by 6-phosphofructo-2-kinase. *Oncogene.* 25(55):7225-7234.
- Testa, J.R., and A. Bellacosa. 1997. Membrane translocation and activation of the Akt kinase in growth factor-stimulated hematopoietic cells. *Leuk Res.* 21(11-12):1027-1031.
- Truitt, K.E., G.B. Mills, C.W. Turck, and J.B. Imboden. 1994. SH2-dependent association of phosphatidylinositol 3'-kinase 85-kDa regulatory subunit with the interleukin-2 receptor beta chain. *J Biol Chem.* 269(8):5937-5943.
- Tsuchiya, Y., and K. Uyeda. 1994. Bovine heart fructose 6-P,2-kinase:fructose 2,6-bisphosphatase mRNA and gene structure. *Arch Biochem Biophys.* 310(2):467-474.
- Van Schaftingen, E. 1987. Fructose 2,6-bisphosphate. *Adv Enzymol Relat Areas Mol Biol.* 59:315-395.

- Van Schaftingen, E., D.R. Davies, and H.G. Hers. 1982. Fructose-2,6-bisphosphatase from rat liver. *Eur J Biochem.* 124(1):143-149.
- Van Schaftingen, E., M.F. Jett, L. Hue, and H.G. Hers. 1981. Control of liver 6-phosphofructokinase by fructose 2,6-bisphosphate and other effectors. *Proc Natl Acad Sci U S A.* 78(6):3483-3486.
- Van Schaftingen, E., F.R. Opperdoes, and H.G. Hers. 1985. Stimulation of *Trypanosoma brucei* pyruvate kinase by fructose 2,6-bisphosphate. *Eur J Biochem.* 153(2):403-406.
- Ventura, F., S. Ambrosio, R. Bartrons, M.R. El-Maghrabi, A.J. Lange, and S.J. Pilkis. 1995. Cloning and expression of a catalytic core bovine brain 6-phosphofructo-2-kinase/fructose-2,6-bisphosphatase. *Biochem Biophys Res Commun.* 209(3):1140-1148.
- Vertommen, D., L. Bertrand, B. Sontag, A. Di Pietro, M.P. Louckx, H. Vidal, L. Hue, and M.H. Rider. 1996. The ATP-binding site in the 2-kinase domain of liver 6-phosphofructo-2-kinase/fructose-2,6-bisphosphatase. Study of the role of Lys-54 and Thr-55 by site-directed mutagenesis. *J Biol Chem.* 271(30):17875-17880.
- Vidal, H., K.M. Crepin, M.H. Rider, L. Hue, and G.G. Rousseau. 1993. Cloning and expression of novel isoforms of 6-phosphofructo-2-kinase/fructose-2,6-bisphosphatase from bovine heart. *FEBS Lett.* 330(3):329-333.
- Wang, B.Y., T. Kalir, E. Sabo, D.E. Sherman, C. Cohen, and D.E. Burstein. 2000. Immunohistochemical staining of GLUT1 in benign, hyperplastic, and malignant endometrial epithelia. *Cancer.* 88(12):2774-2781.
- Wang, R., and D.R. Green. 2012. Metabolic reprogramming and metabolic dependency in T cells. *Immunol Rev.* 249:14-26.
- Wang, T., C. Marquardt, and J. Foker. 1976. Aerobic glycolysis during lymphocyte proliferation. *Nature.* 261:702-705.
- Wang, X., M. Rickert, and K.C. Garcia. 2005. Structure of the quaternary complex of interleukin-2 with its alpha, beta, and gamma receptors. *Science.* 310(5751):1159-1163.
- Warburg, O., K. Posener, and E. Negelein. 1924. Ueber den Stoffwechsel der Carcinomzelle. *Biochem Z.* 152:309-344.

- Watanabe, F., and E. Furuya. 1999. Tissue-specific alternative splicing of rat brain fructose 6-phosphate 2-kinase/fructose 2,6-bisphosphatase. *FEBS Lett.* 458(3):304-308.
- Weber, G. 1977. Enzymology of cancer cells (second of two parts). *N Engl J Med.* 296(10):541-551.
- Werlen, G., E. Jacinto, Y. Xia, and M. Karin. 1998. Calcineurin preferentially synergizes with PKC-theta to activate JNK and IL-2 promoter in T lymphocytes. *EMBO J.* 17(11):3101-3111.
- Wieman, H.L., J.A. Wofford, and J.C. Rathmell. 2007. Cytokine stimulation promotes glucose uptake via phosphatidylinositol-3 kinase/Akt regulation of Glut1 activity and trafficking. *Mol Biol Cell.* 18(4):1437-1446.
- Wilson, J.E. 2003. Isozymes of mammalian hexokinase: structure, subcellular localization and metabolic function. *Journal of Experimental Biology.* 206:2049-2057.
- Wood, I.S., and P. Trayhurn. 2003. Glucose transporters (GLUT and SGLT): expanded families of sugar transport proteins. *Br J Nutr.* 89:3-9.
- Wu, C., S.A. Khan, L.J. Peng, and A.J. Lange. 2006. Roles for fructose-2,6-bisphosphate in the control of fuel metabolism: beyond its allosteric effects on glycolytic and gluconeogenic enzymes. *Adv Enzyme Regul.* 46:72-88.
- Yalcin, A., B.F. Clem, A. Simmons, A. Lane, K. Nelson, A.L. Clem, E. Brock, D. Siow, B. Wattenberg, S. Telang, and J. Chesney. 2009. Nuclear targeting of 6-phosphofructo-2-kinase (PFKFB3) increases proliferation via cyclin-dependent kinases. *J Biol Chem.* 284(36):24223-24232.
- Yamamoto, T., Y. Seino, H. Fukumoto, G. Koh, H. Yano, N. Inagaki, Y. Yamada, K. Inoue, T. Manabe, and H. Imura. 1990. Over-expression of facilitative glucose transporter genes in human cancer. *Biochem Biophys Res Commun.* 170(1):223-230.
- Yap, T.A., L. Yan, A. Patnaik, I. Fearen, D. Olmos, K. Papadopoulos, R.D. Baird, L. Delgado, A. Taylor, L. Lupinacci, R. Riisnaes, L.L. Pope, S.P. Heaton, G. Thomas, M.D. Garrett, D.M. Sullivan, J.S. de Bono, and A.W. Tolcher. 2011. First-in-man clinical trial of the oral pan-AKT inhibitor MK-2206 in patients with advanced solid tumors. *J Clin Oncol.* 29:4688-4695.
- Zhang, X., N. Tang, T.J. Hadden, and A.K. Rishi. 2011. Akt, FoxO and regulation of apoptosis. *Biochim Biophys Acta.* 1813:1978-1986.

Zhao, J.J., and T.M. Roberts. 2006. PI3 kinases in cancer: from oncogene artifact to leading cancer target. *Sci STKE*. 2006(365):pe52.

Zu, X.L., and M. Guppy. 2004. Cancer metabolism: facts, fantasy, and fiction. *Biochemical and Biophysical Research Communications*. 313:459-465.